Actions of NAADP and other agents in cardiac myocytes

SUBMISSION FOR THE DEGREE OF DOCTOR OF PHILOSOPHY

REBECCA ANNE BAYLISS

ACKNOWLEDGEMENTS

First and foremost, I would like to thank Professor Derek Terrar for giving me the opportunity to carry out work in his laboratory and for his tutelage and supervision over a number of years, as both an undergraduate and graduate student.

I have worked with many people over the course of this research for whom I am very grateful. Particularly Dr Rebecca Burton, whose collaboration and friendship has been both scientifically and personally invaluable, and Dr Emma Bolton, who has been responsible for an exponential increase in my tea-drinking capacity. I would also like to thank Professor Peter Kohl for his help in applications to DPhil programmes and for his supervision during my first-year rotations and the British Heart Foundation for their funding of this project and for their continued support in my post-doctoral work.

It is difficult, in a few sentences to really express how grateful I am to friends and family for their support over so many years. Really, this document is dedicated to a number of people. To:

Mum and Dad, for years of unwavering support and for always believing in me.

Ifor, who makes each day a little brighter. Everything is better because I do it with you. And dear Henry, training partner, counsellor and third wheel. There aren't good enough words to say how much I value your friendship.

Gramps, who started with me and is still watching from somewhere, and Grandma, who is my model in faithful living. I hope I am like you when I am 92.

Ifor and Madeline, who have taken me as one of their own. Life wouldn't be as much fun without our discussions and this thesis would look very different without all the things you did for us last year.

Sarah and Jason and Margred and Gareth, who always have an open door, and their respective children, Delaney, Maria, Owain and Carys, who don't care about science but did teach me about High School Musical and Peppa Pig. Sometimes a little perspective is paramount!

William Tew, the one and only, for a significant decline in productivity but a knowledge of 'applied' probability I would never otherwise have gained. Justin, because Bear Camp was awesome, Matt and Rhi, because Masons Road would never have been the same without you and Meera, who was the best Maid of Honour I could have asked for.

TABLE OF CONTENTS

Table of Contents 2

Complete Figure List 6

Abstract 12

1 General Introduction 13

1.1 Calcium as an intracellular messenger 14

1.2 The heart as a pump 15

1.3 Cardiac muscle and the cardiac myocyte 17

1.4 Mechanism of contraction 22

1.5 Electrophysiology of cardiac muscle 25

1.6 Calcium transients: Overview 30

1.7 Calcium transients: Sarcolemmal Calcium Entry 33

1.8 Calcium transients: SR Calcium Release 36

1.9 Calcium transients: Clearing Ca^{2+} from the Cytosol 45

1.10 CaMKII 50

1.11 NAADP 55

1.12 cADPR 63

1.13 IP_3 65

1.14 The Sino-Atrial Node 66

1.15 Specific Bradycardic Agents 72

2 Methods 75

2.1 Cell Isolation Protocols 76

2.2 Multicellular Tissue Preparations 80

2.3 Electrophysiology 81

2.4 Fluorescent Indicators 90

2.5 Epifluorescence Measurements 93

2.6 Measurement of Cellular Contraction 95

2.7 UV Photolysis Systems 96

2.8 Solutions 98

2.9 Suppliers 100

2.10 Statistics 102

3 Identification of a Role for CaMKII in the NAADP Signalling Pathway 104

3.1 Introduction 105

3.2 Methods 109

3.3 Results 112

3.3.1 Photorelease of NAADP enhances cellular calcium transients in atrial myocytes 112

3.3.2 Photorelease of NAADP enhances cellular calcium transients in ventricular myocytes 128

3.3.3 Ned-19 abolishes the cellular response to NAADP photorelease..... 137

3.3.4 Intact CaMKII signalling is essential to the actions of NAADP 147

3.3.5 Consistent effects of UV photorelease protocol in cardiomyocytes... 160

3.4 Discussion 164

4 NAADP Signalling is Physiologically-Relevant in the Heart 171

4.1 Introduction 172

4.2 Methods 174

4.3 Results 176

4.3.1 NAADP signalling is constitutively active in atrial myocytes 176

4.3.2 The calcium transient response to isoprenaline is partially dependent on NAADP signalling in atrial myocytes 178

4.3.3 The calcium transient response to isoprenaline is partially-dependent on the NAADP pathway in ventricular myocytes 181

4.3.4 The L-type calcium current response to isoprenaline is not dependent on the NAADP pathway 187

4.4 Discussion 192

5 Potential of Hydroxychloroquine as a Novel Funny Current Inhibitor 198

5.1 Introduction 199

5.2 Methods 203

5.3 Results 206

5.3.1 HCQ reduced spontaneous beating rate in a multicellular preparation in a dose-dependent manner 206

5.3.2 HCQ reduced spontaneous AP firing rate in isolated SA node cells .. 210

5.3.3 HCQ reduces stimulated $I_{(f)}$ current 217

5.3.4 HCQ reduces stimulated $I_{(f)}$ current in a dose-dependent manner 221

5.4 Discussion 225

6 The Endogenous Peptide Apelin Confers both Positive Inotropy and Positive Lusitropy 231

6.1 Introduction 232

6.2 Methods 236

6.3 Results 238

6.3.1 Apelin increases cellular contractility in mouse ventricular myocytes 238

6.3.2 The effect of apelin on mouse cardiomyocytes is not dependent on temperature 247

6.3.3 Apelin does not increase fractional shortening in rat cardiomyocytes 250

6.3.4 Apelin consistently accelerates contraction and relaxation in rat ventricular cardiomyocytes 253

6.4 Discussion 258

7 References 261

COMPLETE FIGURE LIST

Figure 1.1: Ventricular myocytes 19

Figure 1.2: Atrial and Sino-atrial node myocytes 21

Figure 1.3: Structure of a sarcomere 23

Figure 1.4: Schematic traces of typical action potentials in functionally-distinct areas of cardiac tissue 28

Figure 1.5: Structure of Nicotinic Acid Adenine Dinucleotide Phosphate 56

Figure 2.1: Voltage clamp protocol for the measurement of L-type Ca^{2+} currents 88

Figure 2.2: Voltage clamp protocol for the measurement of $I_{(f)}$ currents in sino-atrial node myocytes 89

Figure 3.1 (i) and (ii): Representative Traces of NAADP Photorelease 114

Figure 3.2 (i) and (ii): Calcium Transient Response to NAADP 115

Figure 3.3 (i) and (ii): NAADP enhances the velocity of atrial calcium transient decay 116

Figure 3.4 (i) and (ii): NAADP enhances the velocity of atrial calcium transient upstroke 117

Figure 3.5: Representative Trace of UV Flash Control 119

Figure 3.6 (i) and (ii): Calcium Transient Response to UV Flash Control 120

Figure 3.7 (i) and (ii): The effect of UV flash on calcium transient velocities 121

Figure 3.8: Representative Action Potential Response to UV Flash Control 124

Figure 3.9: Representative Action Potential Trace to NAADP Photorelease 125

Figure 3.10: Comparison of Control Flash and NAADP Effects on AP Amplitude 126

Figure 3.11: Comparison of control and NAADP effects on Resting Membrane Potential 127

Figure 3.12: Representative traces to show the effect of NAADP on calcium transients in a ventricular myocyte 130

Figure 3.13: The effect of NAADP on calcium transient amplitude in ventricular myocytes 131

Figure 3.14 (i) and (ii): Effect of NAADP on the maximal slope of Ca^{2+} transient decay 132

Figure 3.15 (i) and (ii): The effect of NAADP on calcium upstroke velocity..... 133

Figure 3.16: Representative trace to show the effect of UV flash on calcium transients in a ventricular myocyte 134

Figure 3.17 (i) and (ii): The effect of UV flash on calcium transient amplitude in ventricular myocytes..... 135

Figure 3.18 (i) and (ii): The effect of UV flash on calcium transient decay and upstroke velocities in cardiac ventricular myocytes 136

Figure 3.19 (i) and (ii): Representative Traces, Atrial NAADP Photorelease in the Presence of Ned-19..... 140

Figure 3.20 (i) and (ii): Atrial Calcium Transient Response to NAADP in the Presence of Ned-19..... 141

Figure 3.21: Representative trace to show the effect of NAADP photorelease in the presence of Ned-19 in a ventricular myocyte 142

Figure 3.22 (i) and (ii): The effect of NAADP photorelease in the presence of Ned-19 on calcium transient amplitude in ventricular myocytes 143

Figure 3.23 (i) and (ii): Lack of effect of NAADP on calcium transient upstroke and decay velocities in the presence of Ned-19, atrial myocytes 144
Figure 3.24 (i) and (ii): Lack of effect of NAADP on calcium transient decay and upstroke velocities in the presence of Ned-19, ventricular myocytes 145
Figure 3.25 (i) and (ii): Stability of action potential parameters during NAADP photorelease in the presence of Ned-19 146
Figure 3.26 (i) and (ii): Representative traces to show the effect of KN93 on calcium transients and action potentials in atrial cardiomyocytes 149
Figure 3.27: The Effect of KN93 Superfusion on Calcium Transients 150
Figure 3.28 (i), (ii) and (Iii): The effect of KN93 superfusion on action potential parameters 151
Figure 3.29 (i) and (ii): Representative trace to show the effect of NAADP photorelease in the presence of KN93 153
Figure 3.30: Photorelease of NAADP in the Presence of KN93 154
Figure 3.31 (i) and (ii): Lack of effect of NAADP on calcium transient decay and upstroke velocities in the presence of KN93 155
Figure 3.32: Representative trace to show the effect of NAADP on calcium transients in a ventricular myocyte in the presence of AIP 157
Figure 3.33 (i) and (ii): The effect of NAADP on calcium transient amplitude in ventricular myocytes in the presence of AIP 158
Figure 3.34: Lack of effect of NAADP on calcium transient decay and upstroke velocities in the presence of AIP 159

Figure 3.35: The effect of NAADP, in the presence of various inhibitors, upon diastolic fluorescence in ventricular myocytes 161
Figure 3.36 (i), (ii) and (iii): NAADP photorelease in ventricular myocytes using a different photorelease system 162
Figure 3.37: The effect of NAADP, in the presence of various inhibitors, upon action potential duration in atrial myocytes 163
Figure 4.1 (i) and (ii): The Effect of Bafilomycin on Atrial Myocytes 177
Figure 4.2 (i) and (ii): Representative traces to show the effect of bafilomycin on the β-adrenergic response in isolated atrial myocytes 179
Figure 4.3 (i) and (ii): Effect of Bafilomycin on Cellular Response to Isoprenaline 180
Figure 4.4 (i), (ii) and (iii): Representative traces of responses to isoprenaline 184
Figure 4.5: Timecourse graph of ISO response in the presence of Baf and Ned..... 185
Figure 4.6: Bar graph to show maximal effect of ISO under each condition 186
Figure 4.7 (i) and (ii): Representative traces to show L-type calcium current Iso responses in control conditions and in the presence of Ned-19 189
Figure 4.8: L-type Ca^{2+} current response to ISO over time in the presence and absence of Ned-19 190
Figure 4.9 (i) and (ii): Maximal response of L-type Ca^{2+} current to ISO in the presence and absence of Ned-19 191
Figure 4.10: New model of the NAADP pathway in cardiac myocytes 196
Figure 4.11: A possible role for the NAADP pathway in the development of cardiac hypertrophy 197
Figure 5.1: Chemical structure of hydroxychloroquine 201

Figure 5.2: Dose-dependent effect of HCQ on spontaneous beating rate in mouse atrial preparations 208
Figure 5.3: Normalised dose-dependent change in atrial beating rate compared to control preparations 209
Figure 5.4: Representative traces to show action potentials before and after superfusion of 1 μM HCQ 211
Figure 5.5 (i) and (ii): HCQ reduces action potential firing rate in isolated guinea pig sino-atrial myocytes 212
Figure 5.6 (i) and (ii): Change in rate of spontaneous diastolic depolarisation 214
Figure 5.7 (i) and (ii): Change in action potential duration in the presence of HCQ 215
Figure 5.8: Lack of effect of HCQ on AP amplitude 216
Figure 5.9: Representative trace to show the effect of HCQ on $I_{(f)}$ 219
Figure 5.10 (i) and (ii): The effect of HCQ on $I_{(f)}$ current 220
Figure 5.11: Representative traces to show the effect of different doses of HCQ on $I_{(f)}$ 222
Figure 5.12: The magnitude of $I_{(f)}$ inhibition by HCQ is dose-dependent 223
Figure 5.13: Illustration of HCQ wash-out 224
Figure 5.14: In vivo bolus injections of HCQ affect heart rate but not blood pressure 228
Figure 6.1: Representative trace to show a single contraction of mouse ventricular myocytes under control conditions and in the presence of apelin 240
Figure 6.2 (i) and (ii): The effect of apelin on diastolic sarcomere length and fractional sarcomere shortening in murine ventricular myocytes 241

Figure 6.3 (i) and (ii): The effect of apelin on velocities of contraction and relaxation in murine ventricular myocytes 244

Figure 6.4 (i) and (ii): The effect of apelin on time taken to reach 90% of peak contraction and 90% of full relaxation in murine ventricular myocytes 245

Figure 6.5: Summary graph to show all of apelin's effects on contraction in murine ventricular myocytes 246

Figure 6.6: The effect of temperature on cellular responses to apelin 248

Figure 6.7: The effect of stimulation rate on responses to apelin 249

Figure 6.8: Representative trace to show the effect of apelin on the course of contraction in rat ventricular myocytes 251

Figure 6.9: The effect of apelin on fractional sarcomere shortening in rat ventricular myocytes 252

Figure 6.10 (i) and (ii): The effect of apelin on cellular contraction in isolated rat ventricular myocytes 254

Figure 6.11 (i) and (ii): The effect of apelin on cellular relaxation in isolated rat cardiomyocytes 256

Figure 6.12: Summary graph to show effects of apelin on contraction in rat ventricular myocytes 257

ACTIONS OF NAADP AND OTHER AGENTS ON CARDIAC MYOCYTES

Abstract for DPhil thesis submission of Rebecca Anne Bayliss

Modulation of cardiac rate and contraction through calcium-dependent and independent means are of central import to the ability of an organism to adapt to its environment.

Nicotinic acid adenine dinucleotide phosphate (NAADP) is a potent calcium-releasing second messenger across a broad range of tissues and organisms. In cardiac myocytes, NAADP is thought to stimulate calcium release from acidic stores which then bolsters filling and release during CICR. Questions remain: as to the potential need for amplification to generate the size of responses observed and the physiological role of the NAADP pathway.

In contractile myocytes, photorelease of NAADP caused significant increase in calcium transient amplitude and velocity of transient upstroke and decay. Effects were absent during NAADP photorelease in the presence of Ned-19 or CaMKII inhibitors. Cellular calcium transient responses to β-adrenergic stimulation were significantly reduced in the presence of inhibitors of the NAADP pathway.

These data support the hypothesis that NAADP-induced calcium release is relevant during adrenergic stimulation and requires amplification through CaMKII.

Rate modulation at the sino-atrial node can occur through the hyperpolarisation-activated current $I_{(f)}$. Basal cardiac rate is a major determinant in cardiac mortality and compounds which specifically affect rate have clinical utility.

Hydroxychloroquine, an antimalarial compound, was found to have a significant rate-reducing effect in sino-atrial node preparations mediated by inhibition of $I_{(f)}$.

Apelin, an endogenous peptide, has been reported to potently generate improved contractility without development of hypertrophy. Study of its effects in single cells have provided conflicting information, at least in part because of the difficulty in working with the compound.

A method for the consistent observation of apelin-mediated contractile responses is presented, focusing on the timecourse of cell contraction. These observations suggest a role for apelin in both inotropy and lusitropy and will enable further research

1 General Introduction

1.1 CALCIUM AS AN INTRACELLULAR MESSENGER

In order to initiate and control cellular processes and react to external stimuli, the cells of the body are awash with proteins which act as receptors, effectors, and transporters. Cellular membranes have very low permeability to ions and solutes, and so it is primarily through these specific proteins that external signals are communicated to, and affect, the intracellular environment. One of the most efficient ways to amplify a signal within a physiological system is through the use of second messengers. Second messenger systems allow a stimulus binding in one place to lead to the synthesis or release of a large number of second messenger molecules which can have spatially or temporally varied and far-reaching effects.

Over the past 100 years, calcium ions (Ca^{2+}) have been recognised as one of the most widespread and important second messengers across the full range of living organisms. Changes in intracellular calcium concentration and temporal pattern are the central factor in initiating or controlling a wide range of physiological processes in many different tissues, ranging from fertilisation and development through synaptic plasticity and muscle contraction, all the way to cell death by apoptosis.

Given the huge range of signals that can be mediated by calcium, it is of no surprise that cells maintain tight control of cytosolic calcium concentration, and this is no different in the heart. Free calcium is pumped from the cytosol using active transport and is also heavily buffered. Most calcium stored within cells is maintained in the sarcoplasmic reticulum (SR), a vast, interconnected tubular network running tentacle-like around the contractile machinery, into which it is actively pumped via the

sarco/endoplasmic reticulum calcium ATPase (SERCA). There are also stores of calcium contained within mitochondria and acidic organelles.

1.2 THE HEART AS A PUMP

Double-circulatory systems

Rapid, even distribution of oxygen, nutrients and heat throughout the body, and removal of waste products, is highly important in the function of all living species. Whilst diffusion suffices for single-celled organisms, the time taken for diffusion is proportional to the square of the distance being covered and simple diffusion rapidly becomes too slow to support tissue function in more complex organisms. In this case, a circulatory system is required to distribute nutrients, oxygen and heat appropriately. In mammals and birds this need has been fulfilled by a double-circulatory system driven by the four-chambered heart.

A four-chambered heart consists of two pumps, the right and left ventricles, which drive blood around two separate circulatory systems. This double-circulatory system enables pressure in the pulmonary circulation, that which passes from the right ventricle, through the lungs in order to be oxygenated and get rid of excess carbon dioxide, to be maintained at a lower pressure than the systemic circulation. The systemic circulation carries oxygenated blood to the tissues of the body and transports waste products to the liver and kidneys. It is driven by the left ventricle. Each side of the heart is divided completely from the other and consists of two chambers, an atria and a ventricle.

Steps to the generation of each beat

Blood is fed into the heart through veins, the vena cave on the right and pulmonary vein on the left. During ventricular relaxation, diastole, blood first begins to fill the ventricles directly. Contraction of the atria completes filling of the ventricles, topping up their volume, and is followed by ventricular contraction, or systole, expelling blood from the heart through the aorta to the body or the pulmonary artery to the lungs.

The rhythmic generation of cardiac contraction, unlike the rhythmic initiation of breathing, is a fully automated process initiated by the sino-atrial node, and does not require nervous innervation. Nervous innervation of the heart, instead, acts to modulate the rate of sino-atrial node beating through receptor-mediated second-messenger systems and, ultimately, the modulation of calcium signalling.

After generation of an electrical signal at the sino-atrial node, excitation is spread across the atrial tissue, causing atrial contraction. If excitation continued directly into the ventricles, atrial contraction and ventricular contraction would be effectively simultaneous and blood leaving the atria would not be able to bolster ventricular volume. Further, ventricular contraction would begin in the wrong area. A layer of insulating tissue, the annulus fibrosus, ensures that the excitatory signal does not pass directly into the ventricles.

A small pathway of conducting tissue, the atrio-ventricular node (AVN), bridges the annulus fibrosus near to the septum. The AVN slows the signal for a short period of time (~100 ms), allowing contraction of the atria, then shepherds its passage into the

ventricular conduction system. Here, rapid conduction through the His-Purkinje network delivers electrical excitation to the contractile cells of the myocardium, initiating a coordinated contraction of both chambers. Ventricular systole begins at the apex of the heart and continues upwards towards the atria, squeezing blood towards the exit vessels.

In order to translate electrical excitation passed throughout the conduction system into meaningful work, all contractile myocytes require a method of excitation-contraction coupling (ECC). Briefly, in an individual cell electrical excitation is carried as an action potential. This rapid change in cellular voltage signal stimulates entry of calcium through voltage-gated channels in the cellular membrane, and that calcium acts as the stimulus for opening ryanodine receptors in the SR. Opening ryanodine receptors empties the SR calcium store, causing a massive increase in intracellular calcium concentration, and it is this intracellular calcium signal which activates the cell's contractile machinery. The initiation, control and modulation mechanisms of the action potential and calcium transient will be discussed in greater detail in the rest of this chapter. For further introduction to cardiovascular physiology, see An Introduction to Cardiovascular Physiology (Levick, 2009).

1.3 CARDIAC MUSCLE AND THE CARDIAC MYOCYTE

Ultrastructure of a cardiac myocyte

Cardiac muscle is a form of striated contractile tissue, so called because of the alternating dark and light bands visible under light microscopy. A human ventricular

myocyte forms a relatively geometric, oblong shape 50-100 μM in length and 10-20 μM wide. Adjacent cardiac myocytes are joined at the intercalated disk by connexons, which form electrical continuity by allowing the free flow of ions (Yeager and Nicholson, 1996), and desmosomes, which anchor the adjacent cells together and provide mechanical stability. Cardiac muscle, because of its extensive network of connexons, can be considered to be a sheet of electrically continuous cells. Unlike in skeletal muscle there are no distinct muscle fibres or motor units present and, under physiological conditions, every cell contracts with every beat. Under physiological conditions, cardiac metabolism is always aerobic. In order to achieve this, cardiac myocytes are made up of mitochondria 30-35% by volume and these are situated in the gaps between contractile elements.

The striated nature of cardiac muscle is due to the presence of 'thick' and 'thin' filaments which form the myocyte's contractile machinery. The basic contractile unit of a cardiac myocyte is called a sarcomere, and consists of a thick filament flanked by thin filaments on either side. Sarcomeres are arranged end-to-end in bundles called myofibrils. Myofibrils within each cell are arranged in parallel, causing the pattern of dark and light bands. A light micrograph of a ventricular myocyte is presented in Figure 1.1.

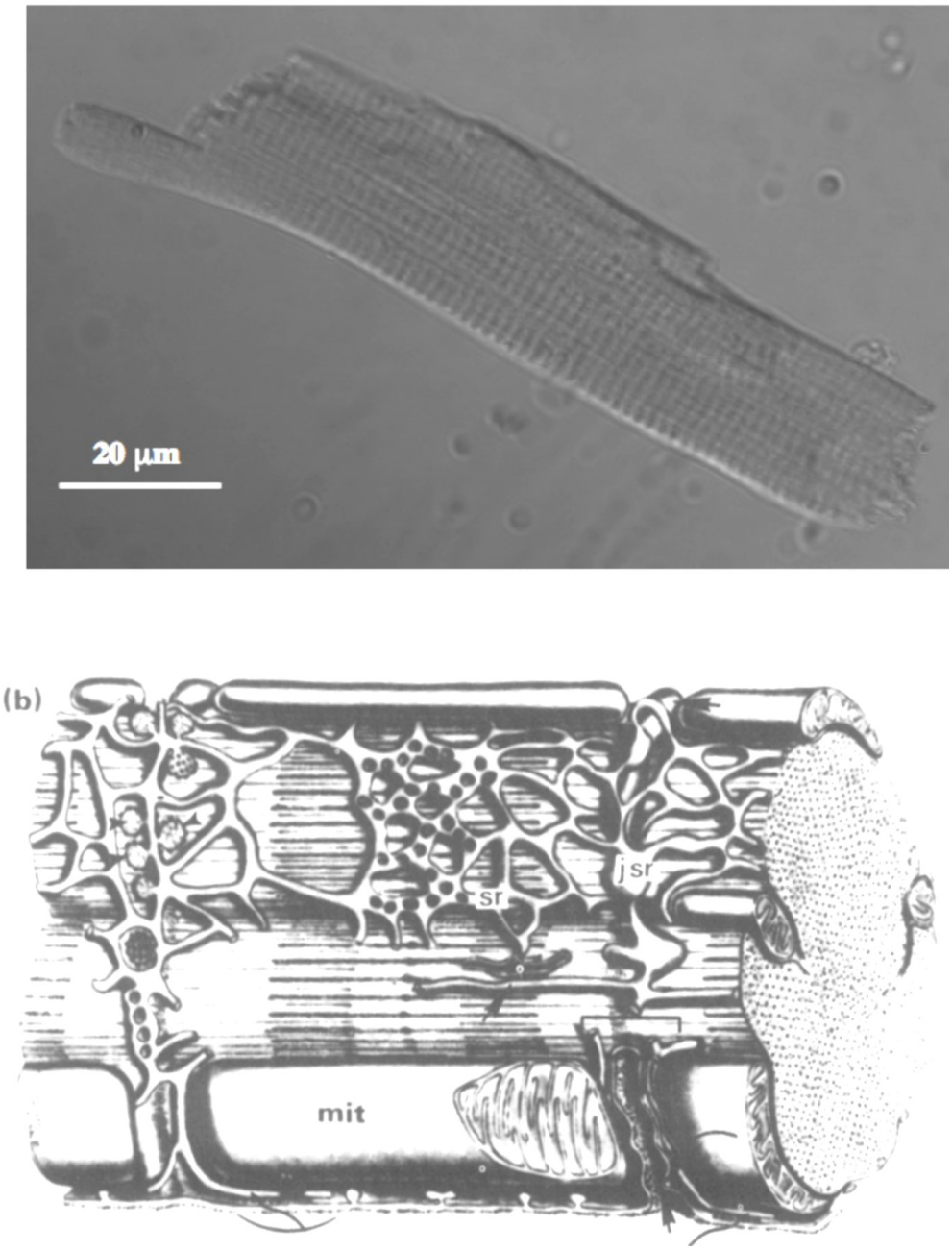


Figure 1.1: Ventricular myocytes
Upper panel: A healthy isolated ventricular myocyte visualised under bright field microscopy, illustrating the relatively geometric, rod-like, nature of the cells and presence of clear striations.
Lower panel: Schematic reproduction of a mammalian cardiac myocyte illustrating the extensive SR network, myofibrils and mitochondria. Arrow indicates a t-tubule. Partial reproduction from Sommer (1982).

Differences between atrial and ventricular myocytes

Within the heart, cells from different areas are functionally distinct and exhibit specialised structural features which make them suitable for these functions. Atrial myocytes, which are required to produce less contractile force, are longer and thinner than their ventricular counterparts but arranged in broadly the same, clearly-striated fashion. Sino-atrial node cells also contain striations of thick and thin filaments however, consistent with the notion that these cells have minimal contractile role, striations are much less distinct. Sino-atrial node cells are thinner, even, than atrial myocytes and often exhibit spindle-like projections which allow them to connect to multiple surrounding cells (DiFrancesco *et al.*, 1986). The morphology of a typical atrial and sino-atrial node myocyte can be seen in Figure 1.2 (ii).

Membrane-staining, for instance using the voltage-sensitive Di-8-ANEPPS, reveals differences in membrane structure between cell types. A large number of invaginations can be visualised in the surface of ventricular myocytes, protruding into the depths of the cell (Ibrahim *et al.*, 2011). These T-tubules extend the cellular membrane (sarcolemma) into the cell such that the voltage and calcium signals associated with the cellular membrane are, in practice, distributed throughout the full volume of the cell instantaneously.

Atrial and sino-atrial myocytes, whilst still containing an array of intracellular SR, lack an organised t-tubule network. In these cells, calcium signals can only reach the deepest areas of the myocyte by diffusion and confocal microscopy using a calcium-selective dye reveals a U-shaped calcium signal, starting at the cell periphery and propagating inwards (Bootman *et al.*, 2006).

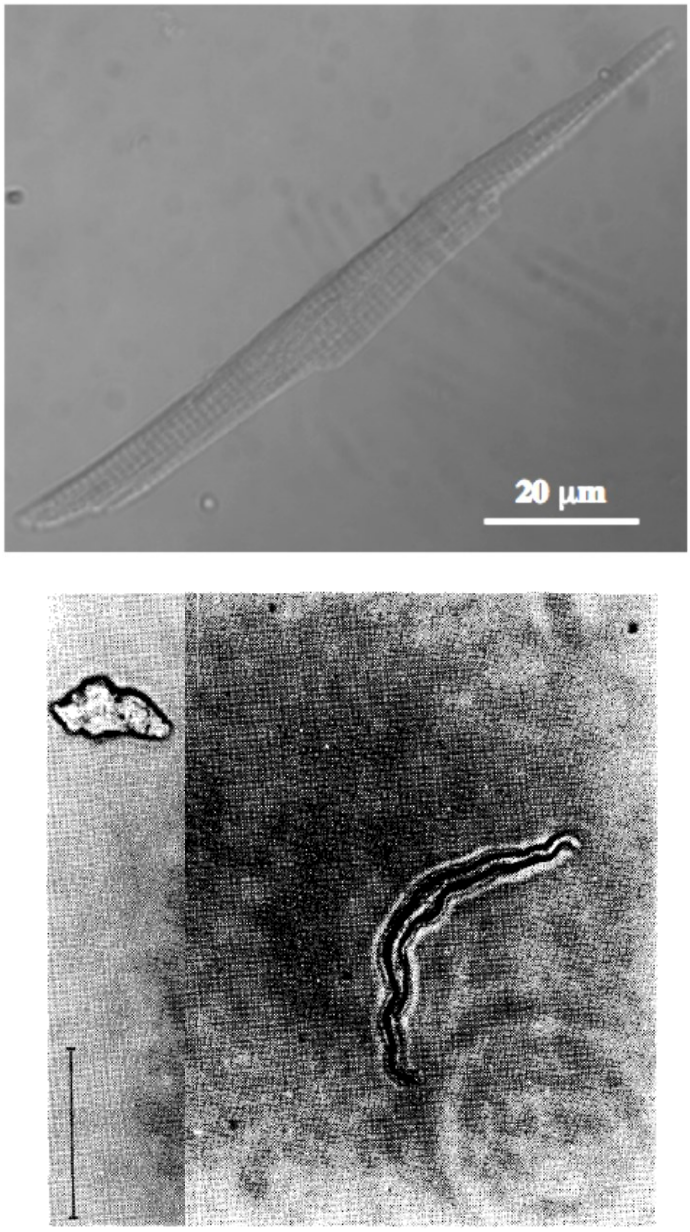


Figure 1.2: Atrial and Sino-atrial node myocytes

(i) Atrial myocyte. Note the presence of clear striations and the elongated but geometric nature of the cell.

(ii) Sino atrial node myocyte. Reproduction from Denyer and Brown (1987, reproduced with permission from The Physiological Society of Japan), one of the first papers to report an isolation method for healthy sino-atrial node cells. Scale bar = 50 μM. Cells are small and thin, do not exhibit strong striations and are more freeform in nature.

1.4 MECHANISM OF CONTRACTION

Muscular contraction in both skeletal and cardiac muscle utilises the mechanical interaction of actin and myosin filaments within each sarcomere to achieve concentric motion by a process termed the sliding filament theory (Huxley and Niedergerke, 1954, Huxley and Hanson, 1954).

An electron micrograph showing a single sarcomere can be seen in Figure 1.3. Within each sarcomere, thick filaments are made up of myosin. Thin filaments consist mainly of actin, with associated troponin and tropomyosin. Actin filaments are tethered at the Z-disk, from where they project across the I-band and into A-bands. Within A-bands, actin and myosin filaments interdigitate in close proximity. A central region, the M-band, contains only myosin.

The SR network, which runs throughout the cell, forms areas of close apposition with t-tubules and the sarcolemma which are estimated to come within 12 nm of the membrane (Langer and Peskoff, 1996). This junctional SR allows formation of signalling clusters, the dyads, where calcium entry through the sarcolemmal membrane is able to rapidly activate CICR through RyR channel opening. These areas are also awash with proteins that act to modulate the calcium signals.

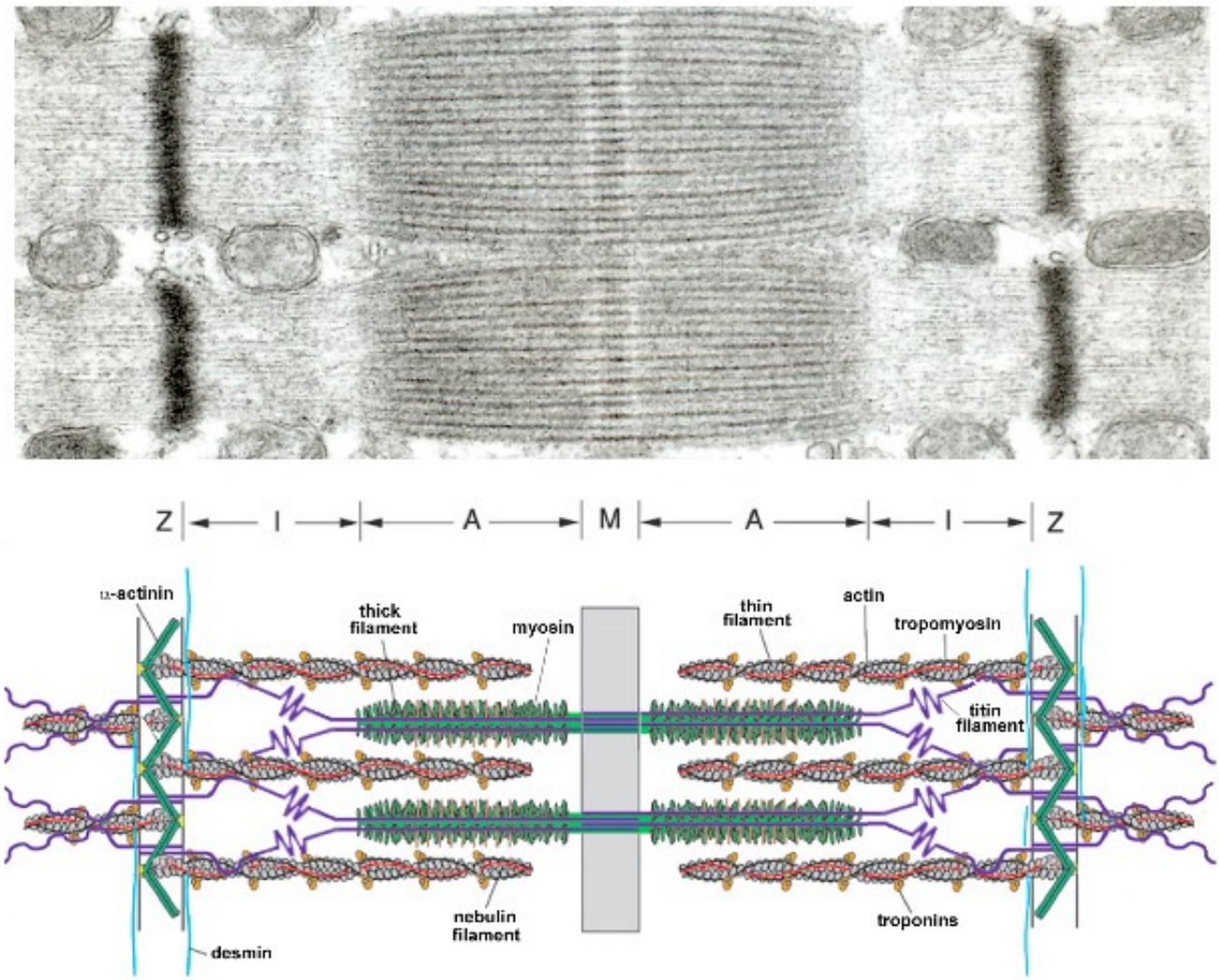


Figure 1.3: Structure of a sarcomere
An electron micrograph showing the thick and thin filaments of two sarcomeres arranged in parallel, and a schematic diagram to illustrate the positions and interactions of the various proteins in the contractile unity of a cardiac myocyte. Figure reproduced from Ottenheijm *et al*. (2008) with permission from Elsevier Limited.

A myosin molecule is frequently described as looking like a golf club with a double head. Each myosin filament is made up of ~400 myosin molecules arranged so that the shafts of the 'golf club' lie lengthways with the heads sticking out into the spaces between filaments.

Actin filaments are made up of long strands of actin monomers. Each thin filament in the cardiac sarcomere consists of two actin filaments arranged in a double-helix formation. Running in the grove of the double helix is the protein tropomyosin. A regulatory complex of Troponins is bound to tropomyosin and actin at regular intervals. Three troponin subunits combine to make each troponin complex; a calcium binding protein, an inhibitory protein and a tropomyosin-binding protein (C-, I-, and T- troponin respectively).

Each actin monomer contains a myosin binding site, however at rest these are physically hidden by tropomyosin. Upon release of calcium into the cytosol, calcium binding at C-troponin produces a conformational change in the troponin complex which reveals the myosin binding sites and allows contraction to take place.

During contraction the energy derived from cleavage of ATP at the myosin heads leads them to stretch backwards, from where they bind the nearest actin monomer and bend forward, dragging the actin filament further into the A-band. This repeated process of 'crossbridge cycling' shortens the I-band and the additive effect of shortening at each sarcomere leads to contraction of the myocyte.

In skeletal muscle, the calcium concentration reached in the cytosol of a muscle cell (~10 μM) is such that crossbridge cycling is maximal with every excitation. The

control of contractile force in a skeletal muscle is brought about by modulation of the number of muscle fibres recruited during any given contraction. In cardiac muscle every cell is recruited during each heartbeat, a property brought about by the extensive electrical continuity between cardiac myocytes. The maximal calcium concentration reached within a cardiac myocyte during each contraction, however, is far lower than in skeletal muscle (0.5-2 μM). Since contractile force is proportional to crossbridge formation and since crossbridge formation is proportional to sarcoplasmic calcium concentration, the modulation of the cellular calcium transient is the most important way in which cardiac myocytes regulate contraction.

1.5 ELECTROPHYSIOLOGY OF CARDIAC MUSCLE

Resting membrane potential

In an electrical circuit, charge is carried by the movement of electrons along a metal wire. In a biological system electrical charge is carried by ions in solution. A difference in the concentration of charged ions across a membrane creates a driving force for movement of ions through any conducting pathways. This driving force is termed potential difference, or voltage. By convention, the voltage of a cell is always given as a comparison to the extracellular environment, with this considered as 0 mV.

At rest, the major factor for determining the voltage of a cardiac myocyte is the movement of potassium ions down their concentration gradient and out of the cell through the inward rectifier I_{K1} (McAllister and Noble, 1966). The movement of positive charge out of the cell creates a negative potential difference across the cell

membrane. Because they are electrically charged the movement of ions across the cell membrane can also be driven by potential difference, so a positively-charged ion will be more inclined to flow from an area of positive charge to an area of negative charge. If the cellular membrane were freely permeable to potassium ions only, then resting membrane potential would be stable at ~-95 mV. At this point the chemical gradient driving potassium ions out of the cell would be equal to the electrical gradient driving ions into the cell and no net movement would take place. At rest, however, the membrane of a cardiac myocyte is permeable to both potassium and sodium ions, leading to a small but constant inward sodium current.

The difference in ionic concentrations across the cell membrane is maintained by the active pumping of sodium ions out of the sarcoplasm and potassium ions back in. This occurs through the Na/K-ATPase, which uses energy released from the breakdown of ATP to transport three sodium ions out of the cell for every two potassium ions pumped back in (Shinoda *et al.*, 2009). Due to the uneven ratio of charge carried into and out of the cell, there is also a slight hyperpolarising influence of the Na/K-ATPase.

The balance of these ion fluxes leads a cardiac myocyte to have a resting membrane potential of ~ -80 mV.

Basic Action Potential Generation

Electrical excitation in the cardiac cell leads to a sudden reversal of the cellular membrane potential from negative to positive. This action potential and its rapid

spread through the electrical conduction system and interconnected sheet of contractile myocytes is the manner in which cardiac muscle is able to achieve coordinated contraction.

A cardiac action potential has five basic phases. Phase 0 denotes rapid depolarisation, the flipping of membrane potential from its negative, resting state to a positive voltage. In contractile cells, it is driven by the rapid opening of voltage-gated sodium channels (I_{Na}). During phase 1, the cell undergoes partial repolarisation as sodium channels become inactive and there is a transient outward current driven by the rapid opening and closing of transiently-open potassium channels (I_{to}). There is then a plateau, phase 2, during which time inward and outward currents are balanced and the cell is held in its depolarised state. Phase 2 is determined by the balance of inward calcium currents and outward potassium currents. The inward flow of calcium during phase 2 of the action potential, carried through voltage-gated calcium channels, is what stimulates CICR, thereby allowing cardiac contraction. As calcium channels close and potassium conductance increases the membrane repolarises to its resting membrane potential, phase 3, where it is maintained until the next excitatory signal. This resting phase is referred to as phase 4.

Typical action potentials expected in ventricular, atrial and sino-atrial myocytes are presented in Figure 1.4.

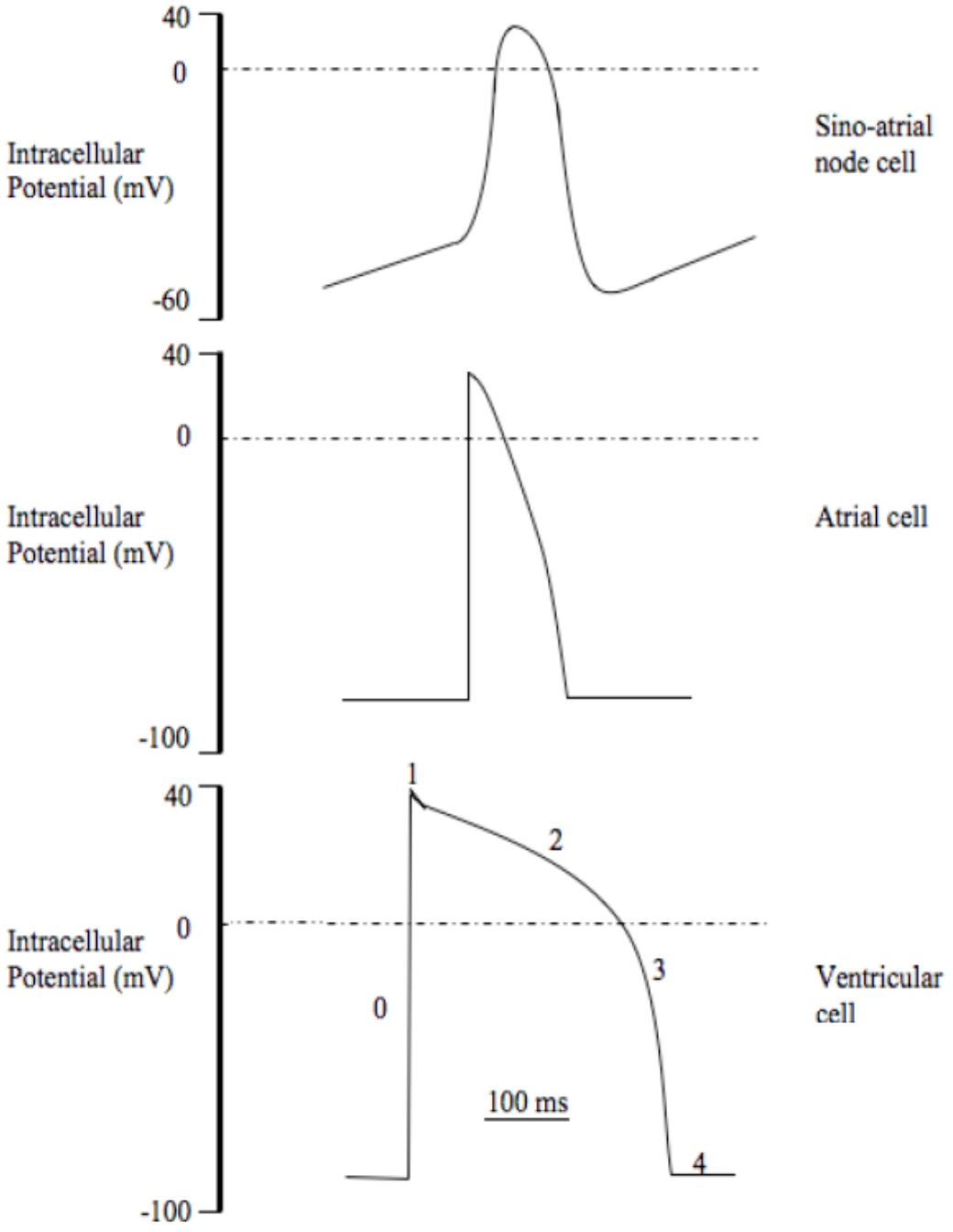


Figure 1.4: Schematic traces of typical action potentials in functionally-distinct areas of cardiac tissue

Differences between atrial and ventricular myocytes

Atrial and ventricular myocytes broadly share the same pattern of ion fluxes during action potential generation: upstroke governed by voltage-gated sodium channel opening which stimulates the opening of voltage-gated L-type Ca^{2+} channels, rapid partial repolarisation due to transient outward potassium currents, a plateau phase driven by the interaction between the inward current of calcium extrusion through the electrogenic sodium-calcium exchanger and the outward currents of voltage-gated potassium channels, and a repolarisation phase driven by the outward flux of potassium ions.

As can be seen in Figure 1.4, ventricular action potentials exhibit a prolonged plateau phase. In skeletal muscle, contraction of a given muscle fibre is maximal with every stimulation. The fibre is also available to be re-activated rapidly, a property which allows skeletal muscle to maintain the generation of force over prolonged periods of time. Prolongation of muscular contraction is not desirable in the heart, where generation of tetany would lead quickly to cessation of circulation. Fortuitously, the long plateau phase of cardiac ventricular action potential creates a prolonged refractory period, during which time cells are not able to be re-stimulated.

The clearest difference between atrial and ventricular action potentials is the much shorter nature of atrial electrical activity. Atrial myocytes exhibit shorter calcium transients and, consequently, a less pronounced plateau phase due to the more rapid predomination of potassium efflux during AP repolarisation. Atrial myocytes express an 'ultra-rapid' delayed rectifier (I_{Kur}), as well as I_{Kr} and I_{Ks} (Ravens and Wettwer,

2011). Current clamp recordings also reveal a slower upstroke velocity, which is linked to a lower expression of voltage-gated sodium channels.

The most striking feature of sino-atrial node myocytes is spontaneous diastolic depolarisation (SDD), a constant and spontaneous decay of cellular membrane potential during phase 4 of the action potential. It is this property which allows myocytes of the sino-atrial node to generate rhythmic action potentials without the need for extracellular nervous input. Even considering SDD, it can be seen that the maximum level of hyperpolarisation reached during a SAN action potential is somewhat more positive than the resting membrane potential of atrial and ventricular cells (~ -60mV). This is due to the fact that SAN myocytes do not express I_{K1} (Cho *et al.*, 2003).

SAN myocytes also exhibit a slow phase 0 depolarisation in comparison to contractile myocytes. True pacemaker cells do not express voltage-gated sodium channels, and rely instead upon the entry of calcium through L-type, and to a lesser extent T-type, voltage-gated calcium channels to mediate depolarisation (Doerr *et al.*, 1989). A more specific consideration of the mechanisms of sino-atrial node depolarisation is given in section 1.14.

1.6 CALCIUM TRANSIENTS: OVERVIEW

Sydney Ringer was the first physiologist to understand the importance of calcium in cardiac contractions, when he recognised that solutions of calcium salts combined with small amounts of sodium and potassium were able to sustain the contractile

actions of a frog heart for many hours, whereas combinations of sodium, potassium and bicarbonate without added calcium halted contractions within minutes (Ringer, 1883). A short-time later, during investigations of cardiac metabolic activity, Locke and Rosenheim found that calcium ions "may be more especially associated with the rendering of the energy of the metabolic process mechanically available" (Locke and Rosenheim, 1907). An overview of the process by which calcium mediates mechanical activity in cardiac myocytes is now given, with a more detailed discussion of the proteins and processes covered over the next sections.

Calcium ions are the direct chemical stimulus to initiate contraction in cardiac myocytes. Although the rapid depolarisation associated with an action potential looks to be an extreme event, the actual change in ionic concentrations inside the cell required to produce the observed changes in potential difference is actually relatively low, for instance a change in cellular sodium concentration of just 0.02%, and calcium ions entering the myocyte through L-type calcium channels are not sufficient to produce the vigorous contraction required for the maintenance of systemic bloodflow.

Instead, the calcium entering through L-type channels provides a 'trigger' for massive calcium efflux from the sarcoplasmic reticulum (SR). Calcium release from this major intracellular calcium store is capable of raising whole-cell calcium concentration from its resting level of ~0.1 μM by an order of magnitude or more (Bers, 2008). The process of calcium influx from the extracellular environment stimulating calcium efflux from the intracellular store is termed calcium-induced calcium release (CICR) (Fabiato and Fabiato, 1978).

The cellular calcium transient is the change in global calcium concentration mediated through CICR, including both calcium influx and RyR release. The magnitude of this transient is directly proportional to the amount of crossbridge cycling which occurs during cardiac contraction, and therefore contractile force.

Muscular contraction will continue to occur for all of the time during which C-troponin is bound to calcium and the myosin binding sites on the actin filaments are available. The return of cellular calcium concentration to its resting level, then, is an essential part of the cardiac cycle, allowing relaxation to occur. During this process, it is also essential for the SR store to be replenished such that it is available to respond to subsequent LTCC opening.

Most calcium leaves the cytosol by active transport into the SR via the sarco/endoplasmic reticular calcium ATPase (SERCA) (Bassani *et al.*, 1994). Calcium leaving the cell by crossing the sarcolemma flows down its concentration gradient, through the sodium-calcium exchanger (NCX) which drives one calcium ion out of the cell in return for the entry of three sodium ions. NCX activity is at its highest level during the plateau of the action potential and is responsible for almost all of the calcium extruded from the cell. A final, small, portion is pumped directly from the cytosol across the cellular membrane or into mitochondria.

1.7 CALCIUM TRANSIENTS: SARCOLEMMAL CALCIUM ENTRY

L-type Calcium Channels

Voltage-gated calcium channels in the sarcolemmal membrane are responsible for converting the swift membrane depolarisation of action potential upstroke into the calcium signal which initiates CICR. The early discovery of voltage-dependent calcium channels was made in the 1950s (Fatt and Katz, 1953), and since then a vast range of 'low' and 'high' voltage-activated, calcium-selective channels have been identified according to pharmacological and biological properties. The major cardiac voltage-gated calcium channel is L-type calcium channel (LTCC), from "L"ong-lasting, and can also be referred to as a dihydropyridine receptor (DHPR). These channels mediated the L-type calcium current (I_{CaL}). L-type calcium channels form heterotetrameric complexes with a total molecular mass of ~400kDa, consisting of four separate classes of subunit: α_1, β, α_2 and δ. LTCCs expressed in skeletal muscle also make use of a γ subunit but this is not commonly expressed in cardiac cells (Bodi *et al.*, 2005).

Each LTCC expresses four identical α1 subunits which form the voltage sensor, ion-selective pore and gating machinery. Multiple different α1 subunit genes have been identified, of which the $Ca_v1.2$ (α_{1c}) form is the only LTCC expressed at high levels in the heart. An individual α1 subunit has 6 transmembrane domains, with the pore-forming loop situated between S5 and S6. Pore-loops contain a conserved glutamate residue which is thought to confer ion-selectivity to the channel (Tikhonov and Zhorov, 2011). The voltage-sensor of the LTCC is thought to reside in the S4 TM

domain (Yamaguchi *et al.*, 1999), which is consistent with the mechanism of voltage-gated activation in potassium and sodium channel families.

The β subunit of LTCC is located fully within the cytoplasm, α2 fully outside the cell and δ associated with the α1 subunit though close proximity of its single transmembrane domain and strong binding to the α2 subunit. The most important roles of both the β and δ/α2 proteins are in trafficking and targeting LTCCS to the sarcolemma, though their presence also modulates channel current and gating.

I_{CaL} Modulation

Given that the magnitude of whole-cell I_{CaL} is directly correlated with RyR-mediated calcium release from the SR (Bassani *et al.*, 1995), increases in I_{CaL} at the sarcolemmal membrane are an important manner in which cardiac myocytes are able to modulate the cellular calcium transient. PKA is able to phosphorylate α_1 subunits at the Ser1928 position (De Jongh *et al.*, 1996). Three sites of PKA-mediated phosphorylation are also noted on the β subunit: Ser-459, Ser-478 and Ser-479 (Gerhardstein *et al.*, 1999). PKA-dependent phosphorylation acts to increase channel open probability and the duration of channel opening, without affecting single-channel conductance (Brum *et al.*, 1984).

PKA is bound in close proximity to the LTCC by A-kinase anchoring proteins (AKAP). Using expression of a mutant AKAP, unable to bind PKA, in HEK-cell expression studies, it was demonstrated that targeting of PKA to the proximity of the LTCC is essential for PKA-mediated phosphorylation of the Ser1928 site (Gao *et al*.,

1997). AKAP tethering has recently also been investigated at the SR membrane, where one AKAP protein, AKAP18-δ has been found to tether PKA to phospholamban, and contribute significantly to the ability of iso stimulation to phosphorylate the PKA-specific site (Lygren *et al.*, 2007).

Cessation of I_{CaL} occurs in part through voltage- and in part through calcium-dependent feedback (VDI and CDI). Under physiological conditions, however, voltage-dependent inactivation is too slow to account for much of the channel gating (Hadley and Hume, 1987) and CDI is the dominant mechanism. CDI acts such that the raising of cleft calcium by CICR acts to cut off the trigger for further CICR. This calcium-dependent inactivation can yield a reduction in I_{CaL} very quickly after initiation of SR release (Puglisi *et al.*, 1999), and is mediated by direct binding of CaM to an IQ sequence on the carboxyl terminus of the channel protein (Zuhlke *et al.*, 1999).

Sodium-Calcium Exchange

The sodium-calcium exchange protein provides a path for passive exchange of ions, i.e. not requiring ATP. NCX is mainly associated with clearance of calcium from the cytosol during recovery from a calcium transient (see section 1.8). As a passive exchanger, it is possible for NCX to function both in calcium extrusion and in calcium entry, with the direction of current flow dependent on intracellular sodium and calcium concentrations and membrane potential. Sodium influx through I_{Na}, coupled with rapid depolarisation to a positive membrane potential should favour

calcium entry through NCX, however the subsarcolemmal calcium concentration generated by CICR is likely to negate these factors in practice. It has been estimated using a wet-lab-based model that inward NCX current, and therefore calcium extrusion, begins quickly after cellular depolarisation, making the scope for calcium entry small (Weber *et al.*, 2002). Other groups have suggested that this early calcium entry is important in the efficiency of CICR and may summate with trigger calcium to hasten RyR opening (Larbig *et al.*, 2010).

1.8 Calcium transients: SR Calcium Release

Ryanodine receptors

The gateway of calcium efflux from the SR, activated by 'trigger' calcium entering through LTCCs, is the ryanodine receptor (RyR). RyRs are so-named for the compound ryanodine, an alkaloid purified from the South American plant *Ryania speciosa*, which was found to cause paralysis without affecting electrical signalling in the nerves or muscle (Edwards *et al.*, 1948). This was later shown to be due to its locking of the channel into a subconductance state (Fleischer *et al.*, 1985).

Each individual RyR channel consists of a massive, ~2.2kDa, protein made up of four identical building blocks (monomers) which each contain ~5000 amino acid residues (Otsu *et al.*, 1990). Crystal structures show RyR homotetramers to resemble a mushroom with the umbrella, ~80% of the protein, projecting into the cytoplasm and the stalk crossing the SR/ER membrane (Sharma *et al.*, 1998, Ludtke *et al.*, 2005).

Three isoforms of RyR exist in mammalian cells: RyR1 is widely expressed in skeletal muscle, RyR2 forms the calcium release channel in the heart and RyR3 was originally identified in the brain. RyR2, which was first cloned in 1990, shares ~70% sequence homology with RyRs 1 and 3 (Otsu *et al.*, 1990).

A major difference between CICR exhibited in cardiac and skeletal muscle occurs due to the differing expression of ryanodine receptor isoforms. The RyR1 expressed in skeletal muscle is physically attached to calcium channels at the cellular membrane such that RyR opening is mechanically stimulated by opening of the surface calcium channels, regardless of whether Ca^{2+} flows into the cell (Armstrong *et al.*, 1972). Instead of mechanically-mediated opening, cardiac RyR2 channels require a rise in calcium concentration within the dyadic cleft.

This calcium-dependent gating is such that calcium release triggered from the SR is directly proportional to the magnitude of I_{CaL} (Bassani *et al.*, 1995). RyR response to cytosolic calcium exhibits a bell-shaped response curve. Studies of SR vesicles isolated from rabbit cardiomyocytes observed a steep rate-dependence centred around 1 μM, peak calcium release rate at 10 μM and near-complete inhibition at 1 mM (Meissner *et al.*, 1986). Although channel open probability is always proportional to intracellular calcium, phosphorylation of proteins within the RyR complex modulates true channel responsiveness to a given stimulus. The open probability of RyRs in cardiac myocytes is also directly modulated by intra-SR lumenal free calcium. Bilayer studies indicate that elevations in calcium on the lumenal side of the channel cause a simultaneous increase in channel open probability and mean open time (Lukyanenko *et al.*, 1996). This response was maintained, albeit at a lower

sensitivity, in the presence of high cytoplasmic calcium concentrations that may be expected during the peak of the calcium transient. In an intact cellular environment an increase in SR calcium loading, achieved by pacing protocol, is correlated with an increase in fractional SR release at a constant level of I_{CaL} trigger (Bassani *et al.*, 1995).

CICR, being ultimately a positive feedback mechanism, could rapidly deplete the SR of calcium if some form of shut-off mechanism did not exist. It has already been discussed that RyRs are gated by subsarcolemmal calcium with a dependence which forms a bell-shaped curve and the rapid rise in cytosolic calcium could reduce channel open probability. Lumenal depletion of SR calcium would act to reduce RyR open-probability (Lukyanenko *et al.*, 1996), and this may contribute to the cessation of the calcium efflux. It is also possible that the coupled gating of RyRs might accelerate the effects of channel closures, by whatever means, across the couplon. Finally, RyR channels have been reported to exhibit inactivation states similar to those of voltage-gated sodium channels, such that rapid channel closure occurs even in the continued presence of calcium and the kinetics of this are related to intracellular Mg^{2+} concentration (Valdivia *et al.*, 1995).

Couplons as a subunit of calcium signalling

Ryanodine receptors are arranged on the SR membrane in groups of ~100 in junctional SR, closely apposed to concentrations of 10-25 LTCCs on the surface membrane, forming a dyad or couplon (Franzini-Armstrong *et al.*, 1999). RyRs

expressed on the SR membrane exhibit coupled-gating, in which the opening of one RyR increases the probability of nearby receptor activation (Marx *et al.*, 1998).

The opening of a small group of RyRs can be detected in quiescent myocytes as a calcium 'spark' using fluorescent indicators and confocal microscopy (Cheng *et al.*, 1993). The fact that sparks can be imaged in quiescent cells itself illustrates the probabilistic nature of channel opening, even under 'resting' conditions. The frequency of spontaneous calcium sparks is now a common method for measuring changes in RyR open probability under different experimental conditions. Even smaller than a 'spark', the smallest unit of RyR opening thus far imaged is a calcium 'quark', which has been proposed to represent the opening of a single RyR channel (Lipp and Niggli, 1996).

The RyR Protein Complex

The massive size of the RyR protein creates a large surface area and a supply of solvent-filled cavities which allow it to act as a scaffold for a vast array of regulatory proteins. In practice the RyR complex, consisting of the receptor and all its associated regulatory units, is so vast that individual channels are visible under electron microscopy.

The RyR complex has been reported to contain a number of proteins, the functions of which will be substantiated over the coming paragraphs, including: Calstabin, PKA, calmodulin, CaMKII, protein phosphatases, phosphodiesterase, sorcin, calsequestrin, junctin and triadin.

RyR Modulation: FKBPs

FKBP proteins are a large family of immunophilins and are individually identified by their molecular mass. Cardiac myocytes express both FKBP 12 and 12.6. Early work postulated a clear-cut difference between cardiac and skeletal muscle, observing that skeletal RyR1 is bound to FKBP12 and cardiac RyR2 is bound to FKBP12.6 in canine-derived SR vesicles (Timerman *et al.*, 1996). More recent work using co-immunoprecipitation suggests that relative ratio of binding to cardiac RyR2 to be species-dependent, with detectable RyR2-FKBP12 binding in mouse, pig and to a lesser extent rabbit, but no detectable binding in the rat (Zissimopoulos *et al.*, 2012).

FK506 and rampamycin, immunosuppressant agents, cause dissociation of FKBPs from the RyR and have been used to investigate their function *in vitro*. FK-506 has been seen to increase resting calcium spark frequency but reduce peak current (Kaftan *et al.*, 1996), prolong channel opening and encourage subconductance states (Xiao *et al.*, 1997).

It is currently thought that FKBP12.6 acts to stabilise RyR channels in their closed state, and may also contribute to coupled gating mechanisms, encouraging openings that are stimulated to be complete and eliminating subconductance states.

One recent bilayer study compared the different RyR gating characteristics of FKBP12 and 12.6 in membrane vesicles derived from sheep hearts. In their hands, FKBP12 was a potent channel activator, mediating a >5-fold increase in channel open probability across a range of concentrations as low as 1pM with characteristics consistent with sensitisation of the channel to cytosolic calcium. FKBP12.6 had no

direct effect upon receptor open probability or the appearance of subconductance states but was able to reduce the effect of FKBP12 by nearly two-thirds (Galfre *et al.*, 2012). The two binding proteins have extremely close sequence homology and may compete for the same binding site on RyR channels. This result suggests the possibility of a dynamic equilibrium between channel activation though FKBP12 and antagonism of its actions through 12.6 in the intact cardiomyocyte.

FKBP12, which is also detectable in the cardiac cytosol, has also been proposed to modulate sarcolemmal voltage-gated sodium channels at its major effect (Maruyama *et al.*, 2011).

RyR Modulation: PKA

Protein kinase A (PKA) is a ubiquitous cellular kinase which is capable of phosphorylating a range of intracellular targets and is modulated by the local concentration of cAMP. PKA is tethered directly to the RyR complex via muscle A kinase anchoring protein (mAKAP) (Marx *et al.*, 2000), allowing it to be held in close proximity to the RyR channel and other proteins of the complex. cAMP binding to the regulatory subunits of PKA relieves inhibition on the catalytic subunits and allows PKA to phosphorylate nearby targets.

PKA specifically phosphorylates RyR Ser-2809, acting to increase Ca^{2+}-sensitivity of the channel (Marx *et al.*, 2000) and this effect is independent of possible FKBP12.6 dissociation (Wehrens *et al.*, 2003).

The physiological role of PKA-mediated phosphorylation at the Ser-2809 site is not clear as mice expressing a mutant RyR with a point mutation that renders Ser-2809 non-phosphorylatable maintain normal responses to isoprenaline *in vivo* and *in vitro* (MacDonnell *et al.*, 2008). Further, studies investigating β-AR stimulation under conditions of a controlled I_{CaL} 'trigger' and SR load have reported that iso enhances the kinetics and amplitude of SR calcium release (Ogrodnik and Niggli, 2010) or enhances kinetics without changing CICR gain (Ginsburg and Bers, 2004).

RyR Modulation: Phosphatases and phosphodiesterase

mAKAP is also able to bind a specific phosphodiesterase (PDE4DE) within the RyR2 macromolecular complex (Lehnart *et al.*, 2005). The localised tethering of a phosphodiesterase, the enzyme which acts to break down cAMP and therefore reduce PKA activity, provides a negative feedback mechanism for modulation of PKA effects at the RyR channel. Indeed, genetic inactivation of PDE4DE leads to hyperphosphorylation of the RyR2 channel without affecting global cAMP signalling measures and results in the development of cardiomyopathy (Lehnart *et al.*, 2005).

The phosphatases PP1 and PP2A are also thought to play an active role in dephosphorylation of proteins in the cardiac RyR complex (Marx *et al.*, 2001).

RyR Modulation: Calmodulin

Calmodulin is a 148 amino acid calcium binding protein with 4 Ca^{2+} binding EF hand motifs. Calcium-binding to CaM is cooperative, such that binding sites are largely unoccupied at diastolic $[Ca^{2+}]_i$ but increase as intracellular calcium concentration is raised.

CaM-binding decreases RyR opening for a given intracellular [Ca] and creates a shift in the calcium concentration required for a given RyR activation (Balshaw *et al.*, 2001) and this process could assist in RyR2 channel closure (Xu and Meissner, 2004). Indeed, mice expressing a RyR2 isoform lacking the CaM binding site exhibit prolonged calcium transients and develop hypertrophy within 10 days of birth (Yamaguchi *et al.*, 2007).

RyR Modulation: CaMKII

CaMKII is a serine-threonine protein kinase activated through binding of calcium-bound calmodulin and subsequent autophosphorylation. CaMKII is physically associated with RyRs and phosphorylates the channels at the CaMKII-specific Ser2815 site (Wehrens *et al.*, 2004). CaMKII-mediated RyR phosphorylation at the Ser-2815 binding site has been reported to increase calcium spark frequency in resting myocytes, leading to a decreased SR calcium content, whilst KN-93, a specific inhibitor of CaMKII, reduced calcium transient amplitude if I_{CaL} and SR load are maintained (Li *et al.*, 1997). CaMKII-mediated phosphorylation is discussed further in section 1.10.

RyR Modulation: Sorcin

Sorcin is a fairly novel, 22kDa, calcium-binding protein whose function in SR calcium handling is only just beginning to become apparent. Co-immunoprecipitation studies found sorcin to be associated with cardiac RyRs (Meyers et al., 1995), and bilayer investigations suggest that sorcin binding is associated with inhibition of RyR opening (Lokuta *et al.*, 1997). In cellular studies, adenoviral over-expression of sorcin led to a significant reduction in cellular shortening, calcium transient amplitude and caffeine-stimulated transient amplitude with an increase in the rate of calcium extrusion by NCX (Seidler *et al.*, 2003), whilst constitutive, cardiac-specific expression of a mis-sense protein in mice led to a significant increase in cell shortening, calcium transient amplitude and calcium spark frequency (Collis *et al.*, 2007).

The physiological role of sorcin is not currently understood, though its binding to SR membranes appears to be modulated by calcium with an EC_{50} of ~200 μM such that increased intracellular calcium leads to an increase in sorcin activity in the region of the RyR (Farrell *et al.*, 2003). This may suggest a role in calcium-dependent inhibition or inactivation of the channels and possibly, given measurements of NCX activity, a mechanism to reduce SR load under conditions of high SR calcium release.

RyR Modulation: Calsequestrin, junctin and triadin

Within the SR, free Ca^{2+} is highly buffered and the major intra-SR buffering protein is calsequestrin, a low affinity calcium buffering protein (apparent Km ~500 μM). A

calsequestrin protein is highly acidic, due to concentrated presence of Glu and Asp residues, and each molecule is capable of binding ~20 Ca^{2+} ions. Junctin and triadin physically couple calsequestrin to the SR-lumenal side of the RyR (Zhang *et al.*, 1997). The observation of a calcium-dependent effect of calsequestrin on RyR open probability suggests it may have a physiological signalling role, contributing to the effect of luminal calcium on RyR function (Gyorke *et al.*, 2004).

Over-expression of calsequestrin leads to a significant increase in SR calcium load as measured by caffeine application. However this has been associated with either a reduction in calcium transient amplitude and calcium spark frequency (Jones *et al.*, 1998) or an increase (Terentyev *et al.*, 2003). The level of over-expression in the Jones study was much more pronounced, and was a result of transgenic over-expression *in vivo* as opposed to adenoviral transfer in cultured myocytes. Both interventions led to hypertrophic changes.

1.9 Calcium transients: Clearing Ca^{2+} from the Cytosol

Free cytosolic calcium concentration is the central factor in cellular contraction in the cardiac myocyte. During diastole in a ventricular myocyte the concentration of cytosolic calcium is very low (~ 0.1 μM), whilst cytosolic calcium can rise 10-fold or more during CICR (Bers, 2002). Removing this calcium from the cytosol in a timely fashion is an essential part of the cardiac cycle. Further, SR calcium must be replenished in order to maintain the gain achieved by CICR.

SERCA

The highest proportion of cytosolic calcium removal is carried out by the sarco/endoplasmic reticulum calcium ATPase (SERCA), which is responsible for clearing ~70% in rabbit and ~98% in rat ventricular cells (Bassani *et al.*, 1994). These percentages are very similar to the estimated contribution of SR calcium release to the cellular calcium transient. The SERCA ATPases are a member of the P-type ATPase family, which also includes the plasma membrane calcium ATPase (PMCA), Na/K ATPase and H/K ATPase.

Three copies of the SERCA gene are found within the mammalian genome, however alternative splicing is capable of generating at least 10 specific isoforms in practice. Cardiac myocytes specifically express the SERCA2a isoform, as well as a small amount of SERCA2b which is found in all cells.

The sequence homology of SERCA isoforms is highly conserved. The tissue-specific nature of subtly different isoforms, however, is an indicator that they fulfil specific functions through the differences they do exhibit. SERCA2a and SERCA2b are structurally similar over the first 993 amino acids, with SERCA2b exhibiting a 49 amino acid extension at the C-terminus. COS-cell expression studies show that SERCA2b has a significantly higher affinity for calcium, and a significantly lower rate of pump turnover (Verboomen *et al.*, 1992, Verboomen *et al.*, 1994). Deletion of the SERCA2 gene, which halts production of isoforms 2a, 2b and 2c, is lethal in most species. SERCA2-/- mice die early in development, with no compensatory increase the expression of SERCAs 1 or 3. Heterozygous animals live to term without

exhibiting overt cardiac pathology under normal physiology, but develop heart failure much more easily under conditions of stress (Periasamy *et al.*, 1999, Ji *et al.*, 2000).

Ver Heyen and colleagues were able to successfully disrupt the splicing mechanism in a mouse model such that a specific SERCA2a-/- was possible. SERCA2a-/- mice were viable, but with an embryonic and neonatal mortality approaching 20% more than controls. Animals surviving to adulthood exhibited impaired relaxation and contraction kinetics *in vivo*, together with concentric hypertrophy (Ver Heyen *et al.*, 2001). Taken together, these data suggest that whilst some compensation between SERCA2a and 2b is possible, the physiologically-expressed SERCA2a is essential for normal cardiac development and mature function.

SERCA regulation

In vivo SERCA2a is closely associated with two further proteins, phospholamban (PLB) and sarcolipin (SLP) which both act to modulate the rate of calcium transport by the ATPase, interfering with the sarcoplasmic binding sites for calcium and are themselves regulated by phosphorylation.

SERCA regulation: Phospholamban

Phospholamban (PLB) is a 52 amino-acid protein which was shown directly to be the target of phosphorylation in the SR region by 32P labelling during stimulation with catechloamines and forskolin (Kranias and Solaro, 1982). PLB is present in the

cardiac SR in a more-active monomeric form and a less-active pentameric form, consisting of five identical monomers. In its native form, PLB binds to SERCA and acts to decrease its affinity for calcium binding at the cytosolic face. Phosphorylation of phospholamban leads to a conformational change in the molecule which relieves its inhibition on SERCA (Kranias and Hajjar, 2012).

PLB has multiple phosphorylation sites which are specific for different substrates and independent, a PKA site at Ser-16, a CaMKII site at Thr-17 and a PKC site at Ser10. Transgenic mice with a PLB that cannot be phosphorylated at Thr-17 show normal responses to iso, whilst those with a non-phosphorylatable Ser-16 have impaired responses (Chu *et al.*, 2000).

PLB over-expression results in a reduction in SR calcium content and magnitude of contraction with concurrent slowing of the time for recovery from the transient, which were fully recovered on stimulation by isoprenaline (Kadambi *et al.*, 1996). Conversely, knock-out animals exhibit enhanced contractility, and this appears to be correlated with the level of PLB expression (Luo *et al.*, 1994, Luo *et al.*, 1996).

Clinically, mutations in PLB have been discovered which lead to either total abolition of PLB binding at SERCA, Leu 39 Stop (Haghighi *et al.*, 2003), or prevention of phosphorylation and therefore constitutive and non-releasable SERCA inhibition, R9C (Schmitt *et al.*, 2003). Both of these mutations result in dilated cardiomyopathy and premature death in human patients, illustrating the importance of SR calcium handling for cardiac health.

SERCA regulation: Sarcolipin

Sarcolipin is a small, 31 amino acid, protein which was initially found to co-purify with SERCA1a in skeletal muscle. Cardiac SLP expression is far more pronounced in the atria than the ventricle (Babu *et al.*, 2007). Inhibitory effects of SLP on contractile function are reversible by isoproterenol, suggesting that it is capable of mediating a portion of the β-adrenergic response, especially in atrial tissue (Periasamy *et al.*, 2008).

SLN-mediated inhibition of SERCA calcium transport can occur independently from that of PLB, as over-expression data and subsequent rescue by β-AR stimulation has also been observed in PLB-/- myocytes (Gramolini *et al.*, 2006).

In support of a more dominant role in the atria, sarcolipin ablation seems to lead specifically to atrial remodelling (Xie *et al.*, 2012), perhaps indicating that PLB is able to carry out the full physiological role in the ventricle but not atrial tissue.

Calcium extrusion across the sarcolemma

The mature form of NCX in cardiac myocytes (NCX 1.1) is a 938 amino acid protein with 9 transmembrane domains which exchanges sodium for calcium in a ratio of 3:1. NCX is vital for life, illustrated by the embryonic death of NCX1.1-deficient mice due to a lack of cardiovascular system development (Wakimoto *et al.*, 2000). NCX is the major pathway for calcium efflux across the sarcolemma in cardiac myocytes. In ventricular myocytes, NCX is located mainly in the t-tubules.

A secondary mechanism for calcium extrusion by active transport also exists in the sarcolemma, the plasma membrane Ca^{2+} ATPase (PMCA). PMCA activity can be activated by Ca-CaM and PKA phosphorylation but makes a relatively small contribution to the clearance of calcium released during calcium transients and acts mainly within t-tubules (Chase and Orchard, 2011).

Species differences exist between the expression and activity levels of the various calcium-clearing mechanisms (Hove-Madsen and Bers, 1993). In the rabbit, which is functionally similar to both human and guinea pig, around 70% of cytosolic calcium is cleared through SERCA uptake and 28% cleared by NCX, leaving very little to be scavenged by the sarcolemmal uniporter and mitochondrial uptake mechanisms (Bassani *et al.*, 1994).

1.10 CaMKII

Introduction to CaMKII

Calcium-calmodulin kinases (CaMK) are a family of serine-threonine protein kinases activated by the calcium-bound form of calmodulin (Ca-CaM). In cardiac myocytes $CaMKII_{\delta}$ is the major isoform found in the sarcoplasm (Jett *et al.*, 1987). CaMKIV is expressed in the nucleus where its activity controls gene transcription, likely via relief of inhibition on the transcription factor MEF2 (Bers, 2011).

CaMKII is a multimeric enzyme made up of 6-12 repeating units arranged in a wheel-like fashion. Each unit consists of a catalytic domain, a regulatory domain and a

carboxyl-terminal association domain responsible for multimerisation. Ca-CaM binds in the regulatory domain, relieving the enzyme of auto-inhibition and exposing the catalytic domain to nearby targets. The enzyme is also capable of autophosphorylation at the Thr-287 site, such that it remains activated during subsequent falls in calcium, and therefore Ca-CaM (Anderson, 2005). Inactivation is mediated by dephosphorylation of the enzyme through the protein phosphatases PP1 or PP2A.

Due to its propensity for autophosphorylation, which is relieved gradually, CaMKII does not undergo rigid cyclical changes in activation and is ideally placed in the cell cytosol to respond to calcium changes over a more prolonged period of time, I_{CaL} facilitation being one example.

A physiological role in the heart?

CaMKII-specific phosphorylation sites in the cardiac myocyte have been found on a number of proteins central to cardiac calcium handling e.g. LTCCs, RyRs, SERCA, and PLB, however the functional role of CaMKII-mediated phosphorylation during acute myocardial responses remains a matter under debate. CaMKII was first reported to be activated during β-AR stimulation in the late 1990s, when it was found that the pool of SR-bound CaMK available to be autophosphorylated by incubation with Ca-CaM was greatly reduced after stimulation with isoprenaline for 2 min (Baltas *et al.*, 1997). That is to say a portion of the SR-bound CaMK had been autophosphorylated

during ISO exposure, and this data was supported by a concomitant increase in phosphorylation at the Thr17 site of PLB.

Since then, studies have been performed to investigate the downstream effectors of CaMKII-mediated phosphorylation and their varying roles under basal, β-stimulated and pathophysiological conditions with mixed results. CaMKII-mediated I_{CaL} facilitation, as described above, is well-supported however conflicting data abound surrounding the acute effects of CaMKII phosphorylation on calcium-handling proteins at the SR.

CaMKII is capable of phosphorylating phospholamban at a CaMKII-specific site, Thr-17. Thr-17 phosphorylation leads to relief of PLB-mediated SERCA inhibition through the same mechanism as PKA-mediated phosphorylation at Ser-16 and allows increased SERCA activity.

CaMKII is tethered within the ryanodine receptor complex (Currie *et al.*, 2004) and CaMKII-mediated RyR phosphorylation at the Ser2815 site has been reported to increase RyR open-probability in bilayer studies (Wehrens *et al.*, 2004). Accordingly, the Bers group were able to show that CaMKII-mediated phosphorylation of RyRs increases the gain of CICR for a given level of trigger calcium and SR content.

Over-expression of $CaMKII_{\delta C}$ by adenoviral transfer can be observed to increase the frequency of spontaneous calcium spark firing and decrease SR load (Kohlhaas *et al.*, 2006). Further, in phospholamban KO mice, application of exogenous activated CaMKII was able to increase the frequency and duration of spontaneous calcium sparks in ventricular myocytes without confounding, concomitant effects on SR load

(Guo et al., 2004). Data from transgenic animals, however, has been inconclusive with over-expression leading to either an increase (Maier et al., 2003) or decrease (Wu et al., 2001) in SR calcium release and expression of constitutive CaMKII inhibitors yielding similarly contradictory results.

Although β-AR stimulation has been linked to CaMKII-activation, whether this has a physiological role at downstream effectors which is appropriate for acute responses is a grey area. CaMKII-mediated phosphorylation of PLB Thr-17 during β-AR stimulation in isolated, perfused rat hearts has been recognised but is abolished if PKA is inhibited (Said *et al.*, 2002), though this may reflect a necessity for PKA-mediated relief of phosphatase activity in order for CaMKII autophosphorylation to remain (El-Armouche *et al.*, 2008).

Recent data has suggested that β-AR stimulation may activate a cAMP-activated guanine nucleotide exchange protein, Epac, through direct cAMP-mediated stimulation and that this protein is capable of driving autophosphorylation in RyR-bound CaMKII. Application of a specific cAMP analogue which specifically activates Epac, led to a significant increase in calcium spark frequency and decrease in spark amplitude measured in isolated rat cardiomyocytes. These changes were associated with a significant increase in level of autophosphorylated CaMKII and were blocked in the presence of KN93 (Pereira *et al.*, 2007).

CaMKII and heart failure

Although opinion about the role of CaMK during acute β-AR stimulation is mixed, chronic exposure to sympathetic stimulation is consistently associated with an increase in CaMK-mediated signalling. Wang and colleagues reported that the contractile and calcium transient response of cultured rat cardiomyocytes to β-AR stimulation remained was no different after 10 min or 24 h of exposure but that early activation could be inhibited by antagonists of PKA whilst the prolonged response was only reversed by CaMKII inhibition (Wang *et al.*, 2004). CaMKII expression and CaMKII-mediated phosphorylation of target proteins are increased in animal models of heart failure, and in cells isolated from human heart failure patients (Hoch *et al.*, 1999), whilst constitutive over-expression of $CaMKII_{\delta C}$ results in the onset of heart failure within 3 months of birth (Maier et al., 2003).

Cardiac-specific constitutive expression of a CaMKII inhibitor, or prolonged pharmacological inhibition of CaMKII using KN93, is significantly protective against ventricular dilatation and loss of cellular contractile function after myocardial infarction (Zhang *et al.*, 2005).

Overall, the evidence would seem to suggest that CaMKII is capable of mediating changes in intracellular calcium handling at either RyRs or SERCA. A physiological basis for contribution of CaMKII to acute β-adrenoceptor responses has yet to be confirmed, although its role in pathophysiology appears to be well substantiated.

1.11 NAADP

Discovery and structure

Nicotinic acid adenine dinucleotide phosphate (NAADP), discovered in 1995 (Chini *et al.*, 1995), is a pyridine nucleotide and the most potent calcium releasing second messenger currently known with an EC_{50} of 16 nM in sea urchin egg homogenates. NAADP-mediated calcium release was initially mistaken for an effect of nicotinamide adenine dinucleotide phosphate (NADP), when it was found that commercially-produced NADP could elicit an immediate calcium release from sea urchin egg homogenates (Clapper *et al.*, 1987). However, it was later recognised that this response was in fact due to the presence of NAADP as a contaminant of the commercial NADP source (Chini *et al.*, 1995). The structure of NAADP is presented in Figure 1.5.

NAADP-mediated calcium signalling is highly specific. Though it differs structurally from NADP only by the conversion of an amide group to a carboxyl group (position marked ** in Figure 1.5), NADP is unable to elicit calcium release in systems which are highly responsive to NAADP (Clapper *et al.*, 1987). Calcium release stimulated by NAADP is distinct from the calcium release stimulated by either inositol trisphosphate (IP_3) or cyclic ADP ribose (cADPR). Desensitisation at the NAADP receptor using high concentrations of NAADP does not inhibit IP_3 or cADPR responses. Further, specific inhibition at the IP_3 or cADPR receptors using heparin and ruthenium red respectively has no effect on the response of sea urchin egg homogenates to NAADP (Chini and Dousa, 1995, Chini *et al.*, 1995).

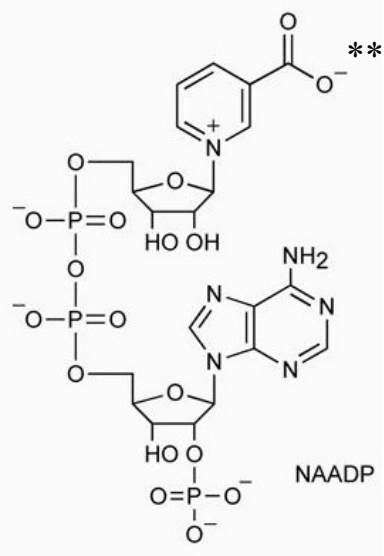


Figure 1.5: Structure of Nicotinic Acid Adenine Dinucleotide Phosphate
Chemical structure of NAADP. ** indicates moiety at which the compound differs from NADP

NAADP synthesis

The simplest method for synthesis of NAADP is a base-exchange reaction substituting the nicotinamide group of $NADP^+$ for nicotinic acid. Brain, liver, myocardium and spleen, with measured activity decreasing in that order, were shown early on to be capable of synthesising NAADP when incubated with β-NADP and nicotinic acid (Chini and Dousa, 1995). CD38, an ADP ribosyl cyclase enzyme (ARC), is capable of carrying out this base-exchange reaction (Aarhus *et al.*, 1995). CD38 has also been shown to be capable of synthesising cyclic ADP ribose (cADPR, discussed in the following section), however acidic conditions appear to favour the generation of NAADP, whereas conversion to a close relative of cADPR, cADPR-phosphate is favoured at a neutral pH (Aarhus et al., 1995). A further member of the ARC family, the bone marrow antigen CD157, has also been put forward as a candidate for NAADP synthesis (Itoh *et al.*, 1994).

Characteristics of NAADP-mediated calcium signals

NAADP-dependent calcium signalling is thought to occur through a 'two-pool system' (Churchill and Galione, 2001a) whereby NAADP first stimulates calcium release from acidic calcium stores and this released calcium then amplifies or stimulates calcium release from the more traditionally accepted reticular stores. In sea urchin oocytes, a robust calcium-releasing model, exposure to NAADP elicits a biphasic response consisting of an initial calcium spike followed by the initiation of calcium waves. Churchill and Galione (Churchill and Galione, 2001a) observed that

inhibition of IP_3 and cADPR was able to stop NAADP from causing oscillations, but not the initial calcium spike. Accordingly thapsigargin, a SERCA inhibitor which abrogates ER-store-filling, was able to abolish the NAADP-mediated oscillations without affecting the initial calcium spike, and also fully inhibited cellular responses to IP_3 and cADPR. This suggested that a calcium store separate to the ER was responsible for the initial calcium spike. Further investigation of the identity of this store was carried out by centrifugation of intact sea urchin oocytes and further separation on Percoll gradients (Churchill *et al.*, 2002). A single fraction was elucidated which was sensitive to NAADP but not IP_3 or cADPR and this was found to be enriched with lysosomal markers.

NAADP receptors

The identity of the NAADP receptor and the effector of its responses has garnered much controversy in the field in recent history, and their true identities still remain elusive.

Ryanodine receptors were considered as a possible receptor for NAADP. This claim is not substantiated by recordings made in planar lipid bilayers and isolated SR microsomes, which both failed to respond to direct stimulation by NAADP (Copello *et al.*, 2001, Pitt *et al.*, 2010). One study did find activation of cardiac RyR2 receptors through direct stimulation with NAADP (Mojzisova *et al.*, 2001), however the concentration required for RyR activation in these experiments is far higher than that required for NAADP-mediated calcium signalling in native cell systems.

Transient receptor potential (TRP) channels, especially TRP-ML1, initially showed promise as the receptor/effector protein for NAADP-mediated calcium release. Reconstruction of lysosomal membrane proteins into lipid bilayers yielded a receptor with all the requisite qualities, namely response to NAADP over a wide range of concentrations with self-inactivating behaviour at concentrations above 10 μM, and these responses were abolished by an anti-TRP-ML1 antibody (Zhang and Li, 2007). Subsequent work, however, has found that the antibodies used in this study were non-specific in their channel-blocking actions.

The most promising evidence proposes two-pore channels (TPC) as the NAADP release channel. Mammals express two TPC genes, and over-expression of TPC2 in HEK or CHO cells has been shown to significantly increase the magnitude of calcium responses seen on NAADP exposure (Calcraft *et al.*, 2009). Mice lacking the TPC2 receptor lack the responses seen to NAADP in cardiac ventricular myocytes (Elson, 2011) and in pancreatic β-cells (Calcraft et al., 2009). Bilayer studies have suggested that TPC2 is a calcium-selective release channel sensitive to NAADP and pH and inhibited by Ned-19 (Pitt et al., 2010).

Photoaffinity labelling studies, in which a compound is modified such that a pulse of UV light will force the formation of permanent covalent bonds if it is in the position to make them, have suggested that the NAADP receptor may actually be a much smaller protein which can then act to open TPCs (Lin-Moshier *et al.*, 2012, Walseth *et al.*, 2012). This possibility would explain why high levels of TPC over-expression in HEK293 cells, increasing TPC2 mRNA 250-fold, have been seen to yield

comparatively modest increases in labelled NAADP binding (Calcraft et al., 2009). Precise identification of the structure of this accessory protein is now awaited.

Ca^{2+}-selectivity of TPC channels

Although NAADP-activated calcium release through TPC channels has been postulated based on the data presented above, and measured in bilayer studies (Pitt et al., 2010) the NAADP field is lacking in direct recordings taken from lysosomal TPC channels in their physiological environment. Lysosomes are too small to be accessed by traditional electrophysiological methods, and some groups have utilised vacuolin to cause lysosomal aggregation, creating larger acidic stores which can be patch-clamped using automated electrophysiological systems. Data from these experiments is conflicting. Shieder *et al*. measured an NAADP-activated current, I_{NAADP}, in vacuolin-treated lysosomes from TPC2 over-expressing HEK293 cells which was consistent with a calcium-selective current (Schieder *et al.*, 2010). Wang *et al*., on the other hand present data indicating that the TPC channel is activated by a lysosome-specific inositol, PI(3,5)P2, and carries a current of mainly sodium ions. This current is increased by TPC1 or TPC2 over-expression, deleted on TPC1,2 double knock-out and unaffected by Ned-19 in vacuolin-treated lysosomes derived from COS-cell expression systems (Wang *et al.*, 2012). A suitable explanation for the discrepancies in this result in the context of the field has not yet been put forward.

Physiological roles of NAADP

Since its discovery, NAADP-mediated calcium signalling has been shown to be functionally relevant in a number of mammalian and non-mammalian systems including: fertilisation, glucose-stimulated insulin release in pancreatic acinar cells, ATP-induced calcium signals in astrocytes and endothelin-mediated constriction in pulmonary smooth muscle cells (Churchill *et al.*, 2003, Cancela *et al.*, 1999, Barcelo-Torns *et al.*, 2011, Kinnear *et al.*, 2004).

NAADP in the heart

NAADP synthesising activity has been demonstrated in cardiac tissue (Chini and Dousa, 1995), whilst NAADP-evoked calcium release has been observed in cardiac rabbit heart microsome preparations and is independent of IP_3 and cADPR (Bak *et al.*, 2001).

Under basal conditions application of NAADP to cardiac myocytes by UV-photorelease of a caged analogue in either atrial (Collins *et al*., 2011), or ventricular (Macgregor *et al*., 2007a) myocytes exhibits a progressive increase in calcium transient amplitude which develops slowly over time and is not associated with any change in the L-type calcium current. After development of this effect caffeine-stimulated calcium transient amplitude is significantly increased, by 21±4% in ventricular and 31±8% in atrial myocytes, illustrating an NAADP-mediated enhancement of SR calcium load.

Application of the membrane-permeant ester NAADP-AM allows NAADP to cross the sarcolemmal membrane and accumulate in an active form in the cytosol through removal of the –AM group by endogenous esterases. NAADP-AM is capable of mediating a significant increase in spontaneous calcium spark frequency in both atrial and ventricular myocytes (Collins *et al*., 2011; Wee Khang Lin, personal communication). In atrial myocytes, this increase required both intact acidic calcium stores and functional SR signalling and was abolished in the presence of bafilomycin, GPN or ryanodine and thapsigargin. Transgenic mouse experiments in ventricular myocytes showed that NAADP-AM-mediated increases in calcium spark frequency were absent in myocytes isolated from TPC2-/- mice but were normal in cells derived from TPC1 knock-outs. They were also abolished during NAADP-AM application in the presence of the NAADP receptor antagonist Ned-19.

The NAADP system is thought to be constitutively active in cardiac myocytes, with application of GPN to atrial cells or self-inactivating NAADP concentrations to ventricular cells causing a decrease in calcium transient amplitude in the absence of further intervention (Collins *et al*., 2011). In ventricular myocytes, high-dose NAADP application yielded significantly more effect on cellular calcium transients during isoprenaline exposure, suggesting that the NAADP pathway is more active during β-AR stimulation (Macgregor *et al*., 2007a). In atrial myocytes this has been more directly observed; prior application of GPN to destroy lysosomes by osmotic lysis resulted in a significantly-blunted calcium transient response to isoprenaline (Collins *et al*., 2011). In support of this notion, the level of NAADP measured in

cardiac tissue is significantly increased during isoprenaline stimulation (Macgregor *et al.*, 2007a, Lewis *et al.*, 2012).

1.12 cADPR

Cyclic ADP ribose (cADPR) is a second calcium-releasing second-messenger, the effects of which were first reported in sea urchin egg homogenates in the same paper that initiated interest in NAADP (Clapper *et al.*, 1987). At the time, it was noted that NAD+ was able to release calcium from sea urchin egg homogenates, but that this response carried a short delay. The time-delay required to elicit calcium release suggested that the effect of NAD+ was mediated by a novel metabolite, which was later identified as cADPR (Lee *et al.*, 1989). Desensitisation of IP_3 or NAADP signalling was unable to inhibit the cellular response to cADPR and, further, self-desensitisation of the cADPR system using high concentrations also desensitised urchin egg homogenates to further applications of caffeine or ryanodine. Based on these observations, and the discovery that inhibitors of the RyR receptor were also able to inhibit cADPR responses (Galione *et al.*, 1991), it was suggested that cADPR acts to sensitise the RyR to cytosolic calcium.

Synthesis of cADPR was first recognised in the sea slug *Aplysia* (Lee and Aarhus, 1991) by an enzyme now referred to as ADP-ribosyl cyclase (ARC), capable of cyclizing NAD+ to cADPR. Candidate ARCs for the synthesis of cADPR in cardiac myocytes are CD38 and CD157. Interestingly, these same enzymes are purported to mediate NAADP-synthesis. A breakthrough in the cADPR field was made in 2012,

when Kannt and colleagues found cADPR cyclase activity localised to cardiac SR membranes (Kannt *et al*., 2012). Unlike the CD38 and 157 enzymes, this cardiac cyclase is not modulated by zinc. Moreover, a massive search of small-molecule compounds resulted in the discovery of two distinct inhibitors of this cyclase which were cardioprotective against arrhythmogenic triggers in guinea pig.

In cardiac myocytes, our laboratory has shown that application of a competitive cADPR antagonist was able to reduce the amplitude of calcium transients and contractions in guinea-pig ventricular myocytes without affecting I_{CaL} or SR calcium load (Macgregor *et al.*, 2007b, Rakovic *et al.*, 1999, Rakovic *et al.*, 1996). Patch application or photorelease of cADPR in ventricular myocytes, on the other hand, mediated an increase in cellular contractile amplitude, calcium transient amplitude and calcium spark frequency which were prevented by 8-bromo or 8-amino -cADPR (Iino *et al*., 1997; Cui *et al*., 1999). The effects of cADPR are now thought to be dependent on FKBP12.6, as myocytes isolated from FKBP12.6 null mice did not respond to patch application of cADPR with the increase in calcium spark amplitude and frequency observed in wild-type cells (Zhang *et al.*, 2009).

In an elegant study, 8-br-cADPR was also seen to inhibit delayed afterdepolarisations associated with oubain-induced SR calcium overload, suggesting that the pathway may be a legitimate anti-arrhythmic drug target (Rakovic *et al.*, 1999). Endogenous cADPR levels were recently found to be increased during β-adrenergic stimulation in Langendorff-perfused hearts (Lewis *et al*., 2012).

Given their propensity to be synthesised by β-AR stimulation, the similarities in potential enzymatic synthesis and seemingly co-operative mechanisms of action, a

focus on the interaction of cardiac cellular cADPR and NAADP signalling during normo- and patho-physiology would seem warranted in the future.

1.13 IP_3

Inositol trisphosphate (IP_3), formed during proteolytic cleavage of the phosphadyl-inositol PIP_2 by phospholipase C, is a ubiquitous cellular calcium-releasing second-messenger first discovered in insect salivary glands (Streb *et al.*, 1983).

IP_3 acts directly as a ligand at the IP_3 receptor (IP_3R), a ligand-gated, calcium-selective ion channel of which the type 2 receptor is expressed in the heart. IP_3-dependent calcium release has long been known to play an important role in the regulation of contraction in vascular smooth muscle cells, critical for the control of peripheral resistance.

IP_3Rs are present on the plasma membrane where they are capable of mediating calcium influx (Dellis *et al.*, 2006), but in most cells IP_3Rs are concentrated in the ER. Unitary IP_3R release events, calcium puffs, have been observed in cat atrial myocytes during RyR inhibition (Zima and Blatter, 2004). The major role of IP_3Rs in cardiac ventricular myocytes under physiological conditions appears to be in control of gene expression (Zima *et al.*, 2007).

Recently, work in our laboratory has suggested a functional role for IP_3 in the cardiac atria during physiological modulation of ECC (Collins, 2009). Phenylephrine, an α_1-AR agonist coupled to G_q that would be expected to increase cellular IP_3 production,

caused an increase in atrial cellular calcium transient amplitude and LTCC conductance by a mechanism which was fully abolished in the presence of 2-APB. Further, type 2 IP_3Rs were immunolocalised to the sarcolemmal membrane and co-localised with the calcium-stimulated adenylyl cyclase AC8. Accordingly, the effect of phenylephrine to increase calcium transient amplitude was less than half in the presence of AC or PKA inhibitors. These data are currently indirect in nature and await investigation using IP_3 directly, in caged or esterified form.

An interest in IP_3 as a mediator of cellular beating rate in the sino-atrial node is also developing, where direct application of IP_3 has been achieved using the esterified form IP_3-BM and is seen to increase calcium spark frequency in the subsarcolemmal space, calcium transient amplitude and most importantly rate of spontaneous node firing (Ju *et al.*, 2011).

1.14 The Sino-Atrial Node

Discovery and anatomy

The sino-atrial node is the epicentre of rhythm generation in the heart, responsible for the initiation of electrical events that lead to the contraction of each beat. The sino-atrial node is situated in the posterior aspect of the right atrium, at the junction between the atrial tissue and vena cave and running adjacent to the crista terminalis. The first suggestion that this anatomical area is responsible for the initiation of heart rhythm was made by Keith and Flack, after a somewhat heroic anatomical study of fixed hearts from across twenty-five species (Keith and Flack, 1907).

SAN action potentials

Action potential firing at the sino-atrial node is rhythmic and self-generated, a property brought about by gradual depolarisation of the cellular membrane during phase 4 of the action potential. The rate of this spontaneous diastolic depolarisation (SDD) determines the length of time between the firing of action potentials at the node; the steeper the rate of SDD the sooner the cell reaches threshold.

The process of firing an action potential in the SAN is relatively well accepted, however the mechanisms responsible for SDD remain under dispute. The central SAN region contains no voltage-gated sodium channels. Instead, the upstroke of the nodal action potential is driven entirely by the opening of voltage gated calcium channels. 'Low-voltage' T-type calcium channels open at ~ -55 mV and are responsible for the start of the acceleration of membrane depolarisation. The much more abundant L-type calcium channels take over relatively quickly as the major driver in depolarisation and are responsible for phase 0 of the action potential (Doerr *et al.*, 1989). The utilisation of calcium as the major ion responsible for depolarisation in the central SAN renders the upstroke of the SAN action potential distinctly slower than that of its contractile colleagues in the atria and ventricle.

Repolarisation of the SAN action potential is primarily driven by the delayed rectifier potassium current. As with atrial and ventricular tissue, there are two components to this current, I_{Kr} and I_{Ks} (Lei and Brown, 1996). Cells of the central sino-atrial node have a maximum diastolic potential around -60 mV, somewhat more depolarised than contractile myocytes. This can be attributed to a lack of the background potassium current I_{K1}.

After an action potential is fired in the SAN, electrical excitation is transmitted to the surrounding atrial tissues, from where it propagates across the atria. Atrial tissue, at rest, is far more hyperpolarised than tissue in the central node and this influence would be in danger of stopping node activity if electrical continuity from central node to atrial tissue was free. In fact, ion channel expression differs in distribution as one moves from the central, rhythm-generating, portion of the node to more peripheral transitional areas. Away from the central SAN, expression of voltage-gated sodium channels is initiated, with graded increases in channel function until the atria proper is entered. Further, whilst cells in the muscular tissue of the heart are made electrically continuous via the connexin-43 protein, central nodal cells express connexin-40. In the transitional areas, however, this expression becomes mixed.

If the hyperpolarising influence of surrounding atrial tissue is completely removed, the peripheral SAN begins to dominate pacemaker activity (Kodama and Boyett, 1985). This suggests that the central SAN, that of HCN4 and Cx-40 expression but lacking in voltage-gated sodium channels, serves as the physiological pacemaker and that the structural and molecular differences seen in the nodal periphery are indeed a form of protective mechanism which counteract the influence of surrounding atrial tissue.

Mechanisms of SDD

Spontaneous diastolic depolarisation (SDD) is the most important feature of SAN tissue for the undertaking of its physiological role. SDD allows the membrane

potential to decay from its most hyperpolarised potential at the end of action potential repolarisation back to the threshold potential for initiation of a new action potential in an automatic, rhythmic and reliable manner.

Two main schools of thought have dominated the debate as to the driving mechanism of SDD in the SAN. The earliest of these, the 'membrane clock' theory, postulates that SDD is brought about entirely by interactions between current flows at the surface membrane and was initially put forward in the late 1950s (Noble, 1960). More recently, the 'calcium clock' hypothesis has been advanced, proposing that the SR itself is acting as a timing mechanism by generating rhythmic calcium release events responsible for driving changes in membrane voltage (Bogdanov *et al.*, 2001).

In the late 1970s, a hyperpolarisation-activated inward current was discovered in sino-atrial node myocytes (Seyama, 1976) which was activated by hyperpolarisation to voltages below -50 mV and became more pronounced with hyperpolarisation to more negative voltages (DiFrancesco, 1986). This current, which became known as the 'funny current' $I_{(f)}$ due to its unusual voltage-gating, is a mixed ionic current encoded by the HCN4 gene (Ishii *et al.*, 1999).

Although the absolute necessity of $I_{(f)}$ in spontaneous SAN firing has been a subject of some controversy (DiFrancesco and Noble, 2012, Lakatta and Maltsev, 2012), it is accepted that the direct binding of cAMP to the $I_{(f)}$ channel (DiFrancesco and Tortora, 1991) is responsible for the chronotropic effect of adrenergic stimulation via modulation of the channel's activation curve (Brown *et al*., 1979). This would suggest that it has an important role in rate modulation. Constitutive knock-out of the HCN4 gene is fatal in utero between ED9.5 and 11.5 (Stieber *et al.*, 2003), this

corresponds to the time of chamber development and 1-2 days after initiation of rhythmic beating. Baruscotti reported cardiac-specific HCN4 ablation in the adult to cause a progressive reduction in atrial beating rate and severity of AV-block resulting in death before the 9th day after knock-out (Baruscotti *et al.*, 2011). Results in other knock-out models have been less severe, reporting more modest rate decreases (Herrmann *et al.*, 2012), however it is clear that ablation of HCN4 leads to a significant reduction in heart rate.

The initial work leading to the advent of the calcium-clock hypothesis was carried out in our laboratory, where Lauren Rigg observed that exposure of spontaneously-beating rabbit sino-atrial node to ryanodine or CPA was able to significantly reduce beating rate and SDD rate as measured with microelectrodes (Rigg and Terrar, 1996). Further data confirmed that the calcium buffering capacity of calcium fluorophores is enough to significantly slow resting pacemaker-cell beating rate in mammalian (Rigg *et al.*, 2000) and amphibian cells (Ju and Allen, 1998).

Lakatta's group have consistently championed the calcium-clock hypothesis, in which rhythmic calcium release from the SR is considered to be the driver of SDD. If sino-atrial node myocytes are forced into electrical quiescence by rapid voltage-clamp to -60 mV, cyclical SR calcium release is seen to continue for several beats (Vinogradova *et al.*, 2004). Under confocal microscopy, this group are able to visualise spark-like calcium release events which begin during diastolic depolarisation and increase in frequency leading into the pacemaker AP upstroke (Bogdanov *et al.*, 2006). These local calcium release events (LCRs) are hypothesised

to mediate membrane depolarisation through activation of inward NCX current as LCR calcium is removed from the cytosol.

Data making use of BAPTA-AM to investigate nodal firing rate has been called into question after one group reported potent potassium current blocking capacity of the ester, but not salt, in HEK cells over-expressing I_{Kr} (Tang *et al.*, 2007). To this end a recent paper was published in which the effect of BAPTA was observed by inclusion in whole-cell patch pipette solution and yielded no change in the beating rate of sino-atrial node cells over the course of several minutes (Himeno *et al.*, 2011). This data, however, cannot explain the effect of other calcium-chelating agents such as calcium dyes on beating rate, nor the propensity for ryanodine and CPA to reduce both resting beat-rate and the magnitude of isoprenaline response (Rigg *et al.*, 2000).

Convergence of M- and C- clocks

In recent years the polarised world of the M and C clocks have begun to be drawn together, with the Lakatta group now advocating a coupled clock mechanism in which $I_{(f)}$ acts as a fail-safe against severe bradycardia, whilst other channels at the cell membrane control C-clock rate by modulating the calcium available for SR store filling (Maltsev and Lakatta, 2012). Further data from our laboratory has provided a mechanism whereby cellular calcium could modulate SAN beating rate without the need for LCRs, as SAN cells have been shown to express calcium-stimulated isoforms of adenylyl cyclase (Mattick *et al.*, 2007). Calcium-modulated generation of cAMP would then be able to alter $I_{(f)}$ currents directly, and regulate the

phosphorylation of a plethora of sarcolemmal and intracellular proteins. Further investigation into this hypothesis is underway in the Terrar laboratory.

1.15 Specific Bradycardic Agents

Heart rate is a major determinant of myocardial oxygen consumption and coronary perfusion time (Laurent *et al.*, 1956). Both resting heart rate and the reduction in heart rate during beta-blocker treatment have been found to be independent predictors of all-cause and cardiovascular mortality in heart failure patients (Lechat *et al.*, 2001).

In an elegant *in vivo* study, Nagatsu *et al*. (2000) induced heart failure in adult mongrel dogs by causing mitral regurgitation and treated them after the development of heart failure with either placebo, beta-blockers, or beta-blockers whilst pacing heart rate at the pre-treatment level. After three months of treatment, they found that all measures of cardiac contractility which had been significantly improved by beta-blocker treatment were not improved in the paced and treated group, suggesting that it was the act of reducing heart rate which had conferred most benefit on cardiac function over that time. Pharmacologically-mediated beta-blocker benefits, on the other hand, were centred in the vasculature.

Lowering heart rate is also an important therapeutic approach to controlling stable angina pectoris, where a lengthening of the diastolic period is desirable to prolong subendocardial bloodflow (Brown *et al.*, 1974) and therefore reduce the development of ischemia.

Specific bradycardic agents (SBAs) are a class of compound which is pharmacologically efficient at cardiac beating rate reduction in comparison to any effects on cardiac contractility and action potentials (Kobinger and Lillie, 1987). The action of early SBAs were found to be different from calcium channel antagonists, as sinus node preparations responding to one SBA could no longer respond further to another but could respond to subsequent application of a calcium channel antagonist (Lillie and Kobinger, 1987).

Ivabradine is the only successful clinically-licenced SBA available today. Ivabradine, initially called S-16257, was first recognised to have dose-dependent specific bradycardic actions in rabbit sino-atrial node preparations and was far less potent at action potential prolongation than the most efficient SBA of the time UL-FS-49 (Thollon *et al.*, 1994). Thollon's experiments, reporting rate change in spontaneously beating atrial preparations, noted a decline in the rate of SAN SDD as measured by microelectrode, and later confirmed to arise from $I_{(f)}$ inhibition (Bois *et al.*, 1996). Ivabradine is now thought to exhibit a similar use-dependent $I_{(f)}$ block to the pharmacological $I_{(f)}$ inhibitor ZD7288, defined by a need for ion channels to be in a specific activation state in order for blocking to occur. $I_{(f)}$ channel block by ivabradine has been putatively attributed to the presence of a protonated amine group which can be attracted into the channel pore during openings and trapped there (Bucchi *et al.*, 2002).

Ivabradine treatment in a rat heart failure model has been seen to improve stroke volume, maintain cardiac output and lessen collagen deposition over three months of treatment (Mulder *et al.*, 2004). Ivabradine treatment has been shown to significantly

reduce the number of reported angina attacks and frequency of supplemental nitrate use in angina pectoris patients (Koster *et al.*, 2009). NICE guidelines sanction the prescription of ivabradine during chronic heart failure and angina (NICE, 2012, BNF, 2012).

This thesis deals with aspects of rhythm generation in the sino-atrial node and modulation of cellular contraction in atrial and ventricular tissue under 'normal' physiology. Chapters 3 and 4 explore the compound NAADP as a modulator of cellular calcium signals, whilst chapter 6 is concentrated on another endogenous modulator of cardiac contraction, apelin. Chapter 5 explores the effect of an exogenous compound, already licensed for therapeutic use in the treatment of lupus, on ionic currents in the sino-atrial node that modulate the rate of cardiac beating.

2 METHODS

2.1 Cell Isolation Protocols

All guinea pig myocytes were isolated using a method modified from Powell *et al*. (Powell *et al.*, 1980) such that it was possible to isolate atrial, sino-atrial and ventricular myocytes from the same heart on a given experimental day. The isolation protocols for each cell type stemmed from digestion with collagenase by retrograde perfusion.

Male guinea pigs (300-500g) were sacrificed by concussion followed by cervical dislocation. The heart was rapidly excised and encouraged to beat several times in heparin-containing zero-Ca^{2+} solution to prevent clotting. The heart was mounted via the aorta on a constant pressure Langendorff system for retrograde perfusion, with solutions maintained at body temperature using water jackets fed from a water bath (Grant Instruments, Cambridge, UK). After 2 min initial wash with zero Ca^{2+} solution (in mM: NaCl 136, KCl 5.4, $NaHCO_3$ 12, Na^+ pyruvate 1, NaH_2PO_4 1, $MgCl_2$ 1, EGTA 0.04, glucose 5; gassed with 95% O_2/5% CO_2 to maintain a pH of 7.4), perfusion was switched to re-circulation with collagenase solution (same as zero Ca^{2+} but with 24-28mg collagenase/50ml – type II Worthington, Worthington Biochemical Corp., Lakewood, NJ, USA – 0.1 mM $CaCl_2$ and no EGTA). The heart was cut down after 25 min of collagenase recirculation and specific protocols were carried out to isolate each individual cell type.

Guinea Pig Atrial Myocytes

Following 25 mins enzymatic digestion, the left atrium was carefully removed and placed in a Sylgard-coated bath containing an oxygenated salt solution (See 2.9, Solution A) at 37 ºC. Atrial tissue was cut into small pieces and immediately moved to a high potassium storage medium (in mM: KCl 70, $MgCl_2$ 5, K^+ glutamine 5, taurine 20, EGTA 0.04, succinic acid 5, KH_2PO_4 20, HEPES 5, glucose 10; pH to 7.2 with KOH) at 4°C, at which temperature the tissue was then stored until use. Isolation of single atrial myocytes was carried out by trituration with a 200µl pipette.

Guinea Pig Ventricular Myocytes

After 25 min enzymatic digestion as described above, the ventricles were separated from the atria and dissected into 8 pieces. These were placed in 10ml of collagenase solution and agitated for 5 min using a mechanical stirrer whilst being maintained at physiological temperature. The resulting cell suspension was filtered through a mesh, leaving the pieces of ventricle behind for further isolations. To stop the digestion process, collagenase was replaced with Dulbecco's Modified Eagle Medium (DMEM, Invitrogen) using repeated centrifugations. The collagenase-containing solution was gently centrifuged for 30 s, the supernatant discarded and replaced with DMEM warmed to 37 ºC and the remaining pellet re-suspended using a 200µl pipette. This centrifugation, discarding of supernatant and replacement with fresh, warm DMEM was repeated and cells re-suspended and stored at room temperature in DMEM until use.

Guinea Pig Sino-Atrial Node Cells

Similar to the isolation of atrial myocytes described above, following 25 min enzymatic digestion, the right atrium and major blood vessels were dissected away from the ventricles and placed in oxygenated Solution A warmed to 37 ºC.

Under a binocular microscope, overlying tissue was cleared away from the posterior surface of the right atrium to expose the entrance of the superior vena cava and likely position of SA node. The right atrium was pinned in a Sylgard-coated bath, opened by anterior incision and the SA node identified from anatomical features and tissue appearance. Under a binocular microscope, the SA node appears as a translucent, smooth, white structure in contrast to the thicker, pinker surrounding atrial tissue. The SA node was dissected into thin strips (~2x5mm) and transferred to warmed, oxygenated high potassium storage medium (as described above and in 2.9). Single cells were isolated by gentle trituration with a fire-polished glass pipette and stored thereafter at 4 ºC until use.

Mouse Ventricular Myocytes

Murine ventricular myocytes were isolated using a method adapted from O'Connell *et al*. (O'Connell *et al.*, 2007). Adult male C57/BL6 mice were killed by concussion followed by cervical dislocation. The heart was excised, placed in Tyrode solution (in mM: NaCl 140, KCl 10, $CaCl_2$ 1.8, $MgCl_2$ 1, HEPES 5, glucose 11) and mounted on a constant flow Langendorff system (4 ml/min, body temperature) for retrograde perfusion via the aorta. The heart was washed with zero-Ca^{2+} perfusion buffer for 4

min (in mM: NaCl 120.4, KCl 14.7, KH_2PO_4 0.6, Na_2HPO_4 0.6, $MgSO_4$ 1.2, HEPES 10, $NaHCO_3$ 4.6, Taurine 30, BDM 10, Glucose 5.5, pH to 7.0 with HCl) before switching to digestion buffer for 3 min (Perfusion buffer plus 2.4 mg/mL collagenase type II, Worthington). Finally, perfusion was continued for a further 8 min in low-Ca^{2+} digestion buffer (zero-Ca^{2+} digestion buffer plus 40 μM $CaCl_2$). After this time the heart was removed from the perfusion system and ventricles dissected into small pieces. Digestion was stopped with a myocyte stopping buffer (9 parts perfusion buffer, 1 part bovine calf serum plus 12.5 μM $CaCl_2$), cells were mechanically dissociated using a soft pipette and calcium was gradually re-introduced (3 min centrifugation at 20 g, supernatant removed and replaced with myocyte stopping buffer containing, sequentially, 100, 400 and 900 μM Ca^{2+}).

2.2 MULTICELLULAR TISSUE PREPARATIONS

Spontaneously-Beating Mouse Atrial Preparations

Male CD-1 mice (7-9 weeks of age) were terminated by concussion followed by dislocation in accordance with the Animals (Scientific Procedures) Act (1986). The chest cavity was opened and heparinised solution (10 U/ml) applied around the heart to minimise clotting during dissection. The heart was rapidly excised and placed in warm, oxygenated modified Tyrode solution (PSS, in mM: NaCl 125, $NaHCO_3$ 25, KCl 5.4, NaH_2PO_4 1.2, $MgCl_2$ 1, glucose 5.5, $CaCl_2$ 1.8, pH to 7.4 with NaOH and oxygenated with 95 % O_2/5% CO_2), the ventricular tissue discarded and the sino-atrial node region cleared of any overlying tissue.

Loops of thin suture were tied to the lateral edges of each atrium by directly knotting around a small area of the tissue, taking care to avoid contact with the node itself. One loop was anchored to a hook, which also provided oxygenation to the organ bath, and the other tied to a tension transducer. The preparation was hung in a 20ml organ bath, filled with PSS and maintained at 37 ºC. Tension data was digitised using a PowerLabs bridge amplifier and recorded on Chart5 software (all from ADInstruments, UK). Beating rate was calculated in real-time from the upstroke of the tension signal using the Chart5 Ratemeter function.

Spontaneously-beating atrial preparations were allowed to stabilise for 20 min, solution was exchanged for fresh PSS and the preparation was again allowed to stabilise for 30 min. Drugs were added directly to the organ bath by pipette and allowed to equilibrate for 30 min before rate data was sampled.

2.3 ELECTROPHYSIOLOGY

Whole-Cell Patch Clamp

Whole-cell patch clamp was used in both atrial and ventricular myocytes in order to deliver membrane-impermeable substances, and to both stimulate and record electrical activity.

Glass microelectrodes were manufactured from thin-walled, filamented borosilicate glass capillary tubing with an external diameter of 1.5 mm and an internal diameter of 1.17 mm (GC150TF, Harvard Apparatus Ltd, Kent, UK). A two-step heating process with gravity-driven pulling (PP-83, Narishige, Japan) was used to produce electrodes of resistance 3.0±1.5MΩ when filled with whole-cell patch solution.

Electrodes were filled with whole-cell patch solution containing (in mM): K^+ Aspartate 110, KCl 10, NaCl 5, $MgCl_2$ 5.2, HEPES 5, K_2ATP 5, pH to 7.2 with KOH. The filled electrode was placed in a Perspex holder with an electrical connection made between the holder and relevant headstage made using an Ag/AgCl coated wire. As per electrophysiological convention, the extracellular solution was taken to have a value of zero and all current and voltage measurements recorded with reference to this value, monitored by a bath probe (Ag/AgCl pellet).

When the AxoClamp 2A amplifier was to be used, for all current clamp recordings, the electrode holder was mounted in a HS-2A headstage.

The investigation of whole-cell currents using voltage clamp recording utilised an AxoPatch 200B amplifier and during these experiments, the electrode holder was mounted in a CV203BU headstage.

After correction for tip potential, the driving force for current flow at the tip of the electrode where two differing salt solutions come into contact, a piezoelectric manipulator (Burleigh Manipulators, part of Thorlabs, NJ, USA) was used to bring the tip of the micropipette into gentle contact with the surface membrane of the cell under study. Gentle suction was then applied using a syringe in order to produce a high-resistance, or Giga-, seal between the pipette and cell membrane.

During current clamp experiments using the AxoClamp amplifier, the process of seal formation was followed using an oscilloscope and auditory feedback. 200 ms current pulses of -1.1 nA were applied to the cell every 400 ms to allow correction for the pipette resistance. During seal formation the pulse was changed to -0.1 nA and changes in voltage signal used to assess seal resistance in a qualitative manner.

During experiments with the AxoPatch amplifier, seal formation was monitored using the PClamp Seal Test function. Seals of greater than 1 GΩ were considered reasonable and used to begin experiments.

After formation of a high resistance seal, the seal was allowed to stabilise and develop further over the course of at least 30 s. Electrical access to the cell was then achieved by rapid suction, carried out manually using a syringe attached to the back of the pipette holder. Where the AxoPatch amplifier allowed the use of Seal Test to monitor the patch, rupture could be seen as the instantaneous development of large capacitative transients at the beginning and end of the test pulse. During use of the AxoClamp amplifier, patch rupture was recognised by the recognition of a membrane voltage close to that which would be expected for an isolated myocyte together with

the presence of very small deviations in voltage caused by -0.1 nA pulses, where before deviations had been very large.

Perforated Patch Clamp

The electrical activity of sino-atrial node myocytes was investigated using perforated patch clamp.

Similar to the process for whole-cell patch clamp, glass microelectrodes were manufactured from filamented borosilicate glass capillary tubing with an external diameter of 1 mm and an internal diameter of 0.58 mm (GC100F, Harvard Apparatus Ltd, Kent, UK). A two-step heating process with gravity-driven pulling (PP-83, Narishige, Japan) was used to produce electrodes 5±1.5 MΩ in resistance.

Electrodes were filled with whole-cell patch solution containing as above, but also containing amphotericin B at 250µg/ml. Filled electrodes were mounted in a CV203BU headstage and both voltage and current clamp recordings were made using an AxoPatch 200B amplifier. Amphotericin B is an ionophore which inserts itself into the membrane and creates a pore capable of passing monovalent cations.

Seal formation during perforated patch experiments was exactly the same as that for whole-cell experiments using the AxoPatch amplifier. After the formation of a giga-seal, however, no further suction was applied and amphotericin was allowed to form electrical continuity between the cell and electrode. This process was usually satisfactory after 10 min but sometimes required up to 15 min and was monitored

using the PClamp Seal Test function, where capacitative transients became increasingly clear during rupture.

Micromanipulators

Electrode holders were mounted securely on a metal plate and controlled using a piezoelectric micromanipulator (Burleigh Manipulators, part of Thorlabs, NJ, USA).

Steps to reduce and correct for noise

In order to improve the quality of signals recorded during electrophysiological experiments a number of steps were taken to reduce recording noise. Electrical recordings were made inside a Faraday cage, with recording and imaging equipment maintained outside. All cables and leads used to connect equipment to the mains were screened such that transmission of 50 Hz noise would be minimal. Equipment was connected to a 'star earth' from where they were grounded. Experiments were carried out using solution level kept to a minimum reasonable depth in order to reduce the capacitive effects of the pipette wall.

Current clamp for action potential recording

On placing the electrode into solution, the measured voltage was manually zeroed to compensate for any microelectrode tip potential with respect to the bath solution. A repeating current pulse of -1.1 nA was applied across the end of the electrode and the

resistance of the electrode compensated using the ‘bridge balance’ such that the injection of current did not cause any deviation of the measured voltage.

Using a piezoelectric micromanipulator and under both visual and audio guidance, consisting of a video system relaying the bright-field microscope image and a voltage-controlled oscillator attached to a speaker giving a pitch that varied with recorded potential, the electrode was carefully manoeuvred to touch the cell under study. Gentle suction was then applied using a 10ml syringe attached to the electrode holder with narrow rubber tubing in order to generate a high resistance seal. Once a stable, high-resistance seal had been achieved a rapid suction pulse was manually applied using the 10ml syringe in order to rupture the cell membrane encompassed by the high resistance seal and allow electrical, and solution, access across the cell membrane.

At least 5 min was allowed for equilibration of the patch solution throughout the cell and further time was given if an inhibitor was added in order for it to achieve its full effect. If a fluorescent dye was being introduced, recordings did not take place until a stable fluorescence had been achieved.

Cells were stimulated to fire action potentials using a 2 ms current pulse applied via the microelectrode, at a rate of 1 Hz and a magnitude 0.3 nA above threshold. Action potentials were recorded in the current clamp configuration, digitised using a DigiData 1200 (Axon Instruments, Molecular Devices, CA, USA) analogue-to-digital converter and recorded using PClamp7 software.

Sampling frequency during recording was 10 kHz, except during $I_{(f)}$ recordings where the longer sweep duration necessitated the use of 2 kHz sampling frequency.

Voltage clamp protocols for various currents

On placing the electrode into the superfusion solution, the measured current was manually zeroed to compensate for any microelectrode tip potential with respect to the bath solution. The electrode tip was brought into gentle contact with the cell surface and a high resistance 'Gigaseal' (a seal resistance of greater than 1GΩ) formed by gentle suction using a 10ml syringe attached to the headstage with silicone rubber tubing to create a sealed system. The syringe plunger was set to 5 ml. Access was then gained to the cell either by rapid suction in the case of whole-cell recordings, or via the ionophore amphotericin in the case of perforated patch recordings.

During whole-cell recordings, cells were immediately clamped at -40 mV and voltage protocols initiated. Liquid junction potentials were considered to be negligible.

When conducting voltage clamp using perforated patch clamp in sino-atrial node myocytes at least 10 min was allowed for good access to develop, during which time the cell was placed in the current clamp configuration and spontaneous activity left to continue in order to help maintain appropriate intracellular conditions. After good access had been achieved, the cell was clamped at -40 mV and voltage protocols were initiated.

A holding potential of -40 mV is appropriate for all voltage protocols used during the experiments of this thesis as it is a voltage at which voltage-gated sodium channels will be held in the inactive state and will not be activated by depolarisation.

The protocol used for measurement of L-type Ca^{2+} currents, together with a representative current is shown in Figure 2.1. Myocytes were clamped at a holding potential of -40 mV and 200 ms step depolarisations to a potential of 0 mV were applied once every 5 s. The magnitude of the L-type Ca^{2+} current was measured as the maximum current minus the current at the end of the voltage pulse.

The protocol used for measurement of $I_{(f)}$ in sino-atrial node cells is shows in Figure 2.2. Myocytes were, again, clamped at a holding potential of -40 mV and step hyperpolarisations were applied for a duration of 2 s, once every 20 s. Before switching to HCQ and 5 min after exposure to the drug a set of hyperpolarising potentials was applied with steps to -80, -100 and -120 mV. During wash-in of the drug, steps to -100 mV were applied repeatedly.

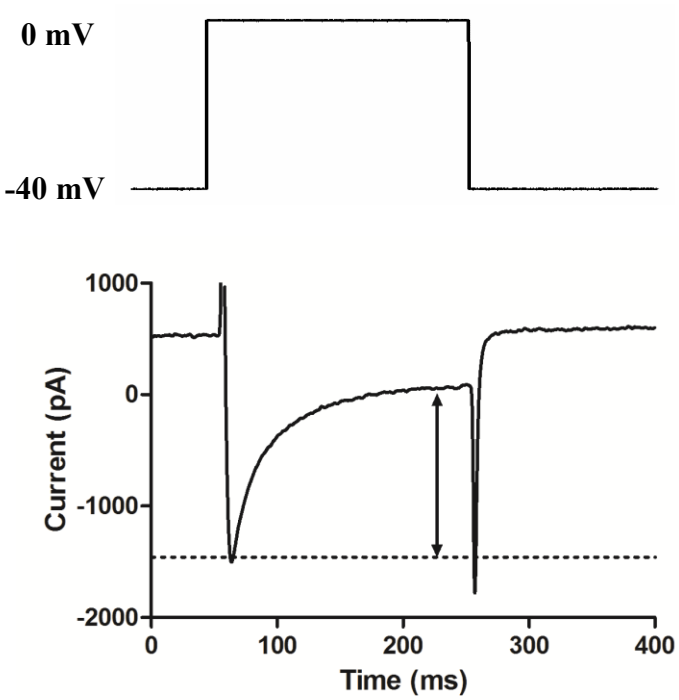


Figure 2.1: Voltage clamp protocol for the measurement of L-type Ca^{2+} currents
Panel to illustrate the voltage step applied to ventricular myocytes to stimulate L-type Ca^{2+} current. Cells were maintained at a holding potential of -40 mV and a step depolarisation made to a final membrane potential of 0 mV made for the duration of 200 ms (upper trace). The lower trace illustrates a typical whole-cell I_{CaL} obtained with arrow to indicate the difference between peak current and current at the end of the pulse used to measure amplitude.

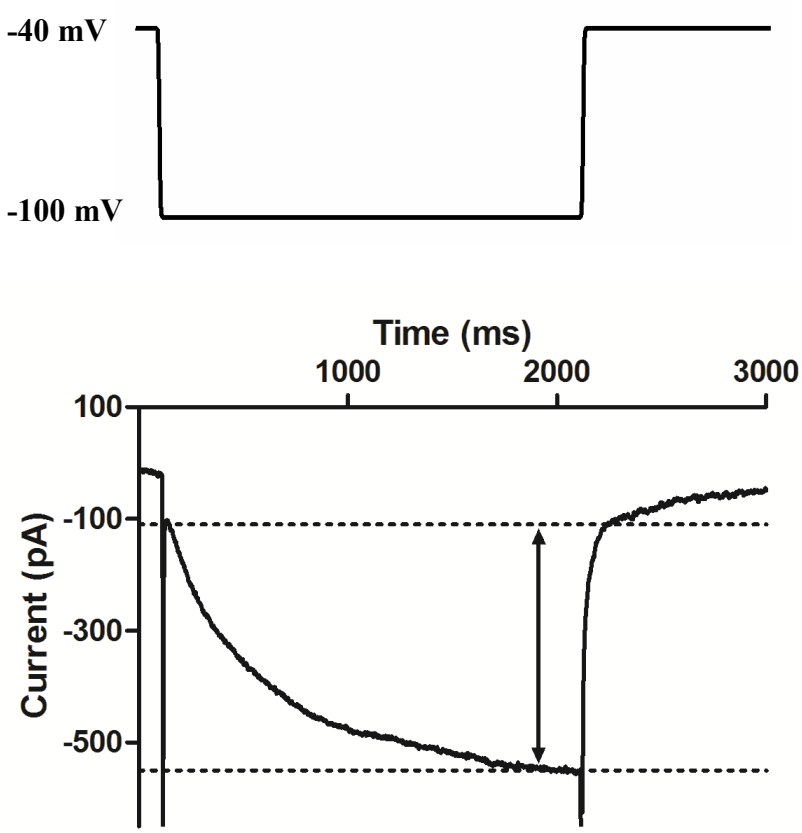


Figure 2.2: Voltage clamp protocol for the measurement of $I_{(f)}$ currents in sino-atrial node myocytes

Upper trace to illustrate the voltage step applied to sino-atrial node myocytes to stimulate the hyperpolarisation-activated inward current ('funny current' or $I_{(f)}$). Cells were maintained at a holding potential of -40 mV and a step hyperpolarisations made to a final membrane potential of -100 mV made for the duration of 2 s. Lower trace illustrates a typical whole-cell $I_{(f)}$ obtained with arrow to indicate the difference between peak current and current at the start of the pulse used to measure amplitude.

2.4 FLUORESCENT INDICATORS

As well as using voltage clamp methods, it is possible to use a fluorescent indicator, or fluorophore, to monitor in real-time changes in the concentration of a specific ion within the intracellular environment. This is especially useful in enabling the measurement of cellular action potentials to be combined with recording of real-time changes in a particular ion concentration. A range of fluorescent indicators are available which respond to various stimuli and absorb and emit photons at various wavelengths.

Fluorescence is defined as the emission of one or more photons from a molecule (in this case, the fluorophore) stimulated by the absorption of a quantum of electromagnetic radiation. Chemically-speaking fluorescent indicators work by absorbing a quantum of electromagnetic radiation at a specific wavelength. It is the decay of this electron from its higher energy state, back to its ground state, usually via multiple transition states, which releases energy in the form of a photon at a longer wavelength. Fluorescent indicators such as those used in these experiments exhibit fluorescent properties upon the binding of the ion they are designed to measure.

Throughout these experiments the fluorophore fluo-5F has been used to measure changes in intracellular calcium over time, a dye originally developed for use in flow cytometry and laser-scanning confocal microscopy by Tsien and colleagues (Minta *et al.*, 1989). Fluo-5F exhibits peak excitation at 494 nm and emission at 518 nm. Its major advantage is a very low affinity for calcium (K_d ~2.3 μM at 22 ºC), which results in minimal interference with the biological functions of calcium within the cell

and, further, decreases the likelihood of signals becoming saturated during recordings made at body temperature.

The relationship between emitted fluorescence of a non-ratiometric calcium indicator dye and free calcium is not directly proportional, especially at high concentrations of free calcium. Changes in measured fluorescence, therefore, indicate a change in free calcium but cannot measure the true calcium concentration within the myocyte.

When electrophysiology was to be carried out at the same time as recording calcium fluorescence, fluo-5F was loaded into the cell through the patch pipette at a concentration of 100 μM. This has the major advantage that dye concentration is always held constant within the cell but has the disadvantage that whole-cell recordings allow the free flow of substances between electrode and solution and may alter the concentrations of intracellular compounds.

During experiments in which concurrent electrophysiology was not required, fluo-5F was loaded into the myocytes by incubation with the acetoxymethyl (-AM) ester. Esterification of the dye renders it uncharged and hydrophobic, allowing for ready movement across the cell membrane. Once inside the cell, native esterases cleave the ester group away from the rest of the molecule, leaving the free form of the dye within the cytoplasm.

Stock solutions of fluo-5F salt, for use in whole-cell patch solutions, were prepared in double-distilled water at 1mM, separated into aliquots and stored at -20 ºC protected from light. For use, a single aliquot of fluo-5F stock was thawed and added to the whole-cell patch solution to produce a final concentration of 100 μM.

Stock solutions of fluo-5F-AM were prepared at a concentration of 100 μM or 400 μM in anhydrous dimethyl sulfoxide (DMSO) and stored in small aliquots, protected from light and maintained at -20 ºC. For use, a single aliquot was thawed and mixed with isolated myocytes in their appropriate storage solution to produce a final concentration of 3 μM for use with atrial myocytes. The cells were incubated with dye for 10 min at room temperature and plated onto a glass coverslip. At least 10 min of PSS superfusion at 35±2 ºC was allowed before experiments were initiated to ensure complete de-esterification of the dye.

2.5 EPIFLUORESCENCE MEASUREMENTS

All atrial myocyte work and all work investigating the role of NAADP signalling in beta-adrenergic responses were carried out using a Leica DMIRB inverted microscope and photomultiplier system (Cairn Research Ltd, Kent, UK). Cells were loaded with fluo-5F calcium dye and visualised using a x40 oil immersion objective and video monitor. Illumination from a blue LED (470nm) was passed through a bandpass interference filter to select for light at 475±15 nm and transmitted to the microscope via a liquid light guide. Excitation light was reflected towards the cell by a dichroic mirror which reflects light shorter than 505 nm wavelength but transmits longer wavelengths. Light emitted from the sample passed back down through the objective and was transmitted through the dichroic mirror before being reflected through a further 520 nm long-pass filter into a photomultiplier. In order to minimise background fluorescence and so increase the signal to noise ratio in fluorescence recordings as much as possible, a mechanical aperture placed in the light path between the microscope and photomultiplier tube was manually closed to obscure the area around the chosen cell. The photomultiplier signal was directed through an amplifier, followed by a low pass 100 Hz electronic filter. Signals were digitised by an Axon Digidata 1200 and recorded with pClamp software.

For analysis of the photomultiplier-derived calcium traces, a set of at least 8 signals taken at the same timepoint were averaged together to remove noise. This averaged signal was subjected to a digital low pass Gaussian filter (30 Hz cutoff, 353 coefficients) to remove as much noise as possible without affecting the timecourse of the transient. Background fluorescence was subtracted, and the resulting trace

analysed using ClampFit software. UV uncaging in this system was carried out using the Cairn arc lamp system described in section 2.7.

All ventricular myocyte work using caged NAADP, unless specifically stated, was carried out using a Zeiss Axiovert 200 inverted microscope, with attached Nipkow spinning disk confocal unit (CSU-10, Andor Technology, UK). Excitation light was provided by a 488 nm diode laser (Cairn Research Ltd, Kent, UK) passed though the Nipkow unit and delivered, via the side-port of the microscope, to the sample through a x40 oil immersion objective, which was also used to collect light emitted by the fluorescent probe fluo-5F. Emitted light passed back through the CSU-10 unit and was detected using an Electron Multiplying Charge Coupled Device (EM-CCD) camera, the Andor iXON897 (Andor Technology, UK). Images were captured at a frame rate of 50 per second. To avoid dye bleaching, the frame capture of the camera was linked directly to the laser such that 488 nm light was only transmitted to the cell during the recording of an image. Images were recorded using Andor iQ software (Andor Technology, UK). The fluorescence signal (arbitrary units) for each full trace was exported as a .txt file for full analysis. Again, the result of at least 8 transients was averaged to produce a model transient for each timepoint. This signal was then filtered and analysed using ClampFit software as above. This system was connected to the Rapp UV uncaging system, as described in section 2.7.

2.6 Measurement of Cellular Contraction

In some experiments, cellular contraction was monitored in real-time using an IonOptix system. Cells were studied on a Leica DMIRB inverted microscope, visualised using the IonOptix Myocam and recorded with IonWizard software (all supplied by IonOptix, MA, USA).

The IonOptix camera system detects sarcomere length over time at a sampling rate of 240 Hz, achieved by splitting the recording chip into four sections each capturing at a rate of 80 Hz staggered by time. IonWizard software assumes sarcomeres are a sinusoidal grating and utilises a fast Fourier transform of this grating to process sarcomere length at any given time.

Sarcomere contraction measurements were converted into .txt files and imported to MatLab, where they were analysed using self-written scripts to asses systolic and diastolic sarcomere length, fractional sarcomere shortening, rate and time of contraction and relaxation and cycle length. Further scripts were then used to compare these values under control conditions and in the presence of an intervention.

2.7 UV PHOTOLYSIS SYSTEMS

Caged compounds were applied to both atrial and ventricular myocytes by whole-cell patch clamp as described previously. Due to differences in the UV intensity of the two uncaging systems and differences between syntheses, 5 μM pipette concentration was used in atrial cell recordings and 1.5 μM in ventricular cells. There were no instances in which two different NAADP syntheses were used within the same set of experiments. Once equilibrated in the cell, the biologically inactive caged NAADP was uncaged by a UV light flash to release NAADP.

The concentration of NAADP actually applied within the cell after UV flash is difficult to ascertain. Previously, caged cAMP was used within the Terrar laboratory to estimate the efficiency of photorelease and a figure of ~1% uncaging was estimated. However the use of a commercially-available caged analogue of known concentration differs significantly from the use of an in-house-synthesised compound. Estimation of the absolute amount of compound synthesised is carried out by chromatography and is, merely, an estimation. It is therefore likely that differences in this initial estimation contribute to differences in the perceived potency of the NAADP batches.

In all atrial experiments and some ventricular experiments, a Cairn uncaging system was used to provide controllable light flashes for uncaging of compounds. This consisted of a xenon arc lamp fitted with a 355 nm filter, with light conveyed to the microscope by a liquid light guide, and a controller system allowing manipulation of flash intensity. During these experiments, when photomultipliers were being used to measure fluorescence before and after uncaging, a ‘gate’ system was also in place

such that the photomultiplier tubes were briefly inactivated during the UV flash. This avoided the high intensity UV light causing saturation of the photomultipliers and allowed accurate recording of cellular calcium transients to continue immediately. All parts of this system were sourced from Cairn Instruments (Kent, UK).

UV light reaching the microscope via the liquid light guide was reflected to the sample from below and passed through the oil objective to achieve illumination.

During UV photolysis on the Zeiss confocal setup, a Rapp photolysis system was used to generate UV pulses. This system is very similar to the Cairn system described above, utilising rapid discharge of capacitors to drive a short light flash, which is passed through a UV filter. UV light is transmitted to the back of the microscope via a quartz fibre optic and reflected to the sample through the objective.

2.8 SOLUTIONS

Solutions used during guinea pig experiments (Chapters 3-5, in mM unless otherwise stated):

- Physiological Salt Solution (PSS)

NaCl 125, $NaHCO_3$ 25, KCl 5.4, NaH_2PO_4 1.2, $MgCl_2$ 1, glucose 5.5, $CaCl_2$ 1.8, pH to 7.4 with NaOH and oxygenated with 95 % O_2/5% CO_2.

- High Potassium Storage Solution

KCl 70, $MgCl_2$ 5, K^+ glutamine 5, taurine 20, EGTA 0.04, succinic acid 5, KH_2PO_4 20, HEPES 5, glucose 10; pH to 7.2 with KOH

- Whole-cell Patch Solution

K^+-aspartate 110, KCL 10, NaCl 5, $MgCl_2$ 5.2, HEPES 5, K_2ATP 5, pH to 7.2 with KOH

- Solution A

NaCl 136, KCl 5.4, $NaHCO_3$ 12, Na^+ pyruvate 1, NaH_2PO_4 1, $MgCl_2$ 1, glucose 5; gassed with 95% O_2/5% CO_2 to maintain a pH of 7.4

- Zero Calcium Solution

Solution A + EGTA 0.04

- Collagenase Solution

As zero calcium, replacing EGTA with $CaCl_2$ at 0.1 mM and with the addition of collagenase at 24-28mg/50ml.

Solutions used during mouse experiments (Chapter 6, in mM unless otherwise stated):

- Tyrode solution

NaCl 140, KCl 10, $CaCl_2$ 1.8, $MgCl_2$ 1, HEPES 5, glucose 11

- Zero Ca^{2+} Perfusion Buffer

NaCl 120.4, KCl 14.7, KH_2PO_4 0.6, Na_2HPO_4 0.6, $MgSO_4$ 1.2, HEPES 10, $NaHCO_3$ 4.6, Taurine 30, BDM 10, Glucose 5.5, pH to 7.0 with HCl

- Digestion Buffers

First 3 min = Zero Ca^{2+} perfusion buffer + collagenase at 2.4mg/ml

Next 8 min = As above + 40 μM $CaCl_2$

- Myocyte Stopping Buffer

9 parts perfusion buffer, 1 part bovine calf serum plus, in sequential treatments 12.5, 100, 400 or 900 μM $CaCl_2$

2.9 SUPPLIERS

All animals used during the course of this thesis were supplied by Harlan (Harlan Laboratories, UK).

Compounds used during the course of this thesis were purchased from a number of suppliers.

Where powders were supplied as a salt, stock solutions were made by dissolving in double-distilled water. When using –AM compounds and bafilomycin, stock solutions were made by dissolving in DMSO. Stock solutions were aliquoted and maintained at -20°C, protected from light until required. Aliquots were used or discarded after defrosting and never re-frozen. The final concentration of DMSO maintained during any experiment was never greater than 0.1%.

Salts used to make Solution A, Zero-Ca^{2+} Solution, Collagenase solutions, PSS, whole cell patch solution and high potassium storage solution were purchased from VWR (VWR International, Leicestershire, UK) or Sigma-Aldrich (Sigma-Aldrich, Poole, UK).

Isoprenaline and hydroxychloroquine, were purchased from Sigma-Aldrich (Sigma-Aldrich, Poole, UK).

KN93 was purchased from Calbiochem (part of Merck-Millipore, Nottingham, UK) as KN93 InSolution.

AIP and bafilomycin A1 were purchased from Tocris (Tocris Bioscience, Bristol, UK).

Fluo5F salt, Fluo5F-AM and DMEM were purchased from Invitrogen (Life Technologies, Paisley, UK).

Caged NAADP and Ned-19 were both kind gifts from the laboratory of Dr G Churchill, Department of Pharmacology, University of Oxford.

2.10 Statistics

Statistical comparisons were made using paired or unpaired Student's t-tests, or repeated measures ANOVA when more than two groups or repeated measures of more than two sampling points were to be compared. A statistically significant difference was concluded when $P < 0.05$.

If ANOVA analysis revealed a significant effect of the factor under study, post-hoc testing was carried out to ascertain from where these statistical differences arose. The use of ANOVA/post-hoc analysis reduces type-1 error which would be introduced if multiple t-tests were carried out upon the same data set. Type-1 error is the probability of rejecting the null hypothesis when it is, in fact, true. Using a value for statistical significance of $P < 0.05$ is accepting a type-1 error of 5%, however when multiple t-tests are carried out on the same data set using a p-value for rejection of the null hypothesis at $P < 0.05$ then type-1 error is actually $1-(1-0.05)^{\text{number of tests}}$. ANOVA analysis is used to counteract this problem, maintaining the accuracy of the statistical method.

Post-hoc testing was carried out using the Tukey adjustment, if multiple comparisons were to be made between multiple groups, and the Dunnett's method if the means of several groups were to be compared to a control group. Again, a p-value of <0.05 was considered to indicate statistical significance. Post-hoc correction is a further way to maintain type-1 error at an acceptable level.

All statistical analysis carried out in chapters 3-5 were made using the Prism software (GraphPad Software Inc., California, USA). Statistical analyses carried out in chapter 6 were evaluated using SPSS (IBM, NY, USA).

For all data presented within this thesis, the responses of cells/tissues from at least three different animals contributed to a given data set. This was done to ensure that results were repeatable and not biased by an individual but representative of the cell types and pathways under study.

3 IDENTIFICATION OF A ROLE FOR CaMKII IN THE NAADP SIGNALLING PATHWAY

3.1 INTRODUCTION

Nicotinic acid adenine dinucleotide phosphate (NAADP) is a pyridine nucleotide and calcium-releasing second messenger which was first studied in sea urchin oocytes (Chini *et al.*, 1995). NAADP is a potent signalling molecule, with an EC_{50} measured at 16 nM in sea urchin egg homogenates (Chini *et al.*, 1995).

NAADP-synthesising capacity can be demonstrated in a range of tissues isolated from rabbit, including myocardium (Bak *et al.*, 2001) and endogenous NAADP signalling has now been demonstrated to play a physiological role across a range of systems and organisms. These include fertilisation (Churchill *et al.*, 2003), glucose-stimulated insulin release in pancreatic β-cells (Cancela *et al.*, 1999) and ATP-dependent calcium signalling in astrocytes (Barcelo-Torns *et al.*, 2011).

Cellular responses to NAADP in the sea urchin oocyte are biphasic in nature, consisting of an initial calcium release followed, after a short gap, by the generation of oscillations arising from calcium release at the ER (Churchill and Galione, 2001a). In this two-pool model, NAADP directly causes calcium release from one calcium pool, the first spike, and this released calcium then bolsters signalling at the ER, leading to the second signal. Subcellular stratification techniques suggested that NAADP is releasing calcium from areas consistent with lysosomal activity (Churchill *et al.*, 2002) and, indeed, agents which interfere with acidic stores have been shown to abolish NAADP responses in sea urchin (Calcraft *et al.*, 2009) and in mammalian cardiac myocytes (Macgregor *et al.*, 2007a). NAADP-mediated calcium signalling is distinct from that of IP_3 and cADPR, illustrated by the fact that de-sensitisation at the

receptor for one compound is unable to alter the calcium-releasing properties of the other two (Chini and Dousa, 1995).

Strong evidence from *in vitro* over-expression and *in vivo* knock-out studies indicates that the two-pore channel TPC2 is essential to the generation of NAADP-mediated calcium release. For instance, pancreatic-β cells isolated from TPC2 -/- mice fail to respond to NAADP exposure with the expected oscillatory inward current (Calcraft *et al.*, 2009), whilst cardiac ventricular cells isolated from TPC2 -/- mice have an impaired response to β-adrenergic stimulation (Elson *et al.*, 2010, Elson, 2011). TPC2 over-expressing HEK293 cells respond to NAADP with a dose-response curve very similar to that found for native NAADP responses (Zong *et al.*, 2009). Direct measurements of the TPC2-mediated current, however, have provided conflicting results with different studies concluding a calcium-selective current stimulated by NAADP (Schieder *et al.*, 2010) or a sodium-selective current stimulated by PI(3,5)P2 (Wang *et al.*, 2012).

Observations made in both atrial and ventricular myocytes confirm that application of NAADP to cardiac contractile cells elicits a significant increase in calcium transient amplitude which requires the presence of both intact acidic organelles and functional SR calcium handling (Macgregor *et al.*, 2007a, Collins *et al.*, 2011). Questions have arisen, however, as to whether the changes observed in stimulated calcium transient amplitude and SR calcium load can be achieved and maintained through direct uptake of calcium sequestered into the acidic stores. These are especially pertinent given questions as to the nature of the TPC2 current.

In sea urchin oocytes, application of NAADP elicits a distinct calcium release which can be visualised using calcium dyes and is directly attributable to release from the acidic stores. In these cells acidic stores may make up as much as 10% of the cell volume (Morgan, 2011). In cardiac myocytes a distinct and immediate calcium signal of this nature has not been observed and electron micrograph studies have reported lysosomes make up just 0.08±0.04% of cell volume (Frenzel *et al.*, 1988). Although the concentration of calcium reported to reside within an acidic store is high, 400-60 μM in macrophages (Christensen *et al.*, 2002), the proportion of acidic stores contributing to a given signal and the timecourse of this contribution is unknown and the lack of visible NAADP-mediated calcium 'spike' led us to consider further mechanisms by which lysosomal calcium release may elicit large and prolonged changes in the cellular calcium transient.

CaMKII is a ubiquitous serine/threonine protein kinase which, when activated, is known to phosphorylate sites on SR calcium handling proteins, especially Thr-17 on phospholamban and Ser-2815 on ryanodine receptors. CaMKII is tethered into the RyR protein complex and can be visualised by immunocytochemistry in distinct bands co-localised with RyRs (Collins and Terrar, 2012). A role for CaMKII in cardiac β-adrenergic responses has been suggested but its true role in β-AR responses has not been elucidated and it has been suggested that CaMKII-mediated phosphorylation is not required for normal responses (Kuschel *et al.*, 1999). Expression of a CaMKII inhibitory peptide has been reported to reduce β-adrenergic responses concomitant with a reduction in Thr-17 phosphorylation (Ji *et al.*, 2003, Ji *et al.*, 2006).

The aims of this section of work were to ascertain whether the actions of NAADP in cardiac contractile myocytes are reliant on CaMKII as an amplification mechanism. We hypothesised that CaMKII-mediated amplification of lysosome-dependent calcium release is required to observe the full response to NAADP in cardiac myocytes and tested this using a range of pharmacological inhibitors.

3.2 METHODS

Guinea pig myocytes were isolated using a method modified from previous work in this department (Powell *et al.*, 1980). Briefly, guinea pigs were terminated by concussion followed by cervical dislocation, the hearts washed and mounted on a constant-pressure retrograde perfusion system. Individual myocytes were obtained by enzymatic digestion followed by mechanical dissociation. Isolated myocytes were stored in DMEM at room temperature (ventricular cells) or high potassium storage solution at 4°C (atrial cells). See section 2.8.

NAADP was 'caged' with the group 1(2-nitrophenyl)diazoethane (NPE). This process allows the cell to be loaded with an inactive compound which is then activated ubiquitously throughout the cytosol by uncaging with a UV light pulse. Caging reactions and subsequent purification steps were carried out by Mr D Bloor-Young of the Churchill laboratory.

Micropipettes were manufactured from borosilicate glass capillary tubing (GC150TF, Harvard apparatus) using a two-step gravity-driven pulling process which produced electrodes in the range of 3±1.5 MΩ once filled. Standard whole-cell patch solution (see section 2.8) was used, to which the calcium fluorophore Fluo5F, caged NAADP, Ned-19 or AIP were added as appropriate. Electrical measurements were made using an AxoClamp 2 amplifier and are given with reference to an AgCl bath electrode.

Whole-cell calcium transients were recorded with the non-ratiometric calcium indicator Fluo5F (100 μM in the patch solution). Fluo-5F-emmitted light was passed through a 520 nm long-pass filter and detected using either a photomultiplier system

(atrial experiments) or an EMCCD camera (ventricular experiments). Photomultiplier signals were passed through a 100 Hz hardware filter, digitised using a Digidata 1200 and recorded using pClamp software. Camera signals were analysed using Andor iQ software and converted to txt files for analysis. Before analysis obtained signals were digitally smoothed with a low-pass Gaussian filter.

Both fluorescence systems gather an emitted signal in arbitrary units. Fluo5F fluorescence can be considered proportional to free calcium in the cytosolic compartment during conditions in which the temperature, pH, and loading concentration are constant. The signal is also affected by dye loading, background fluorescence and cell size. To control for changes in these parameters and allow comparison between cells of different sizes, arbitrary fluorescence units were converted into F/F0, which denotes a proportional change in emitted fluorescence over time compared to the diastolic signal. Calcium transient amplitude, in F/F0, was used to indicate changes in cytosolic calcium available during each beat and was measured as the maximal value of F/F0 during the course of each transient. This value provides information about changes in calcium concentration but cannot be taken to indicate specific concentration within the cell. Upstroke and decay velocities, measured as the maximal change in F/F0 value per ms during the calcium transient upstroke and the first half of calcium transient decay respectively, were also assessed.

UV uncaging systems used for both cell types deliver a flash of UV light to the preparation through the objective lens. UV flashes were generated by passing illumination from a ~1 ms high-intensity arc lamp flash through a 355 nm filter.

Statistical analyses were carried out using Prism software and all data are presented as mean±SEM. One-way ANOVA analysis with repeated measures was used to identify statistically significant effects occurring over time. Post-hoc testing with appropriate correction was carried out if ANOVA analysis identified a statistically significant effect over time. $P < 0.05$ was considered to indicate a statistically significant difference.

3.3 RESULTS

3.3.1 Photorelease of NAADP enhances cellular calcium transients in atrial myocytes

In order to investigate the effects of inhibitors on the NAADP pathway, it was first essential to confirm the actions of NAADP in cardiac myocytes. To this end, guinea-pig atrial and ventricular myocytes were loaded with fluo-5F calcium dye and caged NAADP via the patch pipette in the whole-cell configuration. Cells were stimulated to fire action potentials at a rate of 1 Hz via the patch pipette and maintained at 35±2°C in PSS.

The typical response of an atrial myocyte to photorelease of NAADP (pipette concentration, 5 μM caged NAADP) can be seen in the representative trace, Figure 3.1. Release of NAADP into the cell induced a significant increase in peak cellular calcium transient amplitude ($P < 0.05$, One-way ANOVA with repeated measures). This effect was gradual in its development, becoming statistically significant 2 min post UV flash (14±4% increase, $P < 0.05$, Dunnett's post-hoc testing) and continuing to increase over the course of the experiment (to 37±8% at 5 min, $P < 0.05$ compared to pre-release value, Dunnett's post-hoc testing). The effect of NAADP on calcium transient amplitude over time is summarised in Figure 3.2.

Analysis of calcium transient parameters revealed that the NAADP-induced increase in calcium transient amplitude was accompanied by a significant enhancement of the velocity of transient decay ($P < 0.05$, One-way ANOVA with repeated measures), as measured by the change in (F-F0)/F0 fluorescence units per ms during recovery of the calcium transient. This became significant at the 3 min timepoint (27±6% increase

$P < 0.05$ compared to pre-release value, Dunnett's post-hoc testing) and further increased to 46±11% faster than control at the end of 5 min ($P < 0.05$ compared to pre-release value, Dunnett's post-hoc testing).

There was also a significant increase in the velocity of transient upstroke ($P < 0.05$, One-way ANOVA with repeated measures) which was significantly larger than control by the third minute after photorelease (28±5% increase, $P < 0.05$ compared to control, Dunnett's post hoc testing) and developed to a 41±5% increase at the 5 min timepoint ($P < 0.05$ compared to control, Dunnett's post-hoc testing). Summary graphs of transient decay and upstroke velocities are presented in Figure 3.3 and 3.4 respectively.

No significant changes were noted in diastolic fluorescence, nor the time taken for transient upstroke and decay during the course of 5 min after the photorelease of NAADP in atrial myocytes.

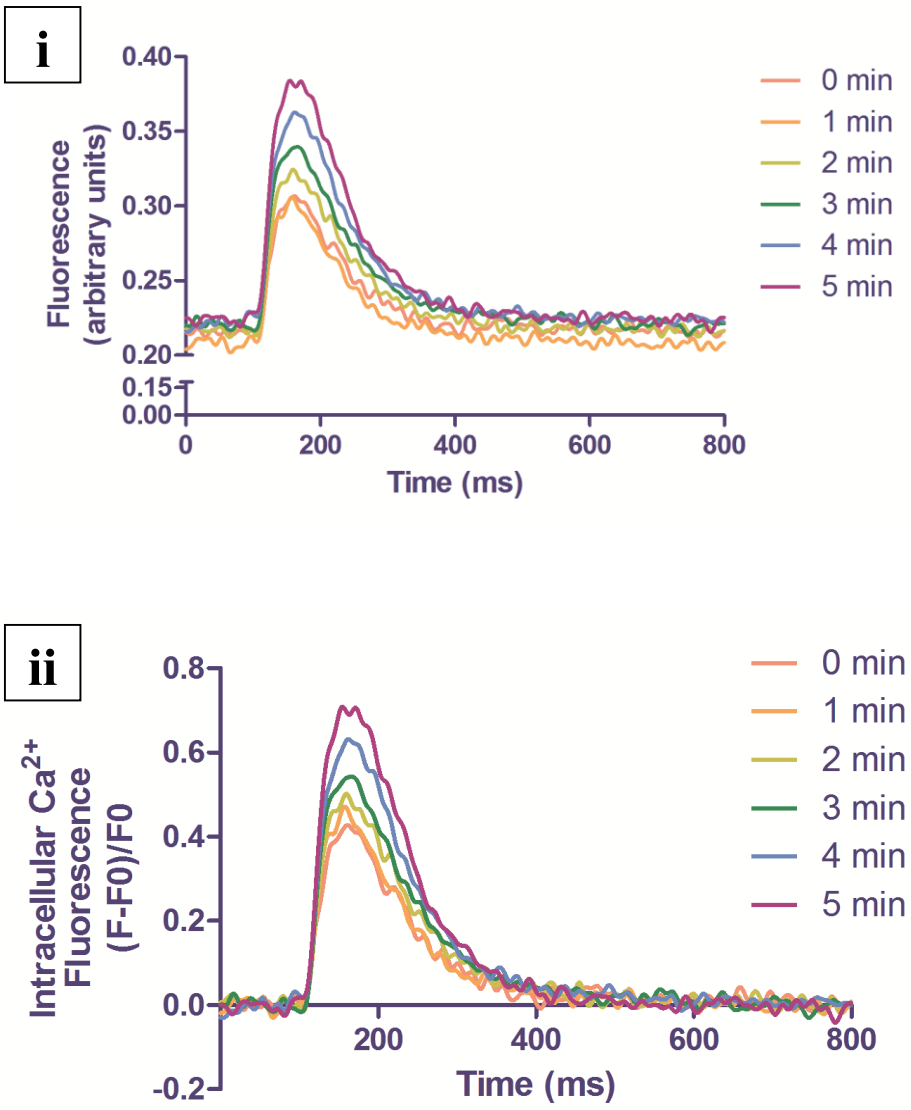


Figure 3.1 (i) and (ii): Representative Traces of NAADP Photorelease
Representative traces to show calcium transients in the same, single, guinea pig cardiac atrial myocyte recorded over the course of a 5 min experiment in which NAADP was photoreleased at time 0. Traces show calcium signals measured once per minute presented as raw Fluo5F (100 µM loaded through the whole-cell patch pipette) fluorescence signal (i) and the more traditional (F-F0)/F0 (ii), which is used throughout this thesis to control for changes in baseline and background fluorescence between cells. Each signal represents the average of at least 8 individual, whole-cell, calcium transients stimulated to fire at 1 Hz via the patch pipette. All experiments were carried out at 35±2 ºC.

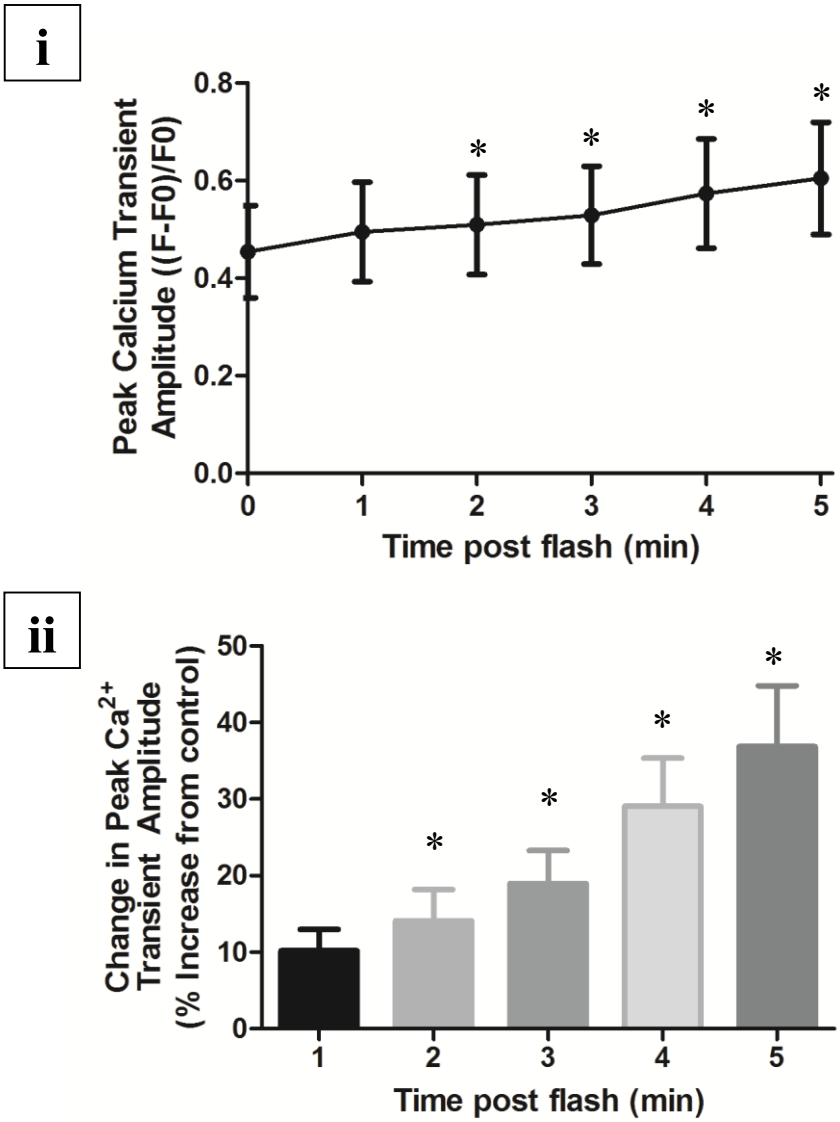


Figure 3.2 (i) and (ii): Calcium Transient Response to NAADP
Maximum calcium transient amplitude (i), defined as maximal (F-F0)/F0 signal, and percentage change (ii) in response to NAADP photorelease over the course of a 5 min experiment (n=10, where 1n = 1 cell, cells from at least 3 different guinea pigs were used). All data were recorded from atrial myocytes patched in the whole-cell configuration, with calcium dye (Fluo5F, 100 μM) and caged NAADP (5 μM) applied via the patch pipette. Cells were stimulated to fire action potentials at 1 Hz and all experiments were carried out at 35±2 ºC. Data are presented as mean±SEM. Repeated measures ANOVA analysis confirmed a significant ($P < 0.05$) increase in calcium transient amplitude from 2 min post flash (14±4% increase) when compared to the control, pre-flash level. Over 5 min, calcium transient amplitude increased by 37±8%. * indicates significant difference from pre-photorelease level (0 min) during Dunnett's post-hoc testing

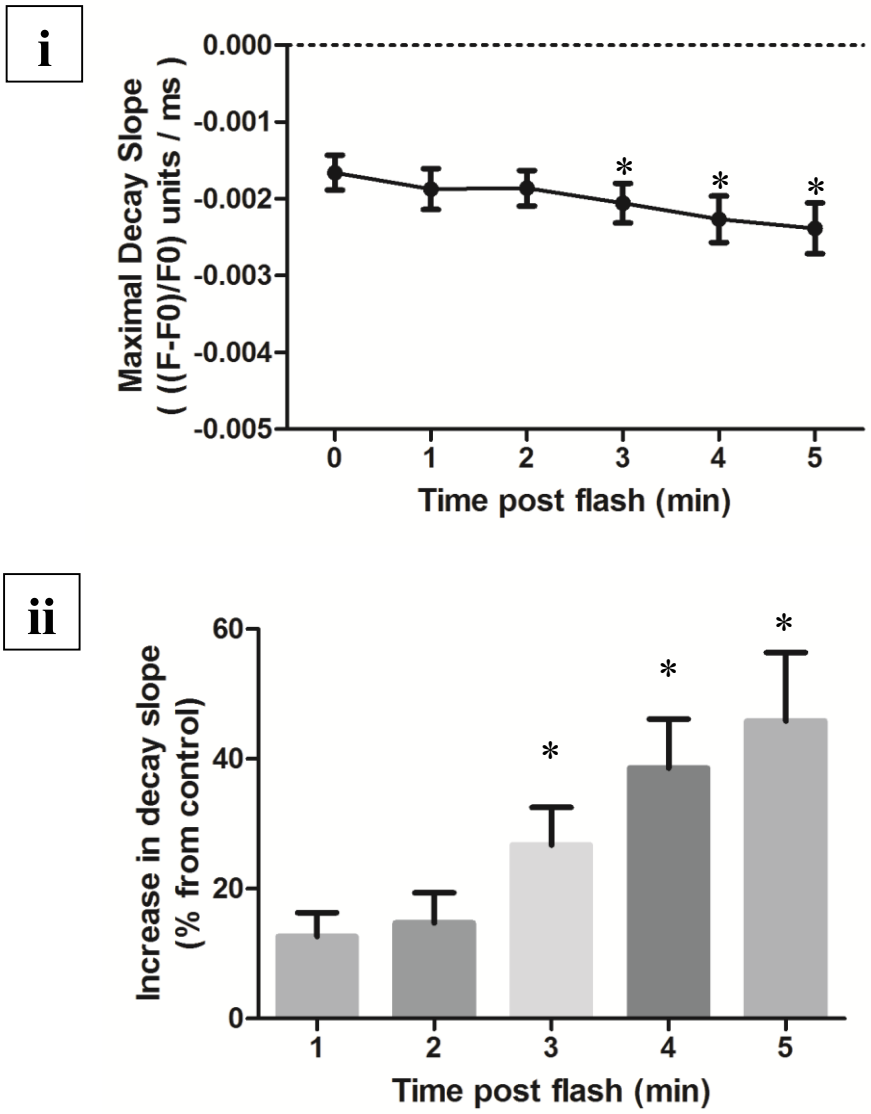


Figure 3.3 (i) and (ii): NAADP enhances the velocity of atrial calcium transient decay
Summary graphs to show the effect of NAADP photorelease in guinea pig atrial myocytes on the maximal velocity of calcium transient decay as both (i) raw values and (ii) percentage change over time. NAADP caused a significant quickening of the rate of calcium transient decay, measured as maximal velocity during the recovery phase of the stimulated calcium transient ($P < 0.05$, One-way ANOVA with repeated measures, n=10). Data are presented as mean±SEM. Post-hoc testing (Dunnett's) revealed a significant increase from control by 4 min, 17±8% increase, which was further enhanced at 5 min, 23±6% increase from 0 min (both $P < 0.05$ by post-hoc testing, n=10). NAADP (5 µM caged compound in the patch solution) was released at time 0 by UV flash. Cells were maintained in PSS at 35±2°C and stimulated to fire action potentials at 1 Hz via the patch pipette. Velocities measured for each timepoint represent the average of at least 8 transients. * indicates significant difference from pre-photorelease level (0 min) during post-hoc testing

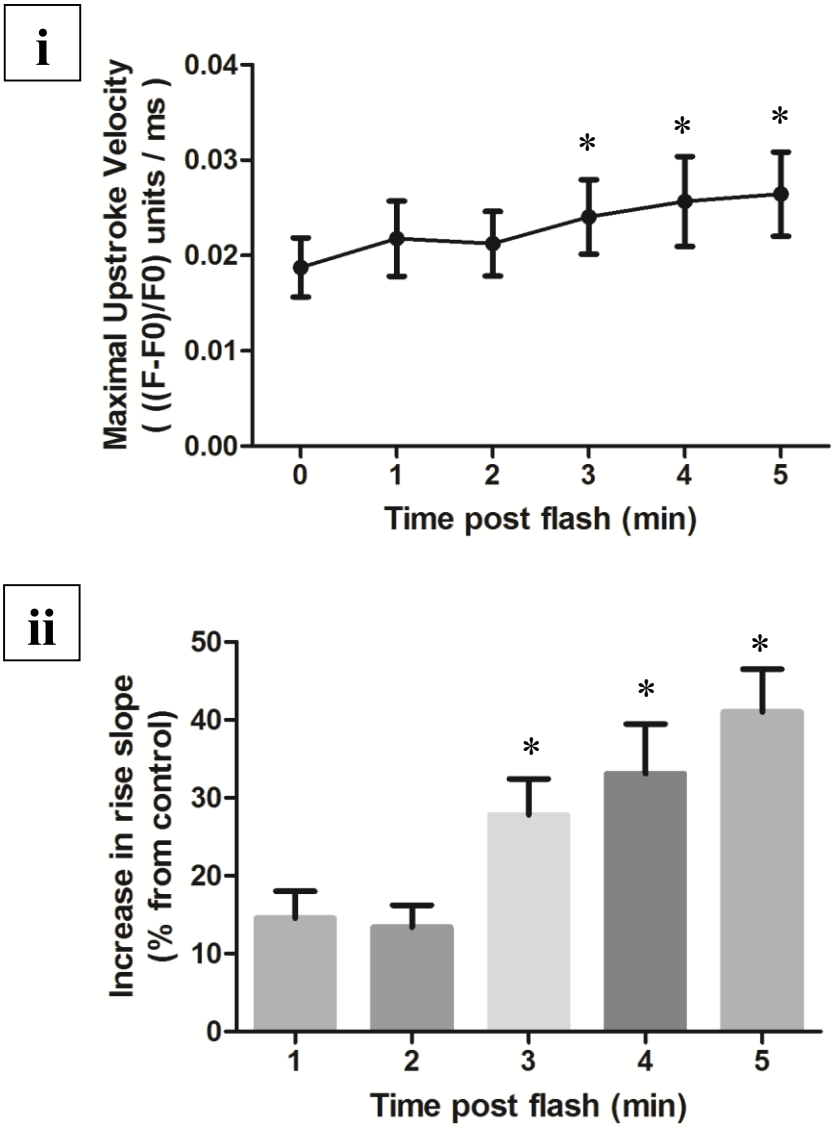


Figure 3.4 (i) and (ii): NAADP enhances the velocity of atrial calcium transient upstroke
Summary graphs to show the effect of NAADP photorelease in guinea pig atrial myocytes on the maximal velocity of calcium transient upstroke as both (i) raw values and (ii) percentage change over time. NAADP significantly enhanced the rate of calcium transient development, measured as maximal velocity achieved during the upstroke of the calcium transient ($P < 0.05$, Data are presented as mean±SEM. One-way ANOVA with repeated measures, n=10). Upstroke velocity was significantly greater than control after 3 min (28±4%) and was further increased at 5 min post UV photorelease of NAADP (41±5%). NAADP (5 µM caged compound in the patch solution) was released at time 0 by UV flash. Cells were maintained in PSS at 35±2°C and stimulated to fire action potentials at 1 Hz via the patch pipette. Velocities measured for each timepoint represent the average of at least 8 transients.
* indicates significant difference from pre-photorelease level (0 min) during Dunnett's post-hoc testing

Although flash-photolysis is a good method for releasing active compound instantaneously throughout the cell, it is also known that a pulse of UV light can lead to the generation of unwanted ionic species such as free radicals which may have their own effects on cardiac myocytes over the timecourse studied. In order to account for this possibility, a set of control experiments were carried out in which the full method was repeated without adding caged NAADP to the whole-cell patch solution.

A representative trace showing calcium transients recorded once per minute from the time of UV flash can be seen in Figure 3.5. Under these conditions, in guinea pig atrial myocytes, UV flash had no significant effect on calcium transient amplitude over the course of 5 min across 6 cells studied (from at least 3 different guinea pigs). In fact, no changes in any measured calcium transient parameters were observed in atrial myocytes in response to UV flash alone. Summary graphs illustrating the lack of effect of UV flash on calcium transient amplitude and velocities are presented in Figures 3.6 and 3.7 respectively.

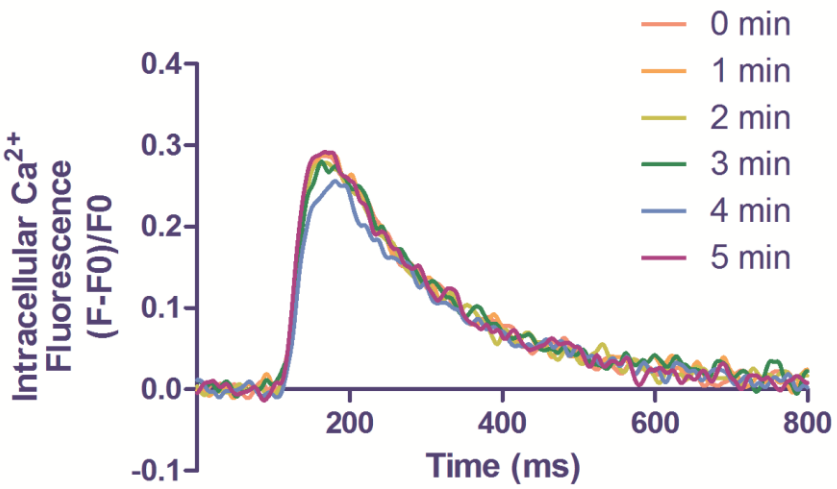


Figure 3.5: Representative Trace of UV Flash Control
Representative trace to show the effect of UV flash alone (flash at time 0) on atrial cell calcium transients. Each signal is the average of at least 8 stimulated calcium transients and was measured once per minute after application of the UV pulse.

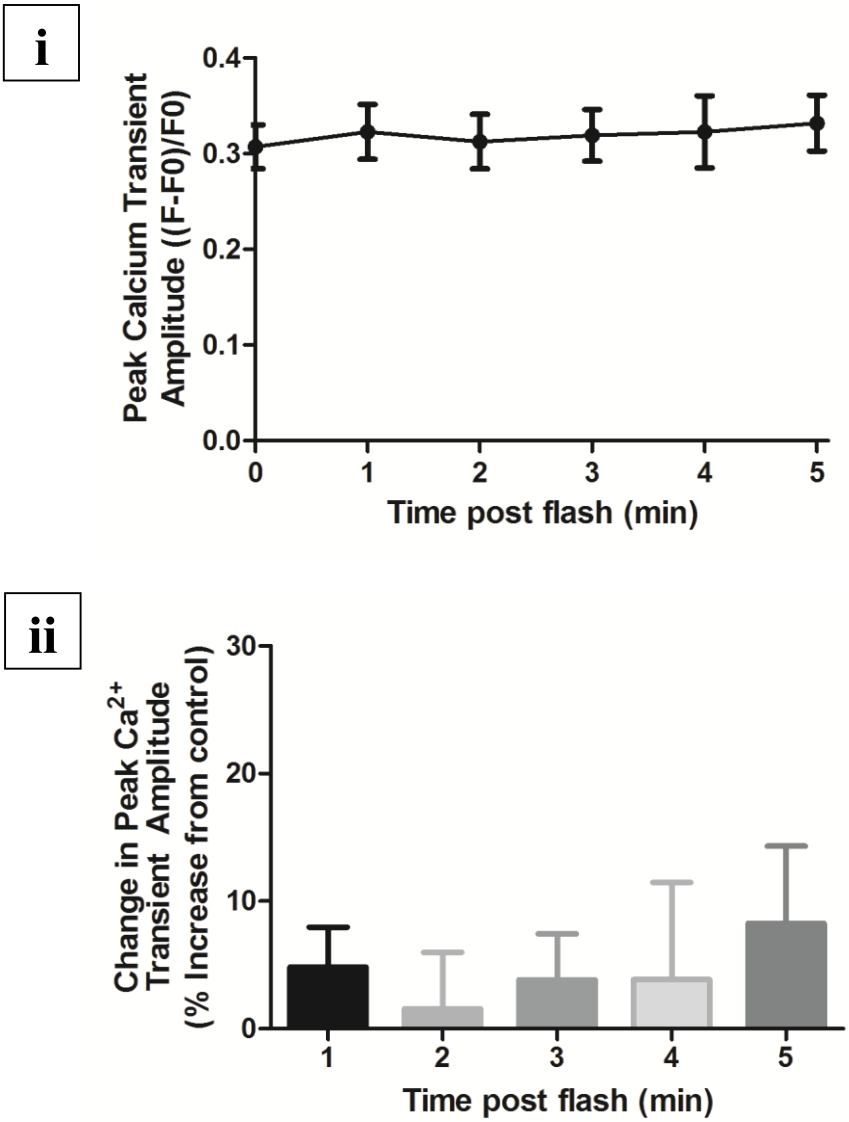


Figure 3.6 (i) and (ii): Calcium Transient Response to UV Flash Control
The effect of UV flash pulse on atrial myocytes under control conditions presented as absolute peak calcium transient amplitude (i) and percentage change from the 0 min, pre-flash, value (ii). Data are presented as mean±SEM. UV flash did not elicit a significant change in calcium transient amplitude over the course of 5 min ($P > 0.05$, ANOVA analysis, n=6).

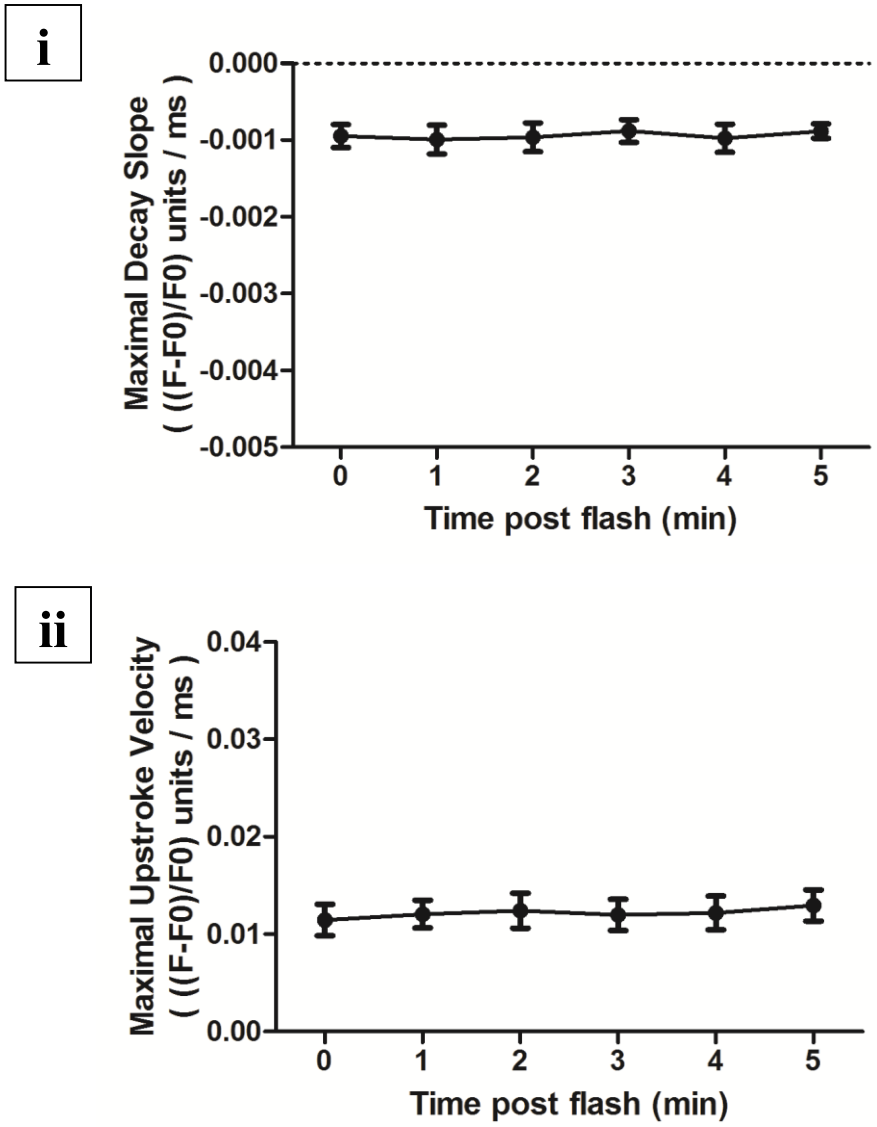


Figure 3.7 (i) and (ii): The effect of UV flash on calcium transient velocities
Summary graphs to show velocities of calcium transient (i) decay and (ii) upstroke over time from UV flash at 0 min in the absence of caged compound. Data are presented as mean±SEM. ANOVA analysis revealed no significant effect of UV flash control on either value over the course of 5 min (both $P > 0.05$, One-way ANOVA with repeated measures, n=6). Both measures indicate maximal velocity during the course of the transient.

At the same time as calcium transient data was being collected, cellular action potentials were recorded through the whole-cell patch electrode. Representative traces to show the effect of UV flash alone and NAADP photorelease on cellular action potentials before and 5 min after UV light exposure are presented in Figure 3.8 and 3.9 respectively.

Over the course of 5 min, a pulse of UV light elicited a significant reduction in action potential duration measured as time to 20%, 50% or 90% recovery (APD20, APD50, and APD90). This effect occurred both when caged NAADP was present in the patch pipette and in UV flash controls (all measures $P < 0.05$, effect over time, One-way ANOVA with repeated measures, n=10 and 6 respectively for NAADP and UV flash control groups). Overall, a reduction in action potential duration was a common theme observed after UV flash under all conditions studied, and the changes were not found to be significantly different between treatment groups ($P > 0.05$, Two-way ANOVA). A comparison of changes in action potential duration across all photorelease experiments conducted in this study is presented in the latter part of the results section, Figure 3.37.

During UV flash control experiments, a slight reduction in action potential amplitude, amounting to 4±2 mV or 3±1%, was observed over the course of 5 min ($P < 0.05$, One-way ANOVA with repeated measures, n=6). Measurement of the peak of the action potential, however, is subject to some error because of the speed of the upstroke, rapid onset of return, sampling rate of the recording and application of filtering. This change, therefore, is not thought to represent any physiological effect,

nor effect of UV flash. No change was observed in resting membrane potential over time.

No effect of UV photorelease of NAADP was found on resting membrane potential or amplitude over the course of 5 min (both $P > 0.05$ compared to pre-flash value, One-way ANOVA with repeated measures, n=10).

Summary graphs showing comparisons between the effect UV flash control and NAADP photorelease are presented for action potential amplitude in Figure 3.10 and for resting membrane potential in Figure 3.11.

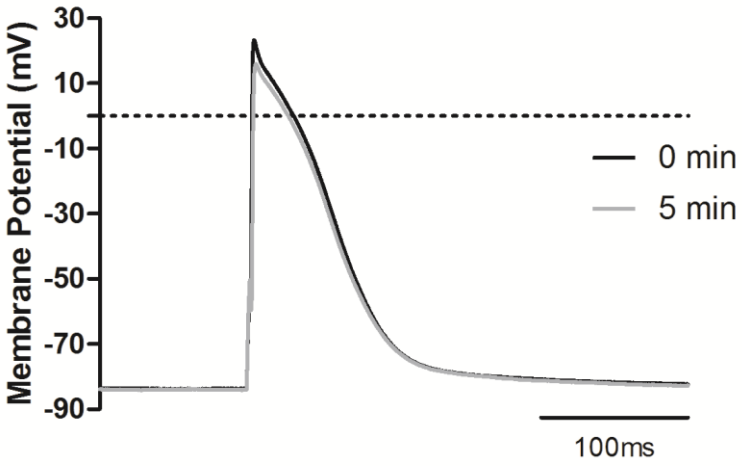


Figure 3.8: Representative Action Potential Response to UV Flash Control
Representative action potential trace recorded from an isolated guinea pig atrial myocyte patched in the whole-cell configuration under UV flash control conditions, in which cells were loaded with whole cell patch solution containing 100 μM Fluo-5F but not caged compound or any inhibitors. Action potentials are shown just before, 0 min, and 5 min after exposure to UV flash. Each trace represents the average of at least 8 action potentials recorded at each timepoint.

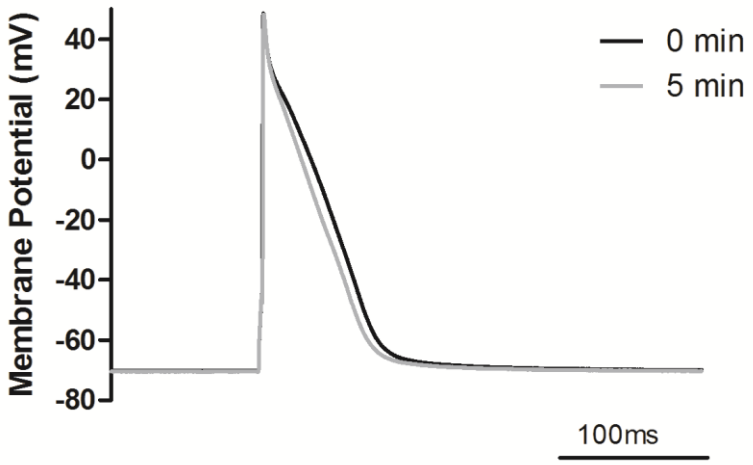


Figure 3.9: Representative Action Potential Trace to NAADP Photorelease
Representative traces to show action potentials recorded from isolated guinea pig atrial myocytes just before (0 min) and 5 min after photorelease of NAADP. Each trace represents the average of at least 8 action potentials recorded at the appropriate timepoint.

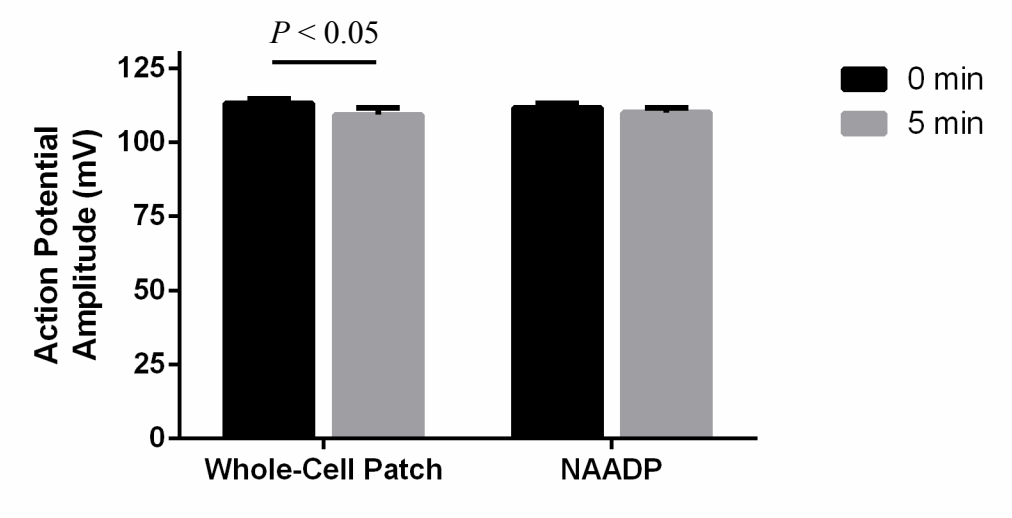


Figure 3.10: Comparison of Control Flash and NAADP Effects on AP Amplitude
Summary bar graph to show the effect of NAADP photorelease (n=10) and UV-flash control (Whole-Cell Patch, n=6) on action potential amplitude in cardiac atrial myocytes recorded just before (0 min) and 5 min after UV exposure. Data are presented as mean±SEM. UV flash caused a small but significant reduction in action potential amplitude over the course of 5 min ($P < 0.05$, One-way ANOVA with repeated measures), reaching 3±1% lower than control 5 min after photorelease. UV photorelease of NAADP had no significant effect on action potential amplitude over time ($P > 0.05$, One-way ANOVA with repeated measures).

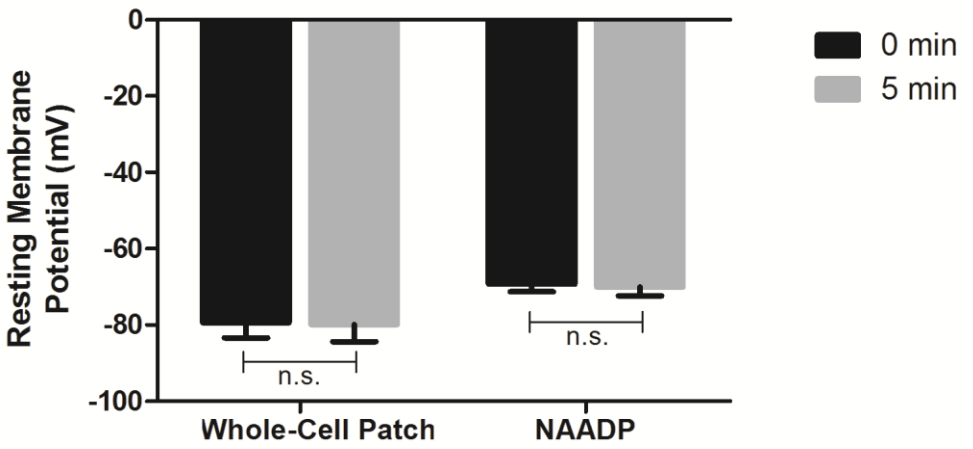


Figure 3.11: Comparison of control and NAADP effects on Resting Membrane Potential
Summary bar graphs illustrate the lack of effect of NAADP on resting membrane potential over the course of 5 min of either UV flash only (n=6) or UV flash to release NAADP (n=10) (both $P > 0.05$, One-way ANOVA with repeated measures). Data are presented as mean±SEM.

3.3.2 Photorelease of NAADP enhances cellular calcium transients in ventricular myocytes

A representative response of a ventricular myocyte to photorelease of NAADP (pipette concentration 1.5 μM caged NAADP) can be seen in figure 3.12. Exposure to NAADP resulted in a significant increase in calcium transient amplitude ($P < 0.05$, One-way ANOVA with repeated measures), becoming significant 3 min post flash and rising over the course of the experiment to a peak of 31±4% above control ($P < 0.05$ compared to pre-flash value, Dunnett's post-hoc testing). These data are summarised in Figure 3.13. For this set of experiments cellular fluorescence is given in units (F-F0)/F0i, where F0i is the baseline signal of the 0 min recording. This was done to control for a gradual drift in baseline fluorescence observed in all recordings on this system (see p159).

As with photorelease of NAADP in atrial myocytes, there was a significant enhancement in the velocity of calcium transient decay on exposure to NAADP in ventricular myocytes ($P < 0.05$, One-way ANOVA with repeated measures), which rose to a value of 28±9% faster than before photorelease at the 5 min timepoint ($P < 0.05$ compared to pre-flash value, Dunnett's post-hoc testing). Further, NAADP caused a significant increase in calcium transient upstroke velocity in ventricular myocytes ($P < 0.05$, One-way ANOVA with repeated measures) which reached a height of 39±15% faster than pre-photorelease (0 min) value after 5 min ($P < 0.05$ compared to pre-flash value, Dunnett's post-hoc testing). The effect of NAADP on calcium transient decay and upstroke velocities over time can be seen in Figures 3.14 and 3.15 respectively.

Control recordings, in which caged NAADP was not included in the whole-cell patch solution, were also carried out in ventricular myocytes to control for any effects which may be an artefact of the UV exposure protocol. A representative trace to show the effect of UV flash alone on calcium transients recorded from an isolated ventricular myocyte can be seen in Figure 3.16.

In ventricular myocytes, control UV flash produced no significant increase in calcium transient amplitude, upstroke or decay velocities (all $P > 0.05$, One-way ANOVA with repeated measures, n=5). The effect of UV flash alone on calcium transient amplitude can be seen as raw data in Figure 3.17, where the normalised amplitude over time is also presented against the effect of NAADP photorelease. Line graphs to illustrate the lack of effect on calcium transient velocities are presented in Figure 3.18.

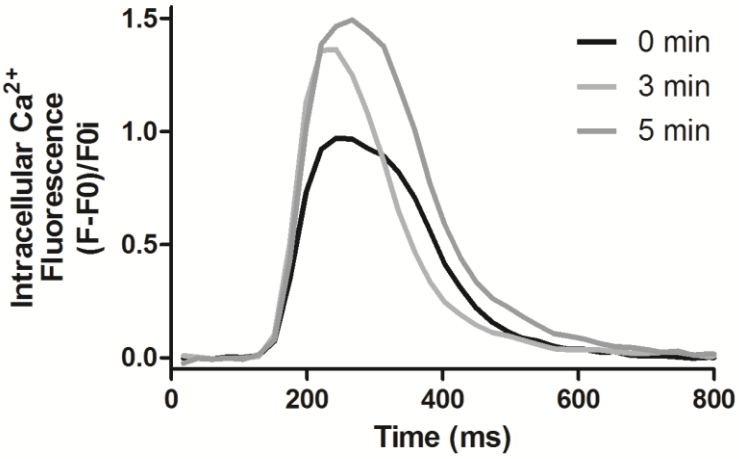


Figure 3.12: Representative traces to show the effect of NAADP on calcium transients in a ventricular myocyte

Representative traces to show calcium transients recorded from an isolated guinea pig cardiac ventricular myocyte over the course of an NAADP photorelease experiment before, 3 min and 5 min after UV flash to release NAADP. Traces are presented as Fluo5F signal normalised to diastolic fluorescence measured at 0 min (F0i). Caged NAADP (1.5 μM) and the calcium indicator Fluo5F (100 μM) were included in the whole-cell patch solution. Cells were stimulated to contract via the patch pipette at a rate of 1 Hz and the preparation was maintained at 34±2°C.

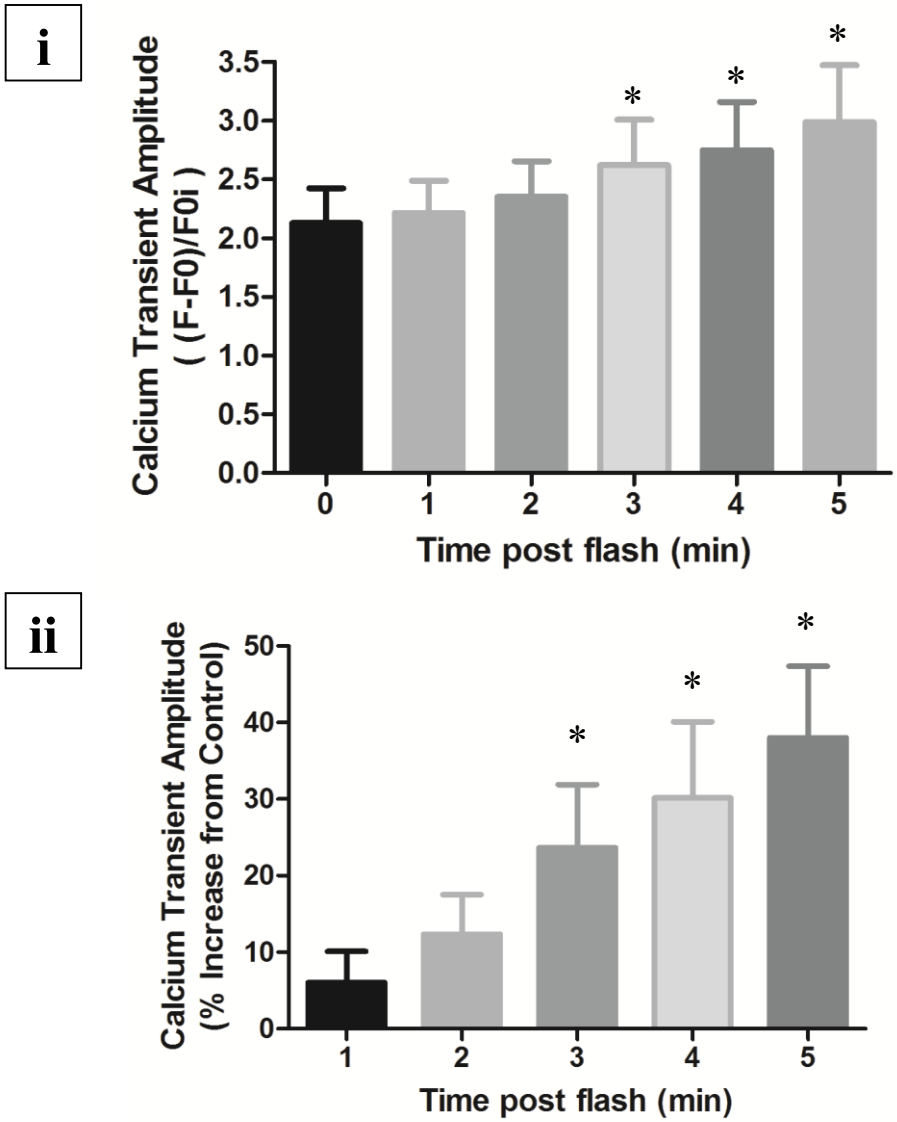


Figure 3.13: The effect of NAADP on calcium transient amplitude in ventricular myocytes

Summary bar graphs to illustrate the effect of NAADP on calcium transient amplitude in isolated guinea pig ventricular myocytes over the course of a 5 min experiment presented as:

(i) Peak calcium transient amplitude.

(ii) Percentage increase in calcium transient amplitude

Data are presented as mean±SEM and use (F-F0)/F0i, or peak signal normalised to diastolic fluorescence at 0 min (F0i). Photorelease of caged NAADP (1.5 µM included in the patch solution) caused a significant increase in calcium transient amplitude over time ($P < 0.05$ One-way ANOVA with repeated measures, n=8). This effect was significantly different from the amplitude measured in control 3 min after photorelease, 24±8% increase from pre-flash value, and continued to rise, reaching 30±10% after 4 min and 38±9% greater than pre-flash value at 5 min (all three $P < 0.05$, post hoc testing, n=8). * indicates significant difference from pre-photorelease level (0 min) during post-hoc testing (Dunnett's)

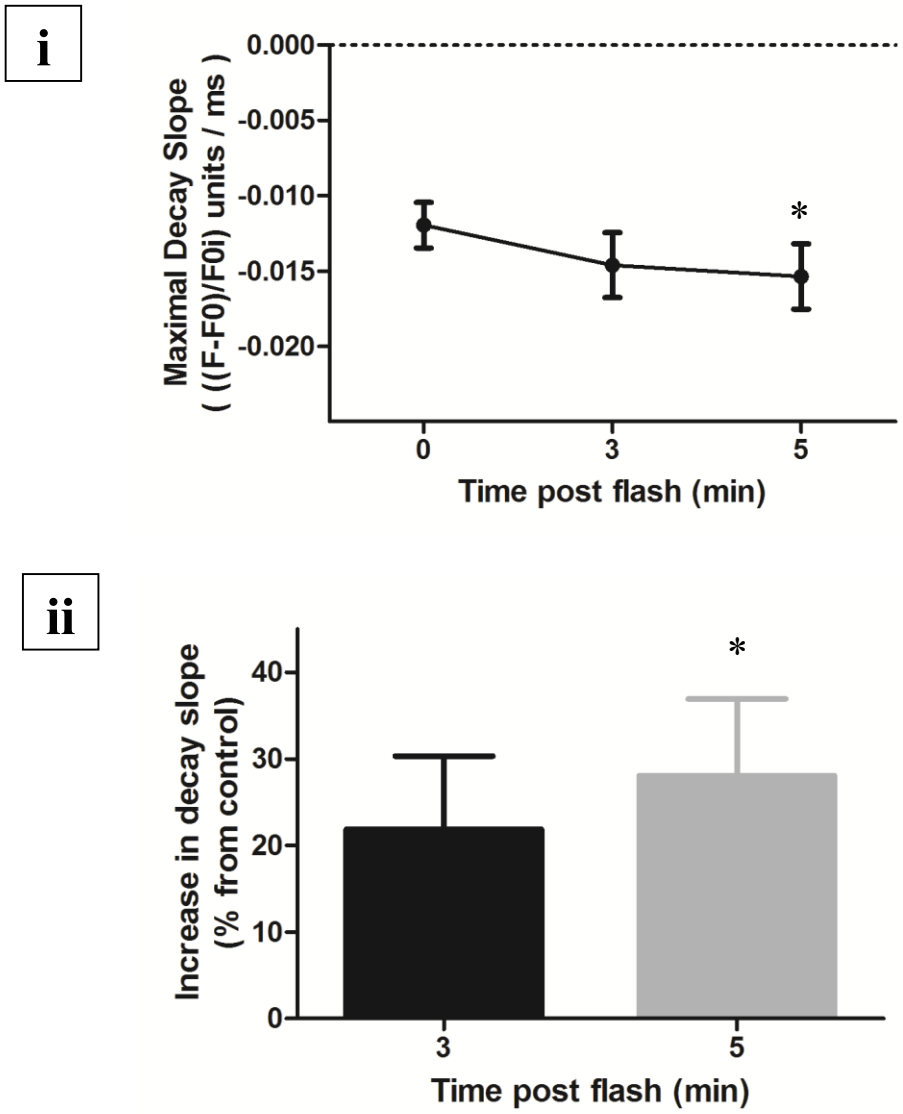


Figure 3.14 (i) and (ii): Effect of NAADP on the maximal slope of Ca^{2+} transient decay

(i) Line graph to show maximum decay velocity of the calcium transients measured in control and 3 and 5 min after photorelease of NAADP by UV flash.

(ii) Summary bar graphs to show percentage increase in decay velocity over time in the same set of recordings.

Data are presented as mean±SEM. UV photorelease of NAADP resulted in a significant enhancement of the calcium transient decay velocity over time ($P < 0.05$, One-way ANOVA with repeated measures, n=8) which reached a maximum of 28±9% greater than that measured before exposure to NAADP after 5 min ($P < 0.05$, Dunnett's post-hoc testing, n=8). * indicates significant difference from pre-photorelease level (0 min) during post-hoc testing

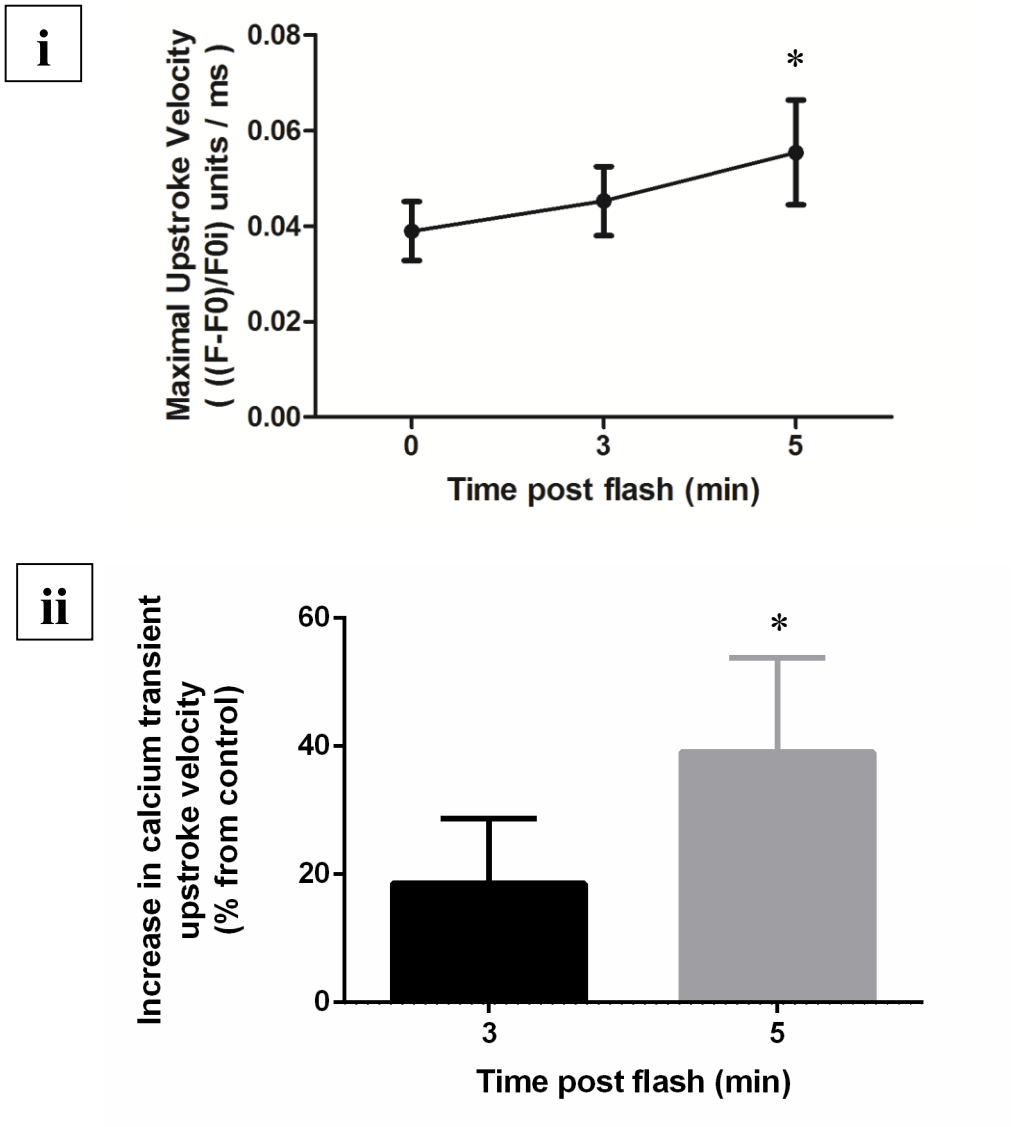


Figure 3.15 (i) and (ii): The effect of NAADP on calcium upstroke velocity
Summary graphs to show the effect of UV photorelease of NAADP on calcium transient upstroke velocity in guinea pig cardiac ventricular myocytes presented as:

(i) Maximal velocity of F/F0 fluorescence increase measured during calcium transient upstroke

(ii) Percentage change in upstroke velocity compared to 0 min value

Data are presented as mean±SEM. UV photorelease of NAADP resulted in a significant increase in calcium transient upstroke velocity over time ($P < 0.05$, One-way ANOVA with repeated measures, n=8), which reached 39±15% increase from the pre-release value after 5 min ($P < 0.05$, Dunnett's post-hoc testing, n=8). * indicates significant difference from pre-photorelease level (0 min) during post-hoc testing

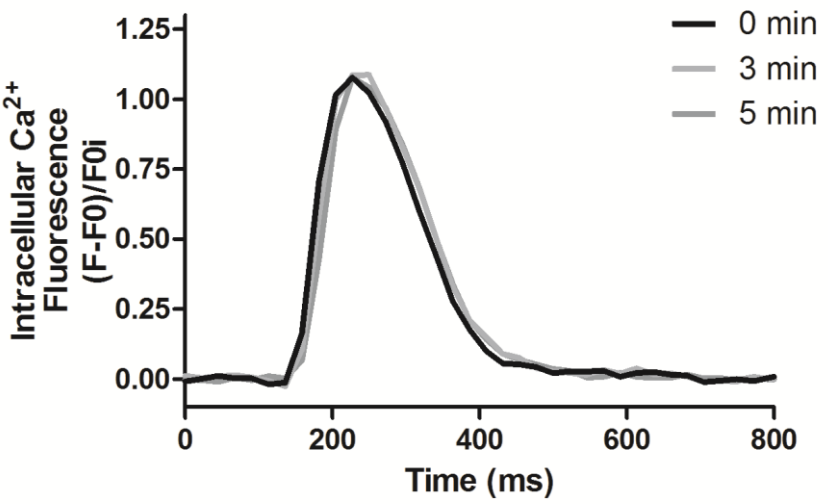


Figure 3.16: Representative trace to show the effect of UV flash on calcium transients in a ventricular myocyte

Representative trace to show Fluo5F calcium transients under UV flash control conditions, in which no caged compound or inhibitor was added to the whole-cell patch solution. UV flash delivered just after the 0 min recording. Each trace represents the average of at least 8 calcium transients measured at the appropriate timepoint. Cells were loaded with Fluo5F (100 μM) via the patch pipette and stimulated to contract at a rate of 1 Hz. Data are presented as fluorescence signal normalised to diastolic fluorescence measured at 0 min.

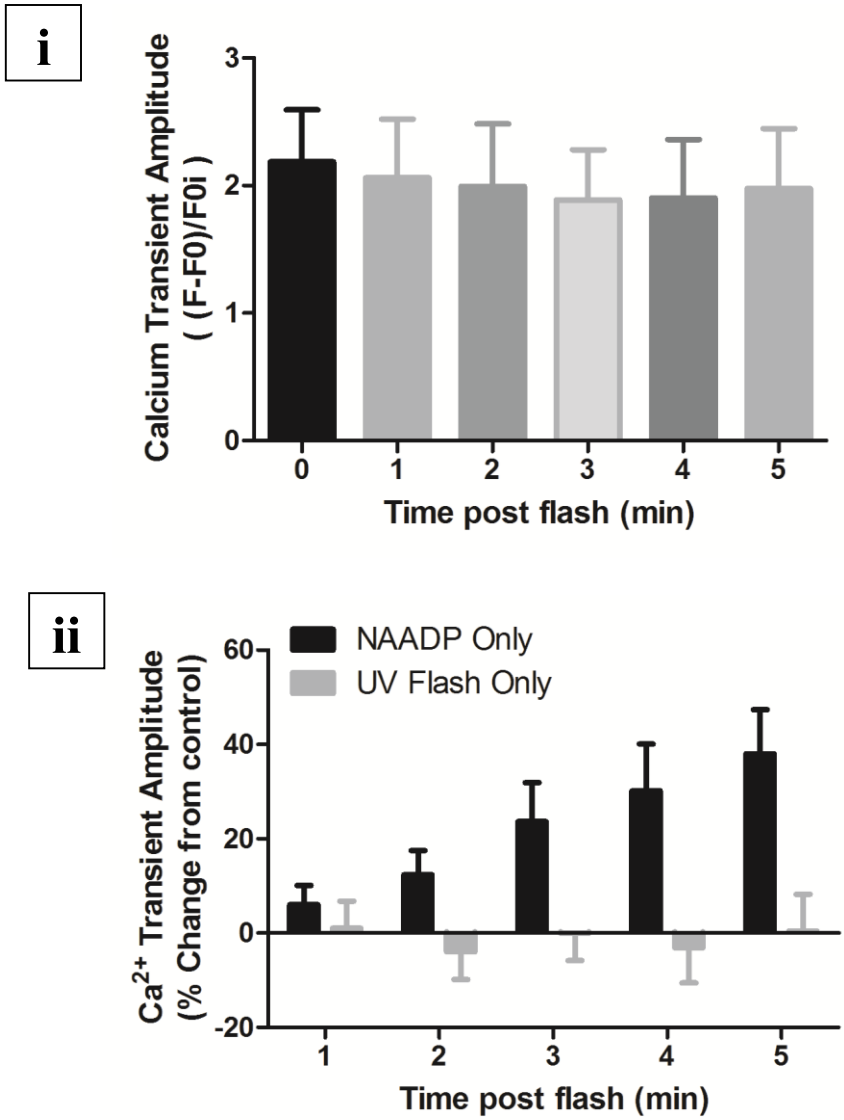


Figure 3.17 (i) and (ii): The effect of UV flash on calcium transient amplitude in ventricular myocytes

Summary bar graphs to illustrate the lack of effect on calcium transient amplitude seen during UV flash control in isolated guinea pig ventricular myocytes patched in the whole-cell configuration. Data are presented as:

(i) Calcium transient amplitude (peak F/F0 signal calculated from Fluo5F fluorescence)

(ii) Percentage change in transient amplitude compared to that observed during NAADP photorelease experiments

Data are presented as mean±SEM. UV flash in the absence of caged compound and any inhibitors failed to cause any effect on calcium transient amplitude over the course of a 5 min experiment ($P > 0.05$, One-way ANOVA with repeated measures, n=5).

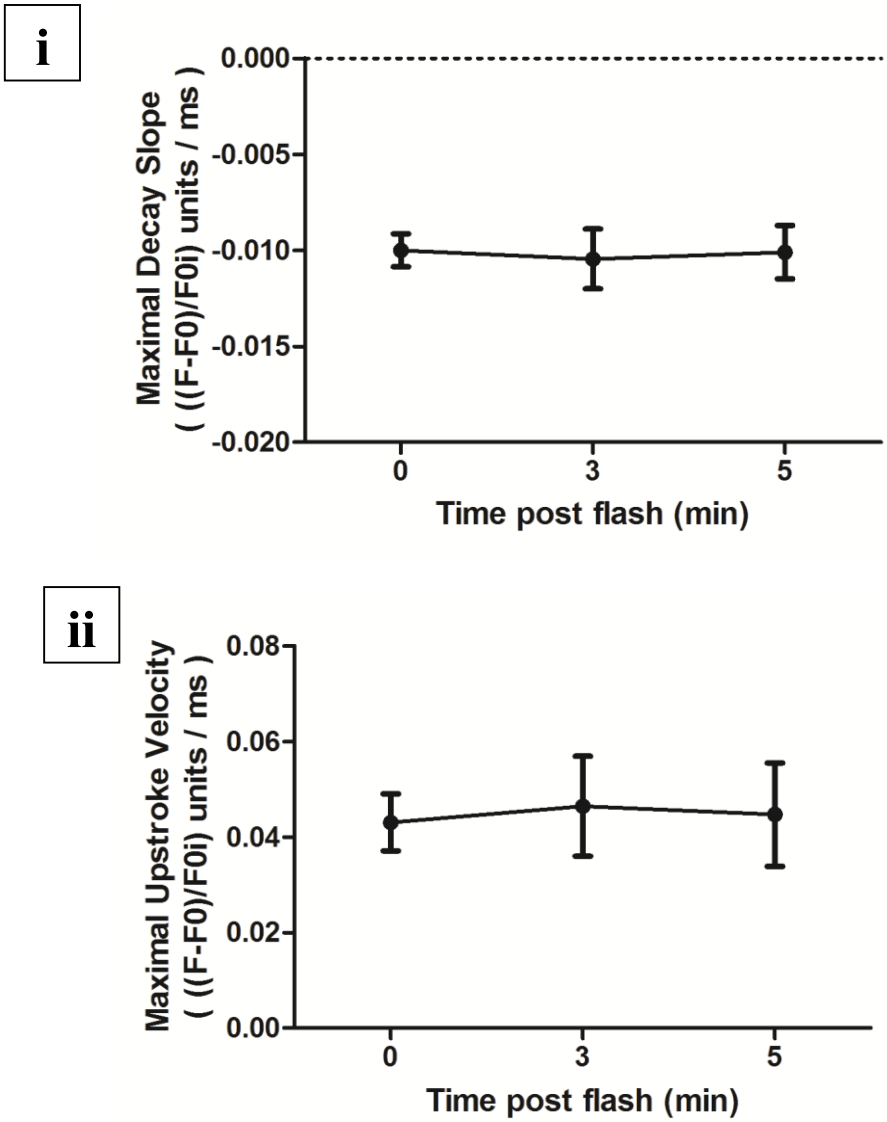


Figure 3.18 (i) and (ii): The effect of UV flash on calcium transient decay and upstroke velocities in cardiac ventricular myocytes

Summary line graphs to illustrate the lack of effect of UV flash control on calcium transient decay and upstroke velocities over the course of a 5 min experiment in isolated guinea pig ventricular myocytes (both $P > 0.05$, One-way ANOVA with repeated measures, n=5). Data are presented as mean±SEM. Cells were loaded with 100 μM Fluo5F via the patch pipette and stimulated to contract at a rate of 1 Hz, also via the patch pipette. Data are presented as maximal velocity achieved during the appropriate phases of the calcium transient and represent the average of at least 8 transients from each timepoint for each n-number included.

3.3.3 Ned-19 abolishes the cellular response to NAADP photorelease

In 2009 a specific inhibitor of the NAADP pathway, Ned-19, was discovered using a virtual screening method (Naylor *et al.*, 2009). This inhibitor is thought to bind at the same site as NAADP and therefore stop NAADP from acting on its receptor. It has previously been shown that Ned-19 abolishes the response of ventricular myocytes to NAADP-AM applied by the rapid-switch system (Elson, 2011) but it has not been used during NAADP uncaging in cardiac myocytes.

If caged NAADP is to be used to investigate how inhibition of other cellular functions may affect the response to NAADP, then it is important to confirm that the responses seen to NAADP photorelease is inhibited by Ned-19. Further, to this point in time, Ned-19 has neither been tested in atrial myocytes, nor previously been used with the photorelease method in either cell type.

Trans-Ned-19 which, unlike its *cis*- counterpart, has no inhibitory action on the L-type calcium current (Elson *et al.*, 2011), was applied via the patch pipette at 1 μM at the same time as caged NAADP (5 μM, atrial myocytes, 1.5 μM, ventricular myocytes) and allowed to equilibrate for at least 10 min.

As was expected, in the presence of patch-applied Ned-19 the response of atrial myocytes to UV photorelease of NAADP was completely abolished ($P > 0.05$, One-way ANOVA with repeated measures, n=7). In ventricular myocytes, three trials consistently showed no change or even a reduction in calcium transient amplitude after photorelease of NAADP in the presence of Ned-19. This data is in complete agreement with previous observations, although the n-number is insufficient to carry out a rigorous statistical test. The maximal changes in calcium transient amplitude

compared to the height of pre-photorelease (0 min) transients was 6±5% in atrial cells (at 4 min) and -13±11% in ventricular cells (at 5 min).

A representative trace to show the effect of NAADP photorelease on calcium transients and action potentials in the presence of Ned-19 in atrial myocytes can be seen in Figure 3.19. A summary graph to show the lack of effect on calcium transient amplitude and percentage change in transient amplitude over time across all atrial myocyte experiments can be seen in Figure 3.20.

A representative trace recorded from a guinea pig ventricular myocyte which shows the lack of effect of NAADP photorelease on calcium transients in the presence of Ned-19 is presented in Figure 3.21. Summary graphs to show the absolute calcium transient amplitude and to compare the effect of NAADP in the presence of Ned-19 to that of NAADP photorelease alone is presented in Figure 3.22.

In both cell types, the enhancement of calcium transient upstroke and decay velocities seen during photorelease of NAADP were completely abolished in the presence of Ned-19 (atrial myocytes, $P > 0.05$, One-way ANOVA with repeated measures, n=7). Summary graphs to show the effect of NAADP photorelease in the presence of Ned-19 on calcium transient decay and upstroke velocities are presented for atrial myocytes in Figure 3.23 and for ventricular myocytes in Figure 3.24.

Action potential analysis of atrial cell data showed that UV photorelease of NAADP in the presence of Ned-19 had no effect on resting membrane potential, nor action potential amplitude (both $P > 0.05$, One-way ANOVA with repeated measures, n=7). Graphs to compare the 0 and 5 min timepoints for both of these parameters are

presented in Figure 3.25. Consistent with action potential measurements recorded in NAADP and UV flash control myocytes, there was a significant reduction in action potential duration measured over the course of 5 min. This was apparent when measured as time to 20, 50 or 90% action potential repolarisation (all $P < 0.05$, One-way ANOVA with repeated measures, n=7). Summary graphs to compare action potential duration across all conditions under study are presented in Figure 3.37.

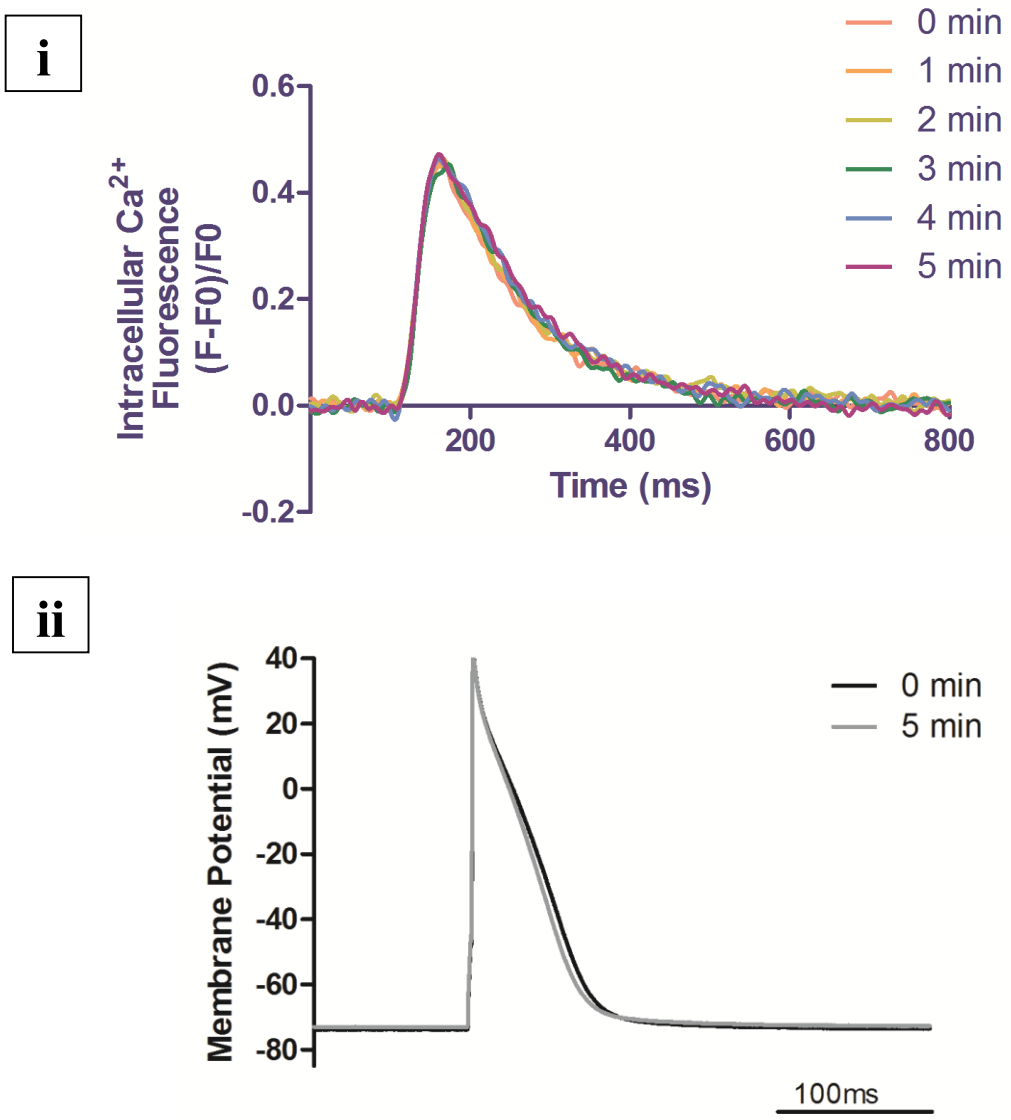


Figure 3.19 (i) and (ii): Representative Traces, Atrial NAADP Photorelease in the Presence of Ned-19

Representative traces to show stimulated calcium transients and action potentials in an atrial cell recorded over the course of a 5 min experiment in which NAADP was photoreleased at time 0 in the presence of patch-applied Ned-19 (1 µM). Traces show calcium signals measured as (F-F0)/F0 (i) and action potentials recorded in current clamp (ii). Calcium signals were recorded as Fluo5F emission (100 µM dye included in patch solution) and represent the average of at least 8 signals recorded at the timepoint stated. Cells were stimulated at a rate of 1 Hz using the patch electrode and maintained at 35±2°C.

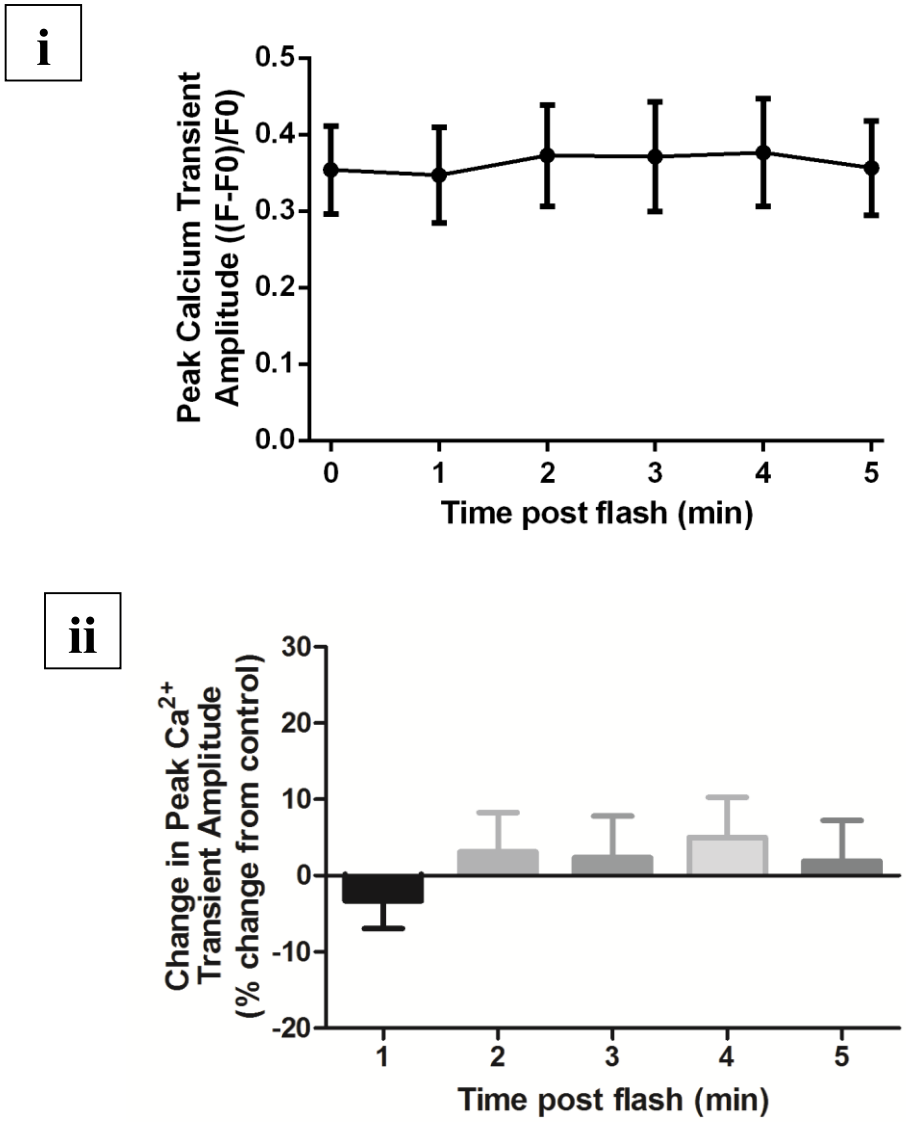


Figure 3.20 (i) and (ii): Atrial Calcium Transient Response to NAADP in the Presence of Ned-19

Summary graphs to show peak calcium transient amplitude (i) and percentage change in peak value (ii) in response to NAADP photorelease at time 0, over the course of a 5 min experiment (n=7). Data are presented as mean±SEM. ANOVA analysis did not identify a significant effect of NAADP on calcium transient amplitude in the presence of Ned-19 ($P > 0.05$, One-way ANOVA). All data were recorded from atrial myocytes patched in the whole-cell configuration, with calcium dye (Fluo5F, 100 μM) and caged NAADP (5 μM) applied via the patch pipette. Cells were stimulated to fire action potentials at 1 Hz and all experiments were carried out at 35±2 ºC.

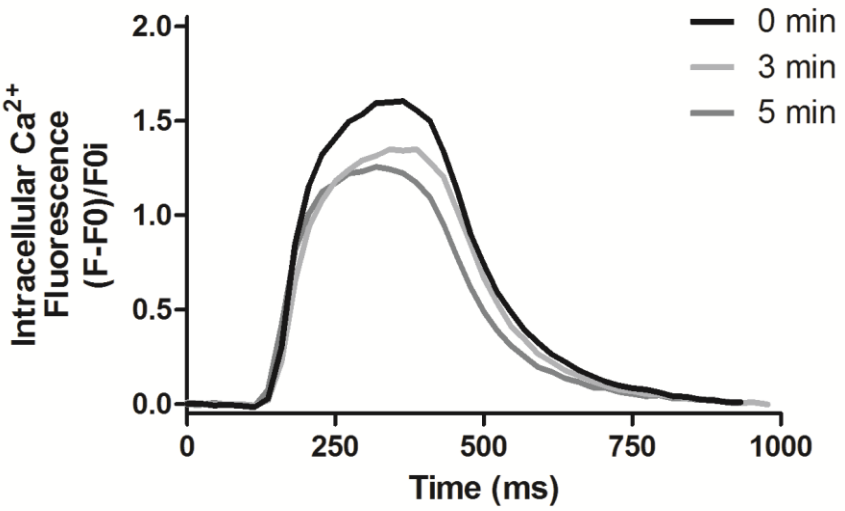


Figure 3.21: Representative trace to show the effect of NAADP photorelease in the presence of Ned-19 in a ventricular myocyte

Representative trace to show calcium transients recorded from an isolated guinea pig ventricular myocyte during a photorelease experiment in which NAADP (1.5 μM caged compound) was released into the cytosol in the presence of Ned-19 (1 μM). Ned-19 had been allowed to equilibrate within the cell for at least 10 min after patch rupture to achieve the whole-cell configuration. Each trace represents the average of at least 8 transients recorded at the appropriate timepoint after UV photorelease (time given in min).

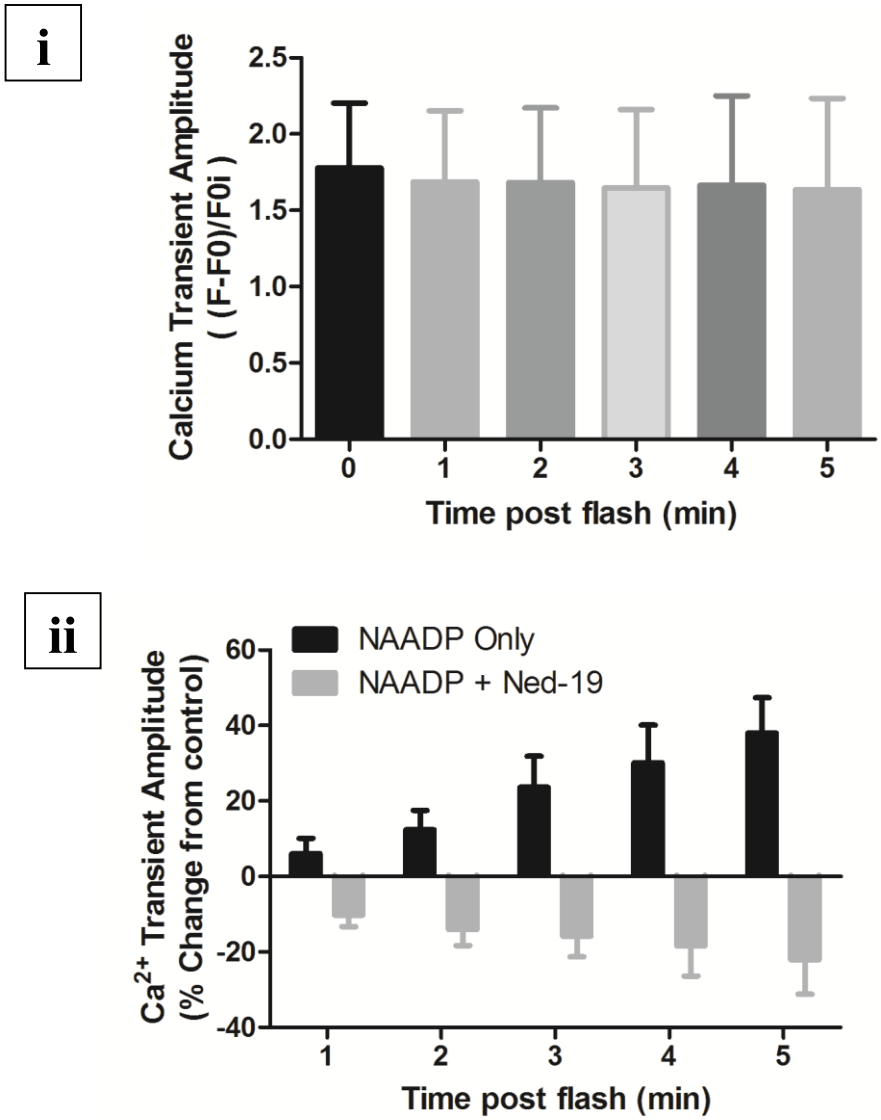


Figure 3.22 (i) and (ii): The effect of NAADP photorelease in the presence of Ned-19 on calcium transient amplitude in ventricular myocytes

Summary bar graphs to show the effect of NAADP on calcium transient amplitude in isolated cardiac guinea pig ventricular myocytes when photoreleased in the presence of 1 μM Ned-19. Data are presented as:

(i) Peak calcium transient amplitude measured from the F/F0 signal

(ii) Percentage change in calcium transient amplitude over time during photorelease in the presence of Ned-19 compared with the response seen to photorelease of NAADP alone.

Data are presented as mean±SEM. No effect of NAADP on calcium transient amplitude was observed when photorelease was carried out in the presence of Ned-19.

.

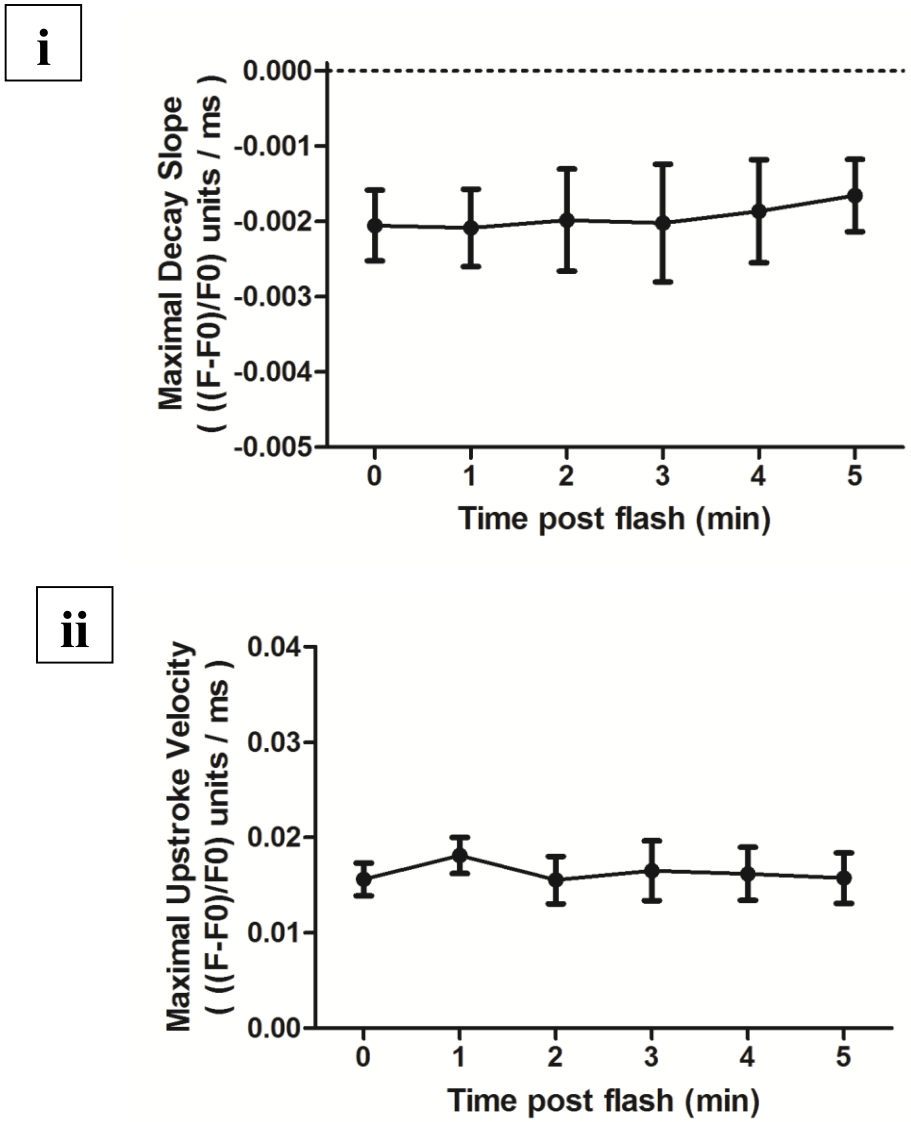


Figure 3.23 (i) and (ii): Lack of effect of NAADP on calcium transient upstroke and decay velocities in the presence of Ned-19, atrial myocytes

Summary line graphs to illustrate the lack of effect of NAADP on calcium transient (i) decay and (ii) upstroke velocities when photoreleased in the presence of the NAADP-receptor antagonist Ned-19. Data are presented as mean±SEM. Both parameters $P > 0.05$, separate One way ANOVAs with repeated measures, n=7. Data are presented as maximal velocity achieved during the appropriate phase of the calcium transient in F/F0. Each n-number at each timepoint represents the average of at least 8 transients, stimulated via the patch pipette at a rate of 1 Hz.

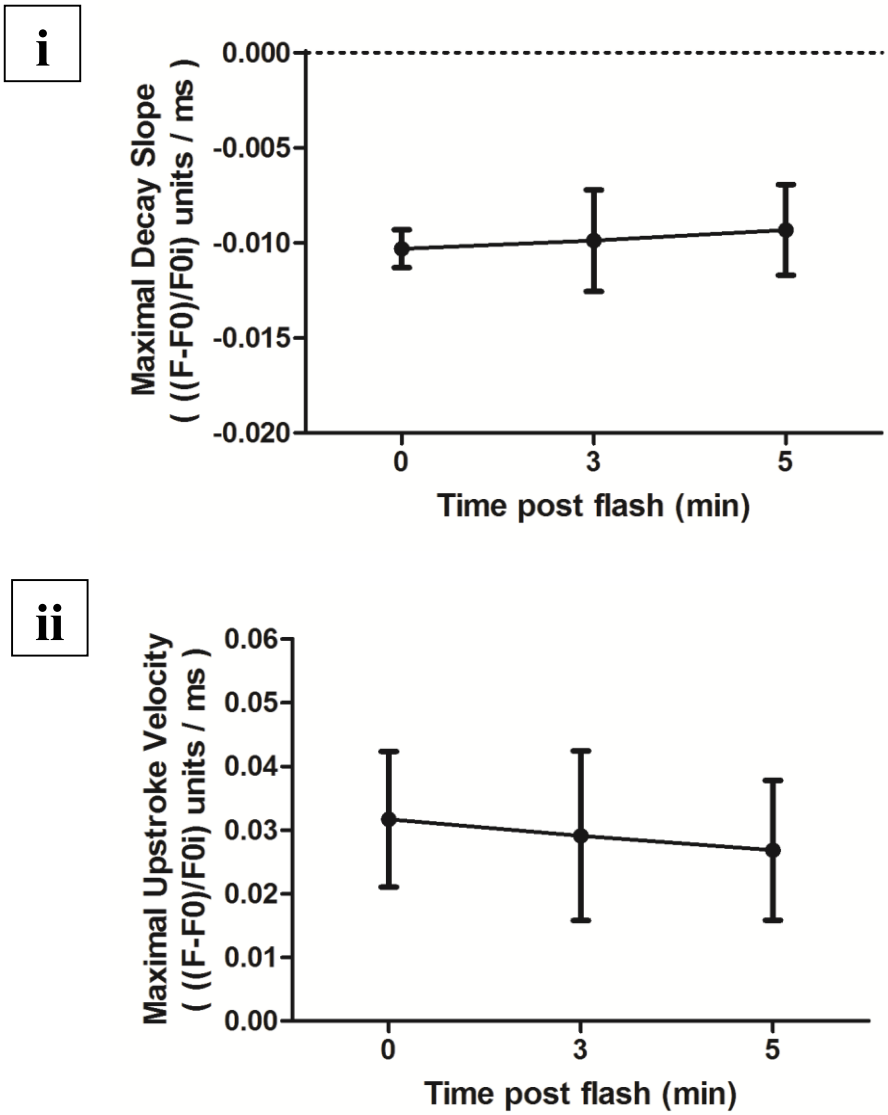


Figure 3.24 (i) and (ii): Lack of effect of NAADP on calcium transient decay and upstroke velocities in the presence of Ned-19, ventricular myocytes

Summary line graphs to show the absence of change in calcium transient (i) decay and (ii) upstroke velocities during NAADP photorelease in the presence of the NAADP-receptor antagonist Ned-19 in guinea pig cardiac ventricular myocytes. Data are presented as mean±SEM. Data are maximal velocity achieved during the appropriate phase of the calcium transient in F/F0. Each n-number at each timepoint represents the average of at least 8 transients, stimulated via the patch pipette at a rate of 1 Hz.

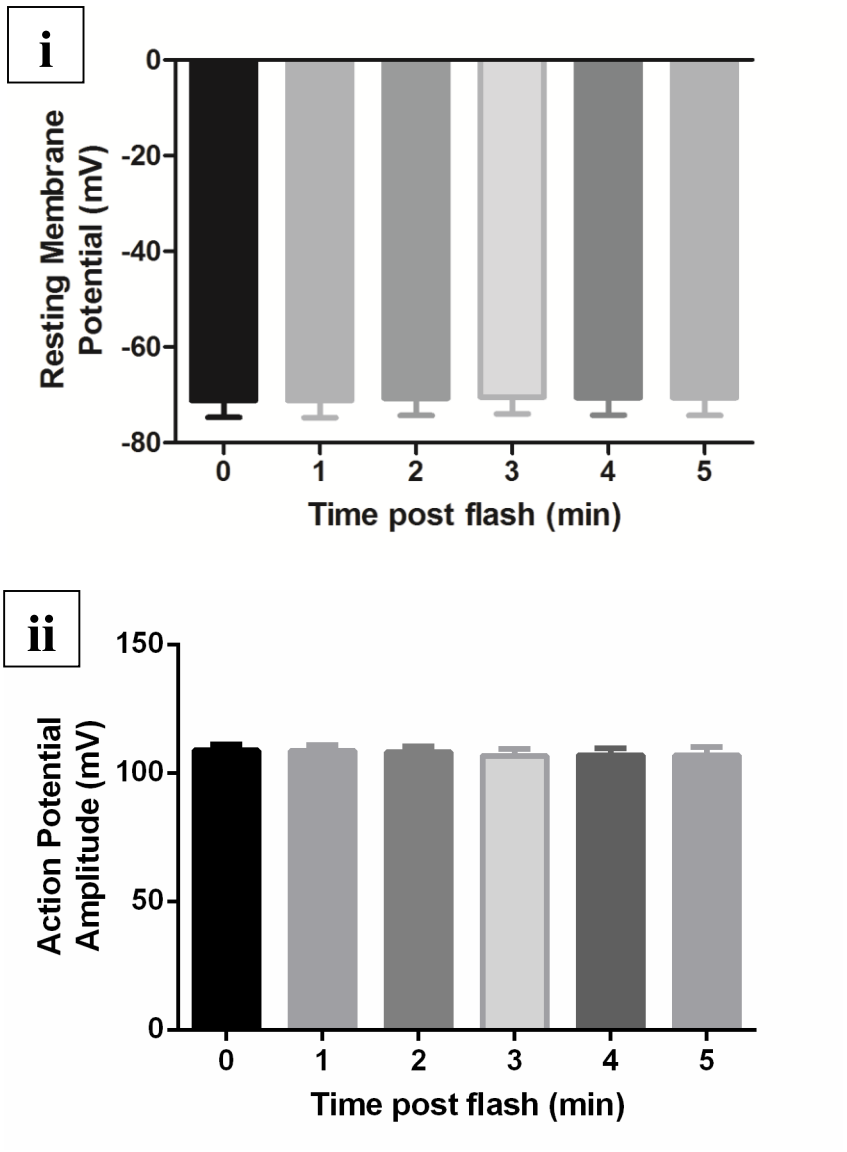


Figure 3.25 (i) and (ii): Stability of action potential parameters during NAADP photorelease in the presence of Ned-19

Bar graphs to show the lack of effect of NAADP on (i) resting membrane potential and (ii) action potential amplitude over the course of 5 min when photoreleased in the presence of Ned-19 (both $P > 0.05$, separate One-way ANOVAs with repeated measures, n=7). Data are presented as raw figures and are mean±SEM.

3.3.4 Intact CaMKII signalling is essential to the actions of NAADP

Previous evidence from our laboratory supported the two-pool model for the actions of NAADP, whereby NAADP releases calcium from the acidic stores which is taken up by the SR, increasing SR calcium release and the gain of CICR (Macgregor *et al.*, 2007a, Collins *et al.*, 2011). Question marks remained, however, as to whether such a gradual, large and prolonged increase in calcium transient amplitude could be achieved solely by the release of calcium from acidic stores.

Recent literature has not been able to confirm whether the postulated calcium release channel opened by NAADP, TPC2, is truly a calcium channel. Pitt *et al*. (2010), utilising bilayer studies, reported TPC2 channels to be Ca^{2+}-selective and respond to NAADP on the cytosolic face of the channel by an increase in open probability. Studies employing vacuolin, to selectively enlarge acidic vesicles and allow electrophysiological recordings directly from the acidic stores, have concluded that TPC2 is a calcium-selective channel responsive to NAADP (Schieder *et al.*, 2010) or that TPC2 is in fact a sodium-selective channel responsive to the endolysosome-specific phosphoinositol PI(3,5)P2 (Wang *et al.*, 2012).

We postulated that CaMKII would be the most likely mechanism to account for amplification between the lysosome and SR, if this were taking place. To test this hypothesis, UV photorelease of NAADP was carried out in guinea-pig atrial and ventricular myocytes during superfusion of KN93, a cell-permeable inhibitor of CaMKII, and in the presence of AIP, a peptide inhibitor of CaMKII, respectively.

KN93 was superfused across atrial myocytes for 5 min before NAADP photorelease in order to allow complete inhibition of CaMKII. A representative trace to show the

effect of superfusion, in the absence of stimulation by NAADP, can be seen in Figure 3.26.

Superfusion of atrial myocytes with KN93 (1 μM) caused no change in the overall calcium transient amplitude but did lengthen the transient significantly. Calcium transient amplitude was not affected over the course of 5 min KN93 superfusion, maximum change 11±7% ($P > 0.05$, One-way ANOVA with repeated measures, n=6). Calcium transient duration, defined as time taken to reach 90% calcium transient recovery, was significantly prolonged by superfusion of KN93 ($P < 0.05$, One-way ANOVA with repeated measures, n=6). Summary bar graphs to illustrate the effect of 1 μM KN93 on calcium transients in atrial myocytes is presented in Figure 3.27.

Action potential data collected during superfusion of KN93 is summarised in Figure 3.28. Analysis revealed a small but significant decrease in action potential amplitude ($P < 0.05$, One-way ANOVA with repeated measures, n=6) reaching a maximum of 3±1% less than control 3 min after the onset of superfusion. This was accompanied by a small but significant hyperpolarisation in resting membrane potential ($P < 0.05$, One-way ANOVA with repeated measures, n=6) which was maximal 4 min after switching to KN93 (2±1% change). These values are not considered to be of physiological importance. Action potential duration was unchanged over the course of 5 min KN93 superfusion ($P > 0.05$, One-way ANOVA with repeated measures, n=6).

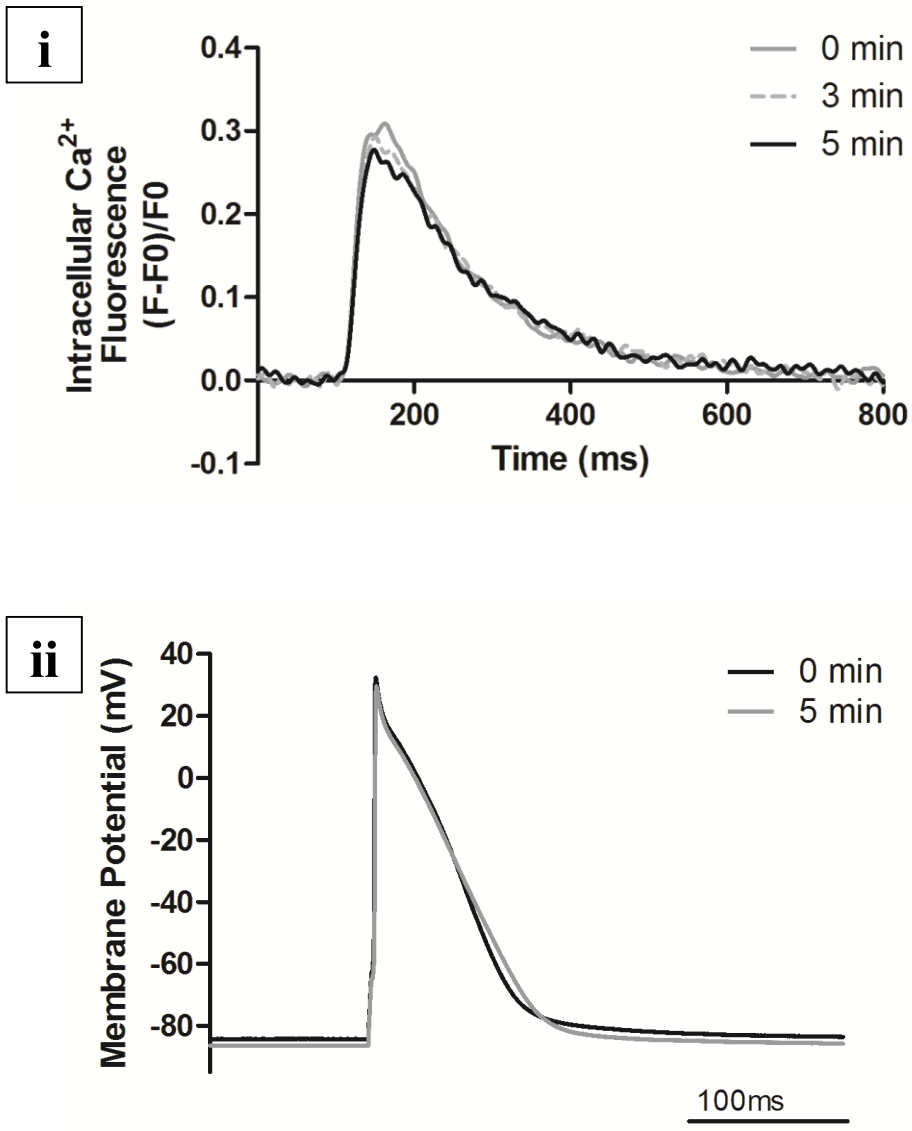


Figure 3.26 (i) and (ii): Representative traces to show the effect of KN93 on calcium transients and action potentials in atrial cardiomyocytes

Representative traces to show the effect of 5 min of 1 μM KN93 superfusion on isolated guinea pig atrial cardiomyocytes:

(i) Calcium transients, as measured by Fluo5F fluorescence, presented as F/F0

(ii) Action potentials

Atrial myocytes were patched in the whole-cell configuration with patch solution containing Fluo5F at 100 μM and caged NAADP at 5 μM in preparation for photorelease. Cells were stimulated to fire action potentials at a rate of 1 Hz via the patch pipette and maintained at a temperature of 35±2°C.

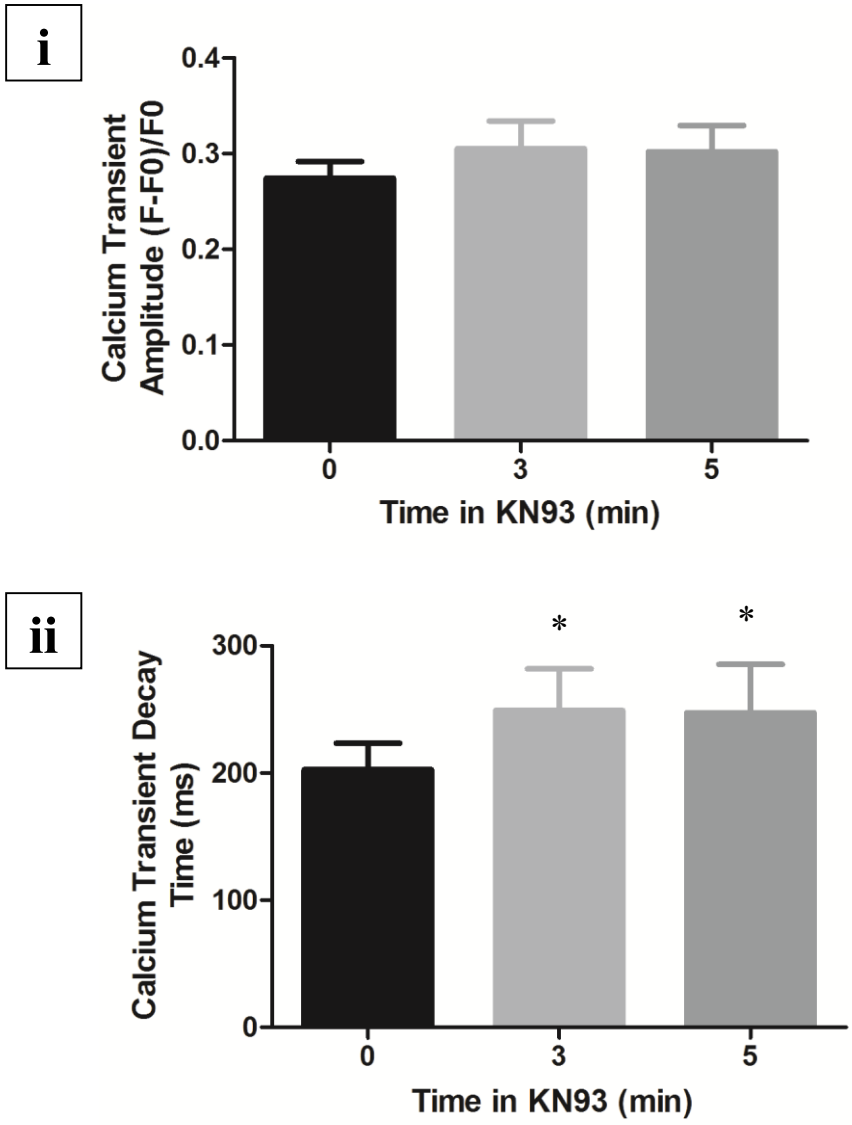


Figure 3.27: The Effect of KN93 Superfusion on Calcium Transients

(i) Summary bar graph to show calcium transient amplitude, measured as peak F/F0 value attained, during the course of 5 min from switch to1 µM KN93. A small but not statistically significant increase in calcium transient amplitude was observed ($P > 0.05$, One-way ANOVA with repeated measures, n=6).

(ii) Summary bar graph to illustrate calcium transient lengthening during KN93 superfusion. One-way ANOVA with repeated measures indicated a significant lengthening in calcium transient, measured as time taken to reach 90% recovery, over the course of 5 min ($P < 0.05$, n=6). This reached a maximal change of 20±11%. * denotes significant increase from 0 min by Dunnett's post-hoc testing

All data are presented as mean±SEM.

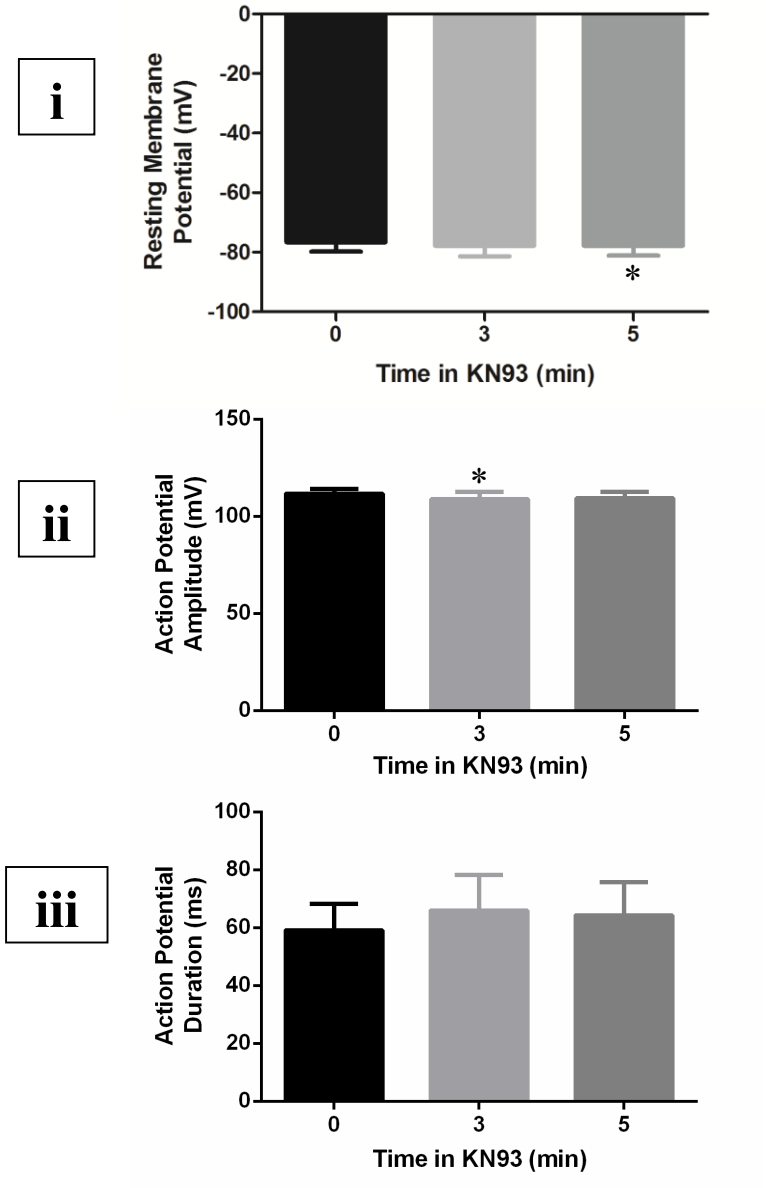


Figure 3.28 (i), (ii) and (Iii): The effect of KN93 superfusion on action potential parameters

Data presented to show action potential parameters as raw data recorded over the course of 5 min KN93 superfusion at 1 µM and are shown as mean±SEM. * denotes significant difference when compared with parameter in PSS (0 min) by Dunnett's post-hoc testing

(i) Cells exposed to KN93 underwent a slight but significant hyperpolarisation ($P < 0.05$, One-way ANOVA with repeated measures, n=6) which reached a maximum of 2±1%

(ii) Action potential amplitude observed was slightly but significantly smaller after 5 min KN93 superfusion ($P < 0.05$, One-way ANOVA with repeated measures, n=6) which reached a maximum change of 3±1%

(iii) Action potential duration was not significantly altered by KN93 ($P > 0.05$, One-way ANOVA with repeated measures, n=6)

Five minutes after the onset of KN93 superfusion, a flash of UV light was applied to release NAADP into the cell. A representative trace to show the effect of NAADP photorelease in the presence of KN93 on action potential and calcium fluorescence signals can be found in Figure 3.29. After KN93 superfusion (1 μM), NAADP photorelease (5 μM caged compound) caused no change in calcium transient amplitude over the course of 5 min ($P > 0.05$, One-way ANOVA with repeated measures, n=6). These data are presented in Figure 3.30.

During the same photorelease experiments described above, no significant acceleration of calcium transient upstroke or decay velocity was observed ($P > 0.05$, One-way ANOVA with repeated measures in both instances, n=6). Summary graphs to illustrate the absence of any effect of NAADP under these conditions are shown in Figure 3.31.

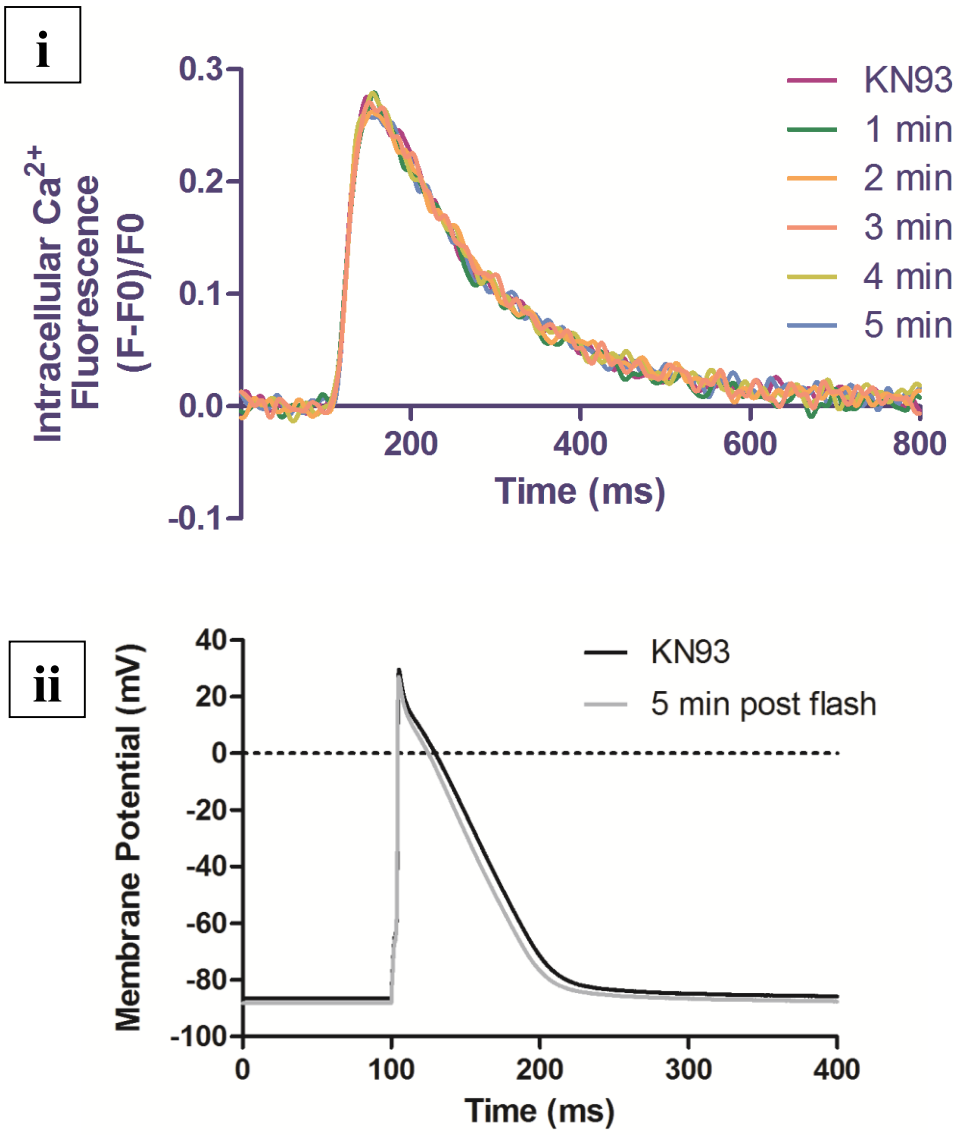


Figure 3.29 (i) and (ii): Representative trace to show the effect of NAADP photorelease in the presence of KN93

Representative traces to show response to photorelease of NAADP (5 µM caged NAADP) in the presence of the CaMKII inhibitor KN93 (1 µM) in both (i) calcium transients and (ii) action potentials over the course of 5 min. Traces presented at each timepoint are the average of at least 8 transients/action potentials, stimulated at a rate of 1 Hz via the patch pipette. Fluorescence signals are given as fluo5F (100 µM in the patch pipette) fluorescence normalised to diastolic fluorescence (F/F0).

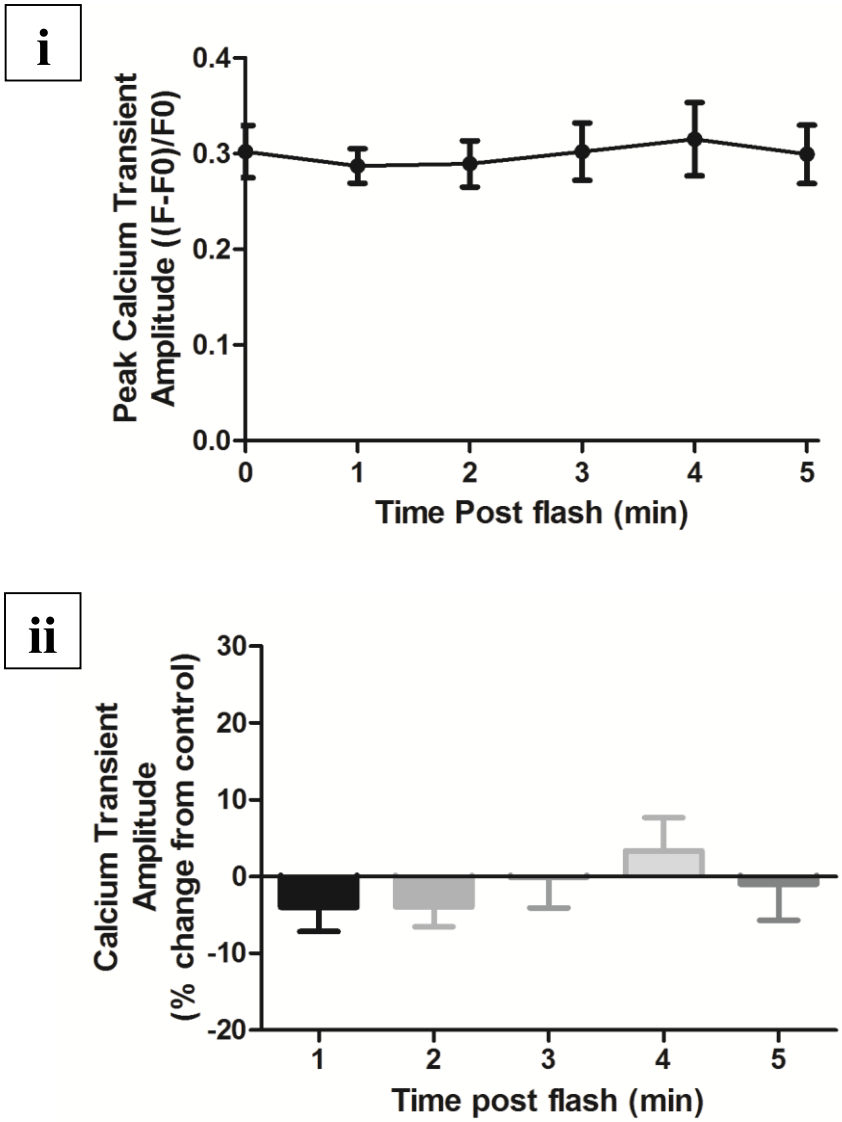


Figure 3.30: Photorelease of NAADP in the Presence of KN93

Summary graphs to show the absence of change in calcium transient amplitude, defined as peak F/F0, after photorelease of NAADP (5 μM caged NAADP) in the presence of KN93 (1 μM) in guinea pig isolated cardiac atrial myocytes. Data are presented as:

(i) Raw fluorescence normalised to diastolic calcium, F/F0

(ii) Percentage change in peak F/F0 amplitude as measured against transients recorded after 5 min of KN93 exposure

Data are presented as mean±SEM. No change in calcium transient amplitude was observed over time ($P > 0.05$, One-way ANOVA with repeated measures, n=6).

All cells were patched in the whole-cell configuration, from which Fluo5F calcium dye (100 μM) and caged NAADP (5 μM) were suffused into the cell. Cells were stimulated at 1 Hz via the patch pipette and maintained at 35±2°C. KN93 was superfused, dissolved in PSS, at a concentration of 1 μM.

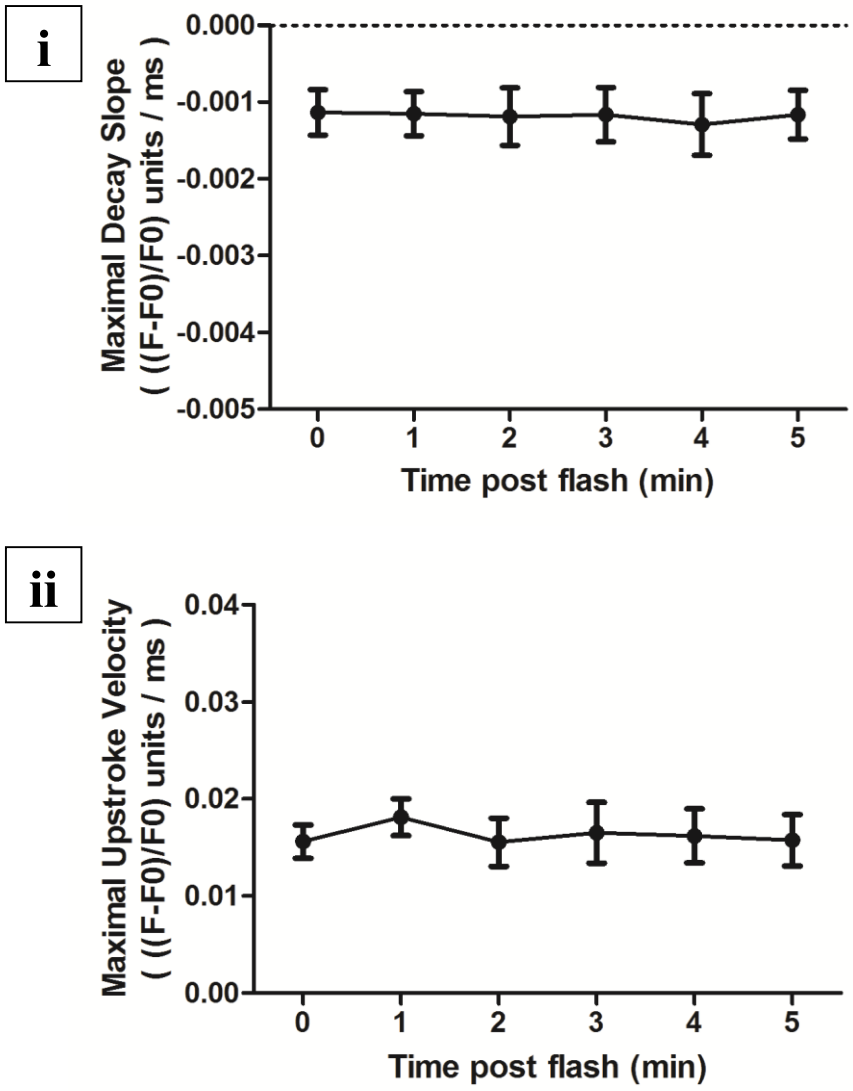


Figure 3.31 (i) and (ii): Lack of effect of NAADP on calcium transient decay and upstroke velocities in the presence of KN93

Summary line graphs to illustrate paucity of change in calcium transient decay and upstroke velocities measured after photorelease of NAADP in the presence of KN93 in isolated guinea pig ventricular myocytes (both $P > 0.05$, One-way ANOVA with repeated measures, n=6). Data are presented as mean±SEM. Data are given as maximally achieved velocity during recovery and upstroke of the calcium transient, analysed using an average of at least 8 transients recorded at each timepoint from each n-number included.

In ventricular myocytes AIP, a peptide inhibitor of CaMKII, was applied via the patch pipette at a concentration of 1 μM together with fluo-5F calcium dye and caged NAADP. After satisfactory seal formation and patch rupture, the preparation was stimulated at 1 Hz for 15 min to allow first equilibration of the patch solution, and then time for the inhibitor to fully abolish CaMKII activity. A representative trace to show the effect of NAADP in the presence of AIP can be seen in figure 3.32.

In the presence of AIP, photorelease of NAADP had no significant effect on calcium transient amplitude ($P > 0.05$, One-way ANOVA with repeated measures, n=6). Bar graphs to show the amplitude of calcium transients over time and a direct comparison of the effect of NAADP in the presence and absence of AIP is shown in figure 3.33.

Consistent with results presented in atrial myocytes, and observations made during photorelease of NAADP in the presence of Ned-19 in ventricular cells, no change in calcium transient decay velocity could be discerned over time during these experiments ($P > 0.05$, One-way ANOVA with repeated measures, n=6). Calcium transient upstroke velocity was also unchanged over the course of 5 min after photorelease of NAADP ($P > 0.05$, One-way ANOVA with repeated measures, n=6). Calcium transient velocity data recorded from guinea pig ventricular myocytes are presented in Figure 3.34.

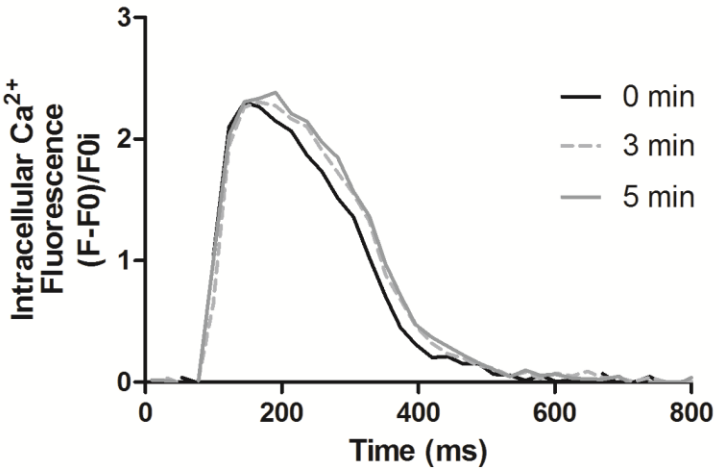


Figure 3.32: Representative trace to show the effect of NAADP on calcium transients in a ventricular myocyte in the presence of AIP

Representative trace to show calcium transients recorded before and then 3 and 5 min after photorelease of NAADP (1.5 μM) in the presence of the peptide inhibitor of CaMKII, AIP (1 μM). Both compounds, together with the calcium dye Fluo5F (100 μM) were applied through the patch pipette. Cells were stimulated at a rate of 1 Hz through the patch pipette and maintained at a temperature of 34±2°C throughout.

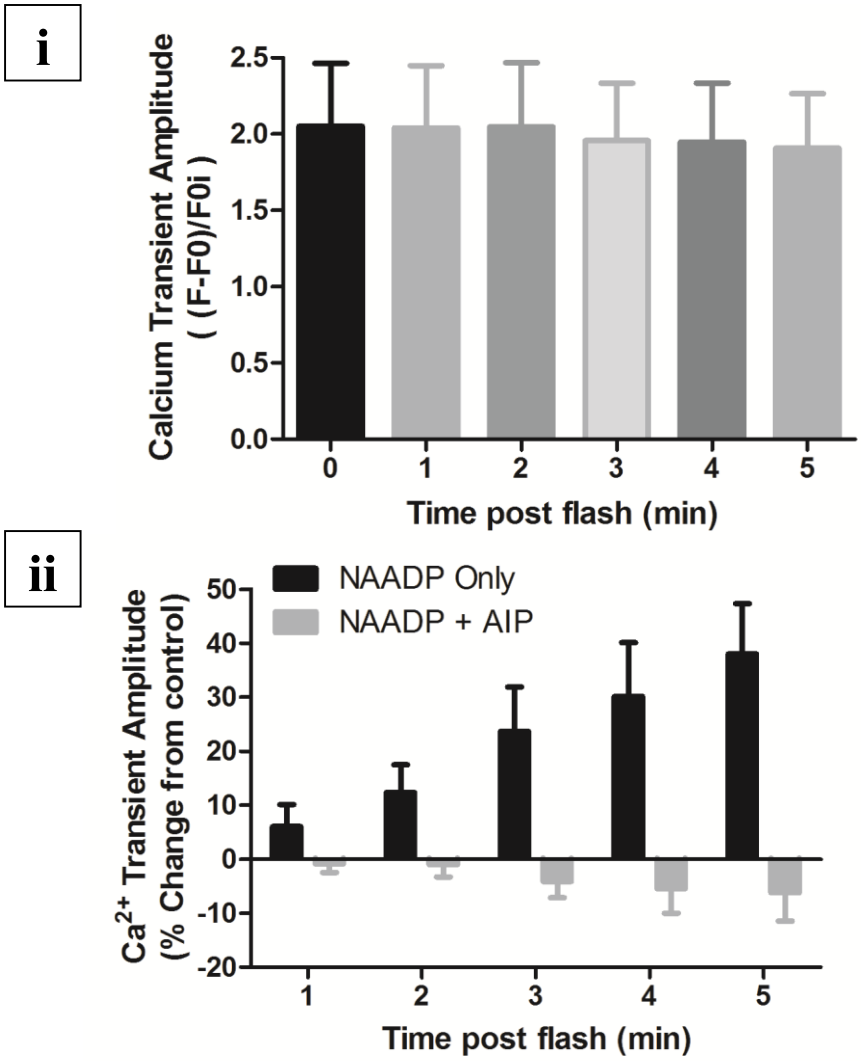


Figure 3.33 (i) and (ii): The effect of NAADP on calcium transient amplitude in ventricular myocytes in the presence of AIP

Photorelease of NAADP in the presence of AIP in guinea pig ventricular myocytes had no significant effect on calcium transient amplitude, defined as peak F/F0 during each stimulated transient ($P > 0.05$, One-way ANOVA with repeated measures, n=6). Data are presented as:

(i) Peak transient amplitude

(ii) Change in calcium transient amplitude from recordings made before photorelease. The effect of NAADP photorelease in the absence of any inhibitors is also presented for comparison.

All data were collected from isolated guinea pig ventricular cardiomyocytes patched in the whole cell configuration, through which Fluo5F calcium dye (100 µM), caged NAADP (1.5 µM) and AIP (1 µM) were administered. Cells were stimulated to fire at a rate of 1 Hz via the patch pipette and data collected at each timepoint represent the average of at least 8 transients per cell (1 cell = n of 1). Experiments were carried out at 34±2°C. Data are presented as mean±SEM.

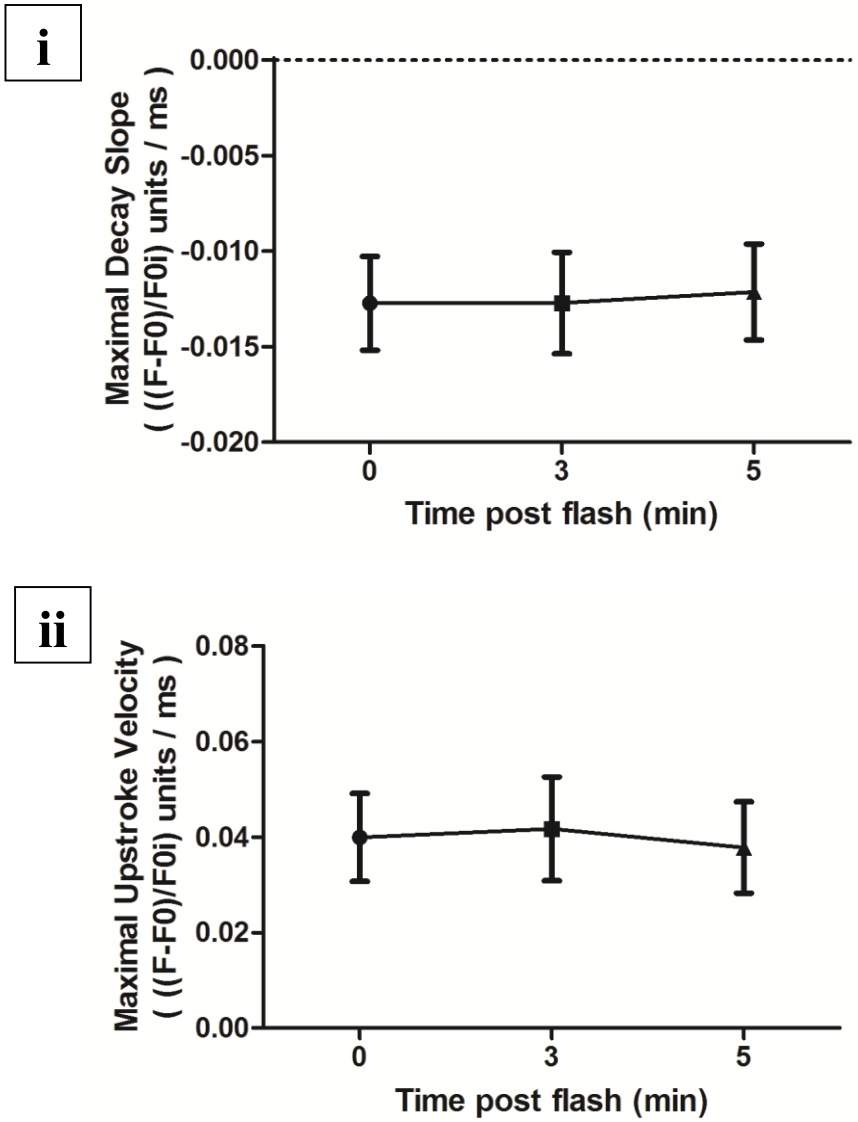


Figure 3.34: Lack of effect of NAADP on calcium transient decay and upstroke velocities in the presence of AIP

Photorelease of NAADP (1.5 µM caged compound) in the presence of AIP (1 µM) had no significant effect on calcium transient decay velocity or upstroke velocity, defined as the maximal achieved velocity during the appropriate phase of the transient (both $P > 0.05$, separate One-way ANOVAs with repeated measures, n=6). Data are presented as mean±SEM.

3.3.5 Consistent effects of UV photorelease protocol in cardiomyocytes

Two effects were noted over the course of these experiments which appear to be artefacts of the recording systems and UV photorelease protocols used. Firstly, across all photorelease experiments carried out on ventricular myocytes using the Rapp/Andor system there was a significant increase in diastolic calcium signal over time. This occurred regardless of the inclusion or exclusion of caged NAADP and inhibitors under study (Figure 3.35). In a further set of NAADP photorelease experiments carried out on guinea pig ventricular myocytes using the PMT system, unchanged from that used to collect atrial myocyte data, no significant increase in diastolic calcium was observed over the course of 5 min despite a 42±11% increase in calcium transient amplitude. This dataset is presented in Figure 3.36.

Finally, shortening of the action potential duration was a consistent feature of atrial myocyte photorelease experiments (Figure 3.37). Interestingly, cells superfused with KN93 did not exhibit a significant change in action potential duration before exposure to UV flash. Further, this shortening was apparent in control experiments, in which no caged compound had been added to the patch solution. Taken together, these data suggest that reduction in action potential duration is an artefact of the experimental protocol in these cells.

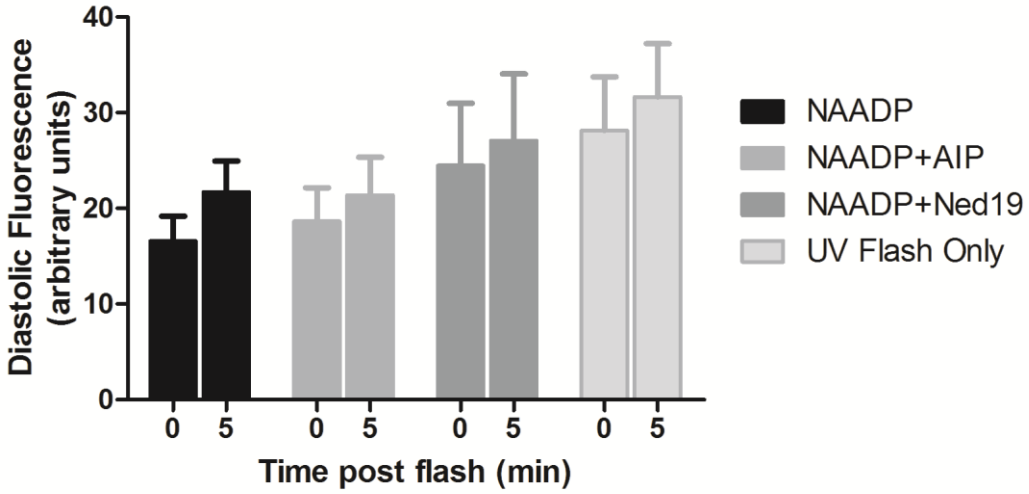


Figure 3.35: The effect of NAADP, in the presence of various inhibitors, upon diastolic fluorescence in ventricular myocytes

Bar graphs to show diastolic fluorescence (arbitrary units) measured from guinea pig ventricular myocytes before and 5 min after UV flash under all conditions presented in this thesis. Data are presented as mean±SEM. A significant increase was noted under all conditions over time ($P < 0.05$, separate One-way ANOVAs with repeated measures, n-numbers as presented in chapter text).

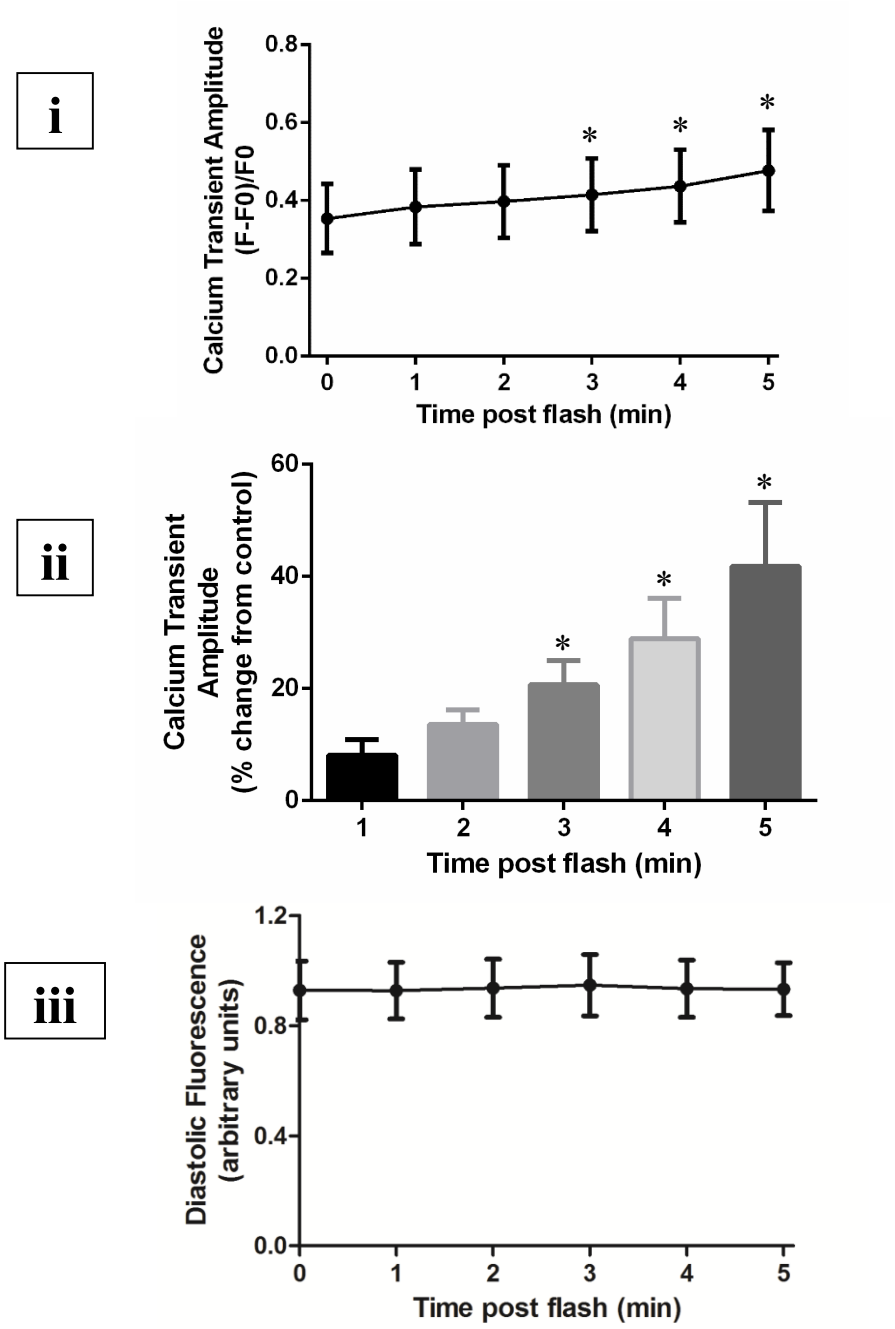


Figure 3.36 (i), (ii) and (iii): NAADP photorelease in ventricular myocytes using a different photorelease system

The effect of photorelease of NAADP on isolated guinea pig ventricular cells measured using the Cairn system. A significant increase in calcium transient amplitude (i, raw data, ii, percentage change) was observed over the course of 5 min ($P < 0.05$, One-way ANOVA with repeated measures, n=6) but NAADP had no significant effect on measured diastolic fluorescence (iii, $P > 0.05$, One-way ANOVA with repeated measures, n=6). Data are presented as mean±SEM. * denotes significant difference from pre-flash value as evaluated by Dunnett's post-hoc testing

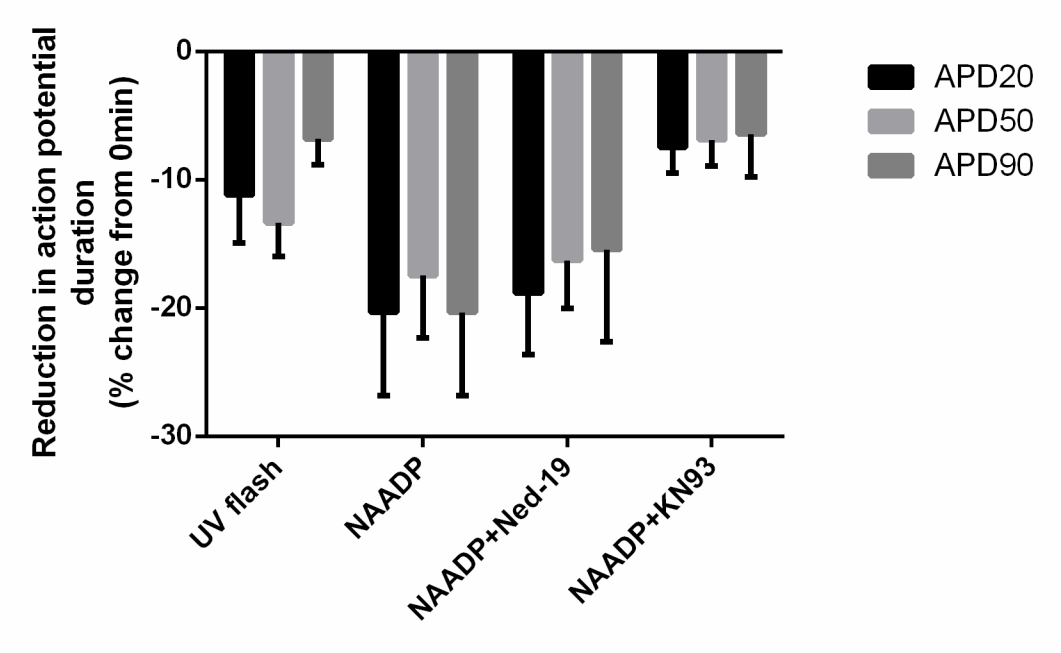


Figure 3.37: The effect of NAADP, in the presence of various inhibitors, upon action potential duration in atrial myocytes

Bar graph to present the change in action potential duration at the three durations measured, comparing the value at 5 min with control. A significant reduction in APD was noted in all conditions and for all durations measured ($P < 0.05$, separate One-way ANOVAs with repeated measures, n-numbers as quoted in thesis text). Data are presented as mean±SEM.

3.4 DISCUSSION

The data presented in this chapter provide the first evidence that functional CaMKII is required for the actions of NAADP in cardiac myocytes. This is also the first time that the NAADP receptor antagonist Ned-19 has been used to inhibit responses to NAADP photorelease in cardiac atrial myocytes, confirming once again the utility of this compound for inhibition of the NAADP pathway. An updated version of our working model for the NAADP pathway in cardiac myocytes in presented at the end of the next chapter, including both the amplification mechanisms discussed here and the physiological role of the NAADP pathway discussed in Chapter 4 (see Figure 4.10).

The actual concentration of NAADP released during experiments in this chapter is very difficult to ascertain, since this depends both on the intensity and timecourse of UV illumination and the efficiency of uncaging within the NAADP batch under study (Ellis-Davies, 2007). Previous experiments carried out in our laboratory utilised caged cAMP to estimate fractional release in the Cairn system, used for atrial myocyte work, and suggested an uncaging rate of 1% for a single high-intensity flash, however this cannot be assumed to be the same for the Rapp system. These experiments, therefore, should be considered as an illustration of the functional pathway and its effector as opposed to a quantitative analysis of the sensitivity of cardiac myocytes to NAADP.

The observation that CaMKII is required for the actions of NAADP in cardiac myocytes raises the question of what downstream effectors are responsible for the translation of CaMKII stimulation into an increase in the cellular calcium transient.

Previous research into NAADP signalling have suggested a range of mechanisms by which calcium released from the acidic store might interact with the reticular store, including increased calcium uptake into the reticular stores (Collins *et al*., 2011) and enhancing the sensitivity of RyRs to cytosolic Ca^{2+} (Chini, 2002).

CaMKII is known to be associated with L-type calcium channels within cardiac myocytes, mediating I_{CaL} facilitation. The responses of the NAADP pathway, however, are localised to the SR and several lines of evidence have led us to believe that the effects of NAADP and, conversely, of CaMKII inhibitors to abolish NAADP responses are unlikely to stem from changes at the L-type channel. Previous studies have shown that photorelease of NAADP in has no effect on I_{CaL} over a similar timecourse to that used in these studies (Collins *et al.*, 2011). Further, photorelease of NAADP was always initiated after the cell had reached a steady state in terms of any response to CaMKII inhibition (5 min superfusion for KN93 and 15 min equilibration for AIP). In atrial myocytes CaMKII is situated in striated bands co-localising with ryanodine receptors but is not strongly labelled at or near the cell surface (Collins and Terrar, 2012). Finally, as will be shown in the next chapter, the response of I_{CaL} to β-adrenergic stimuli is unchanged in the presence of NAADP pathway inhibitors, whilst the pathway does appear to be involved in this response at the level of the calcium transient. Taken together, these data suggest that the major effectors of NAADP pathway signalling beyond the lysosome are found at the SR and that changes in surface calcium entry do not form part of these responses.

It is not surprising that lengthening of the calcium transient was seen on switch to KN93 as this would reflect the inhibition of SERCA caused by a reduction in

CaMKII-mediated phospholamban phosphorylation on exposure to the inhibitor. It is not possible to make the same statement regarding the use of AIP as the patch-loading method did not allow for comparison of signals before and after CaMKII inhibition in the same myocyte.

In cardiac myocytes, NAADP has been observed to increase SR calcium content as measured by caffeine spritz (Macgregor *et al.*, 2007a, Collins *et al.*, 2011) and it would be natural to suggest, therefore, that CaMKII activation leads to phosphorylation at the Thr17 site of phospholamban. The observation that NAADP photorelease causes a significant acceleration of calcium transient decay which is not seen in control cells, nor during NAADP photorelease in the presence of Ned-19 or KN93/AIP, is in support of this as a possible mechanism by which NAADP could increase SR calcium content which deserves further investigation.

The observation that NAADP photorelease leads to a significant acceleration of the calcium transient upstroke, which is abolished during control, Ned-19 or KN93/AIP experiments, also deserves further consideration. An increase in SR calcium content would be expected to accelerate the upstroke of the calcium transient, as an increase in SR $[Ca^{2+}]_i$ would act to increase RyR open probability (Spencer and Berlin, 1995, Xu and Meissner, 1998). It is worth noting, however, that CaMKII is known to be associated with ryanodine receptors in cardiac atrial and ventricular myocytes (Collins and Terrar, 2012) and that CaMKII-mediated phosphorylation of RyR has been suggested to play a central role in the effects of β-adrenoceptor stimulation (Li *et al.*, 1998). Further experiments are required to investigate the downstream targets of NAADP-mediated CaMKII activation from the aspects of both spatial localisation

and molecular targeting before the driving factor(s) in NAADP-mediated calcium signalling can be confirmed.

During the course of atrial action potential analyses presented in this chapter, it was apparent that there was a significant reduction in action potential duration after photorelease of NAADP. However, this reduction is not statistically different from the shortening of the action potential observed in control experiments and when NAADP was photoreleased in the presence of either Ned-19 or KN93. It should not be concluded from these experiments, therefore, that action potential shortening is an effect of NAADP. It is possible that the use of whole-cell patch for delivery of compounds to the cell would cause a shortening of the action potential through dialysis of cAMP. If this were the case, it is unlikely that such an effect would provide an explanation for the effects seen during NAADP photorelease, as a reduction in cAMP would tend to reduce calcium transient amplitude and make the results seen here less likely. No reduction in action potential duration was noted during 5 min superfusion with KN93, and this may lead to the suggestion that APD shortening was in fact a response to UV flash. However, KN93 is known to have a significant blocking effect on a range of voltage-gated potassium channels, including hERG (Rezazadeh *et al.*, 2006) and the most likely explanation is that the maintenance of APD on switch to KN93 represents a balance between the forces of dialysis and potassium channel block until sufficient cAMP has been lost from the cell to begin manifesting as APD shortening.

The data presented in this chapter, suggesting a reliance on CaMKII-mediated amplification of NAADP-mediated Ca^{2+} signals, provide one possible reason why a specific NAADP-mediated Ca^{2+} release has not been visualised in cardiac myocytes to date. There is, however, precedent for a small change in diastolic calcium in ventricular myocytes over the course of the response to NAADP (Macgregor *et al.*, 2007a), though experiments performed during this thesis did not consistently support this observation. In sea urchin eggs, the model system for studying NAADP, it has already been noted that application of NAADP elicits a near-immediate calcium spike which can be attributed directly to release of calcium from lysosomal stores (Churchill and Galione, 2001a).

Electron microscopy studies have suggested that cardiac myocytes contain only around 0.01% lysosomes by volume (Frenzel *et al.*, 1988), whilst a combination of Ca^{2+}- and pH-sensitive dyes have estimated lysosomal calcium concentration to be 500 μM in murine macrophages (Christensen *et al.*, 2002). Assuming a similar concentration of Ca^{2+} in cardiac lysosomes, if an NAADP signal distributed all of this stored calcium immediately throughout the cell then cell calcium would reach a maximum of 500 nM. Although this concentration is far lower than that achieved during the systolic calcium transient, which reaches significantly more than 1 μM, this level of cytosolic calcium increase should be visualised during calcium spark experiments and has not been reported. A pertinent further question, then, is whether all lysosomes respond to NAADP and how much calcium is released by each responding organelle. Do a subset of acidic stores express TPC2 or are there some stores tethered in the vicinity of the SR such that a small cellular release of Ca^{2+}

might cause local changes significant enough to activate CaMKII? In pulmonary vascular smooth muscle cells, calcium microdomains between lysosomes and ER have recently been proposed based on spatial proximity during an electron microscopy study (Nicolas Flameli, personal communication). In these cells, spatiotemporal modelling has previously suggested that such microdomains are capable of activating RyR3, which are more sensitive to cytosolic Ca^{2+} than the RyR2 expressed in cardiac SR, if the lyso-ER junctions are less than 50 nm in width (van Breemen *et al.*, 2013). Whether a similar situation can be predicted for junctions in cardiac myocytes activating CaMKII will require further investigation. The most important initial steps of this work will be to carry out imaging studies, both EM and immunocytochemistry-based, to address the question of whether such lyso-SR microdomains might exist in cardiac myocytes as well.

There are particular differences in the function(s) of NAADP between sea urchin oocytes and mammalian cardiac myocytes which are also of note in respect of the NAADP-mediated cytosolic Ca^{2+} spike or lack thereof. In oocytes the calcium signals under study represent a singular and finite process, signalling fertilisation. In cardiac myocytes, normal calcium signalling is cyclical and continues during the full lifetime of the organism. NAADP is known to bind irreversibly with its' receptor in sea urchin oocytes (Patel *et al.*, 2000), where these cells are unable to respond to further NAADP challenges for at least 25min after an initial response (Churchill and Galione, 2001b). In cardiac myocytes, the observation that bafilomycin (see next chapter) and GPN lead to decreases in cellular calcium transient amplitude in the absence of further intervention (Collins, 2009, Collins *et al.*, 2011) suggest that

cardiac myocytes maintain constant, endogenous NAADP activity, making a similar, prolonged ‘inactivation’ of the system unlikely. Whether this difference stems from reversibility of NAADP binding under the conditions of a cardiac lysosome or whether NAADP binding is permanent but occupies only a small percentage of receptors is yet to be determined. Maybe, then, it is to be expected that NAADP-mediated signals in these cells are more prolonged and/or less pronounced in the acute phase.

Whilst the data presented in this chapter are novel, further work is required to unequivocally establish CaMKII as part of the NAADP signalling pathway in cardiac myocytes. The next steps in this project will repeat the experiments presented above using calcium sparks as a measure of SR calcium handling, and further investigate the molecular targets of NAADP-mediated CaMKII activation.

4 NAADP SIGNALLING IS PHYSIOLOGICALLY-RELEVANT IN THE HEART

4.1 INTRODUCTION

The data presented in the previous chapter provide interesting insights into the intracellular signalling pathway which is activated by NAADP. That the pathway is functional in cardiac myocytes, however, does not establish that it plays a functional role in calcium handling during physiological or pathological processes.

The NAADP pathway has previously been implicated in β-adrenergic responses in the heart. Langendorff perfusion studies in guinea pig found that measured tissue levels of NAADP were raised from 0.22±0.03 to 0.34±0.04 nmol/mg of protein after infusion of the β-adrenoceptor agonist isoprenaline (Macgregor *et al.*, 2007a). In guinea pig atrial myocytes, osmotic lysis of the acidic calcium stores with GPN led to a significant reduction in calcium transient amplitude and a significant reduction in the magnitude of the subsequent response to β-adrenergic stimulation (Collins *et al.*, 2011).

NAADP is thought to stimulate calcium release through two-pore channels (Calcraft *et al.*, 2009). In sea urchin oocytes, three TPC isoforms have been shown to be functionally active (Ruas *et al.*, 2010). Mammals carry only two TPC genes (TPC1 and TPC2) and it has recently been shown that, cells isolated from TPC2 -/- mice show a significantly reduced calcium transient and contractile response to β-adrenergic stimulation with isoprenaline (W. Lin and E. Bolton, personal communication). Conversely, TPC1 -/- mice exhibit normal responses to NAADP-AM and to isoprenaline (Elson, 2011).

Taken together these data suggest that the NAADP pathway is activated during β-adrenergic stimulation, however measurements of the β-adrenergic response during inhibition of the pathway in genetically 'normal' ventricular myocytes have not previously been carried out.

The aims of this section of work were to establish whether the NAADP pathway plays a role during acute responses to beta-adrenergic stimulation and where this role may lie. We hypothesised that NAADP signalling forms a part of the acute cardiac β-adrenergic response and tested this by assessing the response to β-adrenergic stimulation in intact cells and those in which the NAADP pathway had been rendered inactive.

4.2 METHODS

Experiments in this chapter were carried out on isolated guinea pig atrial and ventricular myocytes. Cells were isolated using enzymatic digestion by retrograde perfusion followed by mechanical dissociation as described previously.

Investigations measuring calcium transients utilised the non-ratiometric calcium indicator Fluo5F. This was loaded into cells as the potassium salt at a concentration of 100 μM for ventricular recordings and via the cellular membrane in the –AM form for atrial experiments. Cardiac atrial myocytes were incubated with 3 μM Fluo5F-AM for 15 min at room temperature and PSS solution allowed to superfuse for 5 min before use in order to allow for complete de-esterification to occur within the cells. Cells were maintained at a temperature of 35±2°C during all experiments and stimulated to contract at a rate of 1 Hz using either field stimulation (atrial experiments) or via the patch pipette (ventricular work).

Fluo-5F-emmitted light was passed through a 520 nm long-pass filter and detected using a photomultiplier system (Cairn Research, Kent, UK). Photomultiplier signals were digitised using a Digidata 1200 and recorded using pClamp software. In order to remove stochastic noise inherent in such a high gain system, signals were filtered using a 100 Hz hardware filter and, before analysis digitally smoothed with a low-pass Gaussian filter.

During measurement of the L-type Ca^{2+} current, cells were patched in the whole cell configuration without the addition of a calcium fluorophore and I_{CaL} stimulated at a

rate of 0.2 Hz using a 200 ms duration, 40 mV depolarising voltage step from the holding potential of -40 mV.

All data are presented as mean±SEM. Statistical calculations were carried out using the Prism software, with Student's t-test or ANOVA used to investigate the differences between groups as appropriate. A result of $P < 0.05$ was considered to indicate a statistically significant difference.

4.3 RESULTS

4.3.1 NAADP signalling is constitutively active in atrial myocytes

Whilst NAADP clearly produced a pronounced effect within atrial myocytes, it was important to ascertain whether the system was physiologically relevant in atrial calcium modulation and what its function may be.

Bafilomycin, an inhibitor of the V-type H^+-ATPase, has been shown to abolish the effect of photoreleased NAADP to increase calcium transient amplitude in ventricular myocytes and also disrupted the punctate distribution normally seen on LysoTracker staining (Macgregor *et al.*, 2007a). It is thought that calcium is loaded into the acidic compartments by use of the proton gradient to drive calcium into the compartment, and that bafilomycin leads to a depletion of this store by removing this gradient for driving calcium entry by exchange.

Figure 4.1 (i) shows representative calcium transients from a field-stimulated atrial myocyte before and after superfusion with bafilomycin (100nM). Bafilomycin, in the absence of any further intervention, caused a 19±5% reduction in the amplitude of the stimulated atrial calcium transient ($P < 0.05$, Paired t-test, shown in figure 4.1 (ii)), suggesting that acidic-store-mediated calcium signalling is constitutively active in guinea pig cardiac atrial myocytes.

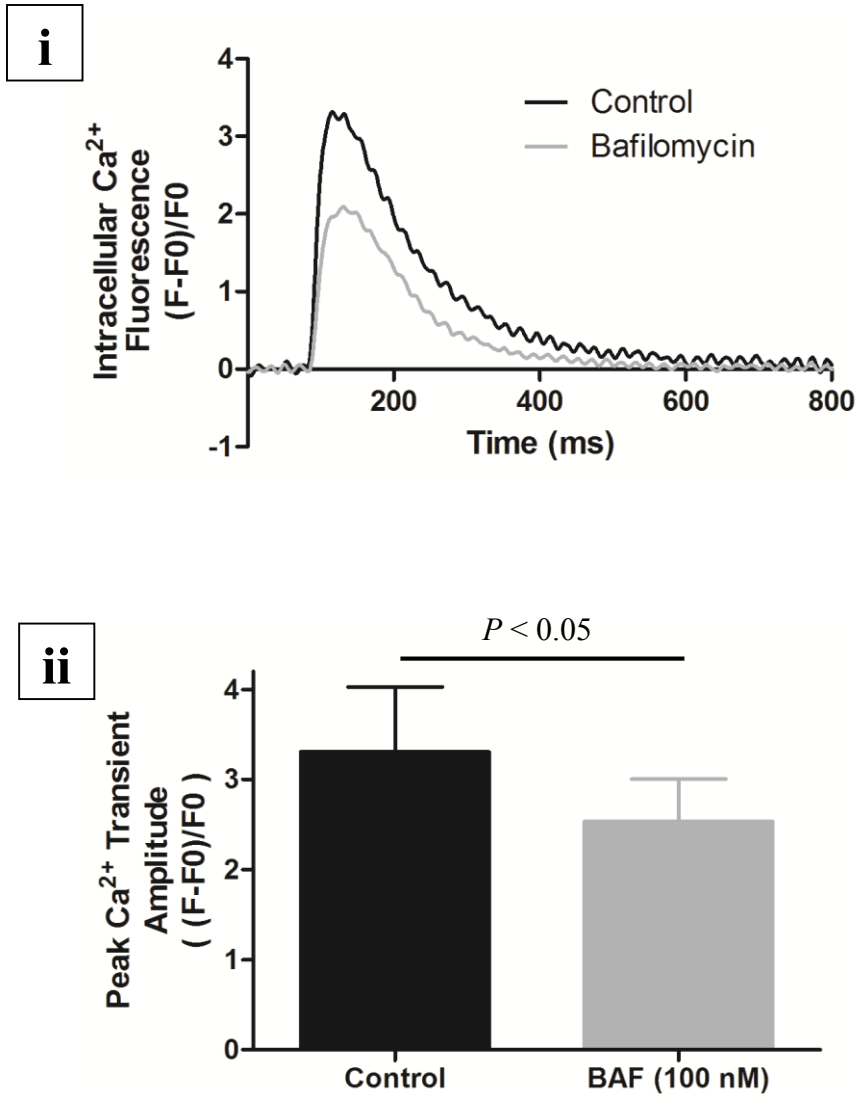


Figure 4.1 (i) and (ii): The Effect of Bafilomycin on Atrial Myocytes

(i) Representative trace to show field-stimulated calcium transients in a guinea pig atrial myocyte before and after superfusion with 100 nM bafilomycin. Each signal is the average of at least 8 stimulated calcium transients under control conditions and at maximal response to bafilomycin.

(ii) Summary graph to show the effect of bafilomycin (BAF, 100 nM, n=6) on guinea pig atrial myocyte calcium transient amplitude compared to calcium transient amplitude in physiological salt solution (PSS, see section 2.8, n=9). The peak height of calcium transients during superfusion of bafilomycin were 19±5% reduced from their amplitude in PSS ($P < 0.05$, Paired t-test).

All experiments were carried out on isolated guinea pig atrial myocytes at physiological temperature (35±2°C), field stimulated at a rate of 1 Hz. Fluo-5F calcium fluorophore was loaded into the cells in the –AM form at a concentration of 3 µM for 10 min. Data are presented as mean±SEM.

4.3.2 The calcium transient response to isoprenaline is partially dependent on NAADP signalling in atrial myocytes

NAADP signalling is thought to be important during β-adrenergic stimulation in the ventricle. Indeed, the level of NAADP measured in ventricular tissue has been shown to significantly increase after stimulation with isoprenaline (Macgregor *et al*., 2007). It has also been shown that mice lacking the postulated NAADP receptor, TPC2, exhibit a significantly blunted calcium transient and contractile response to β-adrenergic stimulation (Elson *et al.*, 2010).

Superfusion of cardiac atrial myocytes with 3 nM isoprenaline led to a 63±8% increase (n=9) in calcium transient amplitude as measured by Fluo5F fluorescence (Fluo5F-AM loaded at 3 μM for 10 min) in field-stimulated myocytes at 1 Hz stimulation rate. In a separate set of cells superfused with bafilomycin, the response to isoprenaline was significantly reduced ($P < 0.05$, Student's t-test), to a 36±9% increase in calcium transient amplitude (n=6). Representative traces of the response to isoprenaline under both conditions can be seen in figure 4.2, whilst a comparison of the complete data sets is presented in figure 4.3.

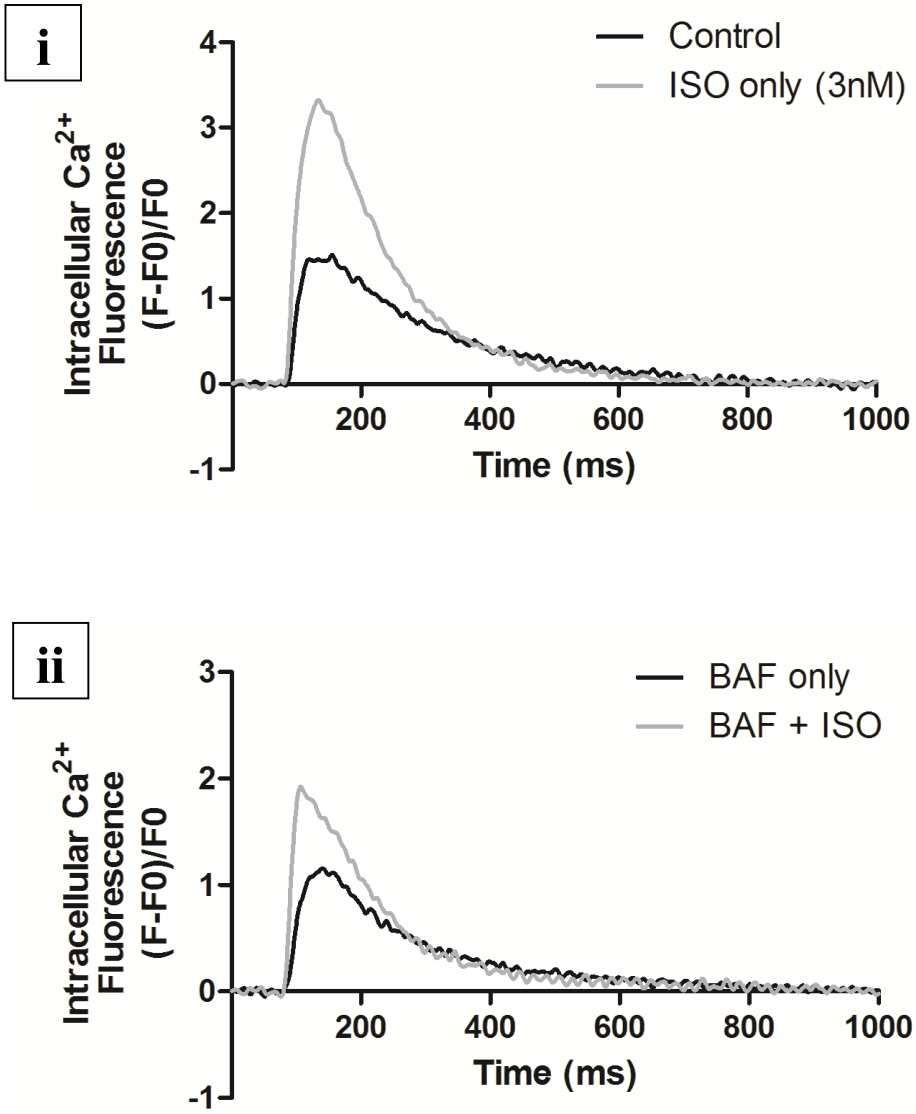


Figure 4.2 (i) and (ii): Representative traces to show the effect of bafilomycin on the β-adrenergic response in isolated atrial myocytes

Representative traces to show the calcium transient response to isoprenaline (3 nM) in isolated ventricular myocytes. Myocytes were loaded with Fluo5F-AM (incubation in 3 µM dye for 15 min at room temperature), superfused with solutions at 35±2°C and stimulated to beat at 1 Hz using field stimulation with a pair of carbon electrodes.

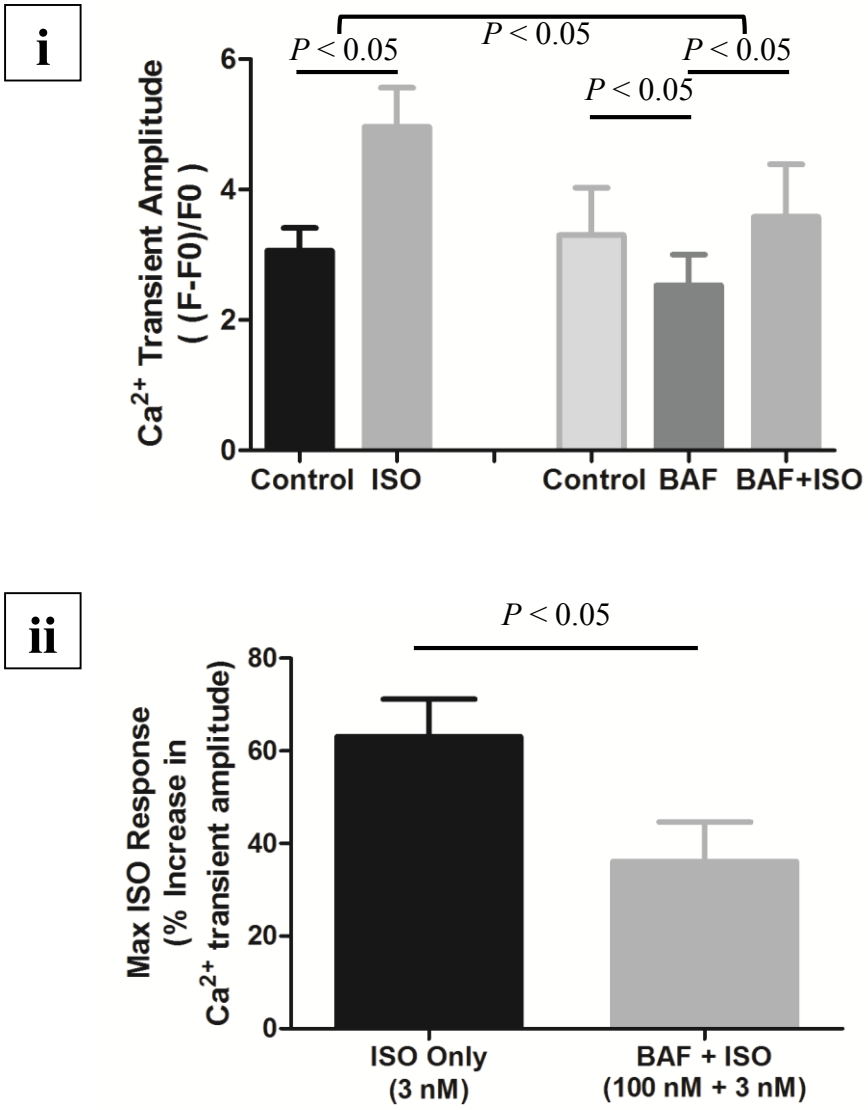


Figure 4.3 (i) and (ii): Effect of Bafilomycin on Cellular Response to Isoprenaline
Summary bar graphs to show the effect of bafilomycin exposure (100 nM) on the calcium transient response to isoprenaline (3nM) in isolated atrial myocytes at 35±2°C, field-stimulated to fire action potentials at a rate of 1 Hz. Data are presented as mean±SEM. Fluo5F-AM (3 μM, 10 min loading) was used as the calcium fluorophore:

(i) Raw data given in (F-F0)/F0.

(ii) Normalised response to isoprenaline under control and bafilomycin conditions. Isoprenaline caused a significant enhancement of the calcium transient under both conditions (both $P < 0.05$, one-sample t-test, n-numbers given below), however this response was significantly smaller in the presence of bafilomycin ($P < 0.05$, Student's t-test). Enhancement under control conditions, 63±8% (n=9) and after exposure to bafilomycin for 5 min, 36±9% (n=6).

4.3.3 The calcium transient response to isoprenaline is partially-dependent on the NAADP pathway in ventricular myocytes

An involvement of the NAADP pathway in ventricular β-adrenergic signalling has been previously suggested based on an increase in measured NAADP levels in ventricular tissue after application of ISO by Langendorff perfusion. Inhibition of the NAADP pathway using a high, self-inactivating, concentration of NAADP (1mM) has been shown to elicit a greater reduction in the amplitude of the ventricular calcium transient during ISO stimulation than in control, indicating that the NAADP pathway is more active during β-stimulation (Macgregor *et al.*, 2007a). The magnitude of the isoprenaline response under the influence of inhibitors of the NAADP pathway, however, had not been investigated.

The data discussed in the previous paragraph were collected before the discovery of Ned-19 as a specific antagonist of the NAADP pathway (Naylor *et al.*, 2009) and, given the findings presented in atrial myocytes, it seemed pertinent to investigate the effect of direct NAADP pathway inhibition on the magnitude of the ISO response in ventricular myocytes.

Isolated guinea pig ventricular myocytes were patched in the whole-cell configuration and Fluo5F Ca^{2+} dye (100 μM) and Ned-19 (1 μM) or bafilomycin (1 μM) included in the patch solution as appropriate. Cells were stimulated to fire action potentials via the patch pipette at a rate of 1 Hz and the response to superfusion of 2 nM ISO compared between conditions. Representative traces to show the 0 min and peak ISO responses attained for a single cell under each condition are presented in Figure 4.4.

Over the course of 4 min from solution switch, ISO was seen to induce a significant increase in calcium transient amplitude over time regardless of the condition under study ($P < 0.05$, Two-way ANOVA). The condition under study was also observed to have a significant effect on the magnitude of calcium transient amplitude response over time ($P < 0.05$, Two-way ANOVA). Post-hoc testing revealed that the increase in calcium transient observed in the presence of Ned-19 (n=6), and that observed in the presence of Baf (n=5), were both significantly smaller than the increase elicited during control ISO superfusion (n=9). This difference became statistically significant 2 min after switch to isoprenaline in bafilomycin-treated cells and 3 min after solution switch in Ned-19-treated myocytes (differences $P < 0.05$, Tukey's post hoc testing). Conversely, there was no significant difference between the responses seen in Ned-19 and Baf treated myocytes at any time during the experiment (differences $P > 0.05$, Tukey's post hoc testing. The increase in calcium transient amplitude stimulated by ISO superfusion over the course of 4 min is summarised in Figure 4.5.

The results presented above were identical when maximal change was considered instead of change over time. Under control conditions 2 nM ISO stimulated an increase in calcium transient amplitude which reached a maximum response of 166±8% increase (n=9) from the transient amplitude during PSS superfusion. In the presence of Ned-19, isoprenaline still elicited a large increase in calcium transient amplitude, peaking at a 105±19% increase (n=6). In the presence of bafilomycin, the response to isoprenaline reached a maximum of 92±20% greater than the transient amplitude measured during PSS superfusion (n=5). Isoprenaline stimulated a significant increase in calcium transient amplitude across all conditions ($P < 0.05$,

One-way ANOVA). The response of cells treated with Ned-19 or Baf was significantly reduced when compared to controls ($P < 0.05$, Tukey's post-hoc testing, n-numbers as above), whilst the responses of cells treated with Ned-19 or Baf were not significantly different from one-another ($P > 0.05$, Tukey's post-hoc testing, n-numbers as above). A summary graph of the maximal recorded responses to isoprenaline under the three conditions is presented in Figure 4.6.

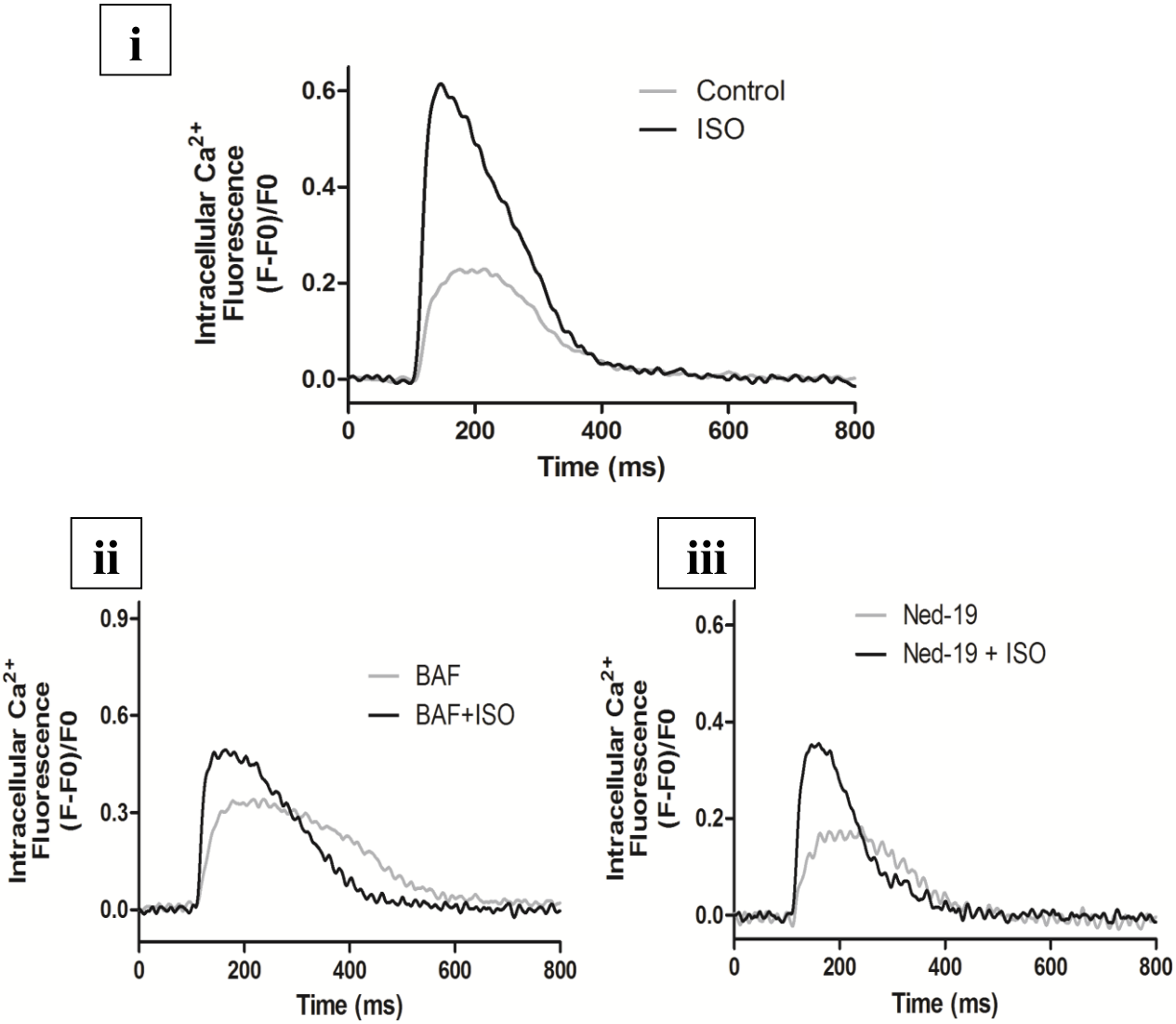


Figure 4.4 (i), (ii) and (iii): Representative traces of responses to isoprenaline
Representative traces to show the calcium transient response of separate, individual ventricular myocytes to 2 nM isoprenaline (i) under control conditions, (ii) in the presence of 1 µM bafilomycin and (iii) in the presence of 1 µM Ned-19. Data are presented as Fluo5F fluorescence normalised to emitted fluorescence at baseline.

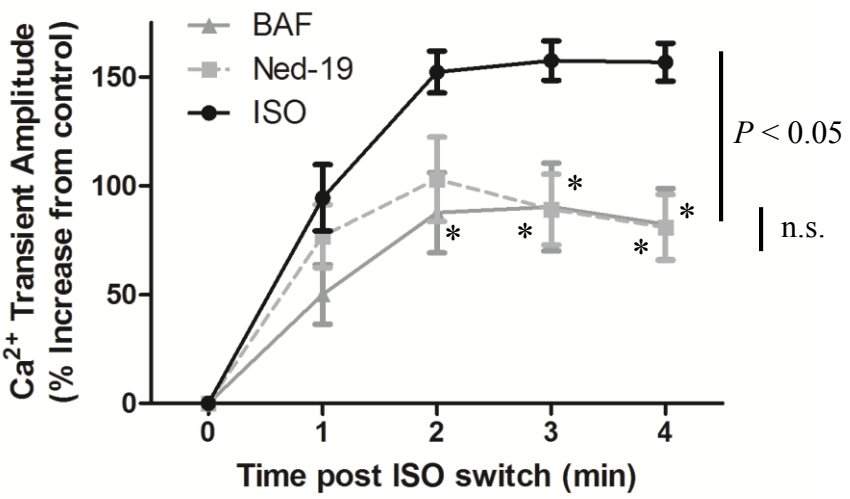


Figure 4.5: Timecourse graph of ISO response in the presence of Baf and Ned
Summary graph to show the response of cardiac ventricular myocytes to 2 nM isoprenaline over time under the three conditions studied. Responses are given as percentage increase in calcium transient amplitude, where calcium transient amplitude is taken to be peak F/F0 fluorescence (Fluo5F calcium indicator) measured across an average of at least 8 transients. Data are presented as mean±SEM. Isoprenaline stimulated a significant increase in calcium transient amplitude across all conditions ($P < 0.05$, Two-way ANOVA). The change in calcium transient amplitude observed during superfusion with 2 nM isoprenaline was significantly smaller in the presence of either bafilomycin or Ned-19 (both 1 µM included in the patch solution, n=5 and n=6 respectively) than under control conditions (n=9). This difference became apparent 2 min after the onset of iso superfusion in Baf-treated cells and 3 min after the onset of superfusion in Ned-19-treated myocytes (differences considered significant as $P < 0.05$ by post-hoc testing with Tukey correction). Individual data points exhibiting a significant difference from the response seen during control ISO exposure are marked as *. Bars to the right of the graph indicate the result of ANOVA analysis.

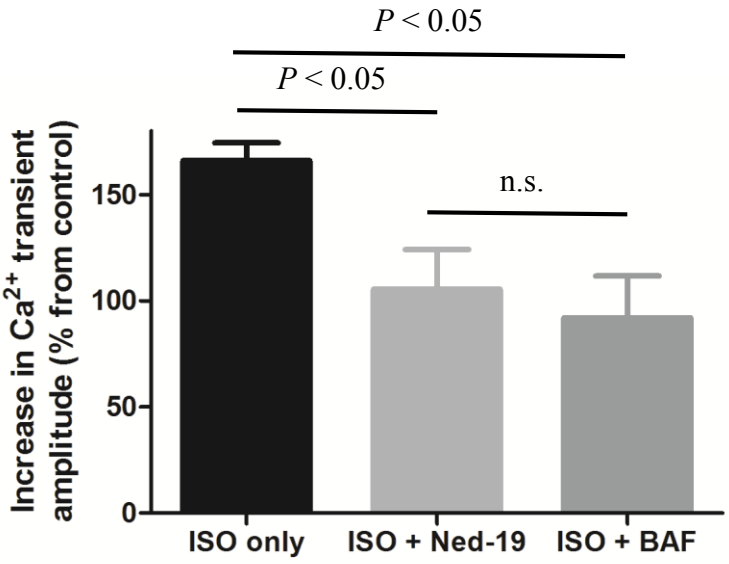


Figure 4.6: Bar graph to show maximal effect of ISO under each condition
Summary bar graph to show the maximal increase in calcium transient amplitude in isolated guinea pig ventricular myocytes in response to superfusion with 2 nM isoprenaline under control conditions and in cells exposed to Ned-19 or bafilomycin (1µM included in the patch solution, incubation for at least 8 min before control recordings initiated). Data are presented as mean±SEM. In whole-cell patch solution, 2 nM iso caused a 166±8% increase in calcium transient amplitude (n=9). When 1 µM Ned-19 was included in the patch solution, this response fell significantly, to 105±19% ($P < 0.05$, Tukey's post-hoc testing, n=6), whilst in the presence of 1 µM Baf the response was also significantly blunted (92±20% increase during iso, $P < 0.05$ compared to control response, Tukey's post-hoc testing, n=5). The responses observed in Ned-19 and baf-treated cardiac ventricular myocytes were not significantly different from one-another ($P > 0.05$, Tukey's post-hoc testing).

4.3.4 The L-type calcium current response to isoprenaline is not dependent on the NAADP pathway

Photorelease of NAADP, as shown in the previous chapter, causes a substantial enhancement of the calcium transient. It has previously been shown that this effect requires intact SR calcium handling. Further, it is known that photorelease of NAADP in cardiac myocytes does not alter the L-type calcium current (Macgregor *et al.*, 2007a, Collins *et al.*, 2011). Accordingly, specific inhibition of the NAADP pathway at the NAADP receptor, using trans-Ned-19 (1 μM) has been shown to have no effect on the L-type calcium current (Elson *et al.*, 2011).

Given that neither NAADP, nor Ned-19 have a significant effect on the calcium current, it would be logical to assume that any effect of the NAADP pathway on calcium signalling is limited to interactions with the SR. However, these observations do not rule out further effects of the pathway when activated by adrenergic stimulation. To investigate whether the physiological role of the NAADP pathway in calcium signalling is confined to interactions between the acidic store and the SR, the response of the L-type calcium current to isoprenaline superfusion was measured under control conditions and in the presence of Ned-19.

Isolated guinea pig ventricular myocytes were patched in the whole-cell configuration using either whole-cell patch solution or whole-cell patch solution containing 1 μM trans-Ned-19. No calcium dye was included during this set of experiments.

Whole-cell L-type calcium currents were stimulated by application of a 200 ms, 40 mV depolarising step from a holding potential of -40 mV at a rate of 0.2 Hz. Control

measurements were taken during superfusion of physiological salt solution, before switching to PSS containing 4 nM ISO. Representative traces to show the effect of 4 nM ISO on I_{CaL} can be seen in Figure 4.7, where baseline PSS recordings are compared to the maximum measured I_{CaL} during ISO exposure in both control (i) and Ned-19-treated cells (ii).

Under control conditions, 4 nM ISO conferred a 90±12% increase in peak I_{CaL} amplitude (n=7). In the presence of 1 μM Ned-19, 4 nM ISO conferred a 119±25% increase (n=6). These two data sets are not considered to be statistically different ($P > 0.05$, Student's t-test). A summary trace showing the development of peak ISO response over time presented as raw whole-cell L-type Ca^{2+} current in control and Ned-19 cells is presented as in Figure 4.8. Maximal current responses are summarised in Figure 4.9.

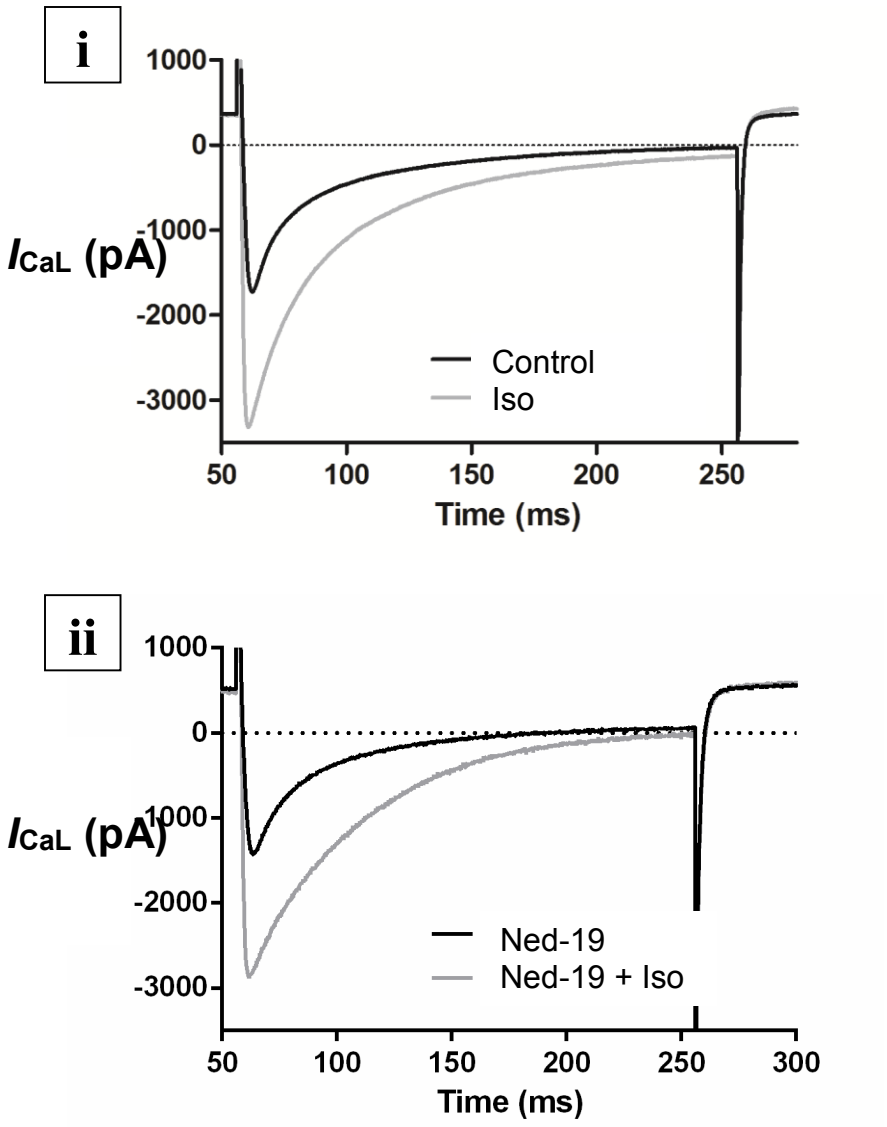


Figure 4.7 (i) and (ii): Representative traces to show L-type calcium current Iso responses in control conditions and in the presence of Ned-19

Representative traces to show whole-cell L-type calcium currents recorded from isolated guinea pig ventricular myocytes in PSS and at the maximal response to 4 nM isoprenaline superfusion. I_{CaL} stimulated by a 200 ms voltage pulse from the holding potential of -40 mV to a pulse potential of 0 mV once every 5 s and measured as peak current minus current at the end of the voltage pulse.

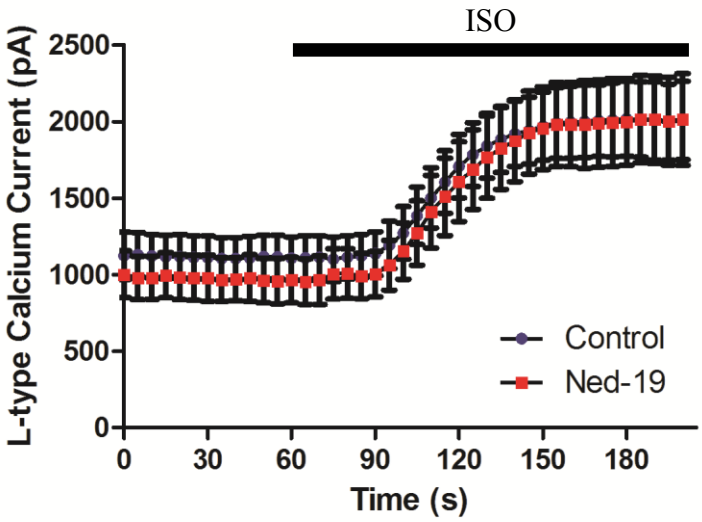


Figure 4.8: L-type Ca^{2+} current response to ISO over time in the presence and absence of Ned-19

Development of the I_{CaL} response to ISO over time presented as whole-cell current in control and Ned-19-treated myocytes (n=7 under control conditions and n=6 in the presence of Ned-19). Data are presented as mean±SEM and represent average whole-cell current across all experiments carried out. I_{CaL} was recorded for 60 s in PSS before switch to 4 nM ISO. All experiments presented were carried out at a temperature of 35±2°C, with temperature fluctuation within any given experiment less than 0.5°C. Calcium currents were stimulated by a 40 mV depolarising voltage step from a holding voltage of 0 mV for 200 ms at a rate of 0.2 Hz.

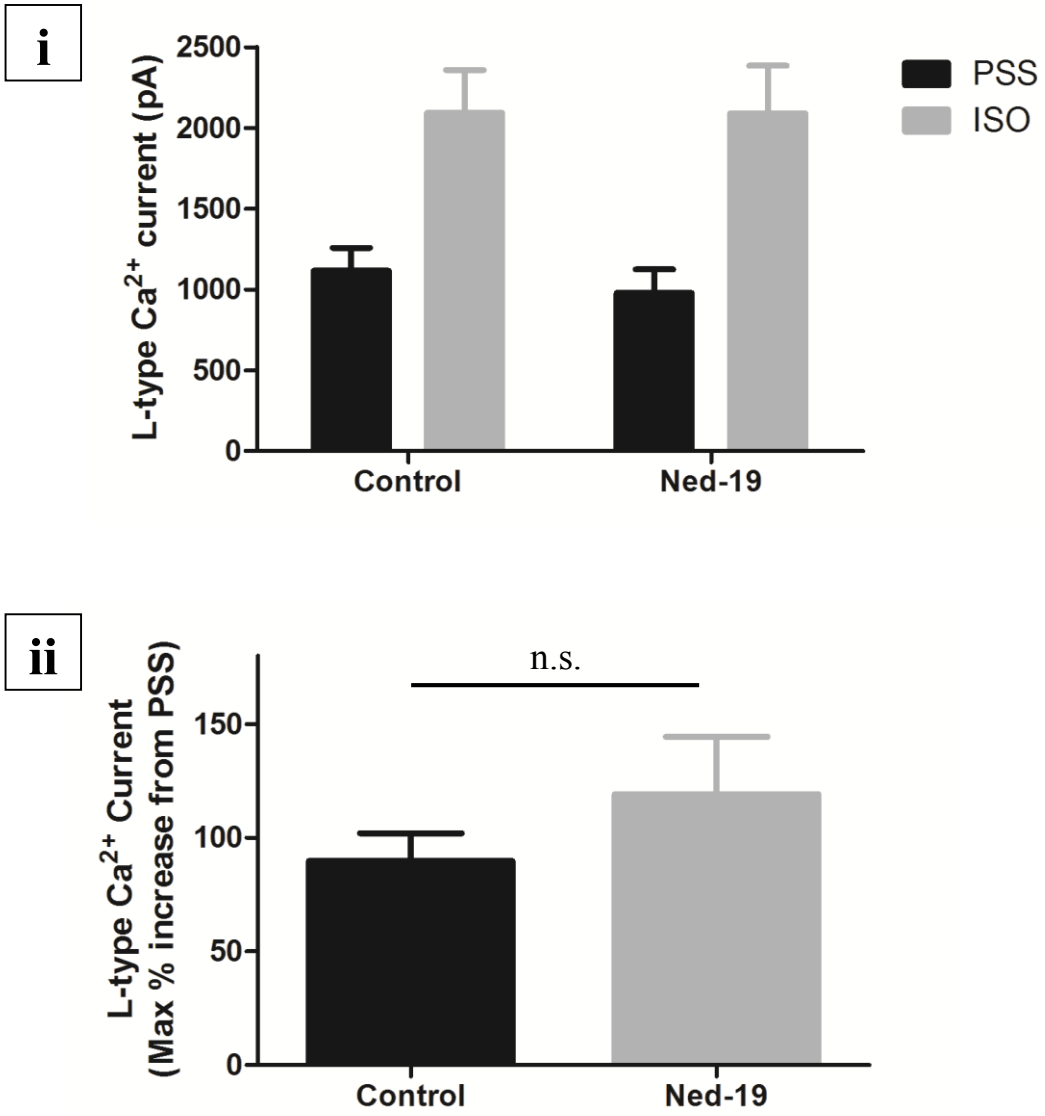


Figure 4.9 (i) and (ii): Maximal response of L-type Ca^{2+} current to ISO in the presence and absence of Ned-19

Comparison of the maximum response of I_{CaL} to ISO stimulation (4nM) in cardiac ventricular myocytes presented as (i) whole-cell I_{CaL} in control and at peak response and (ii) maximum percentage change during ISO superfusion. Iso caused a 90±12% increase in peak I_{CaL} measured under control conditions (n=7) and a 119±25% increase in the presence of Ned-19 (n=6). Maximal response measured under the two conditions was not significantly different ($P > 0.05$, Student's t-test).
Data are presented as mean±SEM, with all experiments carried out at a temperature of 35±2°C, and temperature fluctuation within each experiment <0.5°C. Calcium currents were stimulated by a 40 mV depolarising voltage step from a holding voltage of 0 mV for 200 ms at a rate of 0.2 Hz.

4.4 Discussion

The data presented in this chapter show that inhibition of the NAADP pathway significantly reduces the calcium transient response of contractile myocytes to β-adrenergic stimulation, without affecting the response associated with L-type Ca^{2+} channels. These data are the first to compare calcium transient and calcium current to β-adrenoceptor stimulation during direct inhibition of the NAADP pathway in ventricular myocytes. These data are in full agreement with previous observations using GPN or high dose NAADP to interfere with the pathway (Collins *et al.*, 2011, Macgregor *et al.*, 2007a) and contributes further evidence that NAADP is physiologically relevant during the positive inotropy associated with adrenergic stimulation in the heart.

The observation that interfering with acidic calcium stores results in a significant reduction in the calcium transient response to isoprenaline has now been shown using GPN (Collins *et al.*, 2011), which destroys acidic stores through osmotic lysis, and using bafilomycin, which leaves the store membranes intact but abrogates store calcium-loading. Both of these compounds have inherent disadvantages; lysing of acidic stores by GPN allows the contents of the lysosome to enter into the cytosol, whilst bafilomycin has been reported to impair mitochondrial function by acting as a potassium-selective ionophore (Teplova *et al.*, 2007). The similar data presented in both instances, which also shows good agreement with observations made in ventricular myocytes, suggests that effects seen are associated with actions of the NAADP pathway.

The results presented in chapters 3 and 4 of this thesis together provide an exciting development, being one of the first observations to link a portion of the β-adrenergic response directly to the stimulation of an acute CaMKII-mediated process in cardiac myocytes via a named pathway. Based on these observations, a new schematic model for the development of NAADP-mediated responses in cardiac myocytes is presented in Figure 4.10.

With regards to CaMKII signalling, it is interesting to note the timecourse data collected during isoprenaline exposure in these cells. Computational modelling data suggests that inhibition of CaMKII in cardiac myocytes would be expected to lead to a more rapid peak in the adrenergic response (Koivumäki *et al.*, 2009), since PKA-mediated signalling, is both more rapidly activated than CaMKII-mediated effects and decays at a faster rate. It is not possible using the data collected here, to make a definitive judgement concerning the time of peak response as data were collected only once per minute and not continuously. However there is a tendency in both the atrial and ventricular preparations, for the time of peak measured response to shorten in the presence of Baf and Ned-19 and future work will explore this observation more extensively.

In order to directly confirm a role for CaMKII in this pathway, an important next step will be to assess the phosphorylation state of SR proteins under control conditions and after application of NAADP. Although the role of CaMKII in acute physiological responses to β-adrenergic stimulation remains controversial (see section 1.10), confirmation of changes in CaMKII-mediated phosphorylation of intracellular proteins resulting from NAADP stimulation combined with the clear role for this

pathway in the acute β-adrenergic response would be a very exciting development. Allied to assessment of CaMKII-mediated phosphorylation during NAADP stimulation, measurements of the phosphorylation state of SR calcium handling proteins during stimulation with ISO under control conditions and in the presence of inhibitors of the NAADP pathway would also be prudent.

The involvement of the NAADP pathway in the modulation of calcium signals during the β-adrenergic response raises questions about whether the pathway might be implicated in the development and maintenance of heart failure and cardiac hypertrophy. These questions are especially pertinent given the causal link observed between changes in CaMKII expression or activity and the development of heart failure (Maier *et al.*, 2003) and arrhythmias (van Oort *et al.*, 2010) in animal models.

Since these experiments were carried out, our collaborators in the Lei group (University of Oxford) have carried out *in vivo* and *in vitro* experiments using TPC2 -/- mice which show a significant reduction in the development of cardiac hypertrophy associated with chronic exposure to isoprenaline. A sample of these findings has been kindly provided by members of the Lei group and is presented with permission in Figure 4.11. Further studies in the same group have also indicated that hearts isolated from TPC2 -/- mice after 2 weeks of exposure to isoprenaline exhibited a significantly higher threshold for the initiation of ventricular arrhythmias by electrical pacing (personal communication, data not shown).

A more extensive investigation into the role of the NAADP pathway in the development of cardiac pathology, and the potential of pathway inhibition as a

therapeutic intervention is clearly warranted and the program of experiments for this collaboration is currently being put in place.

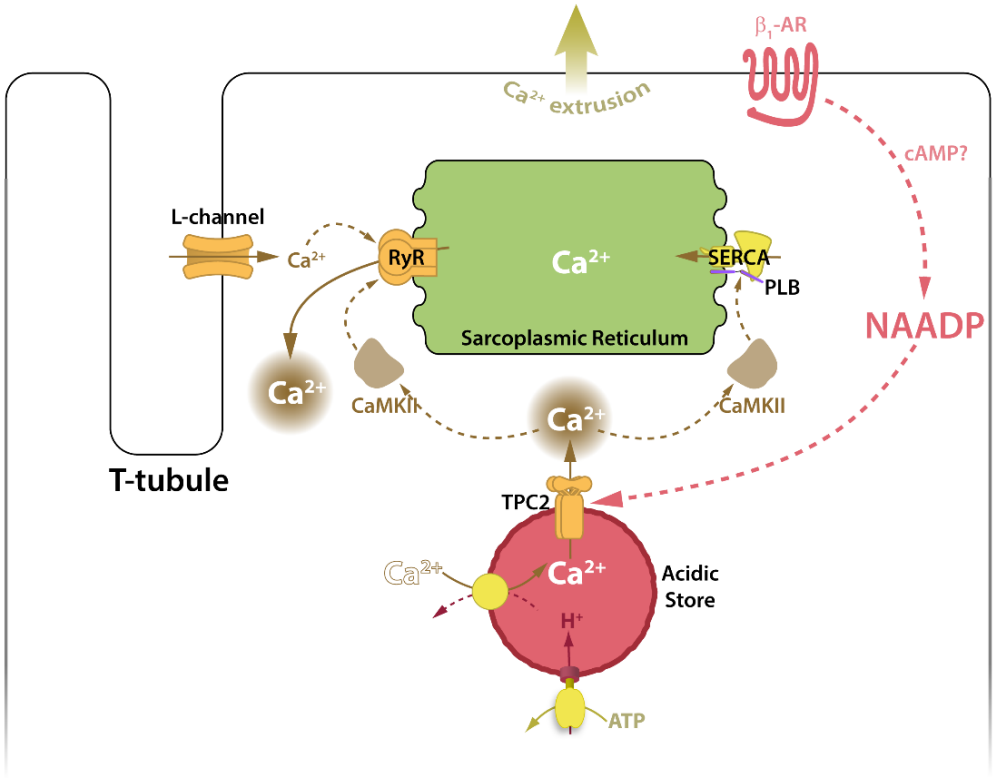


Figure 4.10: New model of the NAADP pathway in cardiac myocytes

Current model representing the known actions of NAADP in cardiac myocytes based on research carried out in the Terrar laboratory.

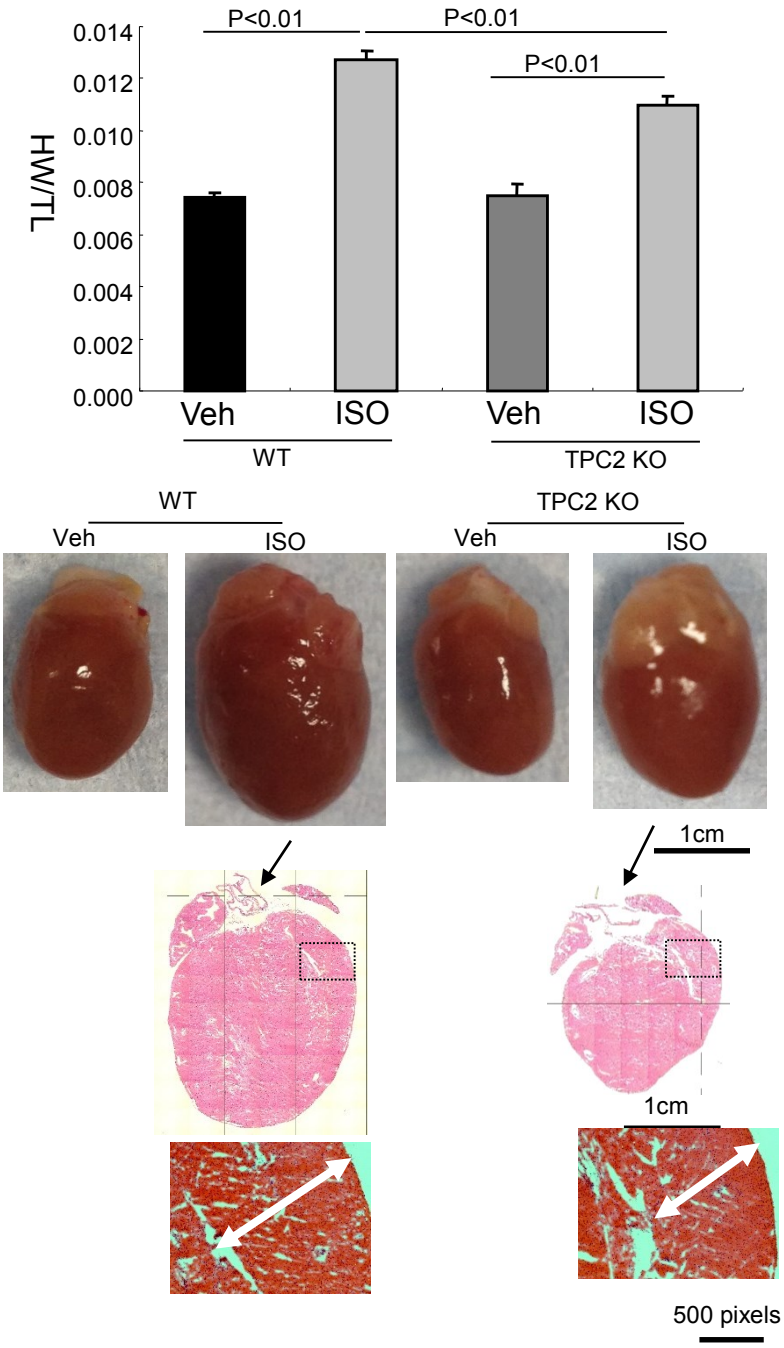


Figure 4.11: A possible role for the NAADP pathway in the development of cardiac hypertrophy

Data to show the effect of 2 weeks of isoprenaline exposure, generated by osmotic mini-pump, on heart weight and ventricular wall thickness in WT and TPC2-/- mice. Iso produced significant hypertrophy in both sets of mice, however the effect was significantly reduced in mice lacking the NAADP-activated calcium release channel TPC2. Data presented with permission from Dr Ming Lei.

5 POTENTIAL OF HYDROXYCHLOROQUINE AS A NOVEL FUNNY CURRENT INHIBITOR

5.1 INTRODUCTION

The sino-atrial node (SAN) is the pacemaker of the heart. Positioned in the posterior aspect of the right atrium, at the juncture of the atrium and superior vena cava and adjacent to the crista terminalis, its myocytes exhibit spontaneous rhythmic electrical activity which initiates each heart-beat. SAN myocytes are specialised for their electrical role, containing very little contractile material, whilst exhibiting spontaneous diastolic depolarisation (SDD) in phase 4 of the action potential.

Heart rate is a major determinant of angina in coronary disease and a high resting heart rate is associated with an increased risk of experiencing a cardiac event (Sulfi and Timmis, 2006). Clinical trials to determine the effect of β-blockers in congestive heart failure demonstrate a correlation between the magnitude of heart rate reduction and survival, regardless of whether this reduction was mediated by drug administration or occurred naturally (Lechat *et al.*, 2001, Waagstein *et al.*, 1993).

Current heart failure therapies which reduce heart rate as part of their action, e.g. β-blockers and calcium channel antagonists, are effective at reducing cardiac beating rate but also convey negative inotropic effects. These agents also result in major side-effects which can include severe hypotension, depression, constipation and peripheral oedema in the case of calcium channel antagonists (BNF, 2012).

In the late 1970s, a hyperpolarisation-activated inward current was discovered in sino-atrial node myocytes (Seyama, 1976) which was activated by hyperpolarisation to voltages more negative than -50 mV and became more pronounced with greater levels of hyperpolarisation (DiFrancesco, 1986). This current, which became known

as the 'funny current' $I_{(f)}$ due to its unusual voltage-gating, is a mixed ionic current encoded by the HCN4 gene (Ishii *et al.*, 1999). $I_{(f)}$ mediates chronotropic changes during adrenergic stimulation (Brown *et al.*, 1979) through direct binding of cAMP at the channel (DiFrancesco and Tortora, 1991). Over-expression of HCN4 in cardiac monolayer cultures results in a significant increase in beating rate (Boink *et al.*, 2008), whilst inducing HCN4 knock-out in adult mice can result in severe bradycardia (Baruscotti *et al.*, 2011).

The search for pharmacological agents which reduce heart rate without negatively affecting myocardial contractility, so-called 'specific bradycardic agents' (Kobinger and Lillie, 1987) is an important pursuit of modern medicine. To date ivabradine, an $I_{(f)}$-channel blocker, is the only SBA which has been successfully added to the NICE guidelines for the treatment of heart failure (NICE, 2012).

Hydroxychloroquine (HCQ), marketed under the name Plaquenil, is an antimalarial which was first synthesised in 1950 (Surrey and Hammer, 1950). It is currently prescribed in the UK for ongoing treatment of the autoimmune inflammatory conditions rheumatoid arthritis (RA) and systemic lupus erythematosus (SLE). The chemical structure of HCQ is shown in Figure 5.1.

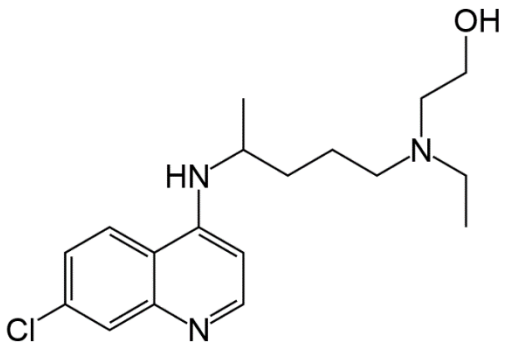


Figure 5.1: Chemical structure of hydroxychloroquine

A fortuitous clinical observation in a patient prescribed Plaquenil (HCQ) for control of SLE was the initial source of our interest in HCQ with relation to cardiac rate control. This patient had experienced sinus tachycardia (heart rate 118bpm at rest) treated with atenolol. Withdrawal of atenolol, attempted on several occasions, was associated with the return of tachyarrhythmia and symptoms of angina. After receiving the diagnosis of SLE, the patient was prescribed Plaquenil at a dose of 200-400mg/day. Within two weeks, cessation of atenolol treatment was attempted again and successful with no tachyarrhythmia or angina and the patient maintained a resting heart rate of 70-80bpm. Approximately 1 year after cessation of beta-blocker treatment the dose of HCQ was halved to 100mg/day and tachyarrhythmias returned within two weeks, with hospital-led ECG recording a rate of 109bpm at rest. At this point HCQ treatment was returned to 200mg/day, and this was associated with a fall in resting heart rate to 70-85bpm which was maintained. In this patient, then, it would seem that: HCQ treatment was associated with a reduction in heart rate and that

lowering of HCQ dose was associated with an increase in heart rate which was reversed upon return to treatment with a higher dose of HCQ.

Early papers did consider the use of hydroxychloroquine in the treatment of cardiac arrhythmias (Burrell and Martinez, 1958), and chloroquine has recently been investigated as a possible treatment in atrial fibrillation (Filgueiras-Rama *et al.*, 2012). None of these studies, however, considered the effects of HCQ on heart rate.

The aims of this section of work were to ascertain whether HCQ has a significant effect on heart rate by actions directly on sino-atrial node myocytes and if this action occurs through inhibition of the funny current. We hypothesised that HCQ would slow cardiac rate and that this effect would be mediated directly at the sino-atrial node through modulation of $I_{(f)}$.

5.2 METHODS

For preparation of spontaneously-beating atrial preparations, male CD1 mice were terminated by concussion followed by cervical dislocation, the thoracic cavity opened and bathed in heparin-containing solution. The heart was rapidly excised and placed in oxygenated, physiological salt solution at body temperature. The ventricles were dissected away and, under a binocular microscope, the major vessels and area posterior to the sino-atrial node were cleared in order to optimise drug access.

The intact, spontaneously-beating atria were mounted onto a force transducer for the measurement of contraction, from which rate data was collected by measuring the time between adjacent contractions. Data were collected and analysed using Chart 5 software.

Sino-atrial node myocytes were isolated using enzymatic digestion followed by mechanical dissociation in a method adapted from Powell *et al*. (1980).

Briefly, male guinea pigs were terminated by concussion followed by cervical dislocation, the hearts rapidly removed, washed in heparin-containing zero calcium solution and mounted for retrograde perfusion with collagenase solution for 25 min.

After digestion, the ventricles were dissected away and the atria transferred to a Sylgard-coated bath containing oxygenated Solution A at body temperature and pinned out for dissection. Debris and connective tissue was removed from the posterior aspect of the right atrium in order to expose the vena cavae and SAN, the SAN region was accessed by dissection of the anterior aspect of the right atrium and cut into thin strips ~2 mm x 5 mm perpendicular to the crista terminalis.

Tissue strips were placed in warmed, oxygenated high potassium storage solution and single cells mechanically dissociated using a fire-polished Pasteur pipette before resting in high potassium storage solution at 4 ºC until use.

In order to maintain the intracellular environment, all electrophysiology was carried out in the perforated patch configuration. Amphotericin B was used as the ionophore, an antifungal compound which inserts itself into the cellular membrane and forms pores permeable to monovalent cations, allowing electrical access with minimal dilution of the cellular milieu.

Patch solution used in these experiments consisted of in mM: K^+ Aspartate 110, KCl 10, NaCl 5, $MgCl_2$ 5.2, HEPES 5, K_2ATP 5, pH to 7.2 with KOH.

Electrodes were manufactured from borosilicate glass capillary tubing (GC100F, Harvard Apparatus, Kent, UK) and used at a tip resistance of 5±1.5MΩ. After sealing onto the cell by manual suction, pipettes were left in the giga-seal stage for at least 10 min to achieve appropriate access.

All cells were initially recorded in the current clamp configuration and an upstroke velocity of less than 10V/s during spontaneous beating used as confirmation that a central sino-atrial node cell had been selected.

Action potential recordings were made in the current clamp configuration. The firing rate of a section of trace at least 15 s long was ascertained using power spectrum analysis. In order to analyse action potential parameters, the same section of action potentials was split into a series of events, which were averaged to produce a typical action potential for the timepoint of recording and assessed for action potential

parameters. All action potential and firing rate analysis were carried out in ClampFit9.

$I_{(f)}$ currents were measured in the voltage clamp configuration. Cells were maintained at a holding potential of -40 mV, at which voltage there is no net current flow, and from which step hyperpolarisations were made for 2 s duration at a rate of 1/20 Hz.

During initial experiments with 1 μM HCQ, voltage steps were made to -80, -100 and -120 mV in repeat cycles over the course of 5 min.

Data were analysed using Student's t-test, or ANOVA where appropriate. In the case of ANOVA analysis, Dunnett's or Tukey corrections were made during post-hoc testing in cases where multiple t-tests were used to compare to control or to all other conditions respectively. $P < 0.05$ was considered to indicate significant change.

5.3 RESULTS

5.3.1 HCQ reduced spontaneous beating rate in a multicellular preparation in a dose-dependent manner

Prior to these experiments all evidence relating to HCQ as a heart rate reducing agent was circumstantial and no direct observations had been published which reported heart rate reduction as a recognised side-effect of taking the drug. The first set of experiments, therefore, were designed to ascertain whether there was any effect of HCQ on spontaneous sino-atrial node beating rate.

Spontaneously-beating mouse atrial preparations were attached to a force transducer using thin suture and hung under gentle tension in oxygenated PSS maintained at 36±1 ºC. HCQ doses were added cumulatively to the bath to investigate the effect, if any, on spontaneous beating rate. Rate change in these preparations when using the specific $I_{(f)}$ channel blocker ZD7288 develops relatively slowly. Rate responses to cumulative doses of HCQ were sampled at 30 min post addition to allow time for a complete response.

Hydroxychloroquine elicited a dose-dependent reduction in spontaneous beating rate ($P < 0.05$, n=7, One-way ANOVA) which was identified as statistically significant at a dose of 3 μM (9±3% reduction from PSS, $P < 0.05$ compared to beating rate in PSS, n=7, Tukey's post-hoc testing) and was further enhanced at a dose of 10 μM (15±2% reduction from PSS, $P < 0.05$ compared to beating rate in PSS and $P < 0.05$ compared to beating rate in 3 μM HCQ, n=7, both Tukey's post-hoc testing). The absolute values of nodal beating rate in the presence of increasing concentrations of

HCQ can be seen in Figure 5.2. In control experiments, whereby preparations were treated in exactly the same way but no drug was added to the bath, rate data taken at matched time-points were extremely stable and showed no significant change over time. Two-Way Repeated measures ANOVA showed a significant difference between control and drug-treated experimental groups which was, again, significant at both the 3 and 10 μM doses of HCQ ($P < 0.05$, Bonferroni post-test). A comparative graph to show percentage change from the control value at increasing concentrations of HCQ against the rate measured in time-match controls is presented in Figure 5.3. During control experiments, the tissue was prepared by the same method and rate data was sampled at matched timepoints without addition of any further agents.

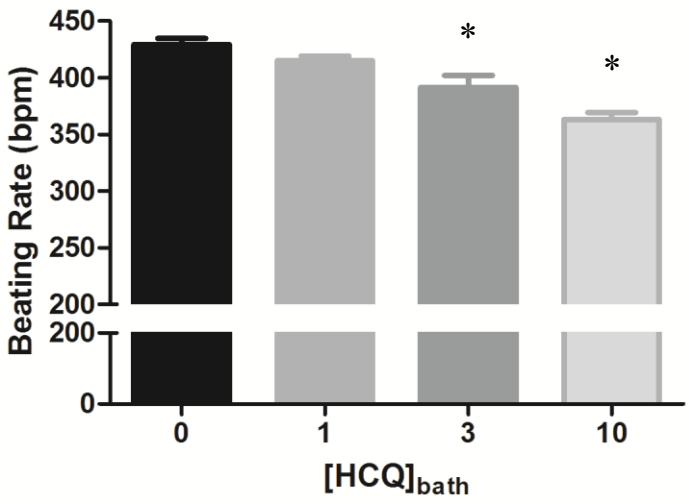


Figure 5.2: Dose-dependent effect of HCQ on spontaneous beating rate in mouse atrial preparations

A bar graph to show the effect of cumulative doses of HCQ on sino-atrial node beating rate in spontaneously-beating mouse atrial preparations maintained at 36±1 ºC. Data are presented as mean±SEM. HCQ elicited a reduction in beating rate ($P < 0.05$, one-way ANOVA) which was significantly different from control at the 3 µM dose (9±3% reduction from 0, $P < 0.05$) and was further reduced at the 10 µM dose (15±2% reduction from control, $P < 0.05$). n=7 for all concentrations. * indicates significant difference from 0 µM by Dunnett's post-hoc test.

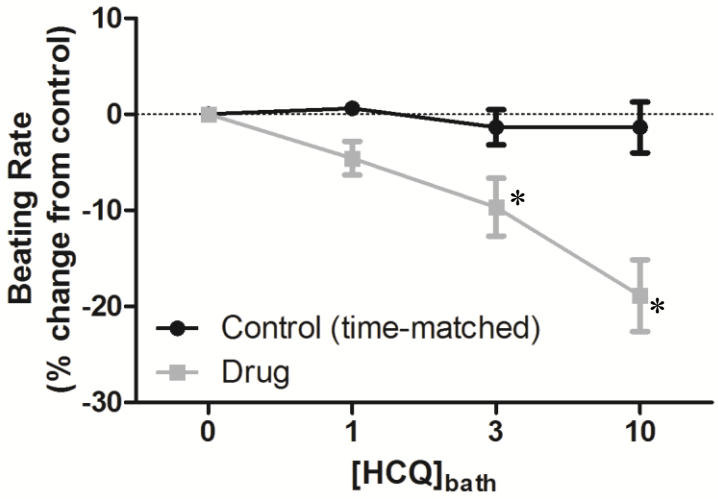


Figure 5.3: Normalised dose-dependent change in atrial beating rate compared to control preparations

A line graph to compare percentage change in atrial beating rate during cumulative HCQ doses with that of control preparations. Data are presented as mean±SEM. There was no significant effect of time beating rate in control preparations ($P > 0.05$, One-way ANOVA, n=6). * indicates a significant difference from Time-matched control, Bonferroni post-test after Two-Way Repeated Measures ANOVA

5.3.2 HCQ reduced spontaneous AP firing rate in isolated SA node cells

In order to investigate the mechanism by which HCQ might be reducing sino-atrial node beating rate, it was first important to investigate spontaneous action potential firing in isolated sino-atrial node myocytes. To this end, the effect of 1 μM HCQ superfusion upon spontaneous action potential generation in isolated guinea-pig sino-atrial node myocytes was investigated. Although the 1 μM concentration had caused a slight but not significant reduction in spontaneous beating rate when bath-applied to the multicellular preparation (4±1% reduction from control, $P > 0.05$, n=7), it was felt that a lower concentration would be more pertinent for the initial investigations into HCQ mechanisms due to the lesser likelihood of non-specific actions.

Isolated guinea-pig sino-atrial node myocytes were accessed by perforated patch and recorded in the current clamp configuration to measure cellular action potentials. HCQ (1 μM) was superfused and spontaneous beating rate followed over the course of 5 min.

Figure 5.4 shows representative traces of action potentials recorded in PSS and after 5 min of superfusion with HCQ. Superfusion with 1 μM HCQ led to a significant reduction in cellular beating rate of isolated sino-atrial node cells ($P < 0.05$, One-way ANOVA, n=6) which had achieved a significant, 10±3%, reduction within 3 min of first exposure ($P < 0.05$, Dunnett's post-hoc testing, n=7). Overall, 1 μM HCQ caused a fall from an average rate of 2.68±0.18 Hz in PSS to that of 2.25±0.24 Hz after 5 min in 1 μM HCQ, a 17±2% reduction ($P < 0.05$, Dunnett's post-hoc testing). The effect of HCQ superfusion on cellular beating rate in isolated guinea pig sino-atrial node myocytes is presented in Figure 5.5.

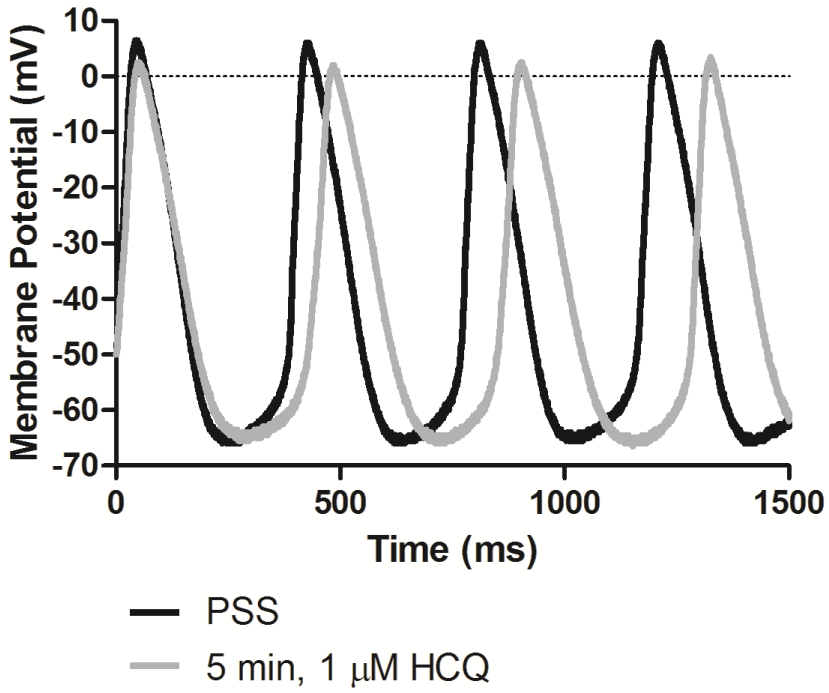


Figure 5.4: Representative traces to show action potentials before and after superfusion of 1 μM HCQ

Representative action potentials from the same SAN myocyte are shown before and after exposure to 1 μM HCQ at 35±0.5 ºC. Cells were electrically accessed by the perforated patch method and allowed to fire spontaneous action potentials. Electrodes were used for recording only, with no stimulation of the cells, and action potentials were recorded in the current clamp configuration.

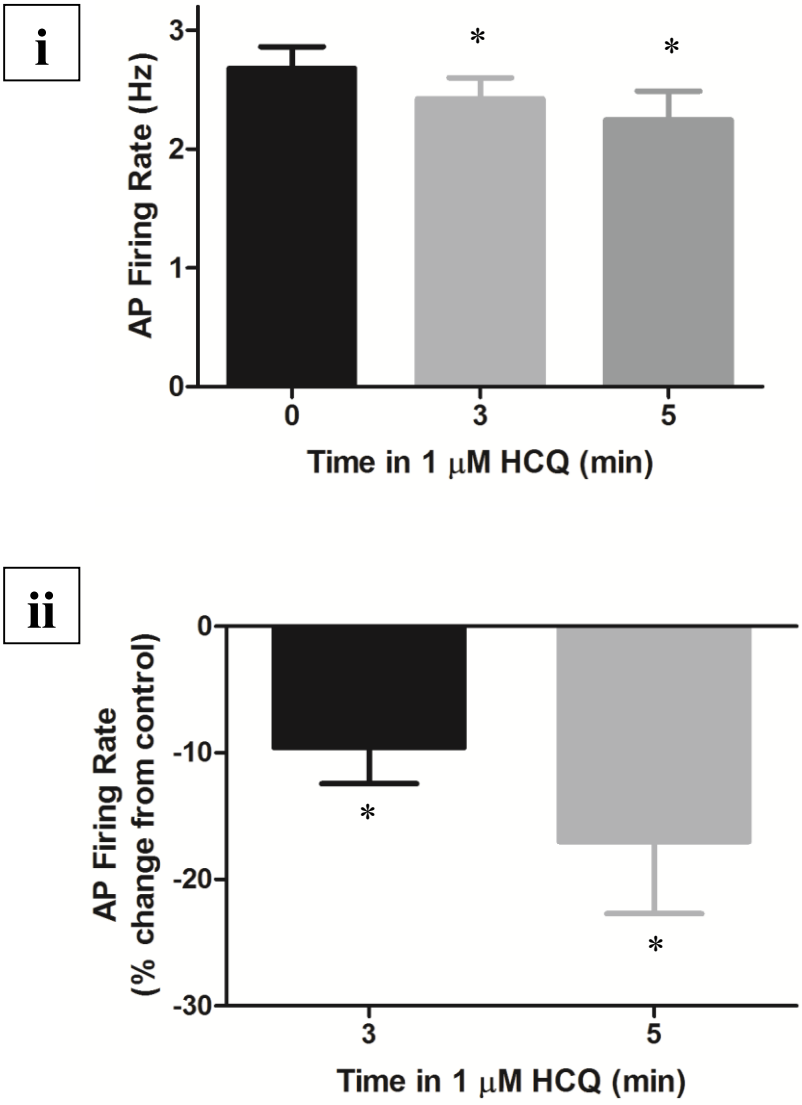


Figure 5.5 (i) and (ii): HCQ reduces action potential firing rate in isolated guinea pig sino-atrial myocytes

Summary bar graphs to show (i) absolute action potential firing rate in Hz before and during 1 μM HCQ application and (ii) percentage change in firing rate 3 and 5 min after switch to superfusion with 1 μM HCQ. n=6 for all groups presented, data are mean±SEM. Solutions were maintained at 35±2 ºC and cells were allowed to fire action potentials spontaneously. AP firing rate was significantly slowed by superfusion of 1 μM HCQ ($P < 0.05$, One-way ANOVA). Compared to control conditions, 1 μM HCQ slowed cellular beating rate significantly by 3 min of exposure (10±3% reduction, $P < 0.05$, Dunnett's post-hoc test) and was further slowed at 5 min (17±6% reduction, $P < 0.05$, Dunnett's post-hoc test). * indicates significant difference from control by post-hoc test.

Analysis of action potential parameters under control conditions and 3 or 5 min after the onset of 1 μM HCQ superfusion confirmed a significant reduction in the rate of spontaneous diastolic depolarisation over time ($P < 0.05$, One-way ANOVA, n=6) which was significant at 3 min (18±5% reduction, $P < 0.05$, Tukey's post-hoc testing, n=6). At the 5 min timepoint there was a further reduction (to 25±4% less than control, $P < 0.05$ Tukey's post-hoc testing, n=6). Summary graphs illustrating the change in slope of SDD are presented in Figure 5.6.

1 μM HCQ caused a lengthening of action potential repolarisation ($P < 0.05$, One-way ANOVA), which was significantly different from control at 3 min of superfusion (9±2% longer than in PSS, $P < 0.05$, Tukey's post-hoc testing, n=6). A summary of action potential duration data is presented in figure 5.7. After 5 min of exposure to 1 μM HCQ, time to 50% action potential repolarisation had lengthened from 88±3 ms to 98±4 ms ($P < 0.05$, Tukey's post-hob testing, n=6). However, the lengthening which was observed at the 5 min timepoint (11±3% longer than in PSS) was not found to be a significant further change from 3 min of HCQ superfusion ($P > 0.05$, Tukey's post-hoc testing, comparison of 3 and 5 min timepoints, n=6). This compares favourably with a reduction of around 8% by ivabradine at the same dose in multicellular preparations (Thollon *et al.*, 1994).

No change in action potential amplitude was observed over the course of these experiments, with amplitude 5 min after switch to HCQ superfusion 79±7 mV, as compared to 83±6 mV before exposure to the compound ($P > 0.05$, paired t-test, n=6). Figure 5.8 presents summary data to show action potential duration during PSS and 3 or 5 min into 1 μM HCQ superfusion.

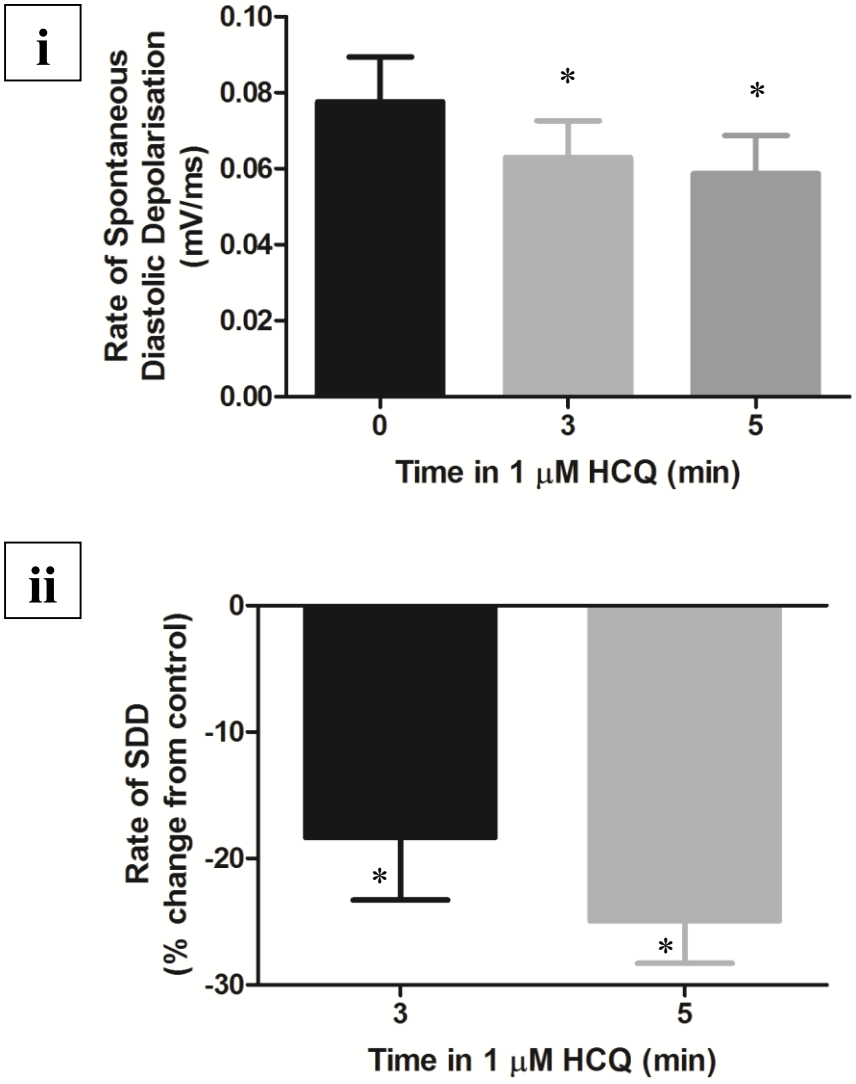


Figure 5.6 (i) and (ii): Change in rate of spontaneous diastolic depolarisation
Summary bar graphs to show (i) absolute value and (ii) percentage change over time in the rate of spontaneous diastolic depolarisation (measured as peak slope of action potential depolarisation during phase 4) of isolated guinea pig sino-atrial node myocytes in PSS and 3 or 5 min after the onset of 1 μM HCQ superfusion. Solutions were maintained at 35±2 ºC and cells were allowed to fire action potentials spontaneously. Data are presented as mean±SEM. 1 μM HCQ caused a significant slowing in the rate of spontaneous diastolic depolarisation by 3 min of exposure (18±5% reduction from 0 min value, $P < 0.05$, One-way ANOVA) and a further significant change at the 5 min timepoint (25±4% reduction from 0 min value, $P < 0.05$, One-way ANOVA). n=6 for all groups presented. * indicates significant difference from 0 min by Dunnett's post-hoc test.

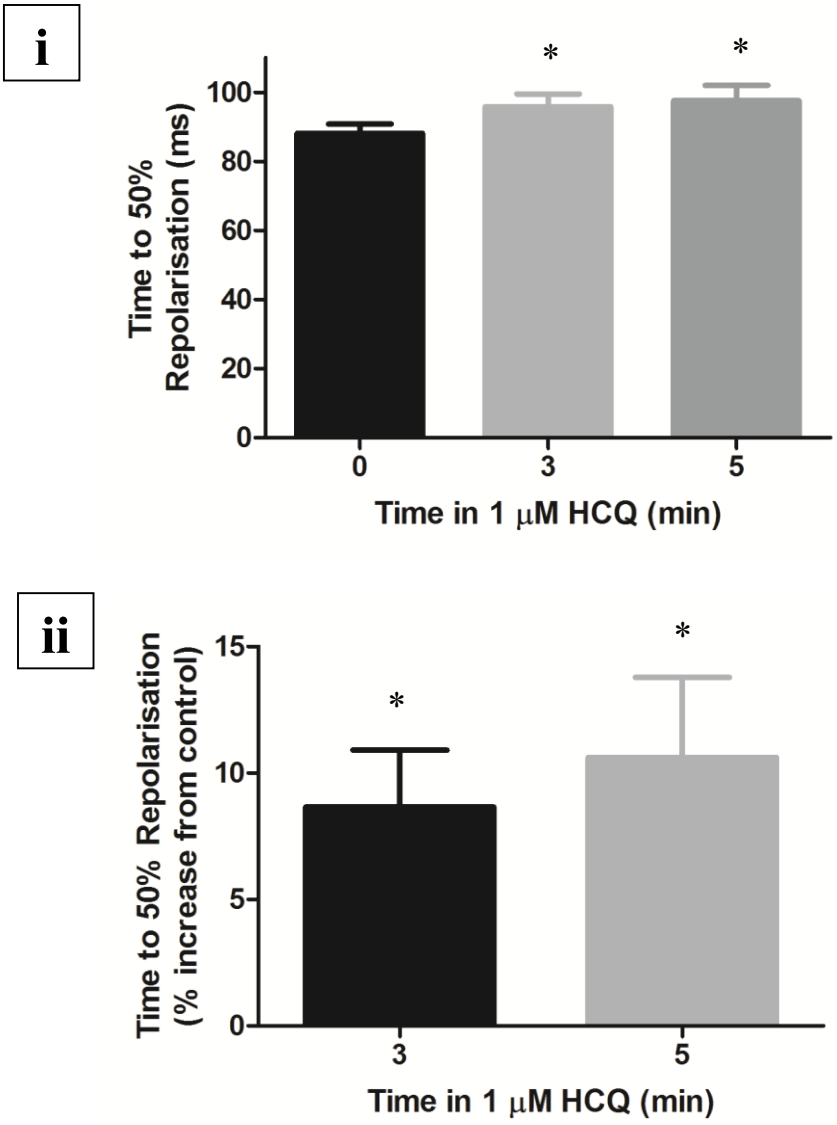


Figure 5.7 (i) and (ii): Change in action potential duration in the presence of HCQ
Summary bar graphs to show (i) absolute values and (ii) percentage change in the action potential repolarisation time in PSS and 3 or 5 min after the onset of 1 μM HCQ superfusion. Solutions were maintained at 35±2 ºC and cells were allowed to fire action potentials spontaneously. Data are presented as mean±SEM. Exposure to 1 μM HCQ led to a significant lengthening of action potential duration, from 88±3 ms before exposure to HCQ, to 96±4 ms 3 min into the experiment and 98±4 ms after 5 min in 1 μM HCQ, prolongations of 9±2% and 11±3% respectively. Both values are significantly different from that at 0 min ($P < 0.05$, One-way ANOVA). n=6 for all groups presented. * indicates significant difference from 0 min by Dunnett's post-hoc test.

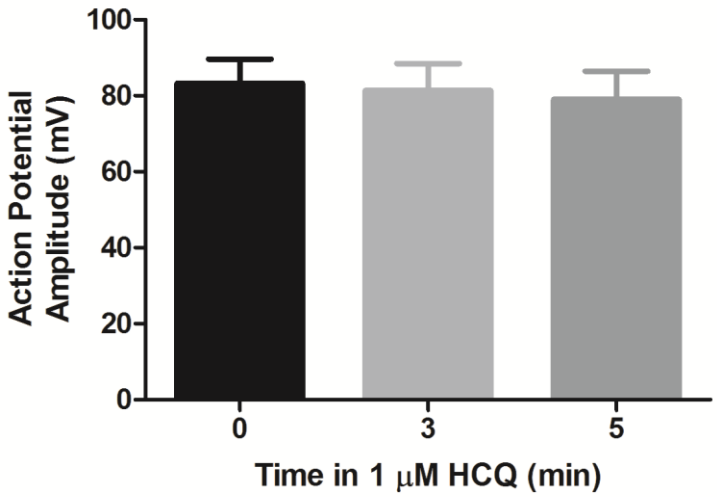


Figure 5.8: Lack of effect of HCQ on AP amplitude
Summary bar graph to show action potential amplitude in mV, recorded in isolated guinea pig sino-atrial node myocytes under control conditions and during superfusion of HCQ at 1 μM. Solutions were maintained at 35±2 ºC and cells were allowed to fire action potentials spontaneously. Data are presented as mean±SEM. No significant change was observed over the course of 5 min ($P > 0.05$, One-way ANOVA, n=6).

5.3.3 HCQ reduces stimulated $I_{(f)}$ current

The previous set of experiments, investigating the effect of HCQ on action potential parameters suggested that the major effect was manifest during phase 4 of the action potential, spontaneous diastolic depolarisation.

We investigated the hypothesis that HCQ could be inhibiting the funny current using voltage-clamp of isolated guinea pig sino-atrial node myocytes. Cells were recorded in the perforated patch configuration to maintain the intracellular milieu and, after full access was gained, membrane voltage was held at -40 mV. Step hyperpolarisations of 2 s in duration were driven at a rate of 1/20 Hz, cycling between steps to -80, -100 and -120 mV and maximal $I_{(f)}$ was measured under control conditions and during HCQ superfusion as the difference between maximal current flow and current at the start of the voltage step. A representative trace showing stimulated $I_{(f)}$ at the three voltage steps before and during superfusion with 1 μM HCQ can be seen in figure 5.9.

1 μM HCQ significantly reduced stimulated $I_{(f)}$ current across the range of voltages tested in this study ($P < 0.05$, Two-way ANOVA, n=7) and this reduction was not affected by the voltage step (interaction effect, $P > 0.05$, Two-way ANOVA, n=7). This data is presented in Figure 5.10 (i), as peak current before and 5 min into 1 μM HCQ superfusion and Figure 5.10 (ii), as proportional change. Post-testing (Bonferroni correction) showed the effect of 1 μM HCQ on change in stimulated voltage to be significant at the -80 and -100 mV voltage steps (both $P < 0.05$, n=7), with reductions over the course of 5 min amounting to 18±5% and 13±3%

respectively. Stimulated current during the -120 mV voltage step was reduced by 8±4% from control ($P > 0.05$, n=7).

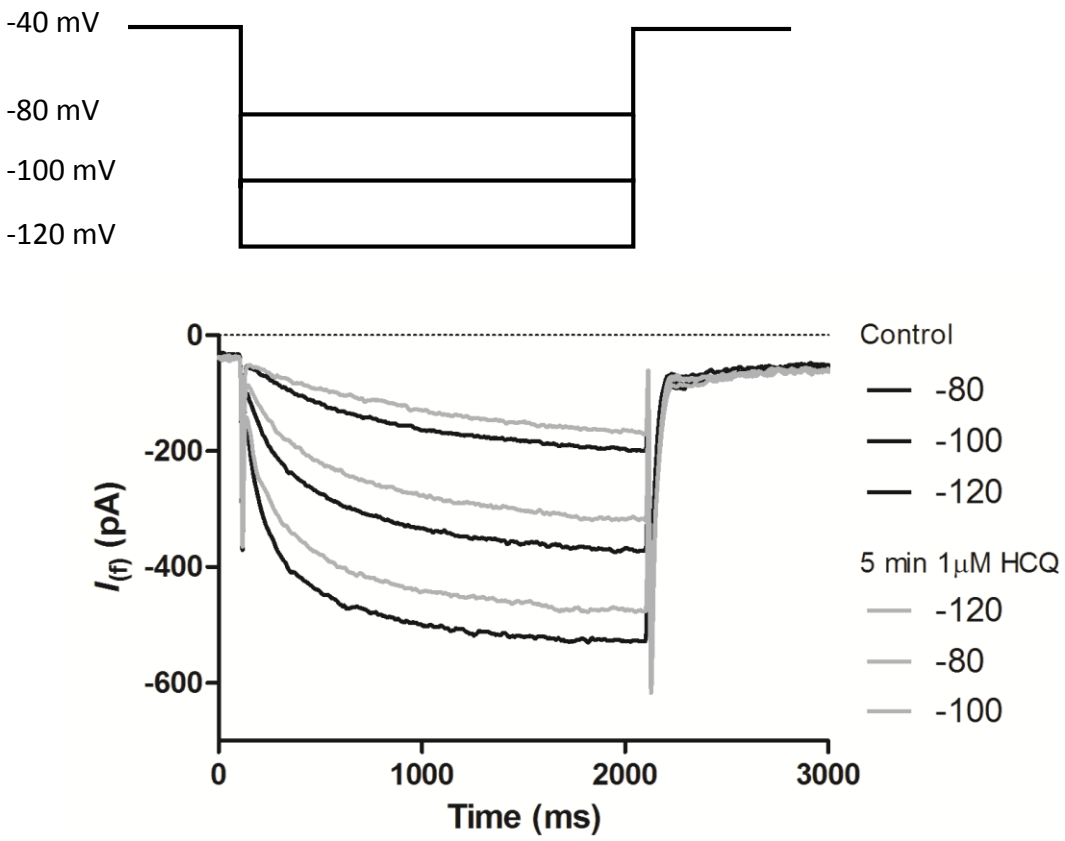


Figure 5.9: Representative trace to show the effect of HCQ on $I_{(f)}$
Representative trace from voltage clamp recording in an isolated guinea pig sino-atrial node myocyte to show $I_{(f)}$ stimulated during hyperpolarising voltage steps to -80, -100 and -120 mV under control conditions (physiological salt solution), and 5 min after switching to 1 μM HCQ. Solutions were maintained at 35±2°C throughout and the cell was stimulated with a 2 s voltage pulse once every 20 s. In between voltage pulses, the cell was held at a membrane voltage of -40 mV.

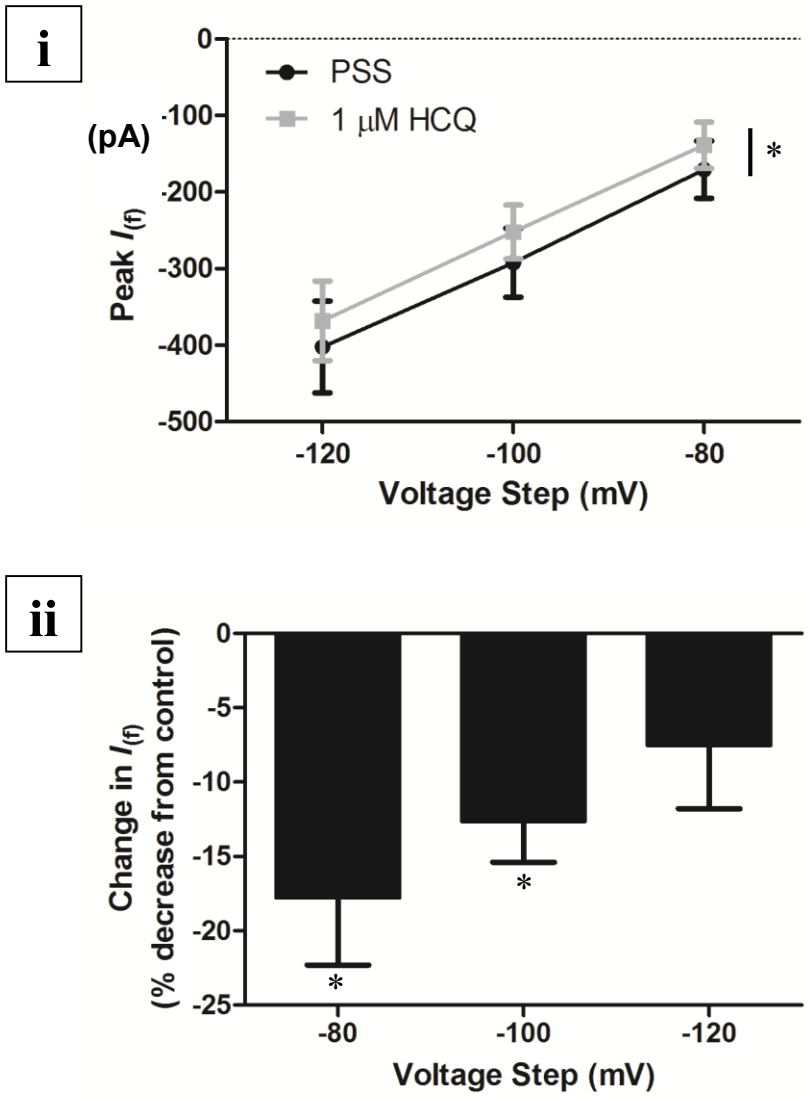


Figure 5.10 (i) and (ii): The effect of HCQ on $I_{(f)}$ current

Summary graphs to show the effect of 1 μM HCQ to reduce stimulated $I_{(f)}$ current in isolated guinea pig sino-atrial node myocytes. n=7 for each group presented, data are given as mean±SEM and all experiments were carried out at 35±2 ºC. Data are presented as:

(i) Peak $I_{(f)}$ current stimulated by voltage steps from -40 mV to -80, -100 or -120 mV at a rate of 1/20 Hz, where peak current is equal to peak stimulated current minus current at the onset of the voltage pulse. 1 μM HCQ caused a significant reduction in stimulated $I_{(f)}$ ($P < 0.05$, Two-way ANOVA, n=7) which was not dependent on the voltage step (interaction effect with voltage step, $P > 0.05$).

(ii) Percentage change in $I_{(f)}$ at each voltage step after 5 min of exposure to 1 μM HCQ. A significant effect of 1 μM HCQ was observed during steps to -80 and -100 mV, reductions of 18±5% and 13±3% respectively from current measured in PSS ($P < 0.05$ and n=7 for both groups). * denotes significant difference from magnitude in PSS by Bonferroni post-test

5.3.4 HCQ reduces stimulated $I_{(f)}$ current in a dose-dependent manner

When investigated in multicellular preparations, the effect of HCQ on spontaneous beating rate in mouse atria was found to be dose-dependent. If the major action of HCQ in reducing beating rate were through inhibition of the funny current, then a dose-dependency in $I_{(f)}$ inhibition would also be expected.

We investigated the dose-dependent effect of HCQ on the funny current in isolated guinea pig sino-atrial node myocytes. Sino-atrial node myocytes were exposed to either 1 μM or 10 μM HCQ and the change in maximal $I_{(f)}$ current at the -100 mV voltage step compared between the two doses, where peak current is measured as maximal current flow minus current at the start of the voltage pulse. A representative trace to show the effect of each dose on stimulated $I_{(f)}$ is presented in Figure 5.11.

Superfusion of either 1 or 10 μM HCQ led to a significant reduction in stimulated $I_{(f)}$ at the -100 mV step, by 13±3% ($P < 0.05$, paired t-test compared to control, n=7) and 32±7% ($P < 0.05$ paired t-test compared to control, n=4) respectively. The inhibition of $I_{(f)}$ on exposure to 10 μM HCQ was significantly greater than that caused by exposure to 1 μM HCQ ($P < 0.05$, Student's t-test) and could be partially reversed by washout for 10 min with PSS. Data comparing the $I_{(f)}$ response to HCQ superfusion at the two doses is compared in Figure 5.12. The effects of HCQ were at least partially recoverable on wash-out. An example of a current-voltage relation collected before 10 μM HCQ, at the point of maximal response and 10 min after switch back into PSS is illustrated in Figure 5.13.

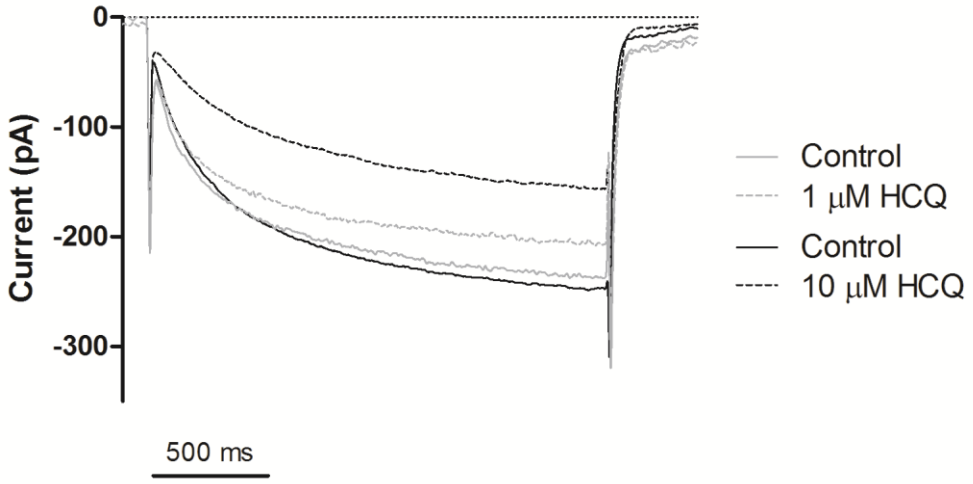


Figure 5.11: Representative traces to show the effect of different doses of HCQ on $I_{(f)}$
Representative traces are presented to show the $I_{(f)}$ measured by step hyperpolarisation to -100 mV before and after exposure to either 1 or 10 μM HCQ. Each cell was exposed to a single concentration of HCQ, so representative traces are presented from two separate experiments. Step hyperpolarisations were applied from a holding potential of -40 mV to -100 mV for 2 s at a rate of 1/20 Hz. Traces shown are the average of at least two currents recorded in control and at maximal response to HCQ. In all experiments, bath temperature was maintained at 35±2 ºC.

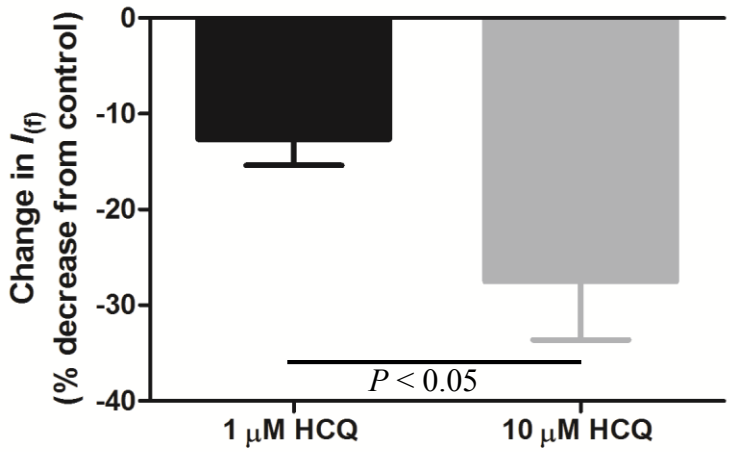


Figure 5.12: The magnitude of $I_{(f)}$ inhibition by HCQ is dose-dependent
Summary graph to show the effect of different concentrations of HCQ on stimulated $I_{(f)}$. Data represent maximal response in both cases. Data are presented as mean±SEM. The inhibition of $I_{(f)}$ caused by exposure to 10 μM HCQ was significantly greater than that caused by exposure to 1 μM HCQ ($P < 0.05$, Student's t-test, n = 5 for the 10 μM dose and n = 7 for the 1 μM dose). $I_{(f)}$ current was stimulated by a step depolarisation from the holding potential of -40 mV, to the test potential of -100 mV for 2 s duration at a rate of 1/20 Hz. Maximal current was measured as maximal current during the test pulse minus current at the start of the test pulse. Change in $I_{(f)}$ is given as percentage change from control (superfusion of PSS) and refers to maximal response. All experiments were carried out at 35±2 ºC.

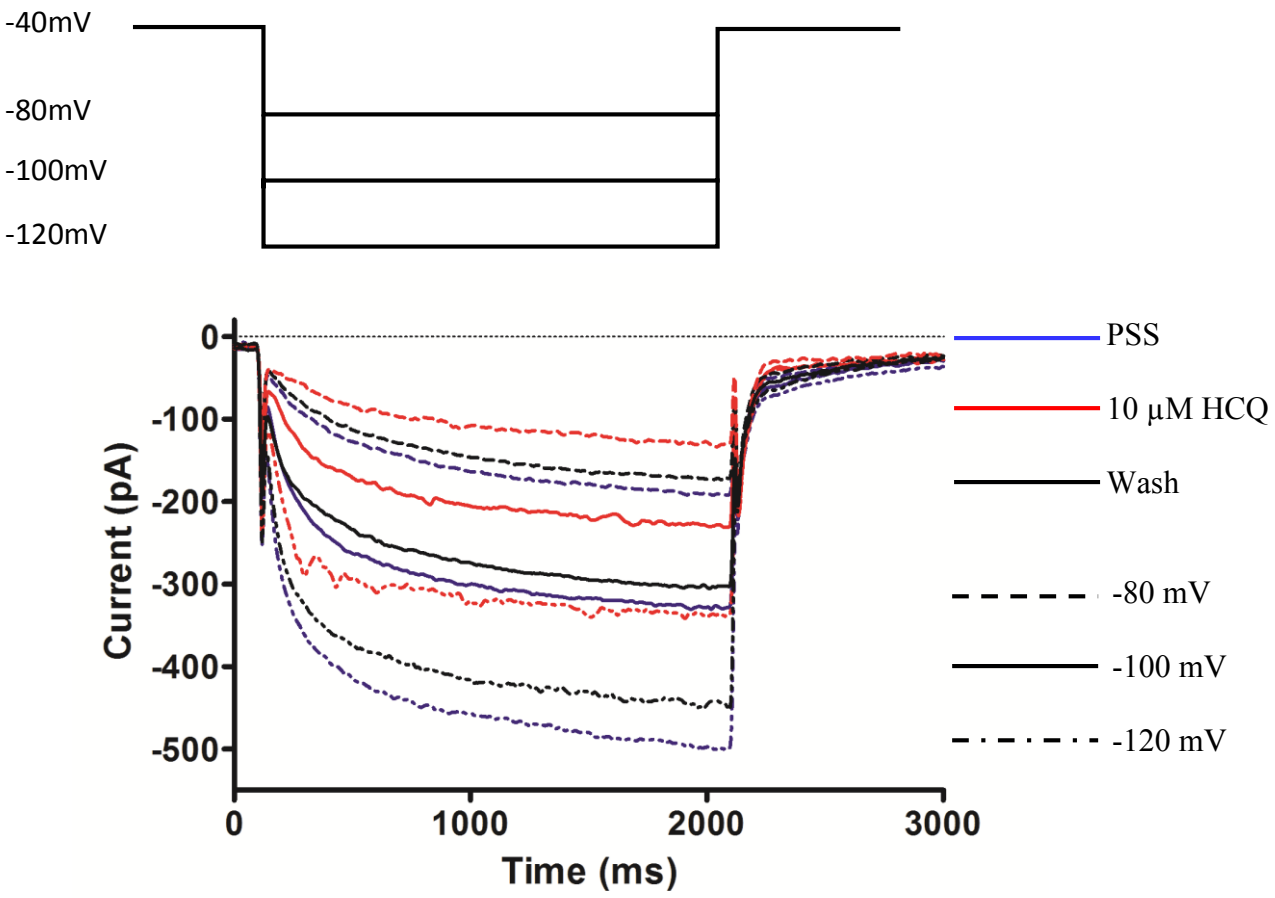


Figure 5.13: Illustration of HCQ wash-out
Attempts to collect wash-out data were not made with every experiment under study due to the prolonged nature of these recordings and the propensity for patch loss during attempts at prolonged wash. Where wash data was collected, however, at least partial recovery of the current was consistently observed. Representative trace above shows $I_{(f)}$ currents stimulated by 2 s voltage pulse to a final potential of -80, -100 and -120 mV under control conditions (blue lines), at maximal response to 10 µM HCQ (red lines) and 10 min after return to PSS (black lines). Lines sharing the same pattern correspond to the same voltage step applied under the three conditions.

5.4 DISCUSSION

The data presented in this chapter are the first evidence of both cardiac rate and SAN-cell 'funny' current modulation by the antimalarial agent hydroxychloroquine. Low doses of HCQ have been shown to cause significant slowing of beating rate in both multicellular preparations and isolated myocytes, with inhibition of the funny current, $I_{(f)}$, the most likely mediator of these effects.

HCQ caused a dose-dependent reduction in beating rate in spontaneously-beating mouse atrial preparations, an effect which was confirmed in isolated myocytes. The reduction in action potential firing rate of isolated myocytes can be mostly attributed to a flattening of phase 4 of the action potential, spontaneous diastolic depolarisation, which was affected to a much greater degree than action potential duration.

When superfused over isolated SAN myocytes at 35±2 ºC, the effect of HCQ on $I_{(f)}$ is relatively slow to develop (Tau = 83 s at 10 μM). It is interesting to note, in this regard, that ivabradine also exhibits a slow onset of channel block in its actions on $I_{(f)}$ (Bois *et al.*, 1996). All tested SBAs, however successful they have been, contain an amide group in their chemical structure which will be protonated at cellular pH, and HCQ is no different.

Ivabradine has been shown to develop use-dependent block of $I_{(f)}$ (Bucchi *et al.*, 2002), defined by the need for a channel to be in a specific state in order for interaction with the blocking compound to take place. For ivabradine, this means that the compound must be within the cell and that an $I_{(f)}$ channel must be open in order for the charged amide to penetrate the core and interfere with the current.

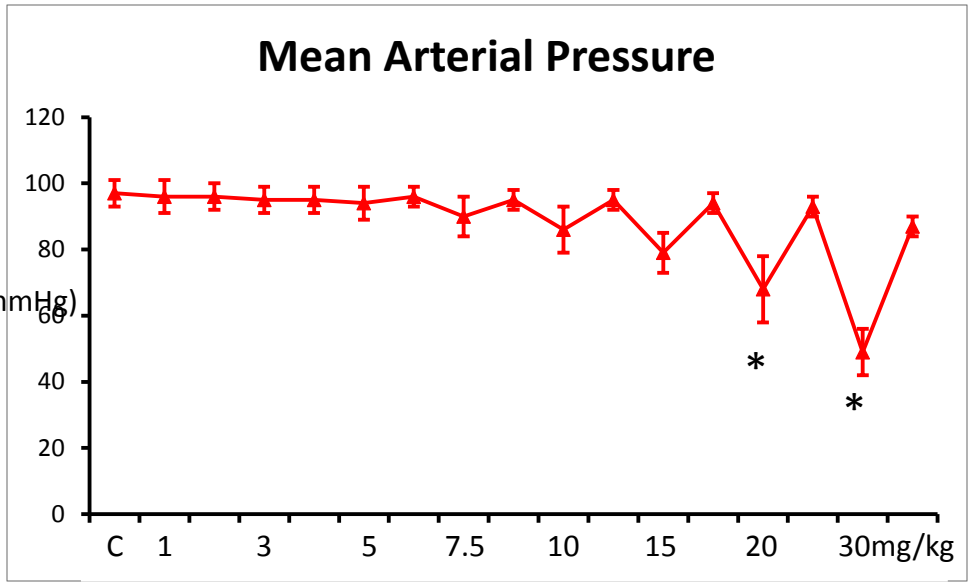
Interestingly, it is actually the brief outward current which passes through HCN4 channels during depolarisation which is responsible for forcing ivabradine into the channel pore. The rapid cycling of membrane voltage in SAN myocytes, then, actually promotes inhibition by ivabradine when it is present in the cytosol. It is likely, given the presence of a similar chemical group in HCQ and the kinetics of onset of inhibition by this compound, that a similar form of use-dependent block is exhibited by HCQ. Testing this hypothesis, for instance by using voltage clamp to hold the channels closed during HCQ superfusion then testing the size of the current at the point where response would be maximal during the step protocols, would be an interesting avenue for further experimentation, both from the perspective of HCQ as an $I_{(f)}$ blocker and the properties of $I_{(f)}$ blockers as a generalised class of agent.

In terms of its clinical actions, the treatment of systemic inflammatory conditions using HCQ is unlikely to arise from the novel mechanism presented in this chapter. Principally, this distinction is made on the basis that clinically beneficial effects of HCQ on RA and/or SLE develop 3-6 months after the onset of treatment, whereas the inhibition of the funny current presented herein is an acute effect. Chloroquine and HCQ are weak bases and, as such, accumulate in acidic stores such as endosomes and lysosomes, where they have the ability to increase compartmental pH (Ohkuma and Poole, 1978). Inhibition of some of the functions of these organelles, for instance production of MHC class II and presentation of antigens, is proposed to account for the anti-inflammatory activity (Abarientos *et al.*, 2011). It is not known whether this activity has a bearing on the NAADP pathway described in Chapters 3 and 4, however it is likely that the calcium concentration within lysosomes will be reduced

under more basic conditions (Morgan and Galione, 2007) and it would be interesting to know if NAADP-mediated responses are reduced after treatment.

One known clinical side-effect of HCQ is the advent of visual disturbance and, in extreme cases, retinopathy which is not always reversed by cessation of drug administration (BNF, 2012). HCN expression occurs in the retina where it is thought that the opening of these channels during rod/cone hyperpolarisation acts to sharpen the voltage signal associated with a light pulse (Della Santina *et al.*, 2010, Della Santina *et al.*, 2012). The acute visual changes and light sensitivity sometimes associated with HCQ use, then, could feasibly arise from an HCN-block-mediated prolongation and of rod and cone responses.

As well as the single cell work presented in this chapter, our collaborator Dr Neil Herring has undertaken *in vivo* studies to investigate the effects of HCQ on heart rate and blood pressure in healthy adult rats. These studies are summarised by the graphs in Figure 5.14. Bolus injections of HCQ are able to reduce heart rate in anaesthetised animals, an effect which is transiently significant at a dose of 7.5mg/kg and reaches a level at which heart rate is maintained below starting levels at a dose of 20mg/kg. No sustained changes in mean arterial pressure were observed over the course of these experiments, though bolus injections of 20 and 30mg/kg did cause significant, transient falls which were recovered to control levels.



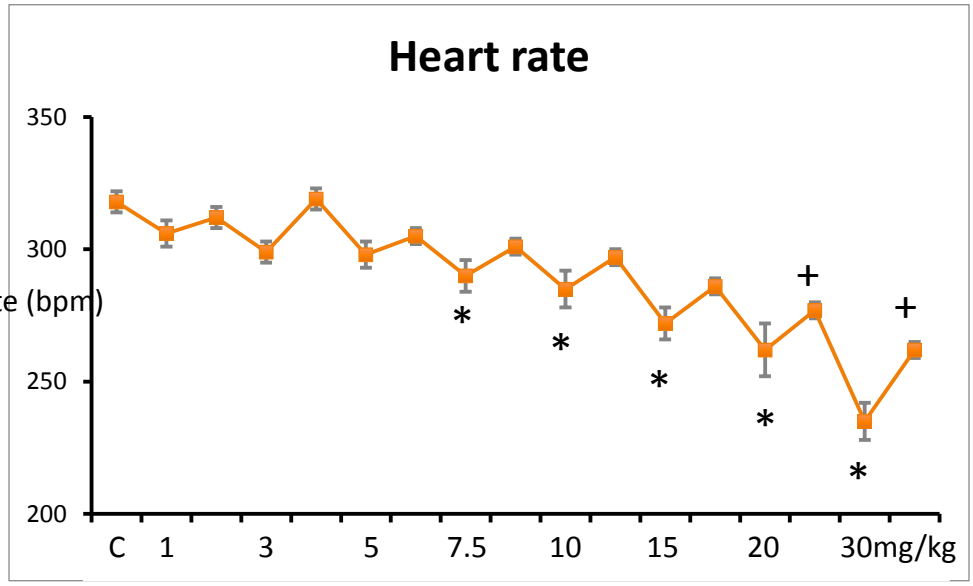


Figure 5.14: In vivo bolus injections of HCQ affect heart rate but not blood pressure
Summary data observed during application of cumulative doses of HCQ given by bolus injection in anaesthetised, adult rats (n=6). * indicates significant response in comparison to rate measured before injection. + denotes maintenance of response over the course of 30 min from injection. Figure presented with permission of Dr N Herring, Department of Physiology, Anatomy and Genetics, University of Oxford.

In clinical terms it is interesting to note that cardiac side-effects with prolonged use of antimalarials, including both chloroquine and HCQ, are reported in the literature but vanishingly rare. It is difficult to assess the absolute role of these agents in the context of the cardiac health of RA and SLE patients because both of these conditions can also affect cardiac tissue over time, however review of the literature from 1948 to 2002 found 3 reported cases of complete AV-nodal block and 7 reported cases of heart failure arising from chloroquine, HCQ or their use in combination (Nord *et al.*, 2004). All cases where dose information was available showed them to be associated with an extremely high dose regimen of chloroquine or hydroxychloroquine, exceeding the recommended maximal mg/kg for prolonged periods of time. It would seem, therefore, that prolonged high-dose administration of HCQ can produce cardiac side-effects in some individuals, and that some of these are consistent with the actions on $I_{(f)}$ described in the this chapter, whilst some are better suited to an explanation including negative inotropy.

HCQ is chemically very close to chloroquine. Chloroquine is known to inhibit both voltage-gated potassium and calcium channels (Sánchez-Chapula *et al.*, 2001) and is therefore likely that HCQ will, at some concentration, have significant effects on the L-type calcium current and I_{Kr} potassium current. All SBAs, at some concentration, lead to negative inotropic effects upon ventricular myocardium, however it is the ratio of dose required for rate-reduction and for negative inotropy which is most pivotal in the therapeutic potential of such compounds (Kobinger and Lillie, 1987).

The experiments presented in this chapter did find a significant lengthening of sino-atrial node action potentials elicited by 1 μM HCQ. To some extent, action potential

lengthening is expected with any slowing of firing rate, however it will be most important during the next stages of this project to measure ionic currents from L-type calcium channels and I_{Kr} and I_{Ks} potassium channels during exposure to HCQ. In one preliminary experiment, 1 μM HCQ was found to reduce I_{CaL} stimulated by 200 ms step depolarisations from -40 mV to 0 mV at a rate of 0.2 Hz by just 1.8% after 10 min of superfusion (from 133 to 130 pA), however more data are required in order to compare the effects of HCQ with those of ivabradine in this regard. It would also be prudent to carry out Langendorff-based studies of the effect(s) of HCQ on both rate and ventricular contractility before further recommendations can be made in respect to the clinical potential of such a compound in cardiac conditions.

The data in this chapter have shown HCQ to be effective at reducing cardiac rate, and suggest that this is due to inhibition of the 'pacemaking current' $I_{(f)}$. There are many further questions to be answered with respect to interaction with other currents but at this stage the compound shows promise as a novel $I_{(f)}$ inhibitor and possible specific bradycardic agent.

6 THE ENDOGENOUS PEPTIDE APELIN CONFERS BOTH POSITIVE INOTROPY AND POSITIVE LUSITROPY

6.1 INTRODUCTION

Apelin, an endogenously-produced peptide first identified from bovine stomach extracts (Tatemoto *et al.*, 1998), is the most potent positive inotropic substance as yet identified in multicellular cardiac preparations, with an EC_{50} of 33pM (Szokodi *et al.*, 2002). This fact alone makes investigation of its actions of interest, however clinically-important observations have further fuelled the need to identify the true role and mechanisms of apelin signalling in the heart.

Increased circulating apelin levels have been reported to correlate with severity of heart failure during the early phase of the condition, as given by NYHA classification (Chen *et al.*, 2003). This was manifest in a significant increase in expression in patients from classes I and II, compared against that measured in healthy control subjects, followed by a fall in class III and IV patients. Furthermore, successful treatment of heart failure by implantation of a left ventricular assist device (LVAD) has been shown by enzyme immunoassay to increase ventricular apelin levels (Chen *et al.*, 2003).

In situ, apelin acts via the APJ receptor, the G-protein-coupled receptor from which apelin derives its name (APJ-receptor ligand). Initially recognised as an 'orphaned GPCR' through the human genome project, APJ is structurally similar to angiotensin-converting enzyme type II but does not bind angiotensin. It has been found by RT-PCR to be present in most tissues (Hosoya *et al.*, 2000), with the highest levels of expression in the lung, brain, and heart. This tissue distribution is very similar to that of apelin mRNA (Kawamata *et al.*, 2001). In the Chen study, APJ receptor was the gene most upregulated by successful LVAD treatment, as measured through gene

array. It is thought that APJ in cardiac myocytes is partially coupled to the G_q signalling pathway as inhibitors of PKC significantly inhibit apelin responses in cardiac tissue (Szokodi *et al.*, 2002, Wang *et al.*, 2008). However, APJ is generally considered to be a G_i-linked receptor (Moon *et al.*, 2007) and pertussis toxin has been shown to inhibit extracellular acidification in cellular expression systems (Scimia *et al.*, 2012). The exact signalling pathway involved in apelin responses in cardiac myocytes is yet to be elucidated.

Apelin is synthesised as preproapelin, a 77 amino acid pre-proprotein (Tatemoto *et al.*, 1998). It is then cleaved to its active forms, of which 46 have been identified in bovine colostrum (Mesmin *et al.*, 2011). At least four fragments are biologically important, the -12, -13, -17 and -36 amino acid proteins (O'Carroll *et al.*, 2013). These all represent fragments of the N-terminal region of the pre-proprotein and increase in potency but decrease in receptor binding affinity as the size of fragment is reduced (Hosoya *et al.*, 2000).

These data have led investigators to suggest that apelin, acting to increase cardiac contractility, may increase in expression during early heart failure as a mechanism of compensation. In *in vivo* studies, prolonged administration of apelin at 2 mg/kg/day caused a significant increase in cardiac output without any evidence of hypertrophy, as assessed by post-mortem organ weight and histological analysis (Ashley *et al.*, 2005). Further, multiple studies have reported that apelin administration has proportionally more effect in failing hearts, whether *in vivo* on stroke volume (Berry *et al.*, 2004) *in vitro* on force generation (Dai *et al.*, 2006). Indeed, Berry and colleagues reported that apelin infusion to Langendorff hearts at 0.01 µg/min was

able to restore cardiac output in adult male rat hearts 6 weeks post MI to near-control levels within 20 min.

For such a potent signalling peptide, relatively little research has been carried out investigating mechanisms of action and effects on contractility in isolated cardiac myocytes. To date, just two papers have been published which show contraction effects in isolated cardiac myocytes (Farkasfalvi *et al.*, 2007, Wang *et al.*, 2008). Both papers utilised isolated rat ventricular cardiomyocytes and both concluded an increase in fractional cell shortening. Farkasfalvi *et al*. (2007), however, reported a rapid onset and short duration of effect at body temperature which was associated with cellular alkalinisation and no change in calcium transient amplitude, whilst Wang *et al*. (2008) reported an increase in cellular contraction at 10 min after the onset of exposure at room temperature associated with a significant increase in calcium transient amplitude. Constitutive apelin knock-out mice are viable but show distinct reduction in sarcomere shortening without a change in cellular calcium transient amplitude when assessed in single cells compared to litter-mate controls (Charo *et al.*, 2009).

One further study has made investigations into the effects of apelin more challenging to interpret; apelin signalling is thought to be stimulated by hypoxia. In cultured cardiomyocytes, apelin mRNA expression was stimulated 3.7-fold by exposure to 2% O_2 for 2 hours, whilst perfused rat atrium exhibited a 2.5-fold increase in apelin mRNA expression after exposure to 12% O_2 for the same period of time (Ronkainen *et al.*, 2007). These observations have important ramifications for the study of apelin on isolated myocytes, in that it is important to maintain good oxygenation throughout

the isolation and storage of cells in order that endogenously-produced apelin does not confound the effects of exogenous administration.

The aim of this section of work was to develop a method for the study of apelin effects in isolated ventricular myocytes and carry out preliminary investigations into which portions of ventricular contraction and/or relaxation these might manifest.

6.2 METHODS

Murine ventricular myocytes were isolated using a method adapted from O'Connell and colleagues (O'Connell *et al.*, 2007). Briefly, adult male C57/BL6 mice were killed by concussion followed by cervical dislocation. The heart was excised, placed in Tyrode solution (in mM: NaCl 140, KCl 10, $CaCl_2$ 1.8, $MgCl_2$ 1, HEPES 5, glucose 11) and mounted on a constant flow Langendorff system (4 ml/min, body temperature) for retrograde perfusion via the aorta. The heart was washed with zero-Ca^{2+} perfusion buffer for 4 min (in mM: NaCl 120.4, KCl 14.7, KH_2PO_4 0.6, Na_2HPO_4 0.6, $MgSO_4$ 1.2, HEPES 10, $NaHCO_3$ 4.6, Taurine 30, BDM 10, Glucose 5.5, pH to 7.0 with HCl) before switching to digestion buffer for 3 min (Perfusion buffer plus 2.4mg/mL collagenase type II, Worthington). Finally, perfusion was continued for a further 8 min in low-Ca^{2+} digestion buffer (zero-Ca^{2+} digestion buffer plus 40 μM $CaCl_2$). The heart was removed from the perfusion system, and ventricles dissected into small pieces. Digestion was stopped with a myocyte stopping buffer (9 parts perfusion buffer, 1 part bovine calf serum plus 12.5 μM $CaCl_2$), cells were mechanically dissociated and calcium was gradually re-introduced (3 min centrifugation at 20g, supernatant removed and replaced with myocyte stopping buffer at, sequentially, 100, 400 and 900 μM [Ca^{2+}]).

Rat ventricular myocytes were kindly provided by the Vaughan-Jones laboratory, Department of Physiology, Anatomy and Genetics, University of Oxford, and were isolated using a collagenase and protease-based enzymatic digestion on a retrograde perfusion Langendorff system, followed by mechanical dissociation.

Pyr-Apelin-13 was used for all experiments presented.

Isolated myocytes were visualised using a Leica DMIRB inverted microscope. Cells were field-stimulated via a MyoPacer. Contraction data was collected using a MyoCamS digital camera system running at a frame rate of 240 Hz, and interpreted using IonWizard software (all products from IonOptix, MA, USA).

Raw data recorded in IonWizard was converted into .txt format and analysed using a MatLab program written in-house to calculate diastolic sarcomere length (DSL), fractional sarcomere shortening (FSS), maximum velocity of contraction (VmaxCon), maximum velocity of relaxation (VmaxRel), time taken to reach 90% of peak contraction (TTP) and time taken to reach 90% of full relaxation (TTRx). For TTP measurements, the TTL pulse which initiated field stimulation was taken to be the start of contraction. TTRx measurements were measured from the moment of peak contraction.

Pilot data carried out in the Kohl laboratory (Dr C Bollensdorff, data not published) suggested that the actions of apelin could change under differing mechanical loads. poly-HEMA coated coverslips were therefore used to ensure cells were not adhered to the cover-slip. Due to the use of poly-HEMA to reduce mechanical association of the cover-slip to the cells, experiments were carried out in static solution and recordings could not be made as paired.

Data from each condition was analysed by multi-way ANOVA and $P < 0.05$ was taken to indicate a significant difference between means.

6.3 RESULTS

6.3.1 Apelin increases cellular contractility in mouse ventricular myocytes

Before mechanisms of apelin actions could be studied, it was important to find an experimental protocol whereby apelin could be studied in a reliable and repeatable manner. Previously, it was reported to us that apelin experiments would be 'successful' in just 30-40% of cases (Dr Cesare Terracciano, personal communication) and it was essential that we found conditions which would allow reliable reproduction of a response. For this we utilised both mouse and rat models. This was carried out such that future investigations were feasible in transgenic mouse models and in order to consider the possibility of species differences between these mouse results and the species used in previously published studies (rat).

Isolated mouse ventricular cardiomyocytes were placed into oxygenated control or apelin-containing (10nM) Tyrode solution maintained at 37 ºC and allowed to settle on a poly-HEMA-coated coverslip. poly-HEMA was used to minimise adhering of myocytes to the coverslip and abolish confounding mechanical effects on the cell. Cells were field-stimulated to fire at 1 Hz. On each experimental day a total of at least 80 recordings were taken, 40 under each condition. Responses on a single day were compared by Student's t-test. To assess the complete data set, n of 6 experimental days, one-way ANOVA analysis was used with $P < 0.05$ considered significant. Fractional sarcomere shortening (FSS), percentage shortening from the diastolic sarcomere length, was used to monitor contractile amplitude.

A representative trace to show the effect of apelin on the course of contraction in isolated murine cardiac ventricular myocytes is presented in Figure 6.1.

Apelin (10nM) caused a significant increase in FSS of 8±2% ($P < 0.05$, ANOVA analysis, n=18). No change in diastolic sarcomere length was noted between the two groups ($P > 0.05$, ANOVA analysis, n=18). Graphs to illustrate the effect of apelin on diastolic sarcomere length and fractional sarcomere shortening can be seen in Figure 6.2.

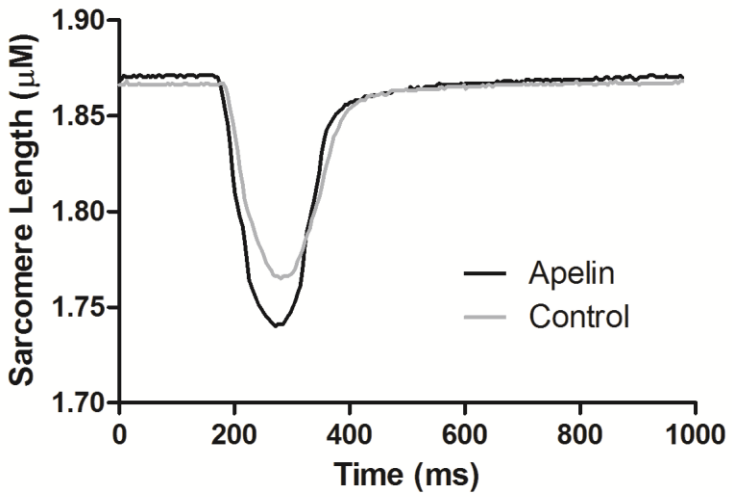


Figure 6.1: Representative trace to show a single contraction of mouse ventricular myocytes under control conditions and in the presence of apelin

Representative trace to show the path of contraction, measured as sarcomere length using the IonOptix system, in two different isolated mouse ventricular myocytes, one contracting in Tyrode solution and the other exposed to 10 nM apelin in Tyrode solution. For this experiment, contractions were field-stimulated at a rate of 1 Hz and experiments were maintained at 36±1°C. Recordings were taken between 5 and 15 min in solution.

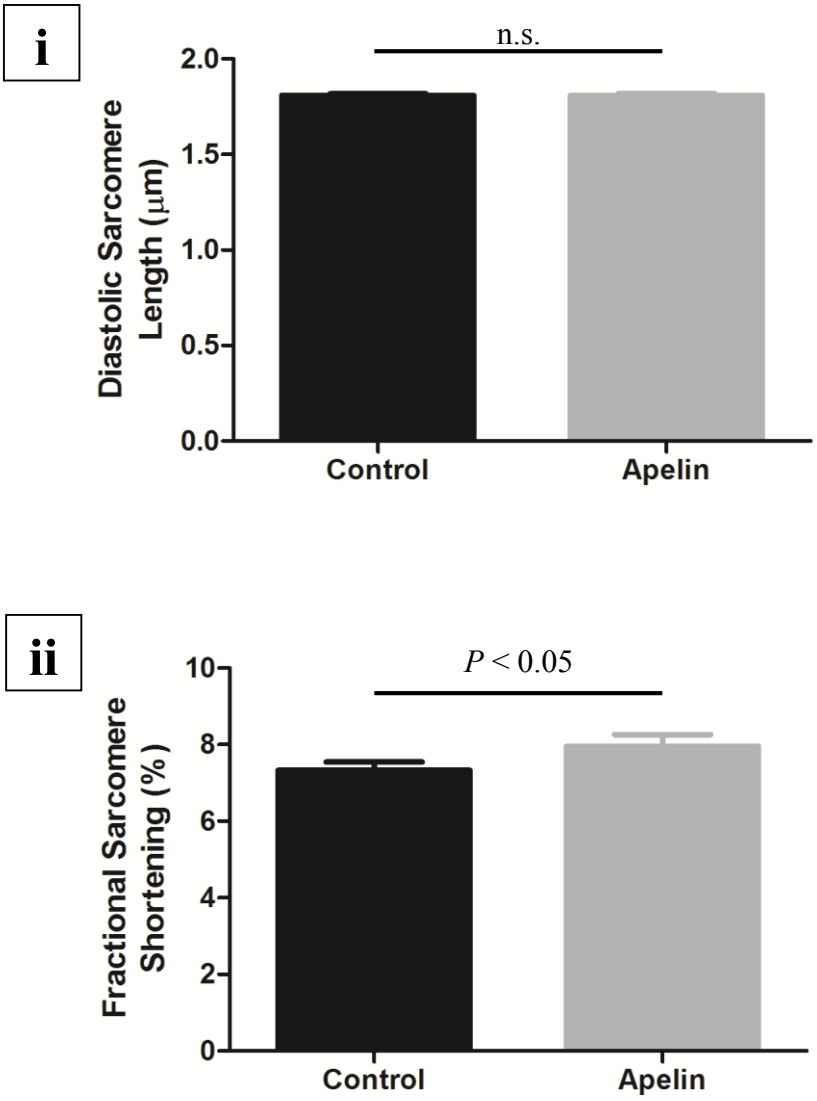


Figure 6.2 (i) and (ii): The effect of apelin on diastolic sarcomere length and fractional sarcomere shortening in murine ventricular myocytes

Summary bar graphs to show the effect of apelin on diastolic sarcomere length and fractional sarcomere shortening in isolated murine ventricular myocytes. Data are presented as mean±SEM. Apelin had no significant effect on DSL ($P > 0.05$, ANOVA analysis, n=18) but did significantly increase FSS, by 8±2% from control ($P < 0.05$, ANOVA analysis, n=18). Each n = data from one animal = at least 40 cells in the presence of control and a further 40 in the presence of 10 nM apelin. Data presented are pooled across recording conditions, n = 6 at 36±1°C 1 Hz stim, n = 6 at 36±1°C 2 Hz stim, n = 6 at 24±1°C 1 Hz stim.

In multicellular preparations an increase in contractility is defined as the intrinsic ability of cardiac muscle to contract against a constant afterload, and independent of preload. Changes in contractility are really changes in force as opposed to strictly an increase the shortening of myocytes in the tissue, encompassing both the rate of pressure development as well as size of contraction, and measurements of FSS alone, therefore, omit the possibility that changes in contractile power are occurring through an increase in contractile velocity. In multi-cellular preparations, contractility is normally investigated using pressure-volume loops however these are not feasible in a single cell model without the use of intricate carbon fibre stretching techniques.

Mouse data collected were therefore investigated for changes in the time taken to reach 90% peak contraction (TTP), time taken to complete 90% relaxation after this peak was reached (TTRx) and the maximal velocities of both contraction and relaxation (VMaxCon and VMaxRel).

The effect of apelin was strikingly consistent when contraction and relaxation times were measured. TTP was reduced in the presence of apelin by 10±1% ($P < 0.05$, ANOVA analysis, n=18) and this change was found to be significant in all individual data sets collected.

TTRx was also reduced in the presence of apelin ($P < 0.05$, ANOVA analysis, n=18). This effect amounted to an average reduction of 11±1% and was found to be significant in 16 out of 18 individual data sets.

The data described above are also complimented by concurrent increases in the peak velocities of contraction and relaxation. VMaxCon was increased by an average of

15±2% ($P < 0.05$, ANOVA analysis, n=18), whilst VMaxRel was increased by 19±3% compared to data measured in normal Tyrode solution ($P < 0.05$, ANOVA analysis, n=18).

Data presenting the effect of apelin on contraction parameters are summarised in Figure 6.3, whilst data presenting the effect of apelin on relaxation parameters are shown in Figure 6.4.

A summary graph to show the percentage change in all parameters under study after apelin administration is presented in Figure 6.5.

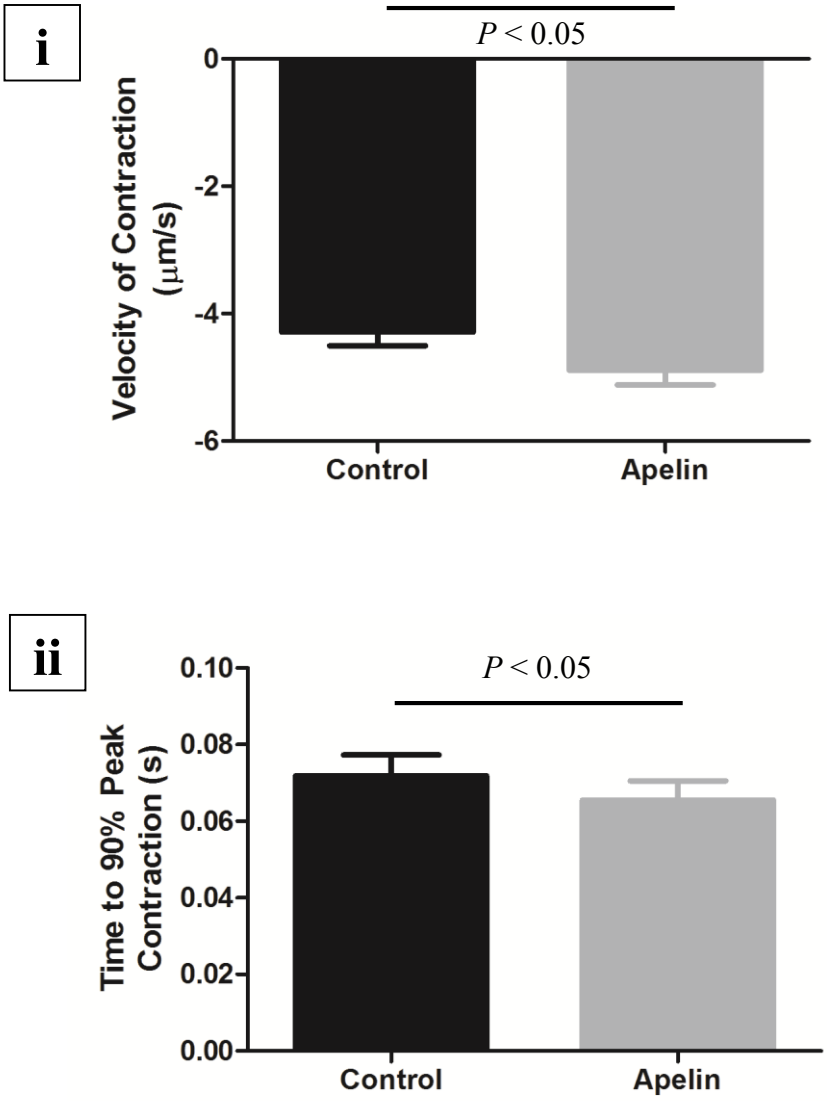


Figure 6.3 (i) and (ii): The effect of apelin on velocities of contraction and relaxation in murine ventricular myocytes

Summary bar graphs to show the effect of apelin on parameters measured during cell shortening, maximal velocity of contraction and time to peak. Data are presented as mean±SEM. 10 nM apelin conferred a significant acceleration in cell shortening, with VMaxCon increased by 15±2% ($P < 0.05$, ANOVA analysis, n=18). This was accompanied by a significant reduction in the time taken to reach 90% of peak contraction from the stimulus to contract (TTP), amounting to 10±1% ($P < 0.05$, ANOVA analysis, n=18). Each n = data from one animal = at least 40 cells in the presence of control and a further 40 in the presence of 10 nM apelin. Data presented are pooled across recording conditions, n = 6 at 36±1°C, 1 Hz stim, n = 6 at 36±1°C 2 Hz stim, n = 6 at 24±1°C 1 Hz stim.

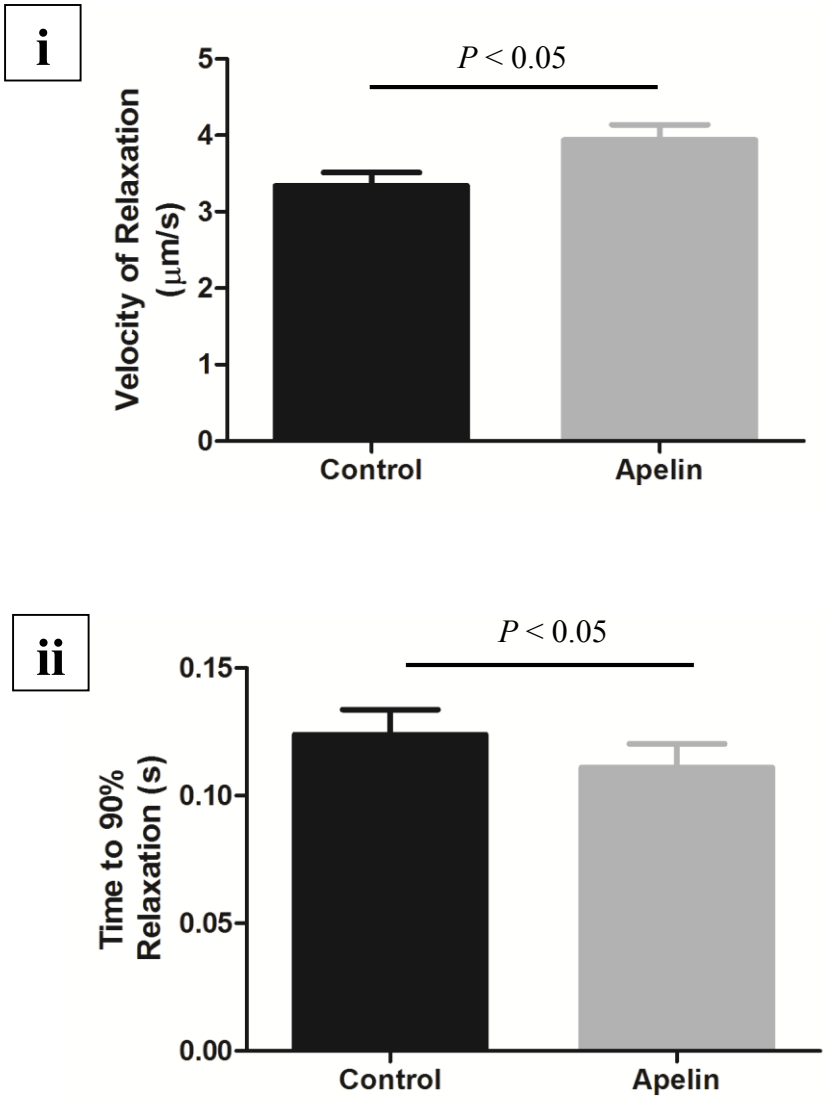


Figure 6.4 (i) and (ii): The effect of apelin on time taken to reach 90% of peak contraction and 90% of full relaxation in murine ventricular myocytes

Summary bar graphs to show the effect of apelin on cellular relaxation, measured through maximal velocity of cellular relaxation and time taken to reach 90% relaxation from the peak of contraction. Data are presented as mean±SEM. Cells exposed to 10 nM apelin exhibited a significant acceleration in cellular relaxation, with VMaxRel increased by 39±3% ($P < 0.05$, ANOVA analysis, n=18). This was accompanied by a significant reduction in TTRx, amounting to 11±1% ($P < 0.05$, ANOVA analysis, n=18). Each n = data from one animal = at least 40 cells in the presence of control and a further 40 in the presence of 10 nM apelin. Data presented are pooled across recording conditions, n = 6 at 36±1°C 1 Hz stim, n = 6 at 36±1°C 2 Hz stim, n = 6 at 24±1°C 1 Hz stim.

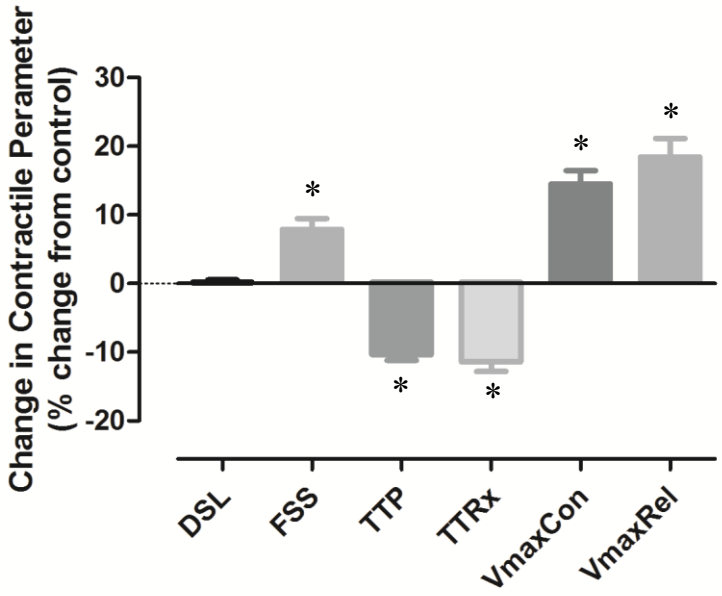


Figure 6.5: Summary graph to show all of apelin's effects on contraction in murine ventricular myocytes

Summary graph to show the percentage change in all parameters under study observed after exposure of murine ventricular myocytes to 10 nM apelin. Data are presented as mean±SEM. ANOVA analysis revealed no difference in diastolic sarcomere length ($P > 0.05$, n=18), a significant increase in fractional sarcomere shortening, VMaxCon and VMaxRel ($P < 0.05$, n=18, changes of 8±2, 15±2 and 18±3% respectively) and a significant reduction in the time taken to reach peak contraction and peak relaxation ($P < 0.05$, n=18, changes of 10±1 and 11±1% respectively). Each n = data from one animal = at least 40 cells in the presence of control and a further 40 in the presence of 10 nM apelin. Data presented are pooled across recording conditions, n = 6 at 36±1°C 1 Hz stim, n = 6 at 36±1°C 2 Hz stim, n = 6 at 24±1°C 1 Hz stim. * denotes a significant difference from control.

6.3.2 The effect of apelin on mouse cardiomyocytes is not dependent on temperature

In previously-published articles the effects of apelin had been suggested to be caused by disparate mechanisms, perhaps affected by differences in experimental conditions. We investigated, therefore, whether there were any gross differences in the effects of apelin on cellular contraction parameters caused by differences in temperature with the aim of replicating these studies using calcium- and pH-sensitive fluorophores in the next stages of the project.

Isolated murine ventricular myocytes were plated on poly-HEMA coated slides and field-stimulated at 1 Hz in control or apelin-containing Tyrode solution and maintained at either 24 or 36 ºC using heating plates surrounding the cover slip.

Under both temperatures, apelin caused a significant increase in FSS, VMaxCon, VMaxRel, TTP and TTRx. These effects were not significantly different between the two temperature conditions ($P > 0.05$, ANOVA analysis, n=12 at 37°C and n=6 at 24°C). A graph illustrating the comparison between the effect of apelin at 37 and 24 °C is presented in Figure 6.6.

It was also possible, using this and the previous set of experiments, to compare the responses of murine ventricular myocytes stimulated to fire at 1 or 2 Hz. Again, the same principal effects were seen under the two conditions, and stimulation rate was not found to have any significant effect on cellular response to apelin (Figure 6.7, $P > 0.05$, ANOVA analysis, n=12 at 1 Hz and n=6 at 2 Hz).

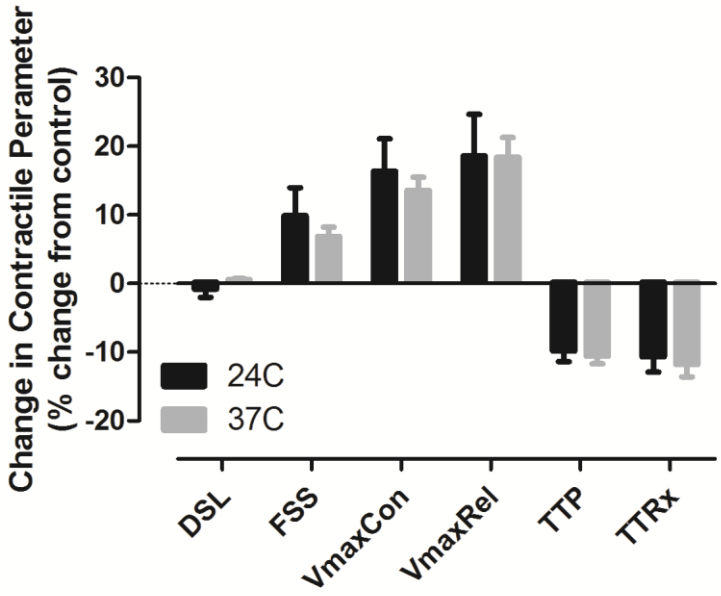


Figure 6.6: The effect of temperature on cellular responses to apelin

A comparison of the effects of 10 nM apelin on contractile parameters in murine ventricular myocytes under different temperature conditions. Across all parameters, no effect of temperature was found ($P > 0.05$, ANOVA analysis, n = 12 at 37°C and n = 6 at 24°C). Sarcomere length was recorded using an IonOptix system and cells were stimulated at 1 Hz during 24°C experiments and either 1 or 2 Hz during 37°C experiments (n = 6 of each frequency). Data are presented by parameter as mean±SEM.

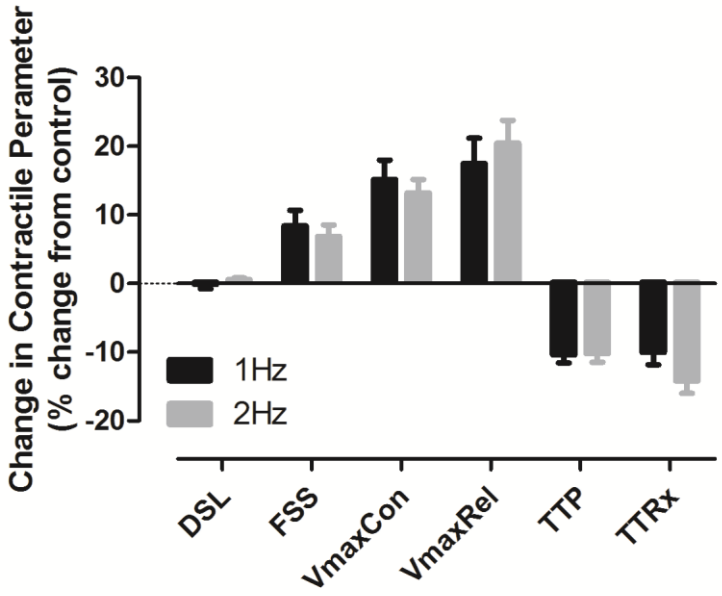


Figure 6.7: The effect of stimulation rate on responses to apelin

A comparison of the effects of 10 nM apelin on contractile parameters in murine ventricular myocytes stimulated to contract at different rates. Across all parameters, no effect of stimulation rate was found ($P > 0.05$, ANOVA analysis, n = 12 at 1 Hz and n = 6 at 2 Hz). Sarcomere length was recorded using an IonOptix system and cells were bathed in control Tyrode or 10 nM apelin containing Tyrode maintained at either 24±1°C (n = 6, all 1 Hz recordings) or 36±1°C (n=12, n = 6 for 1 Hz and 6 for 2 Hz recordings). Data are presented by parameter as mean±SEM.

6.3.3 Apelin does not increase fractional shortening in rat cardiomyocytes

Isolated rat ventricular myocytes were investigated in the same manner as in mouse experiments described above. Ventricular myocytes were plated on a coverslip coated in poly-HEMA and bathed in either control or apelin (10nM) containing Tyrode solution. Cells were stimulated to beat by field stimulation and sarcomere length was filmed using an IonOptix camera system. All experiments using rat ventricular cardiomyocytes were carried out at 36±1°C with a stimulation rate of 1 Hz.

A representative trace to show sarcomere length over the course of a single contraction under control and apelin conditions in rat cardiomyocytes is presented in figure 6.8.

Over the 6 animals studied, apelin (10nM) increased FSS by 6±5% when compared to myocytes contracting in control Tyrode solution. This was not a significant increase from control ($p=0.21$, ANOVA analysis, $n=6$). In fact, daily t-testing revealed that apelin mediated a significant increase in FSS in just 1/6 experiments. The effect of apelin on FSS observed on each experimental day is presented in figure 6.9. A summary of all conditions under study is presented in figure 6.12.

There was a small but significant increase in diastolic sarcomere length of rat cardiomyocytes in the presence of apelin. This difference was small, amounting to 0.02±0.00 μm, or 1.2±0.2%.

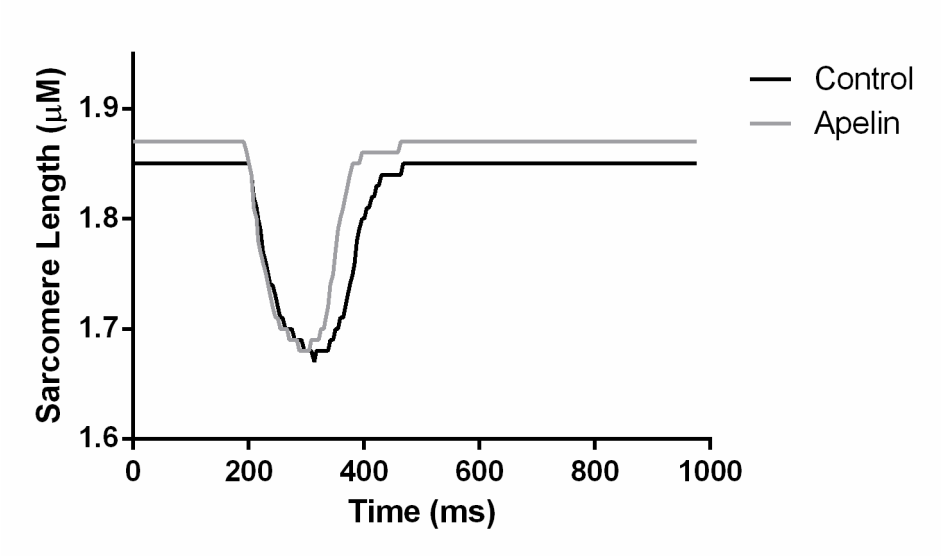


Figure 6.8: Representative trace to show the effect of apelin on the course of contraction in rat ventricular myocytes

Representative trace of a single contraction in an individual myocyte from each condition recorded from the same day of study. Recordings were carried out at 36±1 ºC with 1 Hz field stimulation. Recordings were taken between 5 and 15 min in solution.

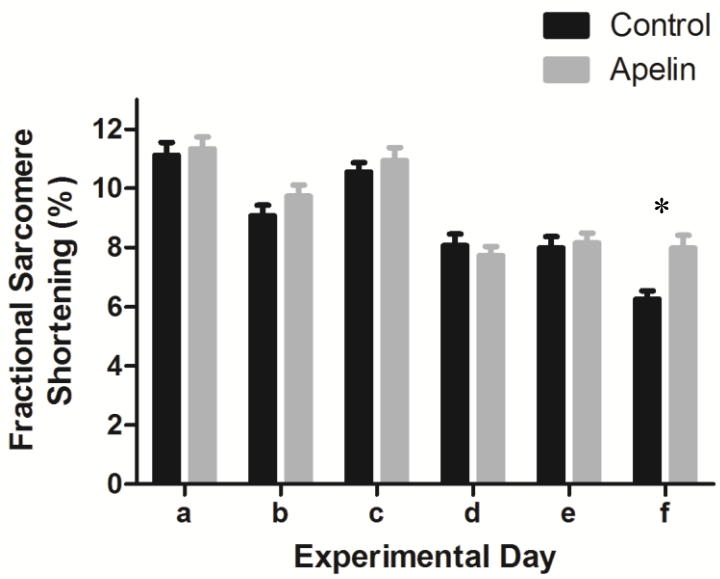


Figure 6.9: The effect of apelin on fractional sarcomere shortening in rat ventricular myocytes

Bar graph to show the effect of apelin on a population of cells recorded from each single animal over the course of an experimental day (at least 40 cells/condition/day). All experiments were carried out at 36±1 ºC, with 1 Hz field-stimulation. FSS increased significantly, by Student's t-test analysis, on only one occasion (Day f, 29% increase, $P < 0.05$). Data are presented as mean±SEM. On average, cells treated with 10 nM apelin showed a 6±5% increase in FSS when compared to control populations (ANOVA analysis p=0.21, n=6). * denotes significant response in individual experiment

6.3.4 Apelin consistently accelerates contraction and relaxation in rat ventricular cardiomyocytes

The same data sets presented above were also analysed for maximum contractile amplitude and time taken to reach 90% of peak contraction.

TTP was significantly reduced in every experiment, amounting to an average fall of 11±2% from control across the full data set (ANOVA analysis, $p<0.001$, n=6). This was complimented by a significant increase in VMaxCon of 14±5% in the presence of 10 nM apelin (ANOVA analysis, $P < 0.05$, n=6). TTP and VMaxCon data are presented as collected from each experimental day in figure 6.10. A summary of changes in all parameters analysed is presented in figure 6.12.

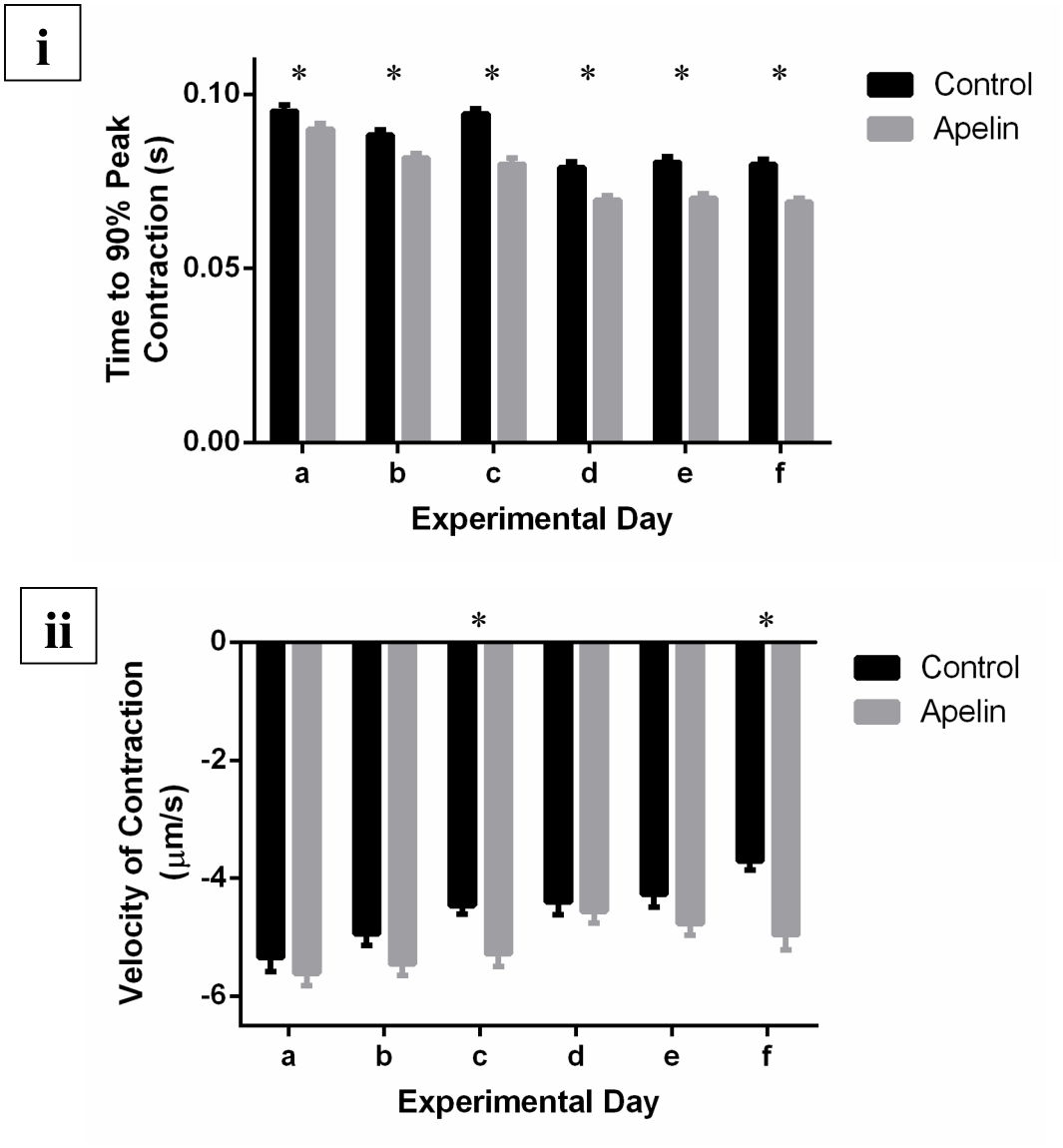


Figure 6.10 (i) and (ii): The effect of apelin on cellular contraction in isolated rat ventricular myocytes

The effect of 10 nM apelin on parameters of cell shortening in rat ventricular myocytes presented by experimental day. All cells were maintained at 36±1°C, stimulated at 1 Hz. Each experimental day consisted of at least 80 recordings, 40 made in control Tyrode solution and 40 in apelin-containing Tyrode solution. Days on which a significant difference was determined ($P < 0.05$ Student's t-test) are marked with an asterisk. Data are mean±SEM.

(i) Across all days under study there was a significant decrease in TTP, amounting to 11±2% ($P < 0.05$, ANOVA analysis, n=6). This was significant difference noted on every individual experimental day.

(ii) Across all days under study there was a significant enhancement in VMaxCon which averaged 14±5% ($P < 0.05$, ANOVA analysis, n=6). This significant difference was noted on 2/6 experimental days.

The effect of apelin on relaxation parameters were also assessed from the raw sarcomere length traces and can be seen in Figure 6.11.

In isolated rat myocytes on a poly-HEMA-coated coverslip, field-stimulated at 1 Hz and maintained at 36±1°C, exposure to 10 nM apelin led to a significant reduction in TTRx in 5/6 experiments. This amounted to a mean reduction of 21±2% ($p<0.001$, $n=6$) across the full data set. Conversely VMaxRel was significantly increased in the presence of 10 nM apelin, by an average of 21±5% ($p<0.01$, $n=6$). This change was significant in individual data sets on 4/6 occasions.

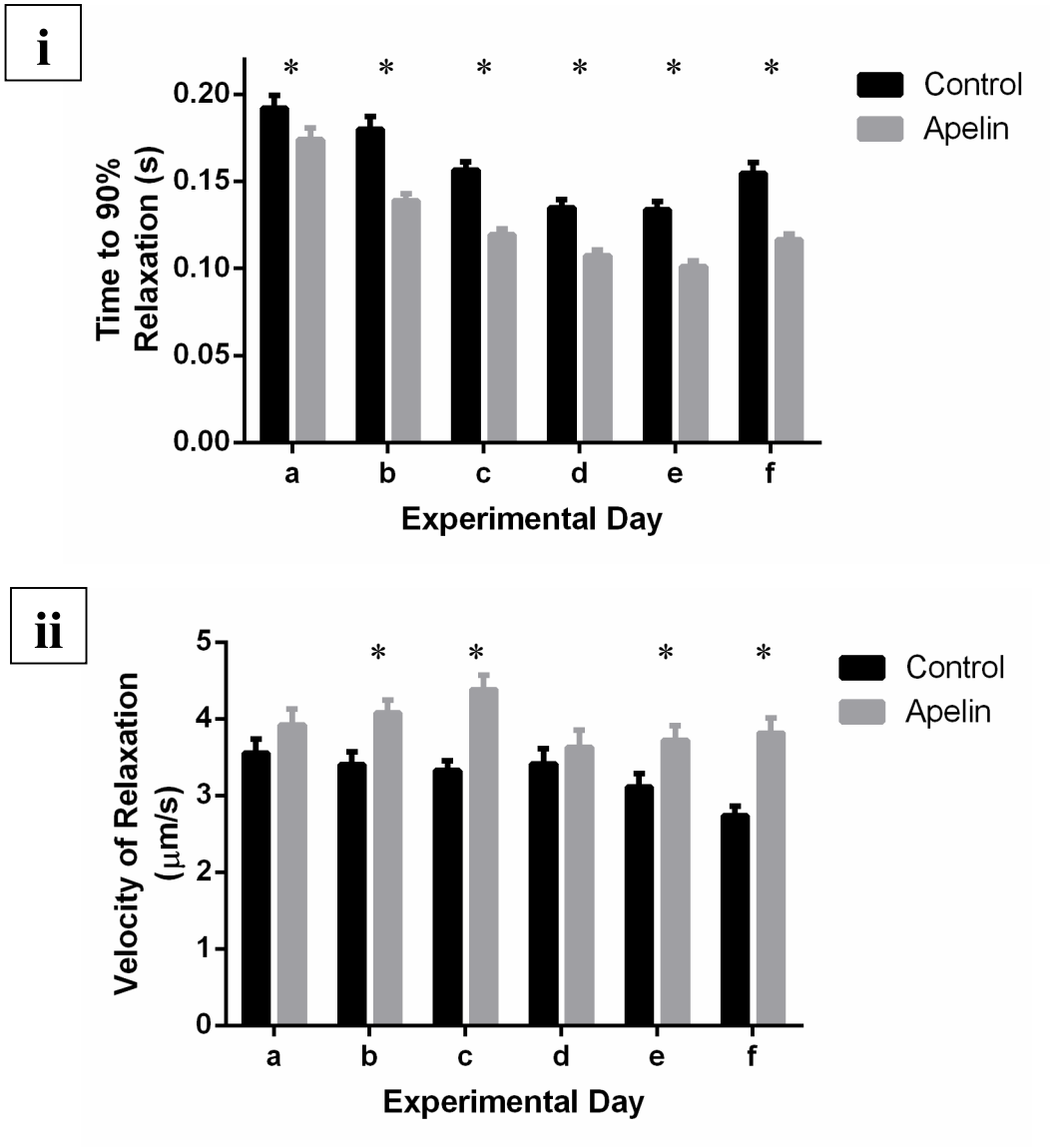


Figure 6.11 (i) and (ii): The effect of apelin on cellular relaxation in isolated rat cardiomyocytes

The effect of 10 nM apelin on parameters of cellular relaxation in rat ventricular myocytes presented by experimental day. All cells were maintained at 36±1°C, stimulated at 1 Hz. Each experimental day consisted of at least 80 recordings, 40 made in control Tyrode solution and 40 in apelin-containing Tyrode solution. Days on which a significant difference was determined ($P < 0.05$ Student's t-test) are marked with an asterisk. Data are mean±SEM.

(i) Across all days under study there was a significant decrease in TTRx, amounting to 21±2% ($P < 0.05$, ANOVA analysis, n=6). This was significant difference noted on 5/6 experimental days.

(ii) Across all days under study there was a significant enhancement in VMaxRel which averaged 21±5% ($P < 0.05$, ANOVA analysis, n=6). Comparing data measured on individual experimental days, this was a significant effect on 4/6 occasions.

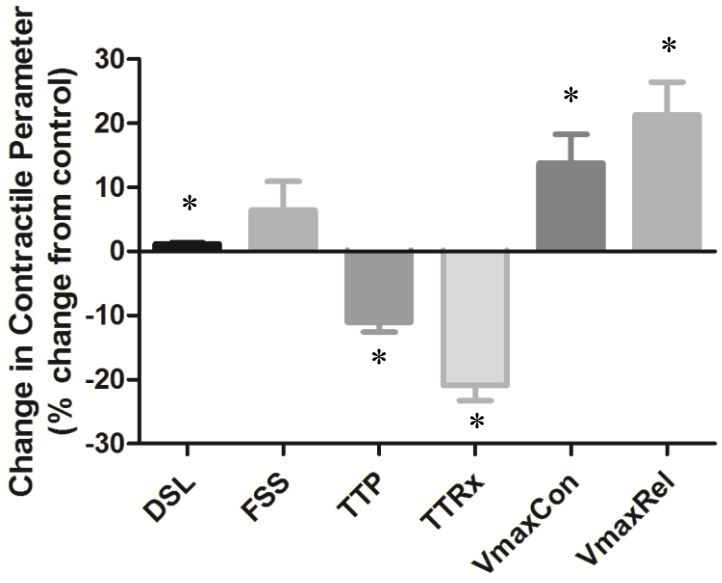


Figure 6.12: Summary graph to show effects of apelin on contraction in rat ventricular myocytes

Summary bar graph to show the percentage change in contractile parameters when 10 nM apelin is compared to control in isolated rat cardiomyocytes maintained at 36±1 ºC with 1 Hz field stimulation. 10 nM apelin did not cause a significant increase in fractional sarcomere shortening (FSS, 6±5% compared with control, p=0.15). Time taken to reach peak contraction, as measured from the contraction stimulus (TTP) and time taken to reach complete relaxation as measured from the peak of contraction (TTRx) were significantly reduced, by 11±2% and 21±2% respectively (both p<0.001), whilst the maximum velocities of contraction (VMaxCon) and relaxation (VMaxRel) were significantly enhanced, by 14±5% ($P < 0.05$) and 21±5% (p<0.01) respectively. There was also a modest but significant increase in diastolic sarcomere length (DSL) of 1±0.2%. All groups analysed are n=6 and data are presented as mean±SEM, p-values are derived from ANOVA analysis and * denotes significant response to apelin exposure

6.4 DISCUSSION

The data presented in this chapter confirm that apelin is a positive inotrope in isolated murine cells, and that this inotropy is combined with a considerable positive lusitropy (i.e. the ability to relax). Taken together, these observations suggest that effects of apelin on cardiac contractility can be most reliably assessed through studying changes in the velocities of contraction and relaxation as opposed to change in absolute cell shortening. This provides a possible explanation as to how the effects of apelin, a potent a compound in multicellular preparations, have often been missed in single cells.

The data presented in this chapter also show that changes in temperature and stimulation rate have no major effect upon the manifestation of cellular response to apelin. It is unlikely, therefore, that differences in the actions of apelin seen in the two previous papers studying single cell effects are due to these recording conditions.

Since the observations above were collected, further experiments have been carried out in the Kohl laboratory using isolated myocytes. It has been confirmed that cells isolated from the APJ knock-out mouse show no response to apelin. This confirms that the measurements described above are due to receptor-mediated effects, rather than non-specific actions of the apelin compound. Responses have also been shown to be similar in cells isolated from apelin knock-out animals. Under these conditions, there can be no confounding effects from endogenously produced apelin.

There is still considerable debate as to the mechanism by which apelin achieves its effects in cardiac myocytes. Evidence is strong that apelin's actions occur fully and

directly through the G-protein-coupled receptor APJ as APJ-deficient mice do not exhibit an increase in contractility in response to apelin exposure (Bollensdorff *et al.*, 2010).

Farkasfalvi *et al*. reported in their 2007 paper that apelin administration led to a significant, transient cellular alkalinisation and that this was accompanied by an increase in the rate of acid extrusion, suggesting a role for activation of sodium-hydrogen exchange (Farkasfalvi *et al.*, 2007). Further, inhibition of NHE in isolated, perfused rat heart preparations was seen to cause a 60% reduction in apelin response (Szokodi *et al.*, 2002).

Two papers have shown an increase in cellular contractility in isolated cardiac myocytes whilst concurrently investigating changes in calcium transients, one observing no change in transient amplitude over the course of a 1 min apelin application and the other observing a significant increase over the course of 10 min (Wang *et al.*, 2008, Farkasfalvi *et al.*, 2007).

More recent papers have begun to investigate the effects of apelin on cellular electrophysiology. In both atrial and ventricular myocytes, apelin superfusion was shown to significantly increase the current carried by voltage-gated sodium channels (Chamberland *et al.*, 2010, Cheng *et al.*, 2013). This was brought about by shifting activation voltage to a more negative level as opposed to increasing the number of channels being opened and was sensitive to PKC inhibition but unaffected by prior maximal activation of PKA (Chamberland *et al.*, 2010). In atrial myocytes, apelin has also been shown to cause a significant reduction in action potential duration through enhancement of the potassium currents I_{Kr} and I_{Ksus} (Cheng *et al.*, 2013).

The sensitivity of apelin actions to PKC inhibition, together with the noted PKC-mediated changes in voltage-gated sodium channels and sodium-hydrogen exchange activity suggest that the acute phase of the apelin response is mediated by PKC and it may warrant investigation as to whether cellular alkalinisation and/or $[Na^+]_i$ are the driving forces behind increased contractility or whether PKC is targeting contractile proteins to enhance myofilament sensitivity. For instance, apelin-mediated activation of PKC has been shown to increase phosphorylation of myosin light chain kinase in vascular smooth muscle cells (Hashimoto *et al.*, 2006). A question that remains is whether it is a prolonged change in $[Na^+]_i$ which leads to the development of increases in calcium transient amplitude over time.

It is important as the next steps in this project to investigate dynamic changes in cellular calcium and sodium during superfusion of apelin. The Kohl laboratory has been able to investigate the effects of apelin on contractile parameters in a paired manner, whilst maintaining the mechanical environment of the cell with poly-HEMA-coated coverslips, by using carbon fibres to anchor the cells. This method has the further benefit that it allows observation of changes in single cell over time and can also be used to assess force of contraction in individual myocytes.

7 REFERENCES

AARHUS, R., GRAEFF, R. M., DICKEY, D. M., WALSETH, T. F. & LEE, H. C. 1995. ADP-ribosyl cyclase and CD38 catalyze the synthesis of a calcium-mobilizing metabolite from NADP. *J Biol Chem,* 270**,** 30327-33.

ABARIENTOS, C., SPERBER, K., SHAPIRO, D. L., ARONOW, W. S., CHAO, C. P. & ASH, J. Y. 2011. Hydroxychloroquine in systemic lupus erythematosus and rheumatoid arthritis and its safety in pregnancy. *Expert Opin Drug Saf,* 10**,** 705-14.

ANDERSON, M. E. 2005. Calmodulin kinase signaling in heart: an intriguing candidate target for therapy of myocardial dysfunction and arrhythmias. *Pharmacol Ther,* 106**,** 39-55.

ARMSTRONG, C., BEZANILLA, F. & HOROWICZ, P. 1972. Twitches in the presence of ethylene glycol bis (-aminoethyl ether)-N, N'-tetracetic acid. *Biochimica et biophysica acta,* 267**,** 605-608.

ASHLEY, E. A., POWERS, J., CHEN, M., KUNDU, R., FINSTERBACH, T., CAFFARELLI, A., DENG, A., EICHHORN, J., MAHAJAN, R., AGRAWAL, R., GREVE, J., ROBBINS, R., PATTERSON, A. J., BERNSTEIN, D. & QUERTERMOUS, T. 2005. The endogenous peptide apelin potently improves cardiac contractility and reduces cardiac loading in vivo. *Cardiovasc Res,* 65**,** 73-82.

BABU, G. J., BHUPATHY, P., CARNES, C. A., BILLMAN, G. E. & PERIASAMY, M. 2007. Differential expression of sarcolipin protein during muscle development and cardiac pathophysiology. *J Mol Cell Cardiol,* 43**,** 215-22.

BAK, J., BILLINGTON, R. A., TIMAR, G., DUTTON, A. C. & GENAZZANI, A. A. 2001. NAADP receptors are present and functional in the heart. *Curr Biol,* 11**,** 987-90.

BALSHAW, D. M., XU, L., YAMAGUCHI, N., PASEK, D. A. & MEISSNER, G. 2001. Calmodulin binding and inhibition of cardiac muscle calcium release channel (ryanodine receptor). *J Biol Chem,* 276**,** 20144-53.

BALTAS, L. G., KARCZEWSKI, P., BARTEL, S. & KRAUSE, E. G. 1997. The endogenous cardiac sarcoplasmic reticulum Ca^{2+}/calmodulin-dependent kinase is activated in response to beta-adrenergic stimulation and becomes Ca^{2+}-independent in intact beating hearts. *FEBS Lett,* 409**,** 131-6.

BARCELO-TORNS, M., LEWIS, A. M., GUBERN, A., BARNEDA, D., BLOOR-YOUNG, D., PICATOSTE, F., CHURCHILL, G. C., CLARO, E. & MASGRAU, R. 2011. NAADP mediates ATP-induced Ca^{2+} signals in astrocytes. *FEBS Lett,* 585**,** 2300-6.

BARUSCOTTI, M., BUCCHI, A., VISCOMI, C., MANDELLI, G., CONSALEZ, G., GNECCHI-RUSCONI, T., MONTANO, N., CASALI, K. R., MICHELONI, S., BARBUTI, A. & DIFRANCESCO, D. 2011. Deep bradycardia and heart block caused by inducible cardiac-specific knockout of the pacemaker channel gene Hcn4. *Proc Natl Acad Sci U S A,* 108**,** 1705-10.

BASSANI, J., BASSANI, R. A. & BERS, D. M. 1994. Relaxation in rabbit and rat cardiac cells: species-dependent differences in cellular mechanisms. *The Journal of physiology,* 476**,** 279-293.

BASSANI, J. W., YUAN, W. & BERS, D. M. 1995. Fractional SR Ca release is regulated by trigger Ca and SR Ca content in cardiac myocytes. *Am J Physiol,* 268**,** C1313-9.

BERRY, M. F., PIROLLI, T. J., JAYASANKAR, V., BURDICK, J., MORINE, K. J., GARDNER, T. J. & WOO, Y. J. 2004. Apelin has in vivo inotropic effects on normal and failing hearts. *Circulation,* 110**,** II187-93.

BERS, D. M. 2002. Cardiac excitation–contraction coupling. *Nature,* 415**,** 198-205.

BERS, D. M. 2008. Calcium cycling and signaling in cardiac myocytes. *Annu. Rev. Physiol.,* 70**,** 23-49.

BERS, D. M. 2011. Ca(2)(+)-calmodulin-dependent protein kinase II regulation of cardiac excitation-transcription coupling. *Heart Rhythm,* 8**,** 1101-4.

BNF 2012. *British National Formulary*, BMJ Publishing Group Ltd.

BODI, I., MIKALA, G., KOCH, S. E., AKHTER, S. A. & SCHWARTZ, A. 2005. The L-type calcium channel in the heart: the beat goes on. *Journal of Clinical Investigation,* 115**,** 3306-3317.

BOGDANOV, K. Y., MALTSEV, V. A., VINOGRADOVA, T. M., LYASHKOV, A. E., SPURGEON, H. A., STERN, M. D. & LAKATTA, E. G. 2006. Membrane potential fluctuations resulting from submembrane Ca^{2+} releases in rabbit sinoatrial nodal cells impart

an exponential phase to the late diastolic depolarization that controls their chronotropic state. *Circ Res,* 99**,** 979-87.
BOGDANOV, K. Y., VINOGRADOVA, T. M. & LAKATTA, E. G. 2001. Sinoatrial nodal cell ryanodine receptor and Na^+-Ca^{2+} exchanger: molecular partners in pacemaker regulation. *Circ Res,* 88**,** 1254-8.
BOINK, G. J., VERKERK, A. O., VAN AMERSFOORTH, S. C., TASSERON, S. J., VAN DER RIJT, R., BAKKER, D., LINNENBANK, A. C., VAN DER MEULEN, J., DE BAKKER, J. M., SEPPEN, J. & TAN, H. L. 2008. Engineering physiologically controlled pacemaker cells with lentiviral HCN4 gene transfer. *J Gene Med,* 10**,** 487-97.
BOIS, P., BESCOND, J., RENAUDON, B. & LENFANT, J. 1996. Mode of action of bradycardic agent, S 16257, on ionic currents of rabbit sinoatrial node cells. *British journal of pharmacology,* 118**,** 1051-1057.
BOLLENSDORFF, C., CHARO, D., HO, M., FAJARDO, G., BERNSTEIN, D., QUERTERMOUS, T., ASHLEY, E. & KOHL, P. 2010. The Effect of Apelin on Single Isolated Cardiac Myocytes from Wild-Type and Apelin/APJ KO Mice. *Biophysical Journal,* 98**,** 710a.
BOOTMAN, M. D., HIGAZI, D. R., COOMBES, S. & RODERICK, H. L. 2006. Calcium signalling during excitation-contraction coupling in mammalian atrial myocytes. *Journal of cell science,* 119**,** 3915-3925.
BROWN, B. G., GUNDEL, W. D., GOTT, V. L. & COVELL, J. W. 1974. Coronary collateral flow following acute coronary occlusion: a diastolic phenomenon. *Cardiovasc Res,* 8**,** 621-31.
BROWN, H., DIFRANCESCO, D. & NOBLE, S. 1979. How does adrenaline accelerate the heart?
BRUM, G., OSTERRIEDER, W. & TRAUTWEIN, W. 1984. Beta-adrenergic increase in the calcium conductance of cardiac myocytes studied with the patch clamp. *Pflugers Arch,* 401**,** 111-8.
BUCCHI, A., BARUSCOTTI, M. & DIFRANCESCO, D. 2002. Current-dependent block of rabbit sino-atrial node I(f) channels by ivabradine. *J Gen Physiol,* 120**,** 1-13.
BURRELL, Z. L., JR. & MARTINEZ, A. C. 1958. Chloroquine and hydroxychloroquine in the treatment of cardiac arrhythmias. *N Engl J Med,* 258**,** 798-800.
CALCRAFT, P. J., RUAS, M., PAN, Z., CHENG, X., ARREDOUANI, A., HAO, X., TANG, J., RIETDORF, K., TEBOUL, L., CHUANG, K. T., LIN, P., XIAO, R., WANG, C., ZHU, Y., LIN, Y., WYATT, C. N., PARRINGTON, J., MA, J., EVANS, A. M., GALIONE, A. & ZHU, M. X. 2009. NAADP mobilizes calcium from acidic organelles through two-pore channels. *Nature,* 459**,** 596-600.
CANCELA, J. M., CHURCHILL, G. C. & GALIONE, A. 1999. Coordination of agonist-induced Ca^{2+}-signalling patterns by NAADP in pancreatic acinar cells. *Nature,* 398**,** 74-6.
CHAMBERLAND, C., BARAJAS-MARTINEZ, H., HAUFE, V., FECTEAU, M. H., DELABRE, J. F., BURASHNIKOV, A., ANTZELEVITCH, C., LESUR, O., CHRAIBI, A., SARRET, P. & DUMAINE, R. 2010. Modulation of canine cardiac sodium current by Apelin. *J Mol Cell Cardiol,* 48**,** 694-701.
CHARO, D. N., HO, M., FAJARDO, G., KAWANA, M., KUNDU, R. K., SHEIKH, A. Y., FINSTERBACH, T. P., LEEPER, N. J., ERNST, K. V., CHEN, M. M., HO, Y. D., CHUN, H. J., BERNSTEIN, D., ASHLEY, E. A. & QUERTERMOUS, T. 2009. Endogenous regulation of cardiovascular function by apelin-APJ. *Am J Physiol Heart Circ Physiol,* 297**,** H1904-13.
CHASE, A. & ORCHARD, C. H. 2011. Ca^{2+} efflux via the sarcolemmal Ca^{2+} ATPase occurs only in the t-tubules of rat ventricular myocytes. *J Mol Cell Cardiol,* 50**,** 187-93.
CHEN, M. M., ASHLEY, E. A., DENG, D. X., TSALENKO, A., DENG, A., TABIBIAZAR, R., BEN-DOR, A., FENSTER, B., YANG, E., KING, J. Y., FOWLER, M., ROBBINS, R., JOHNSON, F. L., BRUHN, L., MCDONAGH, T., DARGIE, H., YAKHINI, Z., TSAO, P. S. & QUERTERMOUS, T. 2003. Novel role for the potent endogenous inotrope apelin in human cardiac dysfunction. *Circulation,* 108**,** 1432-9.
CHENG, C. C., WEERATEERANGKUL, P., LU, Y. Y., CHEN, Y. C., LIN, Y. K., CHEN, S. A. & CHEN, Y. J. 2013. Apelin regulates the electrophysiological characteristics of atrial myocytes. *Eur J Clin Invest,* 43**,** 34-40.
CHENG, H., LEDERER, W. J. & CANNELL, M. B. 1993. Calcium sparks: elementary events underlying excitation-contraction coupling in heart muscle. *Science,* 262**,** 740-4.

CHINI, E. N. 2002. Interactions between intracellular Ca^{2+} stores: Ca^{2+} released from the NAADP pool potentiates cADPR-induced Ca^{2+} release. *Braz J Med Biol Res,* 35**,** 543-7.
CHINI, E. N., BEERS, K. W. & DOUSA, T. P. 1995. Nicotinate adenine dinucleotide phosphate (NAADP) triggers a specific calcium release system in sea urchin eggs. *J Biol Chem,* 270**,** 3216-23.
CHINI, E. N. & DOUSA, T. P. 1995. Enzymatic synthesis and degradation of nicotinate adenine dinucleotide phosphate (NAADP), a Ca^{2+}-releasing agonist, in rat tissues. *Biochem Biophys Res Commun,* 209**,** 167-74.
CHO, H. S., TAKANO, M. & NOMA, A. 2003. The electrophysiological properties of spontaneously beating pacemaker cells isolated from mouse sinoatrial node. *J Physiol,* 550**,** 169-80.
CHRISTENSEN, K. A., MYERS, J. T. & SWANSON, J. A. 2002. pH-dependent regulation of lysosomal calcium in macrophages. *J Cell Sci,* 115**,** 599-607.
CHU, G., LESTER, J. W., YOUNG, K. B., LUO, W., ZHAI, J. & KRANIAS, E. G. 2000. A single site (Ser16) phosphorylation in phospholamban is sufficient in mediating its maximal cardiac responses to beta -agonists. *J Biol Chem,* 275**,** 38938-43.
CHURCHILL, G. C. & GALIONE, A. 2001a. NAADP induces Ca^{2+} oscillations via a two-pool mechanism by priming IP_3- and cADPR-sensitive Ca^{2+} stores. *EMBO J,* 20**,** 2666-71.
CHURCHILL, G. C. & GALIONE, A. 2001b. Prolonged inactivation of nicotinic acid adenine dinucleotide phosphate-induced Ca^{2+} release mediates a spatiotemporal Ca^{2+} memory. *J Biol Chem,* 276**,** 11223-5.
CHURCHILL, G. C., O'NEILL, J. S., MASGRAU, R., PATEL, S., THOMAS, J. M., GENAZZANI, A. A. & GALIONE, A. 2003. Sperm deliver a new second messenger: NAADP. *Curr Biol,* 13**,** 125-8.
CHURCHILL, G. C., OKADA, Y., THOMAS, J. M., GENAZZANI, A. A., PATEL, S. & GALIONE, A. 2002. NAADP mobilizes Ca^{2+} from reserve granules, lysosome-related organelles, in sea urchin eggs. *Cell,* 111**,** 703-8.
CLAPPER, D. L., WALSETH, T. F., DARGIE, P. J. & LEE, H. C. 1987. Pyridine nucleotide metabolites stimulate calcium release from sea urchin egg microsomes desensitized to inositol trisphosphate. *J Biol Chem,* 262**,** 9561-8.
COLLINS, T. 2009. *Regulation of Cardiac Calcium Signalling Mechanisms and Contractile Function by Nicotinic Acid Adenine Dinucleotide Phosphate.* Doctor of Philosophy, University of Oxford.
COLLINS, T. P., BAYLISS, R., CHURCHILL, G. C., GALIONE, A. & TERRAR, D. A. 2011. NAADP influences excitation-contraction coupling by releasing calcium from lysosomes in atrial myocytes. *Cell Calcium,* 50**,** 449-58.
COLLINS, T. P. & TERRAR, D. A. 2012. Ca(2+)-stimulated adenylyl cyclases regulate the L-type Ca^{2+} current in guinea-pig atrial myocytes. *J Physiol,* 590**,** 1881-93.
COLLIS, L. P., MEYERS, M. B., ZHANG, J., PHOON, C. K., SOBIE, E. A., COETZEE, W. A. & FISHMAN, G. I. 2007. Expression of a sorcin missense mutation in the heart modulates excitation-contraction coupling. *FASEB J,* 21**,** 475-87.
COPELLO, J. A., QI, Y., JEYAKUMAR, L. H., OGUNBUNMI, E. & FLEISCHER, S. 2001. Lack of effect of cADP-ribose and NAADP on the activity of skeletal muscle and heart ryanodine receptors. *Cell Calcium,* 30**,** 269-84.
CUI, Y., GALIONE, A. & TERRAR, D. A. 1999. Effects of photoreleased cADP-ribose on calcium transients and calcium sparks in myocytes isolated from guinea-pig and rat ventricle. *Biochem J,* 342**,** 269-73.
CURRIE, S., LOUGHREY, C. M., CRAIG, M. A. & SMITH, G. L. 2004. Calcium/calmodulin-dependent protein kinase IIdelta associates with the ryanodine receptor complex and regulates channel function in rabbit heart. *Biochem J,* 377**,** 357-66.
DAI, T., RAMIREZ-CORREA, G. & GAO, W. D. 2006. Apelin increases contractility in failing cardiac muscle. *Eur J Pharmacol,* 553**,** 222-8.
DE JONGH, K. S., MURPHY, B. J., COLVIN, A. A., HELL, J. W., TAKAHASHI, M. & CATTERALL, W. A. 1996. Specific phosphorylation of a site in the full-length form of the alpha 1 subunit of the cardiac L-type calcium channel by adenosine 3',5'-cyclic monophosphate-dependent protein kinase. *Biochemistry,* 35**,** 10392-402.

DELLA SANTINA, L., BOULY, M., ASTA, A., DEMONTIS, G. C., CERVETTO, L. & GARGINI, C. 2010. Effect of HCN channel inhibition on retinal morphology and function in normal and dystrophic rodents. *Invest Ophthalmol Vis Sci,* 51**,** 1016-23.

DELLA SANTINA, L., PIANO, I., CANGIANO, L., CAPUTO, A., LUDWIG, A., CERVETTO, L. & GARGINI, C. 2012. Processing of retinal signals in normal and HCN deficient mice. *PLoS One,* 7**,** e29812.

DELLIS, O., DEDOS, S. G., TOVEY, S. C., TAUFIQ UR, R., DUBEL, S. J. & TAYLOR, C. W. 2006. Ca^{2+} entry through plasma membrane IP_3 receptors. *Science,* 313**,** 229-33.

DENYER, J. & BROWN, H. 1987. A method for isolating rabbit sinoatrial node cells which maintains their natural shape. *Jpn J Physiol,* 37**,** 963-5.

DIFRANCESCO, D. 1986. Characterization of single pacemaker channels in cardiac sino-atrial node cells. *Nature,* 324**,** 470-3.

DIFRANCESCO, D., FERRONI, A., MAZZANTI, M. & TROMBA, C. 1986. Properties of the hyperpolarizing-activated current I(f) in cells isolated from the rabbit sino-atrial node. *The Journal of physiology,* 377**,** 61-88.

DIFRANCESCO, D. & NOBLE, D. 2012. The funny current has a major pacemaking role in the sinus node. *Heart Rhythm,* 9**,** 299-301.

DIFRANCESCO, D. & TORTORA, P. 1991. Direct activation of cardiac pacemaker channels by intracellular cyclic AMP. *Nature,* 351**,** 145-147.

DOERR, T., DENGER, R. & TRAUTWEIN, W. 1989. Calcium currents in single SA nodal cells of the rabbit heart studied with action potential clamp. *Pflügers Archiv-European Journal of Physiology,* 413**,** 599-603.

EDWARDS, G. A., WEIANT, E. A., SLOCOMBE, A. G. & ROEDER, K. D. 1948. The Action of Ryanodine on the Contractile Process in Striated Muscle. *Science,* 108**,** 330-2.

EL-ARMOUCHE, A., WITTKOPPER, K., DEGENHARDT, F., WEINBERGER, F., DIDIE, M., MELNYCHENKO, I., GRIMM, M., PEECK, M., ZIMMERMANN, W. H., UNSOLD, B., HASENFUSS, G., DOBREV, D. & ESCHENHAGEN, T. 2008. Phosphatase inhibitor-1-deficient mice are protected from catecholamine-induced arrhythmias and myocardial hypertrophy. *Cardiovasc Res,* 80**,** 396-406.

ELLIS-DAVIES, G. C. 2007. Caged compounds: photorelease technology for control of cellular chemistry and physiology. *Nature methods,* 4**,** 619-628.

ELSON, L. 2011. *Regulation of Cardiac Calcium Signalling Mechanisms and Contractile Function by Nicotinic Acid Adenine Dinucleotide Phosphate.* Doctor of Philosophy, University of Oxford.

ELSON, L., CHURCHILL, G., TERRAR, D. A. & RAKOVIC, S. 2011. Actions of the NAADP Antagonist Trans-Ned19 in Cardiac Ventricular Myocytes. *Biophysical Journal,* 100**,** 81a-82a.

ELSON, L. C., OWEN, W. D., GAFSON, A. R., PARRINGTON, J., GALIONE, A., TERRAR, D. A. & RAKOVIC, S. 2010. Role of the Putative NAADP Receptor, Two-Pore Channel 2, in Ventricular Myocyte Responses to Isoproterenol. *Biophysical Journal,* 98**,** 100a.

FABIATO, A. & FABIATO, F. 1978. Calcium-Induced Release of Calcium From the Sarcoplasmic Reticulum of Skinned Cellls From Adult Human, Dog, Cat, Rabbit, Rat, and Frog Hearts and From Fetal and New-Born Rat Ventricles. *Annals of the New York Academy of Sciences,* 307**,** 491-522.

FARKASFALVI, K., STAGG, M. A., COPPEN, S. R., SIEDLECKA, U., LEE, J., SOPPA, G. K., MARCZIN, N., SZOKODI, I., YACOUB, M. H. & TERRACCIANO, C. M. 2007. Direct effects of apelin on cardiomyocyte contractility and electrophysiology. *Biochem Biophys Res Commun,* 357**,** 889-95.

FARRELL, E. F., ANTARAMIAN, A., RUEDA, A., GOMEZ, A. M. & VALDIVIA, H. H. 2003. Sorcin inhibits calcium release and modulates excitation-contraction coupling in the heart. *J Biol Chem,* 278**,** 34660-6.

FATT, P. & KATZ, B. 1953. The electrical properties of crustacean muscle fibres. *The Journal of Physiology,* 120**,** 171-204.

FILGUEIRAS-RAMA, D., MARTINS, R. P., MIRONOV, S., YAMAZAKI, M., CALVO, C. J., ENNIS, S. R., BANDARU, K., NOUJAIM, S. F., KALIFA, J. & BERENFELD, O. 2012. Chloroquine terminates stretch-induced atrial fibrillation more effectively than flecainide in the sheep heart. *Circulation: Arrhythmia and Electrophysiology,* 5**,** 561-570.

FLEISCHER, S., OGUNBUNMI, E. M., DIXON, M. C. & FLEER, E. A. 1985. Localization of Ca^{2+} release channels with ryanodine in junctional terminal cisternae of sarcoplasmic reticulum of fast skeletal muscle. *Proc Natl Acad Sci U S A,* 82**,** 7256-9.

FRANZINI-ARMSTRONG, C., PROTASI, F. & RAMESH, V. 1999. Shape, size, and distribution of Ca^{2+} release units and couplons in skeletal and cardiac muscles. *Biophys J,* 77**,** 1528-39.

FRENZEL, H., SCHWARTZKOPFF, B., HOLTERMANN, W., SCHNURCH, H. G., NOVI, A. & HORT, W. 1988. Regression of cardiac hypertrophy: morphometric and biochemical studies in rat heart after swimming training. *J Mol Cell Cardiol,* 20**,** 737-51.

GALFRE, E., PITT, S. J., VENTURI, E., SITSAPESAN, M., ZACCAI, N. R., TSANEVA-ATANASOVA, K., O'NEILL, S. & SITSAPESAN, R. 2012. FKBP12 activates the cardiac ryanodine receptor Ca^{2+}-release channel and is antagonised by FKBP12.6. *PLoS One,* 7**,** e31956.

GALIONE, A., LEE, H. C. & BUSA, W. B. 1991. Ca^{2+}-induced Ca^{2+} release in sea urchin egg homogenates: modulation by cyclic ADP-ribose. *Science,* 253**,** 1143-6.

GERHARDSTEIN, B. L., PURI, T. S., CHIEN, A. J. & HOSEY, M. M. 1999. Identification of the sites phosphorylated by cyclic AMP-dependent protein kinase on the beta 2 subunit of L-type voltage-dependent calcium channels. *Biochemistry,* 38**,** 10361-70.

GINSBURG, K. S. & BERS, D. M. 2004. Modulation of excitation-contraction coupling by isoproterenol in cardiomyocytes with controlled SR Ca^{2+} load and Ca^{2+} current trigger. *J Physiol,* 556**,** 463-80.

GRAMOLINI, A. O., TRIVIERI, M. G., OUDIT, G. Y., KISLINGER, T., LI, W., PATEL, M. M., EMILI, A., KRANIAS, E. G., BACKX, P. H. & MACLENNAN, D. H. 2006. Cardiac-specific overexpression of sarcolipin in phospholamban null mice impairs myocyte function that is restored by phosphorylation. *Proc Natl Acad Sci U S A,* 103**,** 2446-51.

GYORKE, I., HESTER, N., JONES, L. R. & GYORKE, S. 2004. The role of calsequestrin, triadin, and junctin in conferring cardiac ryanodine receptor responsiveness to luminal calcium. *Biophys J,* 86**,** 2121-8.

HADLEY, R. W. & HUME, J. R. 1987. An intrinsic potential-dependent inactivation mechanism associated with calcium channels in guinea-pig myocytes. *J Physiol,* 389**,** 205-22.

HAGHIGHI, K., KOLOKATHIS, F., PATER, L., LYNCH, R. A., ASAHI, M., GRAMOLINI, A. O., FAN, G. C., TSIAPRAS, D., HAHN, H. S., ADAMOPOULOS, S., LIGGETT, S. B., DORN, G. W., 2ND, MACLENNAN, D. H., KREMASTINOS, D. T. & KRANIAS, E. G. 2003. Human phospholamban null results in lethal dilated cardiomyopathy revealing a critical difference between mouse and human. *J Clin Invest,* 111**,** 869-76.

HASHIMOTO, T., KIHARA, M., ISHIDA, J., IMAI, N., YOSHIDA, S., TOYA, Y., FUKAMIZU, A., KITAMURA, H. & UMEMURA, S. 2006. Apelin stimulates myosin light chain phosphorylation in vascular smooth muscle cells. *Arterioscler Thromb Vasc Biol,* 26**,** 1267-72.

HERRMANN, S., HOFMANN, F., STIEBER, J. & LUDWIG, A. 2012. HCN channels in the heart: lessons from mouse mutants. *Br J Pharmacol,* 166**,** 501-9.

HIMENO, Y., TOYODA, F., SATOH, H., AMANO, A., CHA, C. Y., MATSUURA, H. & NOMA, A. 2011. Minor contribution of cytosolic Ca^{2+} transients to the pacemaker rhythm in guinea pig sinoatrial node cells. *Am J Physiol Heart Circ Physiol,* 300**,** H251-61.

HOCH, B., MEYER, R., HETZER, R., KRAUSE, E. G. & KARCZEWSKI, P. 1999. Identification and expression of delta-isoforms of the multifunctional Ca^{2+}/calmodulin-dependent protein kinase in failing and nonfailing human myocardium. *Circ Res,* 84**,** 713-21.

HOSOYA, M., KAWAMATA, Y., FUKUSUMI, S., FUJII, R., HABATA, Y., HINUMA, S., KITADA, C., HONDA, S., KUROKAWA, T., ONDA, H., NISHIMURA, O. & FUJINO, M. 2000. Molecular and functional characteristics of APJ. Tissue distribution of mRNA and interaction with the endogenous ligand apelin. *J Biol Chem,* 275**,** 21061-7.

HOVE-MADSEN, L. & BERS, D. M. 1993. Sarcoplasmic reticulum Ca^{2+} uptake and thapsigargin sensitivity in permeabilized rabbit and rat ventricular myocytes. *Circ Res,* 73**,** 820-8.

HUXLEY, A. & NIEDERGERKE, R. 1954. Interference microscopy of living muscle fibres. *Nature,* 173**,** 13.

HUXLEY, H. & HANSON, J. 1954. Changes in the cross-striations of muscle during contraction and stretch and their structural interpretation. *Nature,* 173**,** 973-976.

IBRAHIM, M., GORELIK, J., YACOUB, M. H. & TERRACCIANO, C. M. 2011. The structure and function of cardiac t-tubules in health and disease. *Proceedings of the Royal Society B: Biological Sciences,* 278**,** 2714-2723.

IINO, S., CUI, Y., GALIONE, A. & TERRAR, D. A. 1997. Actions of cADP-ribose and its antagonists on contraction in guinea pig isolated ventricular myocytes. Influence of temperature. *Circ Res,* 81**,** 879-84.

ISHII, T. M., TAKANO, M., XIE, L.-H., NOMA, A. & OHMORI, H. 1999. Molecular characterization of the hyperpolarization-activated cation channel in rabbit heart sinoatrial node. *Journal of Biological Chemistry,* 274**,** 12835-12839.

ITOH, M., ISHIHARA, K., TOMIZAWA, H., TANAKA, H., KOBUNE, Y., ISHIKAWA, J., KAISHO, T. & HIRANO, T. 1994. Molecular cloning of murine BST-1 having homology with CD38 and Aplysia ADP-ribosyl cyclase. *Biochem Biophys Res Commun,* 203**,** 1309-17.

JETT, M.-F., SCHWORER, C. M., BASS, M. & SODERLING, T. R. 1987. Identification of membrane-bound calcium, calmodulin-dependent protein kinase II in canine heart. *Archives of biochemistry and biophysics,* 255**,** 354-360.

JI, Y., LALLI, M. J., BABU, G. J., XU, Y., KIRKPATRICK, D. L., LIU, L. H., CHIAMVIMONVAT, N., WALSH, R. A., SHULL, G. E. & PERIASAMY, M. 2000. Disruption of a single copy of the SERCA2 gene results in altered Ca^{2+} homeostasis and cardiomyocyte function. *J Biol Chem,* 275**,** 38073-80.

JI, Y., LI, B., REED, T. D., LORENZ, J. N., KAETZEL, M. A. & DEDMAN, J. R. 2003. Targeted inhibition of Ca^{2+}/calmodulin-dependent protein kinase II in cardiac longitudinal sarcoplasmic reticulum results in decreased phospholamban phosphorylation at threonine 17. *J Biol Chem,* 278**,** 25063-71.

JI, Y., ZHAO, W., LI, B., DESANTIAGO, J., PICHT, E., KAETZEL, M. A., SCHULTZ JEL, J., KRANIAS, E. G., BERS, D. M. & DEDMAN, J. R. 2006. Targeted inhibition of sarcoplasmic reticulum CaMKII activity results in alterations of Ca^{2+} homeostasis and cardiac contractility. *Am J Physiol Heart Circ Physiol,* 290**,** H599-606.

JONES, L. R., SUZUKI, Y. J., WANG, W., KOBAYASHI, Y. M., RAMESH, V., FRANZINI-ARMSTRONG, C., CLEEMANN, L. & MORAD, M. 1998. Regulation of Ca^{2+} signaling in transgenic mouse cardiac myocytes overexpressing calsequestrin. *J Clin Invest,* 101**,** 1385-93.

JU, Y.-K., LIU, J., LEE, B. H., LAI, D., WOODCOCK, E. A., LEI, M., CANNELL, M. B. & ALLEN, D. G. 2011. Distribution and functional role of inositol 1, 4, 5-trisphosphate receptors in mouse sinoatrial node. *Circulation research,* 109**,** 848-857.

JU, Y. K. & ALLEN, D. G. 1998. Intracellular calcium and Na^{+}- Ca^{2+} exchange current in isolated toad pacemaker cells. *J Physiol,* 508 (Pt 1)**,** 153-66.

KADAMBI, V. J., PONNIAH, S., HARRER, J. M., HOIT, B. D., DORN, G. W., 2ND, WALSH, R. A. & KRANIAS, E. G. 1996. Cardiac-specific overexpression of phospholamban alters calcium kinetics and resultant cardiomyocyte mechanics in transgenic mice. *J Clin Invest,* 97**,** 533-9.

KAFTAN, E., MARKS, A. R. & EHRLICH, B. E. 1996. Effects of rapamycin on ryanodine receptor/Ca^{2+}-release channels from cardiac muscle. *Circ Res,* 78**,** 990-7.

KANNT, A., SICKA, K., KROLL, K., KADEREIT, D. & GOGELEIN, H. 2012. Selective inhibitors of cardiac ADPR cyclase as novel anti-arrhythmic compounds. *Naunyn Schmiedebergs Arch Pharmacol,* 385**,** 717-27.

KAWAMATA, Y., HABATA, Y., FUKUSUMI, S., HOSOYA, M., FUJII, R., HINUMA, S., NISHIZAWA, N., KITADA, C., ONDA, H., NISHIMURA, O. & FUJINO, M. 2001. Molecular properties of apelin: tissue distribution and receptor binding. *Biochim Biophys Acta,* 1538**,** 162-71.

KEITH, A. & FLACK, M. 1907. The Form and Nature of the Muscular Connections between the Primary Divisions of the Vertebrate Heart. *J Anat Physiol,* 41**,** 172-89.

KINNEAR, N. P., BOITTIN, F. X., THOMAS, J. M., GALIONE, A. & EVANS, A. M. 2004. Lysosome-sarcoplasmic reticulum junctions. A trigger zone for calcium signaling by nicotinic acid adenine dinucleotide phosphate and endothelin-1. *J Biol Chem,* 279**,** 54319-26.

KOBINGER, W. & LILLIE, C. 1987. Specific bradycardic agents--a novel pharmacological class? *Eur Heart J,* 8**,** 7-15.

KODAMA, I. & BOYETT, M. R. 1985. Regional differences in the electrical activity of the rabbit sinus node. *Pflugers Arch,* 404**,** 214-26.
KOHLHAAS, M., ZHANG, T., SEIDLER, T., ZIBROVA, D., DYBKOVA, N., STEEN, A., WAGNER, S., CHEN, L., BROWN, J. H., BERS, D. M. & MAIER, L. S. 2006. Increased sarcoplasmic reticulum calcium leak but unaltered contractility by acute CaMKII overexpression in isolated rabbit cardiac myocytes. *Circ Res,* 98**,** 235-44.
KOIVUMÄKI, J. T., TAKALO, J., KORHONEN, T., TAVI, P. & WECKSTRÖM, M. 2009. Modelling sarcoplasmic reticulum calcium ATPase and its regulation in cardiac myocytes. *Philosophical Transactions of the Royal Society A: Mathematical, Physical and Engineering Sciences,* 367**,** 2181-2202.
KOSTER, R., KAEHLER, J. & MEINERTZ, T. 2009. Treatment of stable angina pectoris by ivabradine in every day practice: the REDUCTION study. *Am Heart J,* 158**,** e51-7.
KRANIAS, E. G. & HAJJAR, R. J. 2012. Modulation of cardiac contractility by the phospholamban/SERCA2a regulatome. *Circ Res,* 110**,** 1646-60.
KRANIAS, E. G. & SOLARO, R. J. 1982. Phosphorylation of troponin I and phospholamban during catecholamine stimulation of rabbit heart. *Nature,* 298**,** 182-4.
KUSCHEL, M., KARCZEWSKI, P., HEMPEL, P., SCHLEGEL, W. P., KRAUSE, E. G. & BARTEL, S. 1999. Ser16 prevails over Thr17 phospholamban phosphorylation in the beta-adrenergic regulation of cardiac relaxation. *Am J Physiol,* 276**,** H1625-33.
LAKATTA, E. G. & MALTSEV, V. A. 2012. Rebuttal: what I(f) the shoe doesn't fit? "The funny current has a major pacemaking role in the sinus node". *Heart Rhythm,* 9**,** 459-60.
LANGER, G. & PESKOFF, A. 1996. Calcium concentration and movement in the diadic cleft space of the cardiac ventricular cell. *Biophysical journal,* 70**,** 1169-1182.
LARBIG, R., TORRES, N., BRIDGE, J. H., GOLDHABER, J. I. & PHILIPSON, K. D. 2010. Activation of reverse Na^+- Ca^{2+} exchange by the Na^+ current augments the cardiac Ca^{2+} transient: evidence from NCX knockout mice. *J Physiol,* 588**,** 3267-76.
LAURENT, D., BOLENE-WILLIAMS, C., WILLIAMS, F. L. & KATZ, L. N. 1956. Effects of heart rate on coronary flow and cardiac oxygen consumption. *Am J Physiol,* 185**,** 355-64.
LECHAT, P., HULOT, J. S., ESCOLANO, S., MALLET, A., LEIZOROVICZ, A., WERHLEN-GRANDJEAN, M., POCHMALICKI, G. & DARGIE, H. 2001. Heart rate and cardiac rhythm relationships with bisoprolol benefit in chronic heart failure in CIBIS II Trial. *Circulation,* 103**,** 1428-33.
LEE, H. C., WALSETH, T. F., BRATT, G. T., HAYES, R. N. & CLAPPER, D. L. 1989. Structural determination of a cyclic metabolite of NAD^+ with intracellular Ca^{2+}-mobilizing activity. *J Biol Chem,* 264**,** 1608-15.
LEHNART, S. E., WEHRENS, X. H., REIKEN, S., WARRIER, S., BELEVYCH, A. E., HARVEY, R. D., RICHTER, W., JIN, S. L., CONTI, M. & MARKS, A. R. 2005. Phosphodiesterase 4D deficiency in the ryanodine-receptor complex promotes heart failure and arrhythmias. *Cell,* 123**,** 25-35.
LEI, M. & BROWN, H. F. 1996. Two components of the delayed rectifier potassium current, I_K, in rabbit sino-atrial node cells. *Exp Physiol,* 81**,** 725-41.
LEVICK, J. R. 2009. *An Introduction to Cardiovascular Physiology*, CRC Press.
LEWIS, A. M., ALEY, P. K., ROOMI, A., THOMAS, J. M., MASGRAU, R., GARNHAM, C., SHIPMAN, K., PARAMORE, C., BLOOR-YOUNG, D., SANDERS, L. E., TERRAR, D. A., GALIONE, A. & CHURCHILL, G. C. 2012. beta-Adrenergic receptor signaling increases NAADP and cADPR levels in the heart. *Biochem Biophys Res Commun,* 427**,** 326-9.
LI, L., CHU, G., KRANIAS, E. G. & BERS, D. M. 1998. Cardiac myocyte calcium transport in phospholamban knockout mouse: relaxation and endogenous CaMKII effects. *Am J Physiol,* 274**,** H1335-47.
LI, L., SATOH, H., GINSBURG, K. S. & BERS, D. M. 1997. The effect of Ca^{2+}-calmodulin-dependent protein kinase II on cardiac excitation-contraction coupling in ferret ventricular myocytes. *J Physiol,* 501 (Pt 1)**,** 17-31.
LILLIE, C. & KOBINGER, W. 1987. Investigations differentiating the mechanism of specific bradycardic agents from that of calcium channel blockers. *Naunyn Schmiedebergs Arch Pharmacol,* 335**,** 331-3.

LIN-MOSHIER, Y., WALSETH, T. F., CHURAMANI, D., DAVIDSON, S. M., SLAMA, J. T., HOOPER, R., BRAILOIU, E., PATEL, S. & MARCHANT, J. S. 2012. Photoaffinity labeling of nicotinic acid adenine dinucleotide phosphate (NAADP) targets in mammalian cells. *J Biol Chem,* 287**,** 2296-307.

LIPP, P. & NIGGLI, E. 1996. Submicroscopic calcium signals as fundamental events of excitation--contraction coupling in guinea-pig cardiac myocytes. *J Physiol,* 492 (Pt 1)**,** 31-8.

LOCKE, F. & ROSENHEIM, O. 1907. Contributions to the physiology of the isolated heart The consumption of dextrose by mammalian cardiac muscle. *The Journal of physiology,* 36**,** 205-220.

LOKUTA, A. J., MEYERS, M. B., SANDER, P. R., FISHMAN, G. I. & VALDIVIA, H. H. 1997. Modulation of cardiac ryanodine receptors by sorcin. *J Biol Chem,* 272**,** 25333-8.

LUDTKE, S. J., SERYSHEVA, II, HAMILTON, S. L. & CHIU, W. 2005. The pore structure of the closed RyR1 channel. *Structure,* 13**,** 1203-11.

LUKYANENKO, V., GYORKE, I. & GYORKE, S. 1996. Regulation of calcium release by calcium inside the sarcoplasmic reticulum in ventricular myocytes. *Pflugers Arch,* 432**,** 1047-54.

LUO, W., GRUPP, I. L., HARRER, J., PONNIAH, S., GRUPP, G., DUFFY, J. J., DOETSCHMAN, T. & KRANIAS, E. G. 1994. Targeted ablation of the phospholamban gene is associated with markedly enhanced myocardial contractility and loss of beta-agonist stimulation. *Circ Res,* 75**,** 401-9.

LUO, W., WOLSKA, B. M., GRUPP, I. L., HARRER, J. M., HAGHIGHI, K., FERGUSON, D. G., SLACK, J. P., GRUPP, G., DOETSCHMAN, T., SOLARO, R. J. & KRANIAS, E. G. 1996. Phospholamban gene dosage effects in the mammalian heart. *Circ Res,* 78**,** 839-47.

LYGREN, B., CARLSON, C. R., SANTAMARIA, K., LISSANDRON, V., MCSORLEY, T., LITZENBERG, J., LORENZ, D., WIESNER, B., ROSENTHAL, W., ZACCOLO, M., TASKEN, K. & KLUSSMANN, E. 2007. AKAP complex regulates Ca^{2+} re-uptake into heart sarcoplasmic reticulum. *EMBO Rep,* 8**,** 1061-7.

MACDONNELL, S. M., GARCIA-RIVAS, G., SCHERMAN, J. A., KUBO, H., CHEN, X., VALDIVIA, H. & HOUSER, S. R. 2008. Adrenergic regulation of cardiac contractility does not involve phosphorylation of the cardiac ryanodine receptor at serine 2808. *Circ Res,* 102**,** e65-72.

MACGREGOR, A., YAMASAKI, M., RAKOVIC, S., SANDERS, L., PARKESH, R., CHURCHILL, G. C., GALIONE, A. & TERRAR, D. A. 2007a. NAADP controls cross-talk between distinct Ca^{2+} stores in the heart. *J Biol Chem,* 282**,** 15302-11.

MACGREGOR, A. T., RAKOVIC, S., GALIONE, A. & TERRAR, D. A. 2007b. Dual effects of cyclic ADP-ribose on sarcoplasmic reticulum Ca^{2+} release and storage in cardiac myocytes isolated from guinea-pig and rat ventricle. *Cell Calcium,* 41**,** 537-46.

MAIER, L. S., ZHANG, T., CHEN, L., DESANTIAGO, J., BROWN, J. H. & BERS, D. M. 2003. Transgenic CaMKIIdeltaC overexpression uniquely alters cardiac myocyte Ca^{2+} handling: reduced SR Ca^{2+} load and activated SR Ca^{2+} release. *Circ Res,* 92**,** 904-11.

MALTSEV, V. A. & LAKATTA, E. G. 2012. The funny current in the context of the coupled-clock pacemaker cell system. *Heart Rhythm,* 9**,** 302-7.

MARUYAMA, M., LI, B. Y., CHEN, H., XU, X., SONG, L. S., GUATIMOSIM, S., ZHU, W., YONG, W., ZHANG, W., BU, G., LIN, S. F., FISHBEIN, M. C., LEDERER, W. J., SCHILD, J. H., FIELD, L. J., RUBART, M., CHEN, P. S. & SHOU, W. 2011. FKBP12 is a critical regulator of the heart rhythm and the cardiac voltage-gated sodium current in mice. *Circ Res,* 108**,** 1042-52.

MARX, S. O., ONDRIAS, K. & MARKS, A. R. 1998. Coupled gating between individual skeletal muscle Ca^{2+} release channels (ryanodine receptors). *Science,* 281**,** 818-21.

MARX, S. O., REIKEN, S., HISAMATSU, Y., GABURJAKOVA, M., GABURJAKOVA, J., YANG, Y. M., ROSEMBLIT, N. & MARKS, A. R. 2001. Phosphorylation-dependent regulation of ryanodine receptors: a novel role for leucine/isoleucine zippers. *J Cell Biol,* 153**,** 699-708.

MARX, S. O., REIKEN, S., HISAMATSU, Y., JAYARAMAN, T., BURKHOFF, D., ROSEMBLIT, N. & MARKS, A. R. 2000. PKA phosphorylation dissociates FKBP12.6 from the calcium release channel (ryanodine receptor): defective regulation in failing hearts. *Cell,* 101**,** 365-76.

MATTICK, P., PARRINGTON, J., ODIA, E., SIMPSON, A., COLLINS, T. & TERRAR, D. 2007. Ca^{2+}-stimulated adenylyl cyclase isoform AC1 is preferentially expressed in guinea-pig sino-atrial node cells and modulates the I(f) pacemaker current. *J Physiol,* 582**,** 1195-203.
MCALLISTER, R. & NOBLE, D. 1966. The time and voltage dependence of the slow outward current in cardiac Purkinje fibres. *The Journal of physiology,* 186**,** 632-662.
MEISSNER, G., DARLING, E. & EVELETH, J. 1986. Kinetics of rapid Ca^{2+} release by sarcoplasmic reticulum. Effects of Ca^{2+}, Mg^{2+}, and adenine nucleotides. *Biochemistry,* 25**,** 236-44.
MESMIN, C., FENAILLE, F., BECHER, F., TABET, J. C. & EZAN, E. 2011. Identification and characterization of apelin peptides in bovine colostrum and milk by liquid chromatography-mass spectrometry. *J Proteome Res,* 10**,** 5222-31.
MINTA, A., KAO, J. & TSIEN, R. Y. 1989. Fluorescent indicators for cytosolic calcium based on rhodamine and fluorescein chromophores. *Journal of Biological Chemistry,* 264**,** 8171-8178.
MOJZISOVA, A., KRIZANOVA, O., ZACIKOVA, L., KOMINKOVA, V. & ONDRIAS, K. 2001. Effect of nicotinic acid adenine dinucleotide phosphate on ryanodine calcium release channel in heart. *Pflugers Arch,* 441**,** 674-7.
MOON, M. J., OH, D. Y., MOON, J. S., KIM, D. K., HWANG, J. I., LEE, J. Y., KIM, J. I., CHO, S., KWON, H. B. & SEONG, J. Y. 2007. Cloning and activation of the bullfrog apelin receptor: Gi/o coupling and high affinity for [Pro1]apelin-13. *Mol Cell Endocrinol,* 277**,** 51-60.
MORGAN, A. J. 2011. Sea urchin eggs in the acid reign. *Cell Calcium,* 50**,** 147-56.
MORGAN, A. J. & GALIONE, A. 2007. NAADP induces pH changes in the lumen of acidic Ca^{2+} stores. *Biochem J,* 402**,** 301-10.
MULDER, P., BARBIER, S., CHAGRAOUI, A., RICHARD, V., HENRY, J. P., LALLEMAND, F., RENET, S., LEREBOURS, G., MAHLBERG-GAUDIN, F. & THUILLEZ, C. 2004. Long-term heart rate reduction induced by the selective I(f) current inhibitor ivabradine improves left ventricular function and intrinsic myocardial structure in congestive heart failure. *Circulation,* 109**,** 1674-9.
NAGATSU, M., SPINALE, F. G., KOIDE, M., TAGAWA, H., DEFREITAS, G., COOPER, G. T. & CARABELLO, B. A. 2000. Bradycardia and the role of beta-blockade in the amelioration of left ventricular dysfunction. *Circulation,* 101**,** 653-9.
NAYLOR, E., ARREDOUANI, A., VASUDEVAN, S. R., LEWIS, A. M., PARKESH, R., MIZOTE, A., ROSEN, D., THOMAS, J. M., IZUMI, M., GANESAN, A., GALIONE, A. & CHURCHILL, G. C. 2009. Identification of a chemical probe for NAADP by virtual screening. *Nat Chem Biol,* 5**,** 220-6.
NICE 2012. TA267, Chronic Heart Failure - Ivabradine. *In:* EXCELLENCE, N. I. F. H. A. C. (ed.). Manchester, UK.
NOBLE, D. 1960. Cardiac action and pacemaker potentials based on the Hodgkin-Huxley equations. *Nature,* 188**,** 495-7.
NORD, J. E., SHAH, P. K., RINALDI, R. Z. & WEISMAN, M. H. Hydroxychloroquine cardiotoxicity in systemic lupus erythematosus: a report of 2 cases and review of the literature. Seminars in arthritis and rheumatism, 2004. Elsevier, 336-351.
O'CARROLL, A. M., LOLAIT, S. J., HARRIS, L. E. & POPE, G. R. 2013. The apelin receptor APJ: journey from an orphan to a multifaceted regulator of homeostasis. *J Endocrinol,* 219**,** R13-35.
O'CONNELL, T. D., RODRIGO, M. C. & SIMPSON, P. C. 2007. Isolation and culture of adult mouse cardiac myocytes. *Methods Mol Biol,* 357**,** 271-96.
OGRODNIK, J. & NIGGLI, E. 2010. Increased Ca(2+) leak and spatiotemporal coherence of Ca^{2+} release in cardiomyocytes during beta-adrenergic stimulation. *J Physiol,* 588**,** 225-42.
OHKUMA, S. & POOLE, B. 1978. Fluorescence probe measurement of the intralysosomal pH in living cells and the perturbation of pH by various agents. *Proc Natl Acad Sci U S A,* 75**,** 3327-31.
OTSU, K., WILLARD, H. F., KHANNA, V. K., ZORZATO, F., GREEN, N. M. & MACLENNAN, D. H. 1990. Molecular cloning of cDNA encoding the Ca^{2+} release channel (ryanodine receptor) of rabbit cardiac muscle sarcoplasmic reticulum. *J Biol Chem,* 265**,** 13472-83.
OTTENHEIJM, C. A., HEUNKS, L. M. & DEKHUIJZEN, R. P. 2008. Diaphragm adaptations in patients with COPD. *Respir Res,* 9**,** 12.

PATEL, S., CHURCHILL, G. C. & GALIONE, A. 2000. Unique kinetics of nicotinic acid-adenine dinucleotide phosphate (NAADP) binding enhance the sensitivity of NAADP receptors for their ligand. *Biochem J,* 352 Pt 3**,** 725-9.

PEREIRA, L., METRICH, M., FERNANDEZ-VELASCO, M., LUCAS, A., LEROY, J., PERRIER, R., MOREL, E., FISCHMEISTER, R., RICHARD, S., BENITAH, J. P., LEZOUALC'H, F. & GOMEZ, A. M. 2007. The cAMP binding protein Epac modulates Ca^{2+} sparks by a Ca^{2+}/calmodulin kinase signalling pathway in rat cardiac myocytes. *J Physiol,* 583**,** 685-94.

PERIASAMY, M., BHUPATHY, P. & BABU, G. J. 2008. Regulation of sarcoplasmic reticulum Ca^{2+} ATPase pump expression and its relevance to cardiac muscle physiology and pathology. *Cardiovasc Res,* 77**,** 265-73.

PERIASAMY, M., REED, T. D., LIU, L. H., JI, Y., LOUKIANOV, E., PAUL, R. J., NIEMAN, M. L., RIDDLE, T., DUFFY, J. J. & DOETSCHMAN, T. 1999. Impaired cardiac performance in heterozygous mice with a null mutation in the sarco (endo) plasmic reticulum Ca^{2+}-ATPase isoform 2 (SERCA2) gene. *Journal of Biological Chemistry,* 274**,** 2556-2562.

PITT, S. J., FUNNELL, T. M., SITSAPESAN, M., VENTURI, E., RIETDORF, K., RUAS, M., GANESAN, A., GOSAIN, R., CHURCHILL, G. C., ZHU, M. X., PARRINGTON, J., GALIONE, A. & SITSAPESAN, R. 2010. TPC2 is a novel NAADP-sensitive Ca^{2+} release channel, operating as a dual sensor of luminal pH and Ca^{2+}. *J Biol Chem,* 285**,** 35039-46.

POWELL, T., TERRAR, D. A. & TWIST, V. W. 1980. Electrical properties of individual cells isolated from adult rat ventricular myocardium. *J Physiol,* 302**,** 131-53.

PUGLISI, J. L., YUAN, W., BASSANI, J. W. & BERS, D. M. 1999. Ca^{2+} influx through Ca^{2+} channels in rabbit ventricular myocytes during action potential clamp: influence of temperature. *Circ Res,* 85**,** e7-e16.

RAKOVIC, S., CUI, Y., IINO, S., GALIONE, A., ASHAMU, G. A., POTTER, B. V. & TERRAR, D. A. 1999. An antagonist of cADP-ribose inhibits arrhythmogenic oscillations of intracellular Ca^{2+} in heart cells. *J Biol Chem,* 274**,** 17820-7.

RAKOVIC, S., GALIONE, A., ASHAMU, G. A., POTTER, B. V. & TERRAR, D. A. 1996. A specific cyclic ADP-ribose antagonist inhibits cardiac excitation-contraction coupling. *Curr Biol,* 6**,** 989-96.

RAVENS, U. & WETTWER, E. 2011. Ultra-rapid delayed rectifier channels: molecular basis and therapeutic implications. *Cardiovasc Res,* 89**,** 776-85.

REZAZADEH, S., CLAYDON, T. W. & FEDIDA, D. 2006. KN-93 (2-[N-(2-hydroxyethyl)]-N-(4-methoxybenzenesulfonyl)] amino-N-(4-chlorocinnamyl)-N-methylbenzylamine), a calcium/calmodulin-dependent protein kinase II inhibitor, is a direct extracellular blocker of voltage-gated potassium channels. *Journal of Pharmacology and Experimental Therapeutics,* 317**,** 292-299.

RIGG, L., HEATH, B. M., CUI, Y. & TERRAR, D. A. 2000. Localisation and functional significance of ryanodine receptors during beta-adrenoceptor stimulation in the guinea-pig sino-atrial node. *Cardiovasc Res,* 48**,** 254-64.

RIGG, L. & TERRAR, D. A. 1996. Possible role of calcium release from the sarcoplasmic reticulum in pacemaking in guinea-pig sino-atrial node. *Exp Physiol,* 81**,** 877-80.

RINGER, S. 1883. A further contribution regarding the influence of the different constituents of the blood on the contraction of the heart. *The Journal of physiology,* 4**,** 29.

RONKAINEN, V. P., RONKAINEN, J. J., HANNINEN, S. L., LESKINEN, H., RUAS, J. L., PEREIRA, T., POELLINGER, L., VUOLTEENAHO, O. & TAVI, P. 2007. Hypoxia inducible factor regulates the cardiac expression and secretion of apelin. *FASEB J,* 21**,** 1821-30.

RUAS, M., RIETDORF, K., ARREDOUANI, A., DAVIS, L. C., LLOYD-EVANS, E., KOEGEL, H., FUNNELL, T. M., MORGAN, A. J., WARD, J. A., WATANABE, K., CHENG, X., CHURCHILL, G. C., ZHU, M. X., PLATT, F. M., WESSEL, G. M., PARRINGTON, J. & GALIONE, A. 2010. Purified TPC isoforms form NAADP receptors with distinct roles for Ca^{2+} signaling and endolysosomal trafficking. *Curr Biol,* 20**,** 703-9.

SAID, M., MUNDINA-WEILENMANN, C., VITTONE, L. & MATTIAZZI, A. 2002. The relative relevance of phosphorylation of the Thr(17) residue of phospholamban is different at different levels of beta-adrenergic stimulation. *Pflugers Arch,* 444**,** 801-9.

SÁNCHEZ-CHAPULA, J. A., SALINAS-STEFANON, E., TORRES-JÁCOME, J., BENAVIDES-HARO, D. E. & NAVARRO-POLANCO, R. A. 2001. Blockade of currents by the antimalarial drug chloroquine in feline ventricular myocytes. *Journal of Pharmacology and Experimental Therapeutics,* 297**,** 437-445.

SCHIEDER, M., ROTZER, K., BRUGGEMANN, A., BIEL, M. & WAHL-SCHOTT, C. A. 2010. Characterization of two-pore channel 2 (TPCN2)-mediated Ca^{2+} currents in isolated lysosomes. *J Biol Chem,* 285**,** 21219-22.

SCHMITT, J. P., KAMISAGO, M., ASAHI, M., LI, G. H., AHMAD, F., MENDE, U., KRANIAS, E. G., MACLENNAN, D. H., SEIDMAN, J. G. & SEIDMAN, C. E. 2003. Dilated cardiomyopathy and heart failure caused by a mutation in phospholamban. *Science,* 299**,** 1410-3.

SCIMIA, M. C., HURTADO, C., RAY, S., METZLER, S., WEI, K., WANG, J., WOODS, C. E., PURCELL, N. H., CATALUCCI, D., AKASAKA, T., BUENO, O. F., VLASUK, G. P., KALIMAN, P., BODMER, R., SMITH, L. H., ASHLEY, E., MERCOLA, M., BROWN, J. H. & RUIZ-LOZANO, P. 2012. APJ acts as a dual receptor in cardiac hypertrophy. *Nature,* 488**,** 394-8.

SEIDLER, T., MILLER, S. L., LOUGHREY, C. M., KANIA, A., BUROW, A., KETTLEWELL, S., TEUCHER, N., WAGNER, S., KOGLER, H., MEYERS, M. B., HASENFUSS, G. & SMITH, G. L. 2003. Effects of adenovirus-mediated sorcin overexpression on excitation-contraction coupling in isolated rabbit cardiomyocytes. *Circ Res,* 93**,** 132-9.

SEYAMA, I. 1976. Characteristics of the rectifying properties of the sino-atrial node cell of the rabbit. *The Journal of physiology,* 255**,** 379-397.

SHARMA, M. R., PENCZEK, P., GRASSUCCI, R., XIN, H. B., FLEISCHER, S. & WAGENKNECHT, T. 1998. Cryoelectron microscopy and image analysis of the cardiac ryanodine receptor. *J Biol Chem,* 273**,** 18429-34.

SHINODA, T., OGAWA, H., CORNELIUS, F. & TOYOSHIMA, C. 2009. Crystal structure of the sodium–potassium pump at 2.4 Å resolution. *Nature,* 459**,** 446-450.

SOMMER, J. R. 1982. Ultrastructural considerations concerning cardiac muscle. *J Mol Cell Cardiol,* 14 Suppl 3**,** 77-83.

SPENCER, C. I. & BERLIN, J. R. 1995. Control of sarcoplasmic reticulum calcium release during calcium loading in isolated rat ventricular myocytes. *The Journal of physiology,* 488**,** 267-279.

STIEBER, J., HERRMANN, S., FEIL, S., LOSTER, J., FEIL, R., BIEL, M., HOFMANN, F. & LUDWIG, A. 2003. The hyperpolarization-activated channel HCN4 is required for the generation of pacemaker action potentials in the embryonic heart. *Proc Natl Acad Sci U S A,* 100**,** 15235-40.

STREB, H., IRVINE, R. F., BERRIDGE, M. J. & SCHULZ, I. 1983. Release of Ca^{2+} from a nonmitochondrial intracellular store in pancreatic acinar cells by inositol-1,4,5-trisphosphate. *Nature,* 306**,** 67-9.

SULFI, S. & TIMMIS, A. D. 2006. Ivabradine -- the first selective sinus node I(f) channel inhibitor in the treatment of stable angina. *Int J Clin Pract,* 60**,** 222-8.

SURREY, A. R. & HAMMER, H. F. 1950. The preparation of 7-chloro-4-(4-(N-ethyl-N-beta-hydroxyethylamino)-1-methylbutylamino)-quinoline and related compounds. *Journal of the American Chemical Society,* 72**,** 1814-1815.

SZOKODI, I., TAVI, P., FOLDES, G., VOUTILAINEN-MYLLYLA, S., ILVES, M., TOKOLA, H., PIKKARAINEN, S., PIUHOLA, J., RYSA, J., TOTH, M. & RUSKOAHO, H. 2002. Apelin, the novel endogenous ligand of the orphan receptor APJ, regulates cardiac contractility. *Circ Res,* 91**,** 434-40.

TANG, Q., JIN, M. W., XIANG, J. Z., DONG, M. Q., SUN, H. Y., LAU, C. P. & LI, G. R. 2007. The membrane permeable calcium chelator BAPTA-AM directly blocks human ether a-go-go-related gene potassium channels stably expressed in HEK 293 cells. *Biochem Pharmacol,* 74**,** 1596-607.

TATEMOTO, K. 2000. Search for an endogenous ligand of the orphan G protein-coupled receptor--discovery of apelin, a novel biologically active peptide. *Nihon Rinsho,* 58**,** 737-46.

TATEMOTO, K., HOSOYA, M., HABATA, Y., FUJII, R., KAKEGAWA, T., ZOU, M.-X., KAWAMATA, Y., FUKUSUMI, S., HINUMA, S. & KITADA, C. 1998. Isolation and

characterization of a novel endogenous peptide ligand for the human APJ receptor. *Biochemical and biophysical research communications,* 251**,** 471-476.
TEPLOVA, V. V., TONSHIN, A. A., GRIGORIEV, P. A., SARIS, N.-E. L. & SALKINOJA-SALONEN, M. S. 2007. Bafilomycin A1 is a potassium ionophore that impairs mitochondrial functions. *Journal of bioenergetics and biomembranes,* 39**,** 321-329.
TERENTYEV, D., VIATCHENKO-KARPINSKI, S., GYORKE, I., VOLPE, P., WILLIAMS, S. C. & GYORKE, S. 2003. Calsequestrin determines the functional size and stability of cardiac intracellular calcium stores: Mechanism for hereditary arrhythmia. *Proc Natl Acad Sci U S A,* 100**,** 11759-64.
THOLLON, C., CAMBARRAT, C., VIAN, J., PROST, J. F., PEGLION, J. L. & VILAINE, J. P. 1994. Electrophysiological effects of S 16257, a novel sino-atrial node modulator, on rabbit and guinea-pig cardiac preparations: comparison with UL-FS 49. *Br J Pharmacol,* 112**,** 37-42.
TIKHONOV, D. B. & ZHOROV, B. S. 2011. Possible roles of exceptionally conserved residues around the selectivity filters of sodium and calcium channels. *Journal of Biological Chemistry,* 286**,** 2998-3006.
TIMERMAN, A. P., ONOUE, H., XIN, H. B., BARG, S., COPELLO, J., WIEDERRECHT, G. & FLEISCHER, S. 1996. Selective binding of FKBP12.6 by the cardiac ryanodine receptor. *J Biol Chem,* 271**,** 20385-91.
VALDIVIA, H. H., KAPLAN, J. H., ELLIS-DAVIES, G. C. & LEDERER, W. J. 1995. Rapid adaptation of cardiac ryanodine receptors: modulation by Mg^{2+} and phosphorylation. *Science,* 267**,** 1997-2000.
VAN BREEMEN, C., FAMELI, N. & EVANS, A. M. 2013. Pan-junctional sarcoplasmic reticulum in vascular smooth muscle: nanospace Ca^{2+} transport for site- and function-specific Ca^{2+} signalling. *J Physiol,* 591**,** 2043-54.
VAN OORT, R. J., MCCAULEY, M. D., DIXIT, S. S., PEREIRA, L., YANG, Y., RESPRESS, J. L., WANG, Q., DE ALMEIDA, A. C., SKAPURA, D. G., ANDERSON, M. E., BERS, D. M. & WEHRENS, X. H. 2010. Ryanodine receptor phosphorylation by calcium/calmodulin-dependent protein kinase II promotes life-threatening ventricular arrhythmias in mice with heart failure. *Circulation,* 122**,** 2669-79.
VER HEYEN, M., HEYMANS, S., ANTOONS, G., REED, T., PERIASAMY, M., AWEDE, B., LEBACQ, J., VANGHELUWE, P., DEWERCHIN, M., COLLEN, D., SIPIDO, K., CARMELIET, P. & WUYTACK, F. 2001. Replacement of the muscle-specific sarcoplasmic reticulum Ca^{2+}-ATPase isoform SERCA2a by the nonmuscle SERCA2b homologue causes mild concentric hypertrophy and impairs contraction-relaxation of the heart. *Circ Res,* 89**,** 838-46.
VERBOOMEN, H., WUYTACK, F., DE SMEDT, H., HIMPENS, B. & CASTEELS, R. 1992. Functional difference between SERCA2a and SERCA2b Ca^{2+} pumps and their modulation by phospholamban. *Biochem J,* 286 (Pt 2)**,** 591-5.
VERBOOMEN, H., WUYTACK, F., VAN DEN BOSCH, L., MERTENS, L. & CASTEELS, R. 1994. The functional importance of the extreme C-terminal tail in the gene 2 organellar Ca^{2+}-transport ATPase (SERCA2a/b). *Biochem J,* 303 (Pt 3)**,** 979-84.
VINOGRADOVA, T. M., ZHOU, Y. Y., MALTSEV, V., LYASHKOV, A., STERN, M. & LAKATTA, E. G. 2004. Rhythmic ryanodine receptor Ca^{2+} releases during diastolic depolarization of sinoatrial pacemaker cells do not require membrane depolarization. *Circ Res,* 94**,** 802-9.
WAAGSTEIN, F., BRISTOW, M. R., SWEDBERG, K., CAMERINI, F., FOWLER, M. B., SILVER, M. A., GILBERT, E. M., JOHNSON, M. R., GOSS, F. G. & HJALMARSON, A. 1993. Beneficial effects of metoprolol in idiopathic dilated cardiomyopathy. Metoprolol in Dilated Cardiomyopathy (MDC) Trial Study Group. *Lancet,* 342**,** 1441-6.
WAKIMOTO, K., KOBAYASHI, K., KURO, O. M., YAO, A., IWAMOTO, T., YANAKA, N., KITA, S., NISHIDA, A., AZUMA, S., TOYODA, Y., OMORI, K., IMAHIE, H., OKA, T., KUDOH, S., KOHMOTO, O., YAZAKI, Y., SHIGEKAWA, M., IMAI, Y., NABESHIMA, Y. & KOMURO, I. 2000. Targeted disruption of Na^{+}/ Ca^{2+} exchanger gene leads to cardiomyocyte apoptosis and defects in heartbeat. *J Biol Chem,* 275**,** 36991-8.

WALSETH, T. F., LIN-MOSHIER, Y., JAIN, P., RUAS, M., PARRINGTON, J., GALIONE, A., MARCHANT, J. S. & SLAMA, J. T. 2012. Photoaffinity labeling of high affinity nicotinic acid adenine dinucleotide phosphate (NAADP)-binding proteins in sea urchin egg. *J Biol Chem,* 287**,** 2308-15.

WANG, C., DU, J. F., WU, F. & WANG, H. C. 2008. Apelin decreases the SR Ca^{2+} content but enhances the amplitude of $[Ca^{2+}]$i transient and contractions during twitches in isolated rat cardiac myocytes. *Am J Physiol Heart Circ Physiol,* 294**,** H2540-6.

WANG, W., ZHU, W., WANG, S., YANG, D., CROW, M. T., XIAO, R. P. & CHENG, H. 2004. Sustained beta1-adrenergic stimulation modulates cardiac contractility by Ca^{2+}/calmodulin kinase signaling pathway. *Circ Res,* 95**,** 798-806.

WANG, X., ZHANG, X., DONG, X. P., SAMIE, M., LI, X., CHENG, X., GOSCHKA, A., SHEN, D., ZHOU, Y., HARLOW, J., ZHU, M. X., CLAPHAM, D. E., REN, D. & XU, H. 2012. TPC proteins are phosphoinositide- activated sodium-selective ion channels in endosomes and lysosomes. *Cell,* 151**,** 372-83.

WEBER, C. R., PIACENTINO, V., 3RD, GINSBURG, K. S., HOUSER, S. R. & BERS, D. M. 2002. Na^{+}-Ca^{2+} exchange current and submembrane $[Ca^{2+}]$ during the cardiac action potential. *Circ Res,* 90**,** 182-9.

WEHRENS, X. H., LEHNART, S. E., HUANG, F., VEST, J. A., REIKEN, S. R., MOHLER, P. J., SUN, J., GUATIMOSIM, S., SONG, L. S., ROSEMBLIT, N., D'ARMIENTO, J. M., NAPOLITANO, C., MEMMI, M., PRIORI, S. G., LEDERER, W. J. & MARKS, A. R. 2003. FKBP12.6 deficiency and defective calcium release channel (ryanodine receptor) function linked to exercise-induced sudden cardiac death. *Cell,* 113**,** 829-40.

WEHRENS, X. H., LEHNART, S. E., REIKEN, S. R. & MARKS, A. R. 2004. Ca^{2+}/calmodulin-dependent protein kinase II phosphorylation regulates the cardiac ryanodine receptor. *Circ Res,* 94**,** e61-70.

XIAO, R. P., VALDIVIA, H. H., BOGDANOV, K., VALDIVIA, C., LAKATTA, E. G. & CHENG, H. 1997. The immunophilin FK506-binding protein modulates Ca^{2+} release channel closure in rat heart. *J Physiol,* 500 (Pt 2)**,** 343-54.

XIE, L. H., SHANMUGAM, M., PARK, J. Y., ZHAO, Z., WEN, H., TIAN, B., PERIASAMY, M. & BABU, G. J. 2012. Ablation of sarcolipin results in atrial remodeling. *Am J Physiol Cell Physiol,* 302**,** C1762-71.

XU, L. & MEISSNER, G. 1998. Regulation of Cardiac Muscle Ca^{2+} Release Channel by Sarcoplasmic Reticulum Lumenal Ca^{2+}. *Biophysical journal,* 75**,** 2302-2312.

XU, L. & MEISSNER, G. 2004. Mechanism of calmodulin inhibition of cardiac sarcoplasmic reticulum Ca^{2+} release channel (ryanodine receptor). *Biophys J,* 86**,** 797-804.

YAMAGUCHI, H., MUTH, J. N., VARADI, M., SCHWARTZ, A. & VARADI, G. 1999. Critical role of conserved proline residues in the transmembrane segment 4 voltage sensor function and in the gating of L-type calcium channels. *Proc Natl Acad Sci U S A,* 96**,** 1357-62.

YAMAGUCHI, N., TAKAHASHI, N., XU, L., SMITHIES, O. & MEISSNER, G. 2007. Early cardiac hypertrophy in mice with impaired calmodulin regulation of cardiac muscle Ca^{2+} release channel. *J Clin Invest,* 117**,** 1344-53.

YEAGER, M. & NICHOLSON, B. J. 1996. Structure of gap junction intercellular channels. *Current opinion in structural biology,* 6**,** 183-192.

ZHANG, F. & LI, P. L. 2007. Reconstitution and characterization of a nicotinic acid adenine dinucleotide phosphate (NAADP)-sensitive Ca^{2+} release channel from liver lysosomes of rats. *J Biol Chem,* 282**,** 25259-69.

ZHANG, L., KELLEY, J., SCHMEISSER, G., KOBAYASHI, Y. M. & JONES, L. R. 1997. Complex formation between junctin, triadin, calsequestrin, and the ryanodine receptor. Proteins of the cardiac junctional sarcoplasmic reticulum membrane. *J Biol Chem,* 272**,** 23389-97.

ZHANG, R., KHOO, M. S., WU, Y., YANG, Y., GRUETER, C. E., NI, G., PRICE, E. E., JR., THIEL, W., GUATIMOSIM, S., SONG, L. S., MADU, E. C., SHAH, A. N., VISHNIVETSKAYA, T. A., ATKINSON, J. B., GUREVICH, V. V., SALAMA, G., LEDERER, W. J., COLBRAN, R. J. & ANDERSON, M. E. 2005. Calmodulin kinase II inhibition protects against structural heart disease. *Nat Med,* 11**,** 409-17.

ZHANG, X., TALLINI, Y. N., CHEN, Z., GAN, L., WEI, B., DORAN, R., MIAO, L., XIN, H. B., KOTLIKOFF, M. I. & JI, G. 2009. Dissociation of FKBP12.6 from ryanodine receptor type 2

is regulated by cyclic ADP-ribose but not beta-adrenergic stimulation in mouse cardiomyocytes. *Cardiovasc Res,* 84**,** 253-62.
ZIMA, A. V., BARE, D. J., MIGNERY, G. A. & BLATTER, L. A. 2007. IP_3-dependent nuclear Ca^{2+} signalling in the mammalian heart. *J Physiol,* 584**,** 601-11.
ZIMA, A. V. & BLATTER, L. A. 2004. Inositol-1,4,5-trisphosphate-dependent Ca^{2+} signalling in cat atrial excitation-contraction coupling and arrhythmias. *J Physiol,* 555**,** 607-15.
ZISSIMOPOULOS, S., SEIFAN, S., MAXWELL, C., WILLIAMS, A. J. & LAI, F. A. 2012. Disparities in the association of the ryanodine receptor and the FK506-binding proteins in mammalian heart. *J Cell Sci,* 125**,** 1759-69.
ZONG, X., SCHIEDER, M., CUNY, H., FENSKE, S., GRUNER, C., ROTZER, K., GRIESBECK, O., HARZ, H., BIEL, M. & WAHL-SCHOTT, C. 2009. The two-pore channel TPCN2 mediates NAADP-dependent Ca^{2+}-release from lysosomal stores. *Pflugers Arch,* 458**,** 891-9.
ZUHLKE, R. D., PITT, G. S., DEISSEROTH, K., TSIEN, R. W. & REUTER, H. 1999. Calmodulin supports both inactivation and facilitation of L-type calcium channels. *Nature,* 399**,** 159-62.